# DEVELOPMENT AND IMPLEMENTATION OF HIGH PERFORMANCE AND HIGH EFFICIENCY INTERIOR PERMANENT MAGNET SYNCHRONOUS MOTOR DRIVE

By
Bhavinkumar Patel

SUBMITTED IN PARTIAL FULFILLMENT OF THE
REQUIREMENTS FOR THE DEGREE OF
MASTER OF SCIENCE
AT
LAKEHEAD UNIVERSITY
THUNDER BAY, ONTARIO
May, 2013

# Abstract

As the motor consumes more than 50% of total electrical energy produced in the world, the efficiency optimization of the motor is a burning issue in terms of saving energy and the environment. In modern days researchers display immense interest in the control of a high performing interior permanent magnet synchronous motors (IPMSM) drive for general industrial applications. The IPMSM is largely used in low and medium power applications such as adjustable speed drives, robotics, aerospace and electric vehicles due to its several advantageous features such as high power density, greater flux weakening capability, high output torque, high power factor, low noise, robustness and high efficiency as compared to the dc motors and induction motors (IM). Nevertheless, its high efficiency characteristics are influenced by applied control strategies. Most of the reported works developed control algorithms for IPMSM to achieve high performance. However, the efficiency optimization of IPMSM, which is one of the important aspects is often ignored. Therefore, in this thesis the efficiency optimization issues is also considered along with high performance control.

This thesis presents a nonlinear loss model-based controller (LMC) for IPMSM drive to achieve both high efficiency and high performance of the drive. Among numerous loss minimization algorithms (LMA), a LMC approach offers a fast response without torque pulsations. However, it requires the accurate loss model and the knowledge of the motor parameters. Therefore, a difficulty in deriving the LMC lies in the complexity of the full loss model. Moreover, the conventional LMC does not pay attention to the performance of the drive at all. In an effort to overcome the drawbacks of conventional LMC, an adaptive backstepping based nonlinear control

(ABNC) is designed to achieve high dynamic performance speed control for an IPMSM drive is developed in this thesis. The system parameter variations as well as field control are taken into account at the design stage of the controller. Thus, the proposed ABNC is capable of maintaining the system robustness and stability against mechanical parameter variation and external load torque disturbance. To ensure stability the controller is designed based on Lyapunov's stability theory while the LMC ensures high efficiency of the drive. A neuro-fuzzy logic controller (NFC) including LMC is also developed in this work. The proposed NFC overcomes the unknown and nonlinear uncertainties of the drive, the membership function of the controller is tuned online. An important part of this work is directed to develop an adaptive network-based fuzzy inference system (ANFIS) based NFC. In this work, an adaptive tuning algorithm is also developed to adjust the membership function and consequent parameters.

The complete closed-loop system model is developed and then simulated using MATLAB/Simulink software. Performance of the various control algorithms based IPMSM drive is investigated extensively at different dynamic operating conditions such as sudden load change, command speed change, parameter variation, etc. The performance of the proposed loss minimization based ABNC and NFC are also compared with the conventional $i_d$=0 control scheme. The complete IPMSM drive have been successfully implemented in real-time using digital signal processor (DSP) controller board DS1104 for a laboratory 5 hp motor. The experimental results verify the simulation of NFC based loss minimization. It is found from the results that proposed drive algorithms can improve the efficiency by around 3% as compared to without any LMA.

# Acknowledgements

I would like to acknowledge God, who gave me strength and knowledge to complete this thesis. I like to express my most sincere thanks and appreciation to my supervisor, Dr. M. N. Uddin for his continuous inspiration and guidance throughout the program. This thesis would not have been completed without his support. I wish to thank my thesis committee members Dr. K. Natarajan and Dr. D. Alexandrov. I acknowledge the support from Dr. X. Liu for his direction towards experimental demonstrations of this thesis. And finally I would like to give many thanks to my fellow graduate students, especially Nirav Patel for his guidance throughout the last two years, and staff of Lakehead University.

I am also grateful to my parents Mr. Vrundavanbhai Patel and Mrs. Anjanaben Patel and my brother Pratik Patel for their enormous support. I also give many thanks to my friends who has always been positive and helpful.

# Table of Contents

# List of Figures

# List of Acronyms

| | |
|---|---|
| ABNC | Adaptive backstepping based nonlinear controller |
| AC | Alternating current |
| ANFIS | Adaptive network-based fuzzy inference system |
| ANN | Artificial neural network |
| CSI | Current source inverter |
| DC | Direct current |
| DSP | Digital signal processors |
| EKF | Extended kalman filter |
| EMF | Electromotive force |
| FBLC | Feedback linearization control |
| FLC | Fuzzy logic controller |
| FOC | Field oriented control |
| FW | Flux-weakening |
| HPD | High performance drive |
| HPVSD | High performance variable speed drive |
| IM | Induction motor |
| IPMSM | Interior permanent magnet synchronous motor |
| LMA | Loss minimization algorithm |

| | |
|---|---|
| LMC | Loss model-based controller |
| MRAC | Model reference adaptive controller |
| MTPA | Maximum torque per ampere |
| NFC | Neuro-fuzzy Controller |
| NNC | Neural network controller |
| PDF | Pseudo-derivative-feedback |
| PI | Proportional integral |
| PID | Proportional integral derivative |
| PM | Permanent magnet |
| PMSM | Permanent magnet synchronous motor |
| PWM | Pulse width modulation |
| R&D | Research and development |
| SC | Search-based controller |
| SM | Synchronous motor |
| SMC | Sliding mode controller |
| SPMSM | Surface mounted permanent magnet synchronous motor |
| SPWM | Sinusoidal PWM |
| STR | Self-tuning regulator |
| SVM | Space vector modulation |
| VSC | Variable structure controller |
| VSI | Voltage source inverter |

# List of Symbol

| | |
|---|---|
| $e$ | Speed error |
| $e_q$ | q-axis current error |
| $e_{\Gamma}$ | Loss minimization control error |
| $I_a$ | Maximum line current amplitude |
| $L_d$ | d-axis inductance |
| $L_q$ | q-axis inductance |
| $T_e$ | Developed electromagnetic torque |
| $V_a$ | Maximum phase voltage amplitude |
| $\theta_r$ | Rotor position |
| $\omega_r$ | Rotor frequency |
| $\omega_s$ | Stator frequency |
| $I_{dT}$ | d-axis demagnetizing current |
| $I_{qT}$ | q-axis torque generating operating point current |
| $I_{dc}$ | d-axis core loss current |
| $I_{qc}$ | q-axis core loss current |
| $I_d$, $i_d^r$ | d-axis armature current |
| $I_q$, $i_q^r$ | q-axis armature current |
| $V_d$, $v_d^r$ | d-axis armature voltage |

| | |
|---|---|
| $V_q$, $v_q^r$ | q-axis armature voltage |
| $R_s$ | Armature copper loss resistance |
| $R_c$ | Iron loss resistance |
| $I_q^*$ | Command q-axis current |
| $v_a$, $v_b$, $v_c$ | a, b and c phase voltages |
| $P_{Cu}$ | Copper losses |
| $P_{Fe}$ | Iron losses |
| $\eta$ | Efficiency of IPMSM drive |
| $P_{out}$ | Output power |
| $P_L$ | Total electrical power loss |
| $\omega_r$ | Electrical angular velocity |
| $T_L$ | Load torque |
| $B_m$ | Friction coefficient |
| $J$ | Inertia constant |
| $k_1$, $k_2$, $k_3$ | Closed-loop feedback gains |
| $\varphi_1$, $\varphi_2$ | Adaptive gains |

# Chapter 1

# Introduction

## 1.1 History

An electric motor is an electromechanical device that converts electrical energy into mechanical energy and vice versa for electric generator. The very first conversion of electrical energy into mechanical energy was demonstrated by the British scientist Michael Faraday in 1821. The demonstration was done by dipping a free-hanging wire into a pool of mercury, on which a permanent magnet (PM) was placed in the middle of the pool of mercury. When a current was passed through the wire, the wire rotated around the magnet, showing that the current gave rise to a circular magnetic field around the wire. This class of electric motors is called homopolar motors. An advanced improvement is the Barlow's wheel, which was designed and built by English physicist and mathematician, Peter Barlow in 1822. In 1828, Hungarian physicist Anyos Jedlik demonstrated the first device to contain the three main components of practical direct current (DC) motors: the rotor, stator and commutator. The device had no PM; the current flowing through windings produced the magnetic fields of both the rotating and stationary components. The device is known as multipolar motors, it can use attraction and repulsion of magnetic interaction. In 1832, the first commutator type DC electric motor capable of turning machinery was invented by the

British scientist William Sturgeon. The modern DC motor was invented in 1873 by Zenobe Gramme, a Belgium born electrical engineer. He accidentally connected the dynamo he had invented to a second similar unit, driving it as a motor. The Gramme machine was the first electric motor that was successful in the industry; earlier inventions were used as toys or laboratory interests. In 1886, Frank Julian Sprague invented the first practical DC motor, capable of constant speed under variable loads. In 1831, the discovery of a changing magnetic field that is capable of inducing an electric current in a circuit by an English scientist Michael Faraday paved the way towards the invention of AC motors. In 1885, Italian physics and electrical engineer Galileo Ferraris demonstrated a working model of his single phase induction motor (IM) [1]. In 1887, Nikola Tesla built his working two phase IM and demonstrated it at the American Institute of Electrical Engineers in 1888. Working from Farraris's experiments, Mikhail Dolivo-Dobrovolsky developed the very first three-phase IM in 1890. He also invented three-phase generator and transformer and combined them into the first complete AC three-phase system in 1891 [2].

Application of electric motors revolutionized industry. It's providing easy control at the point of use. In agriculture applications, human and animal muscle power is eliminated from such tasks as handling grain or pumping water. Household uses of electric motors reduced heavy labour in the house and made higher standard of convenience, comfort and safety. Over the years electric motor drive systems use has been widely accepted. We find it in applications such as pumps, fans, paper and textile mills, elevators, electric vehicles and subway transportation, home appliances, wind generation systems, servo and robotics, computer peripherals, steel and cement mills, ship propulsion, etc. An electric motor is a complex structure electrically, mechanically and thermally. Although motors were introduced more than one hundred years ago, the research and development (R&D) in this area appears to be never-ending. However, the evolution of motors has not been up

to the mark compared to that of power semiconductor devices and power electronic converters [3]. Most motion control systems were designed to operate at fixed speed but many of these applications requires variable speed operation. As a result, the shift from fixed speed drives to variable speed drives has been in effect since last 40 years. The two main categories of general electric motors are DC motors and AC motors. Each class have numerous types and unique abilities that suit them well for specific applications.

## 1.2 DC Motors

As mention in previous section, first modern DC motor was invented accidently by Zenobe Gramme in 1873. The name dc motor originates from the dc electric power being supply to the motor. By the year 1900 the dc motor was widely used in street railways, mining and industrial applications. Nowadays, dc motors are just cheap options for unimportant uses. However, their behaviour has some very interesting characteristics that make dc motors versatile and desirable for many applications. First, the rotation speed of a dc motor is directly tied to its supply voltage, which can itself be varied within some range to produce variable motor speed. DC motors can also be designed to rotate at any desired speed for a fixed supply voltage. Secondly, dc motors have strong torque at low speeds. And lastly, the decoupled nature of the field and armature makes dc motor control very easy therefore utilizing for high performance variable speed drive (HPVSD) applications [4]. However, there are many disadvantages of dc motors such as, lack of overload capability, limited range of operation, adverse effects of power loss in field circuit, lack of ruggedness, frequent maintenance requirement, low torque density, high weight to power ratio, high cost due to brushes, low life span for high intensity uses, high maintenance cost for replacing

commutator, fire hazards due to sparking and low efficiency [5]. Due to these disadvantages of dc motors researchers were encouraged to develop ac motors such as induction motors (IM) and synchronous motors (SM) for HPVSD applications, where robustness and maintenance free operations are the major concerns.

## 1.3 AC Motors

An ac motor is an electric motor driven by an alternating current (AC). It commonly consists of two basic parts, a stator having coils supplied with AC to produce a rotating magnetic field, and a rotor attached to the output shaft that is given a torque by the rotating field [6]. There are two main types of ac motors, depending on the type of rotor used. The first type is the IM, which runs slightly slower than the supply frequency. The magnetic field on the rotor of this motor is created by an induced current. The second type is the SM, which does not rely on induction and as a result, can rotate exactly at the supply frequency or a sub-multiple of the supply frequency. The magnetic field on the rotor is either generated by current delivered through slip rings or by PM. Ac motors have no commutator therefore, no need for frequent maintenance, no need for housing the commutator, they have rugged construction and have speed which is only limited by the physical constraints of the motor and the supply frequency. Recent development of power electronic devices, very large scale integrated (VLSI) technologies and efficient use of microprocessors, ac motors can also be used for variable speed drives. The ac motors can be used for high performance drive (HPD) systems using closed loop vector control technique [7].

### 1.3.1 Induction Motors

IM was a product of Tesla's amazing brain. The drive current is passed through coils on the stator, just as in the synchronous AC motor. But in IM, the rotor holds nothing except for some windings of wire. No magnet, no current sent through an electromagnet. So how does it work? The drive current in the stator induces a magnetic field in the stator, and the stator field in turn induces one in the rotor wires, and the two fields interact to allow the rotor to be pushed around and effectively convert electrical energy to mechanical energy [8]. IM can be divided into two categories; squirrel cage motors and would rotor motors. Squirrel cage motors have a heavy winding made up of solid bars or conductors, usually aluminum or copper. In squirrel cage rotor aluminum/copper bars or conductors are shorted together at both ends of the rotor by cast aluminum/copper end rings. In wound rotor motors, the rotor winding consists many turns of insulated wire and is connected to slip rings on the motor shaft. The wound rotor motor is used primarily to start a high inertia load or a load that requires a very high starting torque across the full speed range.

As compared to dc motor the main advantages of IM are great reliability, low cost, low maintenance, its ruggedness, simple, direct connection to ac power source and good efficiency [3, 9]. Even though IM has great advantages it also has few disadvantages with their use in HPVSD applications. First disadvantage of IM is that it always operates at lagging power factor as the rotor induced current is supplied from the stator side. Second disadvantage is that IM drive system is not highly efficient due to slip power loss. And last disadvantage is that it always runs at a speed lower than the synchronous speed and rotor quantities depend on slip speed. Hence, the control of these motors is very complex. Furthermore, the real time implementation of the IM drive requires sophisticated modeling and estimation of machine parameters with complex control circuitry.

Some other disadvantages include low torque density, thermal problem at high speed and low efficiency [9, 10]. In 21st century, most of the electric energy in the world is consumed by electric machines thus the need for more energy efficient high performance motor drive becomes the key factor. Due to these disadvantages of IM researchers have looked into the SM for easier control in HPVSD.

### 1.3.2 Synchronous Motors

A synchronous motor rotates at synchronous speed; that is, the speed is uniquely related to the supply frequency. It is a serious competitor to the IM in variable speed drive applications. The stator winding of the SM is same as the IM, but the rotor has a winding that carries dc current and produces flux in the air gap that helps the stator induced rotating magnetic field to drag the rotor along with it. As SM runs at synchronous speed, its control is less complex. It also removes the slip power loss [3, 11]. However, the conventional wire wound excited SM have some disadvantages such as the requirement of extra power supply, slip ring and brush gears at the rotor side to supply the dc field excitation. Therefore, the presence of the dc supply, field coil and slip rings decrease the efficiency of the drive and requires frequent maintenance [12]. Due to the disadvantages of SM, more recently different kinds of special motors have been developed. Among them, the permanent magnet synchronous motor (PMSM) is becoming popular. In PMSM, extra power supply, slip ring, brush and the power loss due to the excitation winding is eliminated.

## 1.4 Permanent Magnet Synchronous Motors

Permanent magnets (PM) have not been used for electric motors for a long time because the development of the PM materials was not established until mid-20th century. The

manufacturing of PM started with magnetic carbon steel from the 18th century in London, the actual history of the PM motors on the industrial basis started with Alnico in the first half of the 20th century. However, Alnico, based on aluminum, nickel, iron and cobalt was replaced by Ferrite in the late 1960s, because of Alnico's high price caused by the complex manufacturing process. In spite of its poor maximum energy capability, Ferrite is still widely used in many applications today because of the abundance of the raw materials and the low production cost. Since Ferrite is composed of fine particles made from iron oxide ($Fe_2O_3$), with barium (Br) or Strontium (Sr), this magnet material is popular for use in complex shapes [13]. Samarium-Cobalt (Sm-Co), a type of rare earth magnet, is a strong PM material developed in early 1970s. They have higher temperature ratings because of its good thermal stability. However, the cost and availability of this type of material limit its commercial achievement [13]. In 1982 General Motors and Sumitomo Special Metals simultaneously announced the development of Neodymium-Iron-Boron (Nd-Fe-B), it is also a rare earth magnet, is a strong PM material widely used in many industrial areas [13]. For its high energy capability and relatively low cost compared to Samarium-Cobalt, Neodymium-Iron-Boron is the best material in applications requiring a small product size. Neodymium-Iron-Boron magnets are the most common rare earth magnets used in motors these days. Rare earth alloys have a high residual induction and coercive force than the ferrite materials. But the cost is also high. So rare earth magnets are usually used for HPVSD as high torque to inertia ratio is attractive.

A PMSM is exactly similar to a conventional SM. Field winding and dc power supply is replaced by PMs. To provide the field flux in PMSM, it consists of a stator with three phase windings and rotor mounted with PM. The absence of the field winding reduces the cost and eliminates the power losses associated with this winding. The PMSM occupies less space than a wire wound motor for a given size, which leads to more compact and robust design. Unlike an IM

there is no slip dependent rotor copper loss in a PMSM. When compared to IM, PMSM is more efficient and has a larger torque to inertia ratio and power density [14]. Current improvement of PM motors is directly associated to the recent achievement in high energy PM materials. Depending on the position of PM, there are different types of PMSM which are discussed in the following section.

## 1.5 Categories of PMSM

The categorization for PMSM can be done based on some different principle such as position of magnet in the rotor, current regulation, the principal motor control method, design of the motor and driving power circuit configuration. The performance of a PMSM drive varies with the placement of the magnet in the rotor, the magnet material, the number of poles, EMF waveform, the presence of dampers on the rotor and configuration of the rotor [15, 16]. Depending on magnet configuration, it can be categorized into three divisions.

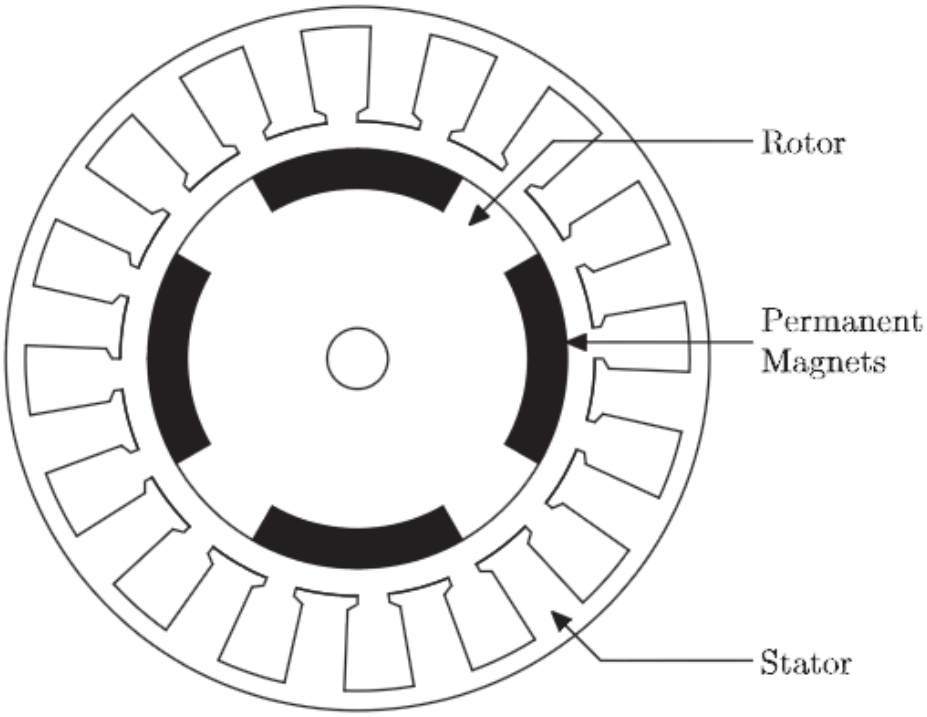


Fig. 1.1: Cross section of inset type PM motor.

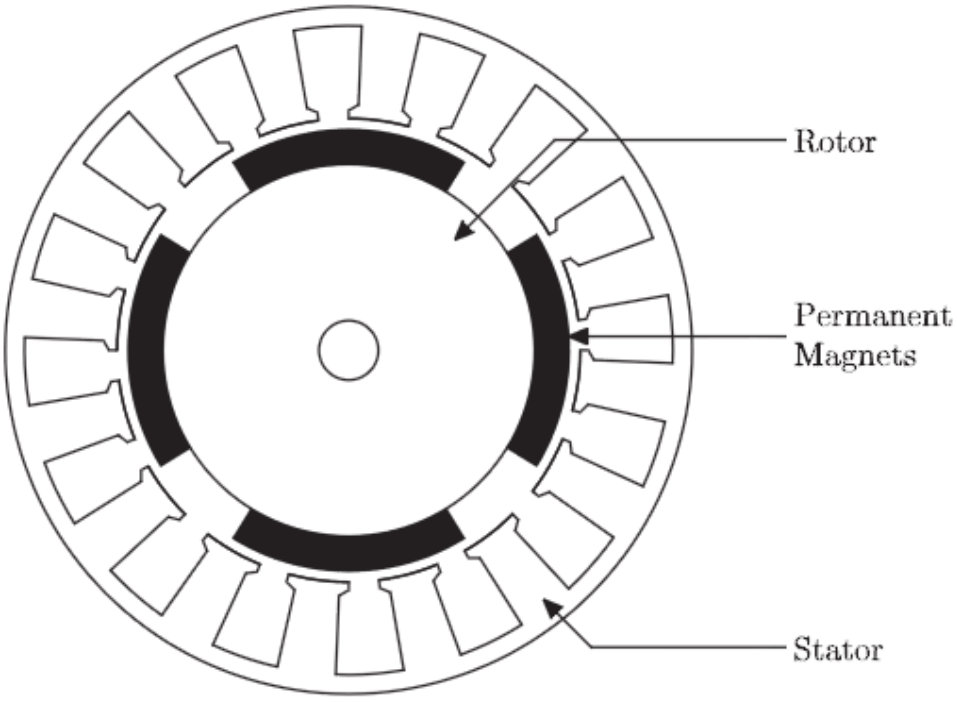


Fig. 1.2: Cross section of surface mounted type PM motor.

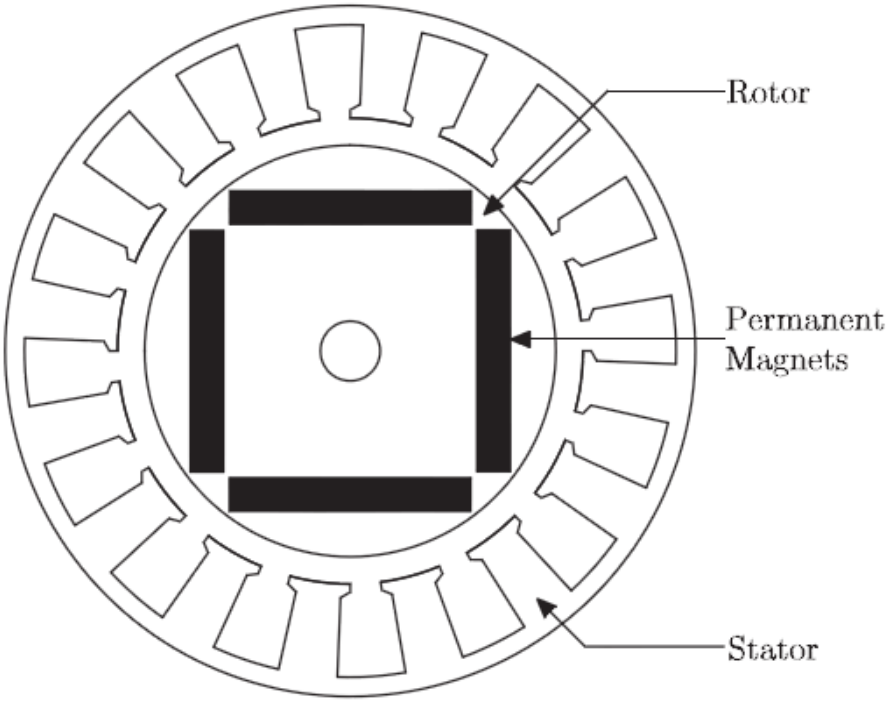


Fig. 1.3: Cross section of interior type PM motor.

**a)** Inset type PM motor: in this type of PM motor, the PMs are typically glued directly or banded with a non-conducting material inside the rotor core as shown in Fig. 1.1. It also has a small but relatively smooth air gap.

**b)** Surface mounted PM motor (SPMSM): In this type of PM motor, the PMs are mounted on the surface of a cylindrical rotor core as shown in Fig. 1.2. Because SPMSM has PMs that are glued on the surface of its rotor, the rotation speed should be limited in order to keep the PMs at the surface of the rotor from the effect of the centrifugal force. Therefore, it can only utilize the developed torque. Though, it has a simple construction, the motor suffers from huge eddy current losses. Eddy current loss occurs on the surface of the stainless steel can that is attached to the outside of the rotor [4, 11]. Since the relative permeability of a PM is very close to one, and magnets are mounted on the rotor surface, the effective air

gap of the machine is large and is essentially non-salient type ($L_q = L_d$) meaning that the permeance of rotor does not vary significantly around the circumference. This contributes to a low armature reaction effect due to low magnetizing inductance [3].

**c)** Interior mounted PM motor (IPMSM): Unlike a SPMSM, in an IPMSM, the magnets are imbedded inside the rotor as shown in Fig. 1.3. Therefore, the mechanical integrity of the IPMSM is better than SPMSM since it is easier to secure the magnets, which are subject to centrifugal forces from rotation as well as intensive transients due to magnetic forces. This mechanical security is especially important in high speed applications. IPMSM is also most economical to manufacture and it provides a smooth rotor surface and reduced air gap. As a result, this type of motor can be used for high speed with quiet operation and better dynamic performance, which are the major worries for HPD systems. Interior permanent magnet type is the most recently developed method of mounting the magnet. The difference in geometry gives the following characteristics to the IPMSM: 1) the machine is more robust, permitting a much higher speed of operation, 2) the effective air gap in the d-axis is larger than that in the q-axis, which makes the machine a salient pole ($L_q > L_d$). 3) with the effective air gap being low, the armature reaction effect becomes dominant. The saliency makes possible a degree of flux weakening, enabling operation above nominal speed at constant voltage and helps reduce the harmonic losses in the motor [3]. By applying closed loop vector control for IPMSM drive and using Park's transformation method, it is possible to decouple the flux and torque controlling components of IPMSM quantities. Therefore, the motor behaves like a separately excited dc motor while maintaining general advantages of ac motor. It is also found that IPMSM is the most

efficient of all motors [4]. Therefore, IPMSM has been considered as a working model in this thesis.

# 1.6 Literature Review

The IPMSM is becoming more popular in HPD applications as compared to other types of ac motors due to its advantageous features including high efficiency, high torque to current ratio, low noise, high power to weight ratio, and robust operation [11]. However, due to the nonlinear nature of IPMSM the dynamics and control of IPMSM drives are complex and their complexity increases for higher performance requirements [11]. Many different control techniques have been implemented.

For a long time a straightforward open-loop volt/hertz (v/f) control method was employed in low performance drives. It may not be a good choice for HPD because of poor speed control accuracy, limitation in torque control and worse performance with any disturbances. The scalar control techniques include torque control, flux control and current angle control. In [17] a scalar control technique for inverter driven motors is proposed. It causes the air gap flux to vary over a wide range, which is proportional to the load. Based on the magnitude of the motor current authors estimated the torque and implemented the PI based speed controller. They developed the control algorithm based on the steady state motor model. The steady state motor model is not sufficient to handle the dynamic uncertainties as the nonlinearity presents in motor model. Therefore, it causes slow responses which are undesirable for HPD applications. Moreover, scalar control has limitations at the high and low ends of the motor's speed range.

In order to achieve the characteristics of HPD the vector control or field oriented control (FOC) technique is being utilized for control of ac motor drives. Vector control is a more complex control technique as it works with vector quantities, controlling the desired values by using space phasors which contain all the three phase quantities in one phasor [18]. Vector control uses feedback from the motor to maintain desired speed or torque output. The principle of vector control is to eliminate the coupling between the direct (d) and quadrature (q) axis component of voltage/current. Both the phase angle and the magnitude of the current must be controlled. This is achieved by transforming the a-b-c quantities into d-q quantities using Park's transformation [6]. The ac motor then behaves like a separately excited dc motor while maintain the advantages of ac over dc motors. Thus, the control of ac motors becomes easier as the q-axis current ($i_q$) is responsible to control the torque and d-axis current ($i_d$) is responsible for control of the flux. As a result of decoupled torque and flux generating currents a faster and smooth transient and error free steady state response can be achieved. Once the system determines the rotor-flux angle, a vector control algorithm determines the optimum timing and magnitude of the voltages to apply to the stator-phase windings. For that reason the vector control provides significantly better performance and reduces torque ripple and current spikes. Therefore, the vector control scheme is used in the proposed work.

As we are aware of environmental problems rising dramatically worldwide, researchers are interested towards developing energy efficient motor drives for the industry in order to address the environmental problem. The product comparison between IPMSM and IM is shown in Figs. 1.4 and 1.5 for Yaskawa Electric Inc. product (15kW, 200V, 1750rpm). It can easily be seen from these figures that efficiency is improved and inverter size is reduced by using IPMSM instead of IM [20]. It is proved that IPMSM can offer significant efficiency advantages over IM when

employed in adjustable speed drives. It also offers more torque density than the IM and the inverter size is also greatly reduced for certain torque and power speed range [19].

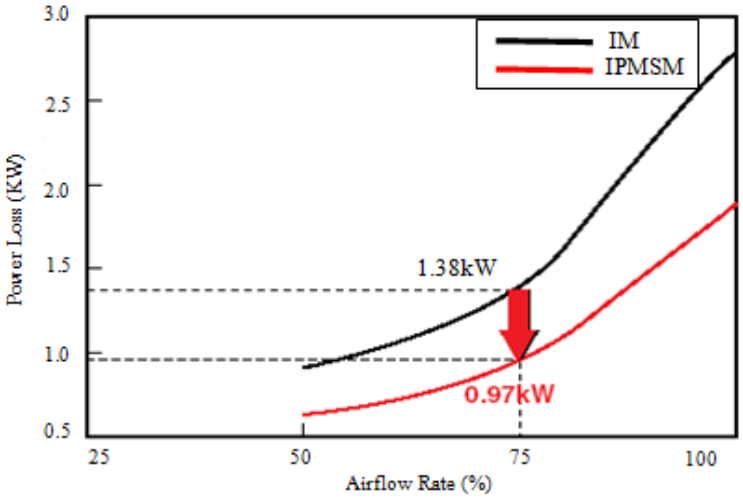


Fig. 1.4: Comparison of power loss of IPMSM with IM at different airflow rate.

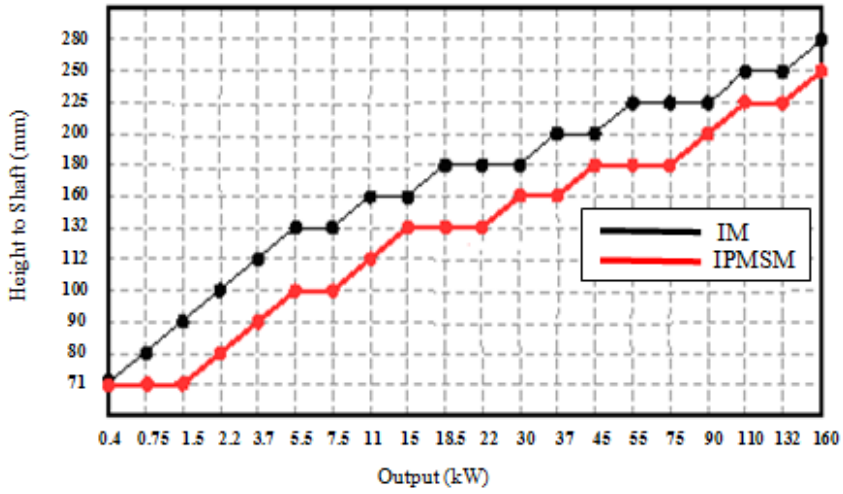


Fig. 1.5: Comparison of size of IPMSM with IM of different rating.

Although, IPMSM drive is well known for their relatively high efficiency, improvement margins still exist in their operating efficiency. Particularly, the reduction of power loss for IPMSM still remains a challenge for researchers. Despite many advantageous features of IPMSM, the precise speed control of an IPMSM drive is a complex issue due to nonlinear coupling among its winding

currents and the rotor speed as well as the nonlinearity present in developed electromagnetic toque ($T_e$) due to magnetic saturation of the rotor core [21]. To solve this issue nonlinear adaptive backstepping speed controller is applied because it's a relatively new technique for the control of uncertain nonlinear systems. In vector control many control works have been described [22-65]. The motor drive controller can be classified as: (a) fixed gain types and (b) adaptive types. The conventional fixed gain controller types include proportional integral derivative (PID), proportional integral (PI) and pseudo-derivative-feedback (PDF). The adaptive controller types are sliding mode controller (SMC), self-tuning regulator (STR), model reference adaptive controller (MRAC), variable structure controller (VSC), fuzzy logic controller (FLC), neural network controller (NNC), neuro-fuzzy controller (NFC), etc. Major works on vector control for IPMSM drive are discussed below.

### 1.6.1 Conventional Fixed Gain Controller

Several researchers have documented their work on the development of high performance IPMSM drives. Essentially, the researchers presented their work during study of the IPMSM fed by a voltage source or current source inverter. Gunmaste and Slemon [22, 23] proposed a vector control scheme with the steady state performance of voltage source inverter (VSI) and current source inverter (CSI) fed PMSM drives. In both schemes to operate inverter in self-control mode they have utilized a position feedback control from a shaft position sensor. Also they investigated the constant torque mode and the constant power mode. To operate motor with stability and reduce harmonic current they suggested removing the damper winding for the VSI fed PMSM drive. Whereas in case of CSI fed PMSM, they reduced the commutating inductance. Bose and Szczesny [24] developed a microcontroller based control system of an IPMSM drive that describes control

of an inverter fed IPMSM. Constant torque region and constant power region are incorporated in the control system. In this work, PI controllers are used to generate d and q axes currents to control the speed of the motor. However, the PI controller is sensitive to parameter variations and load disturbances. Moreover, they implemented the system on a multiprocessor architecture, which makes it costly and gives a good performance only in particular range of speed. Pillay and Krishnan [25] proposed a state space model of IPMSM for a high performance vector control scheme. The authors obtained linearized model of IPMSM by forcing $i_d$ to zero. This makes the design of the controller easy. Using linear model it is particularly challenging to design and predict the performance of the controller. Authors used linear model of the IPMSM to design PID speed controller. However, the drawbacks of this work are, the performance of the drive is sensitive to the motor parameters and operation speed is limited as the flux cannot be controlled with $i_d = 0$. Kazunori et. al. [26] dealt with the effect of inner current control loops on the system performance of a position-sensorless IPM motor drive system. Authors estimated the position based on inductance matrix which can be calculated from current and voltage vector. It is demonstrated that the inner current loops make it plausible to supress interference between the q-axis voltage and d-axis current, subsequently leading to significant improvements in the stability of position control. Though, the authors did not provide any experimental result to verify the possibility of this controller. It is observed that this control method requires a lot of computation, which makes it difficult to implement in real-time. In another work, Ogasawara and Akagi [27] proposed a conventional PI controller based IPMSM, which is characterized by position estimation based on magnetic saliency. A motor inductance matrix, including the rotor position information and the motor current harmonics are detected by real-time estimation algorithm. However, PI controller suffers from many disadvantages which are already mentioned earlier. Mademlis and Agelidis [28]

proposed current vector controlled scheme for IPMSM drives for high performance. They divided the operating region into three regions, constant torque region with maximum torque to current ratio, voltage and current limited region and voltage limited region. The command d-axis current was determined by flowchart of deciding control mode. The q-axis current command was determined from the speed error through PI controller and a current limiter. However, the performance of this controller is parameter sensitive and affected by load disturbance. Furthermore, q-axis current ripple affects the d-axis current too, which will result in increase of ripple at output of developed torque. Bolognani et. al. [29] dealt with the experimental realization of a sensorless IPMSM. They obtained position and angular speed of the rotor through an extended Kalman filter (EKF). They designed estimation algorithm in such a way that it does not require the knowledge of the mechanical parameters and the initial rotor position. This controller is insensitive to mechanical parameters variation of the drive. However, it requires high rate of computation to implement in real-time. Morimoto, et. al. [30] developed flux-weakening control for high speed. The authors modeled q-axis inductance as a function of the q-axis current, and the new value of q-axis inductance was used in the proposed control algorithm to compensate for magnetic saturation and demagnetization effect of PM to achieve high torque and high efficiency. The q-axis current command is decided from the PI controller. The d-axis current command is determined by maximum torque per ampere (MTPA) region or flux-weakening (FW) region as a function of q-axis current, angular speed and calculated value of $L_q$. However, in this work the effects of parameter variations due to noise, temperature, etc. are not considered. Therefore, the drive system suffers from instability unless an on-line adaptive scheme is incorporated.

The conventional fixed gain controllers have been used as the speed controller for PMSM drive in industry for the last several decades because of their simplicity and ease of implementation

in real-time. However, conventional fixed gain controllers such as PI, PID are very sensitive to parameter variations due to saturation, temperature variation, load disturbances, sudden change of command speed and other uncertainties. Therefore, the fixed gain PI controllers are not suitable for HPD systems. So the parameters have to be adjusted online such that it gives optimum performance with dynamic conditions. As a result, researchers have developed adaptive control schemes so that the controller can adapt the controller parameters to system parameter variations and load disturbances to achieve the desired criteria of HPDs.

### 1.6.2 Adaptive Controller

Recently, adaptive controllers have been used for PMSM drives to achieve fast transient response, parameter insensitivity, load handling capability and high adaptability to recover from any kind of uncertainties. Researchers, worked on adaptive gain controllers, developed different ways to achieve adaptations. Cerruto et. al. [31] proposed a MRAC approach to compensate the variations of the system parameters, such as inertia and torque constant for IPMSM drive in robotic applications. A disturbance torque observer is designed to balance the required load torque and reduce the complexity of the adaptive algorithm. However, the proposed controller suffers from a lot of online computational burden and high torque ripple. Consoli and Antonio [32] proposed SMC based self-controlled synchronous motor drive system for torque control and to investigate the performance above the base speed using field weakening (FW) technique. The authors used both the motor currents and line voltages as feedback to generate the torque and flux. The effect of acceleration, speed and deceleration are counted for designing SMC. The authors used variable bandwidth to reduce the chattering problem. However, the drive system has not been investigated in real-time where, the unknown and unavoidable parameter variations and chattering problem

exist. Ghirby and Le-Huy [33] proposed VSC for design of the position and speed controllers for an ac servo drive using a PMSM. They have used two control loops: the inner loop assures the predictive current controllers and uses the digital PWM principle and the outer loop is used for a position or speed controller. The predictive current controller has been used to improve the robustness of the drive. However, the performance of the drive has not been investigated for wide variable speed condition. Moreover, the drive still has chattering problem even in the steady state. Zhang and Li [34] proposed a SMC based on MRAC for PMSM system. The controller employs a SMC strategy in order to reduce the complex identification of MRAC. The proposed control scheme helps the speed response of the system keeps pace with that of the reference mode system and is insensitive to system uncertainties and load disturbance. Combining different control techniques gives superior results to conventional fixed gain controllers; however they increase the computational complexity of the control algorithm. Sepe and Lang [35] proposed a fully digital adaptive velocity controller for the PMSM. Their work is very similar to the self-tuning regulator case. The mechanical state estimation and mechanical parameters estimation of the motor have been estimated in real-time to redesign the gain of the controller. There are two major control loops. The fast inner loop contains the motor, its inverter, its current, velocity controller and a state filter. The slow outer loop consists of the parameter estimator and the redesign algorithm for the velocity controller. The outer control loop adjusts the gains in the velocity controller to affect invariant velocity control in the presence of changing mechanical parameters. They have implemented the complete drive using a Motorola 68020 microprocessor. However, due to the computational limitation of the microprocessor, the performance of the drive has been affected. Therefore, significant noise is introduced in steady state speed responses. Zhou, Wang and Zhou [36] developed a nonlinear adaptive backstepping based speed controller for the field weakening

area of separately excited dc motor with uncertainties. First, the authors derived a nonlinear model of a dc motor with parameter uncertainties such as motor inertia and load torque. Then the control algorithm is derived from the model equations and stability analysis is also carried out. The mechanical speed and the back EMF tracking objectives are satisfied. Rahman et. al. [37] developed a nonlinear adaptive backstepping speed controller for IPMSM drive realizing that the conventional controller designed with the standard linear d-q axis IPMSM model with constant parameters will lead to an unsatisfactory prediction of the performance of an IPM motor owing to the magnetic saturation of these machines even during normal operation. In order to achieve high performance from an IPMSM, the vector control technique is utilized for their proposed drive. In this paper, authors estimated the motor parameters as the d-q axis inductance and load torque. The most appealing point of this work is the use of virtual control variable to make original high order system simple, thus the final control output can be derived step by step through suitable Lyapunov functions ensuring global stability. In this work, authors took an assumption of d-axis current equal to zero to simplify the controller design. This assumption leads to erroneous and/or non-optimal results for motors at all operating conditions. Furthermore, due to this assumption, the operating range of the IPMSM is reduced. Sometimes it cannot even reach the rated speed at rated load. Tan and Chang [38, 39] proposed a combined field orientation and adaptive backstepping approach for the control of IM. The field orientation transformation brings significant simplification to the IM model so that backstepping design technique can be applied more easily. The authors formulated rotor angular speed and rotor flux tracking objectives so that the speed regulation is achieved with the consideration of improving the power efficiency. The designed nonlinear controller successfully achieved rotor angular speed and rotor flux amplitude tracking objectives with uncertainties in the rotor resistance and load torque. Huang and Fu [40] proposed a nonlinear

adaptive controller and an adaptive backstepping controller for linear IM to achieve speed/position tracking. The authors also considered friction dynamics effect and employed observer-based compensation which coped with friction force. Stability analysis based on Lyapunov theory is also performed to guarantee that the controller design is stable. An adaptive controller for the linear IM requires acceleration signals of the motor. Although this signal can be obtained through numerical differencing and digital filtering, it is more susceptible to noise. Therefore, to avoid such problem, authors proposed the nonlinear backstepping position controller. Shieh and Shyu [41] proposed the nonlinear sliding-mode torque and flux control combined with adaptive backstepping approach for an IM drive. Based on the state-coordinates transformed model representing the torque and flux magnitude dynamics, the nonlinear sliding-mode control was designed to track a linear reference model. Furthermore, the adaptive backstepping control approach is utilized to obtain the robustness for mismatched parameter uncertainties. Uddin and Chy [42] developed a nonlinear controller based speed control of an IPMSM incorporating MTPA based flux control. Authors developed an adaptive backstepping based control technique for an IPMSM, where the authors take field control into account at the design stage of the controller. Thus, it is robust to dynamic uncertainties and does not require knowledge of the mechanical system parameters. The authors also estimated load torque, inertia and friction coefficient. Uddin and Lau [43] developed an adaptive backstepping based nonlinear control for an IPMSM. IN this paper Lyapunov's stability theory was used to prove that the control variables were asymptotically stable. Authors estimated online stator resistance, load torque and d-q axis inductances based on speed error and actual currents. However, only simulation results were presented.

Due to well-known disadvantages of adaptive controller such as steady-state chattering problem and dependency of motor model parameters, researchers looked into the application of intelligent computation algorithms for motor drive applications.

### 1.6.3 Intelligent Controller

The main advantages of intelligent controllers are: their designs do not need the exact mathematical model of the system and theoretically they are capable of handling any nonlinearity of arbitrary complexity. Over the last decade researchers [44-59] have done extensive research for application of fuzzy logic controller (FLC), artificial neural network (ANN) and neuro-fuzzy controller (NFC) for HPD systems. Simplicity and less intensive mathematical design requirements are the main features of intelligent controllers, which are suitable to deal with nonlinearities and uncertainties of electric motors [60-62]. Therefore, the intelligent controllers demand particular attention for high performance nonlinear IPMSM drive systems. Tang and Xu [44] developed a direct FLC and an adaptive FLC which is based on MRAC. For the direct FLC, the controller normalizing gains are designed for certain situations, which would then prohibit the machine to achieve desired performance in case of large disturbances. The adaptive FLC uses adaptive model of the motor with FLC to control the motor. Because of two FLCs, the computation burden is large. Therefore, the real-time implementation was not presented in this paper. Uddin and Rahman [45] proposed a FLC based speed control for IPMSM drive. In that work, the vector control technique incorporated with the FLC was used to obtain the highest torque sensitivity of the IPMSM drive. For the design of FLC, the speed error and the rate of change of speed error are considered as the input linguistic variables and the torque producing current component is considered as the output linguistic variable. This controller suffers from ripple in the developed

torque. Butt et. al. [42], proposed FLC based MTPA speed controller. They designed the controller to calculate command torque from which they derived the command q- and d-axis current to control the motor speed. The command q- and d-axis current derived from command torque is dependent on motor parameters. This command torque has lot of ripple which makes the output speed have high ripple. So it is inappropriate for real-time implementation. Uddin et. al. [47] developed a genetic based FLC for the IPM ac motor drive. In this work they reduced the number of membership functions for low computational burden of FLC. A performance index, 'J' is tuned for the parameter of their proposed genetic based FLC such that it reflects small settling time, small steady-state error, and small overshoots. The tuning parameters are adjusted offline in order to minimize the index to predetermined level utilizing genetic algorithm (GA). The optimization process is based on the rated conditions of the motor. Due to difficulties of binary representation when dealing with continuous search space with large dimension, they proposed to implement the optimization using a real-coded GA. Due to high computational burden of GA, it is almost impossible to apply GA in real-time. So the control requirements of IPM motor drive under significant uncertainty of disturbance cannot be satisfied in this controller for all operating points. Zawirski [48] developed an angular speed control scheme for PMSM. The controller was constructed by combining a non-integral fuzzy and a PI algorithm. However, author did not provide any experimental result to prove the feasibility of the controller in real-time application. Uddin and Chy [49] developed a novel FLC based torque and flux controls for wide speed range of IPMSM drive. In that work, a stand-alone FLC is utilized, whose inputs are speed, speed error, and change of speed error. The outputs are d- and q-axis currents. However, this controller suffers from significant ripple in the d- and q-axis currents.

The use of artificial neural network (ANN) in control systems is very attractive because of their ability to learn, to approximate functions, to classify patterns and their potential for massively parallel hardware implementation. Rahman et. al. [50] implemented ANN for online tuning of the gains of PI controller. In this work, radial basis function network (RBFN) based ANN is utilized to control the speed of IPMSM. Like the counter propagation network, the RBFN is designed to perform input-output mapping based on the concept of locally tuned meaning it is "selective" for some part of the input space. The input variables are each assigned to a node in the input layer and pass directly to the hidden layer without weight. The hidden layer nodes are the RBF units. Each node in this latter contains a parameter vector called a center. The node calculates the Euclidean distance between the center and the network input vector and passes the result through a nonlinear function. For learning purpose the orthogonal least square (OLS) method is used in this work. Rahman and Hoque [51] proposed another ANN controller for PMSM drive. In that work, they used offline and online training to tune weights and biases of the ANN if the speed error signal is beyond a prescribed limit. This controller does not ensure the stability in all operating region. Moreover, this controller requires a lot of computation. Elbuluk et. al. [52] suggested another type of controllers with adaptation. This paper presented ANN-based model reference adaptive system (MRAS) to estimate the speed and position of a PMSM. An ANN adaptation method was used as the optimization engine for a comprehensive parameter estimation strategy. Two ANN-based MRASs were presented. First, the use of an ANN adaptation for the estimation of the stator resistance and torque constant was presented. Second, a rotor-speed estimation algorithm with stator resistance adaptation was developed. The estimator used the back EMF to determine the motor position and speed. The adaptation was done based on speed error using back propagation technique. In adaptation process, Jacobian function for the system was chosen equal to one for

simplicity, which may cause some error. The use of low pass filter in the training and adaptation process makes the systems slow. Urasaki et. al. [53] proposed another high efficiency ANN controller for IPMSM drive. The authors control the torque component current by PI controller. So this controller still suffers from the well-known disadvantages of PI controllers. The flux is controlled by an ANN controller. The ANN controller was designed to control the actual flux component of the stator current to the desired flux component of the stator current. But it is tough to calculate the desired flux component of the current as it depends on parameters and operating conditions. This needs a lot of computation in calculating command d-axis current for implementing in real-time. El-Sarkawi et. al. [54] proposed a multi-layer ANN architecture for the identification and control of dc brushless motors operating in a HPD. But they didn't provide any experimental result to verify the feasibility of the controller in real-time.

So far, we have discussed the FLC and ANN techniques independently. The conventional FLC has a narrow speed operation and needs much more manual adjusting by trial and error if high performance is required [55]. On the other hand, it is extremely tough to create a series of training data for ANN that can handle all the operating modes. These techniques can be brought together into a hybrid neuro-fuzzy controller (NFC) system to build a more powerful intelligent system with improved design and performance features. The NFC utilizes the transparent, linguistic representation of a fuzzy system with the learning ability of ANN. Therefore, it takes advantages of both FLC and ANN. Uddin et. al. [55] proposed a fuzzy basis function network (FBFN) based NFC to tune the parameters of PI controller. In this NFC, initially different operating conditions are obtained based on motor dynamics incorporating uncertainties. These are used to optimize the PI controller parameters in a closed-loop vector control scheme in order to get the initial PI controller parameters. In the optimization procedure a performance index is developed

to reflect the minimum speed deviation, minimum settling time and zero steady-state error. However, the weights and centers were trained offline in order to avoid computational burden. Thus, the controller cannot adapt with changing operating condition. Rubaai et. al. [56] proposed an adaptive fuzzy neural network controller (FNNC) for practical application of high performance BLDC drives. The FLC scheme was implemented by using a multilayer neural network. The authors performed learning of the structure based on the partition of input space, whereas learning of the parameter was done on the supervised gradient decent method. To give better performance in all operating condition, it is necessary to tune the membership functions. Lin [57] proposed a new structure and parameter learning scheme for a NFC system. The disadvantages of this learning scheme are that it is suitable only for offline instead of online operation and a large amount of representative data must be collected in advance for the implementation of this scheme. Moreover, the independent realization of the structure and parameter learning is too time consuming. Lin et. al. [58] proposed a self-constructing fuzzy neural network for PMSM drive. They used both structure learning and parameter learning. But it is not suitable to implement in industry because of a lot of computational burden. Furthermore, they didn't consider the flux control. Chy and Uddin [59] proposed a new adaptive intelligent speed controller for IPMSM drive. This paper presents a novel adaptive network-based fuzzy inference system (ANFIS). The back propagation technique is used for the online tuning of ANFIS parameters. To reduce the computational burden Takagi-Sugeno-Kang (TSK) fuzzy rule is used. The membership function and weight parameters were tuned online.

### 1.6.4 Loss Minimization Control

There have been growing concerns over energy consumption and the environment, due to the soaring energy cost and tighter environment protection laws. Increasing the efficiency has become one of the most important factors in the development of the products that consume electrical energy. Considering the fact that more than 50% of electrical energy produced is consumed by motors. In an effort to improve efficiency, there have been improvements in the materials, design and construction technique for the equipment involved IPMSM drive. However, converter loss and motor loss are still greatly dependent on control strategies, especially when the motor operates at light load. The efficiency optimization of IPMSM drives can be realized in various ways by different types of loss minimization control technique. There are two major loss minimization control techniques to improve motor efficiency such as search-based controller (SC) and loss model-based controller (LMC). Both the loss minimization techniques have been used in vector controlled drives.

#### 1.6.4.1 Search-based Controller (SC)

The SC approach to optimal efficiency control is to measure the power delivered to the drive and use a search algorithm to adjust a control variable until it detects a minimum input power condition [63-67]. Colby and Novotny [63] demonstrated a frequency-controlled PMSM drive that employs an adaptive control to find the maximum-efficiency operating point at any speed and load. They achieved efficiency-optimizing control with a frequency-programmed drive, where they had independent control of the voltage and frequency. The authors optimized both the motor-inverter efficiency and motor efficiency by measuring the current on the dc link and adjusting the voltage

output of the inverter. However, there is stability problem associated with frequency-controlled synchronous motor drive. The instability of the system occurs at mid-range frequency. Overall the dynamic performance of the system is not good since the efficiency control will not permit the rapid voltage changes necessary to achieve rapid torque response. Therefore, it is more suited to applications where efficiency and simplicity are more important than HPD. Kirschen et. al. [64] proposed an adaptive control of the rotor flux in a field-oriented drive system. The authors decreased the flux command in small steps until the minimum input power is achieved for the given torque and speed. This task is done by the speed control loop which adjusts the q-axis current to compensate the effect of changes in the rotor flux. It is very simple and easy solution but the problem is the long search time for the convergence. It took approximately 7 seconds for the controller to bring the motor to the minimal loss operating condition. The long search time was necessary because, the flux was reduced in several small steps in order to avoid undesirable speed variation. Even with small step time, the torque pulsation still existed. The steps can cause speed fluctuations and may result in instability in the system. Vaez et. al. [65] proposed an on-line adaptive loss minimization controller for interior permanent magnet motor drives. The adaptive loss minimization controller provides a novel pattern of change in d-axis stator current to achieve a minimum drive input power at any operating condition. The authors eliminated stepwise change of control variable and replaced by a continuous adjustment of the control variable. Therefore, a faster loss minimization is achieved by the continuous changes in the control variable since the relatively long transient period after each step change is evaded. The proposed controller saves more energy in systems with frequent changes in operating point due to the achievement of an accurate minimum input power and a short search time required to find this minimum. However, the continuous pattern of change in d-axis current, employed by the adaptive loss minimization

controller, demands more computations and more memory to store the previous values of the input power. Sul and Park [66] proposed the realization technique that optimizes the flux level to improve the efficiency of an IM. The control strategy is divided into two stages. First, the optimal slip is searched by trial and error, and the results are tabulated in microprocessor memory. Second, the controlled system is forced to track the optimal slip from the lookup table to achieve optimal efficiency. The optimal slip table in the microprocessor memory is made out on the basis of the calculated torque and speed. However, the lookup table cannot cover all the operating point of speed and torque; also this technique can be considered as an indirect way to minimize the input power. Kim et. al. [67] proposed to control IM with maximum power efficiency as well as high performance by means of decoupling of motor speed and rotor flux. Authors adjusted the squared rotor flux according to a minimum power algorithm based on Fibonacci search algorithm until the measured power input reaches the minimum. Since the speed and rotor flux are decoupled by means of nonlinear control the torque ripple is not generated in this configuration. The nonlinear controller requires the accurate value of the rotor resistance to calculate the accurate rotor flux. This value was obtained by an online identification algorithm. The experimental results showed the shorter search time with larger flux steps as compared to that in [64], while no undesirable disturbances appear in the motor speed and torque. However, these improvements on system performance have added sufficient complexity in overall control algorithm.

#### 1.6.4.2 Loss Model-based Controller (LMC)

The LMC computes losses by using the machine model. Also LMC measures the speed and the q-axis current and specifies the optimal d-axis current through the loss minimization condition [68-76]. Morimoto et. al. [68] proposed the loss minimization control algorithm, in

which the current vector is optimally controlled according to the operating speed and the load conditions. The authors utilized the reluctance torque and the d-axis armature reaction effectively to minimize the losses in the proposed control algorithm. The authors also proposed an approximate control algorithm in order to simplify the control algorithm. The approximate control algorithm is applied to the experimental PM motor drive system. The proposed control algorithm can be applied to various types of PM motors, not only the salient pole PM motor, but also the non-salient pole PM motor. The proposed control system also has a good dynamic response. However, authors implemented a conventional gain PI controller which suffers from the disadvantages mentioned earlier and is not suitable for HPD. Mademlis et. al. [69] investigated the problem of efficiency optimization in vector-controlled IPMSM drives using both SC and LMC. The authors proposed a LMC that determines the optimal d-axis component of the stator current that minimizes power losses. They showed that the loss model of the IPMSM can be used as a basis for deriving loss minimization conditions for SPMSM and synchronous reluctance motors as well. Authors also implemented SC but didn't get any satisfactory results, because the drive did not reach a steady-state, causing undesirable torque disturbances. They also determined the motor parameters using experimental procedure which eliminated the knowledge of the exact motor model. In conclusion, no additional feedback signals from the motors were required, beyond those already used in the pre-existing control. Therefore, the LMC controller does not affect the cost, complexity and dynamic performance of the drive. Ojo et. al. [70] proposed the concept of input-output linearization with decoupling which sets forth the speed control of the interior permanent magnet motor drives which simultaneously ensures the minimization of the losses. The motor parameters such as d- and q-axis inductances and the armature reaction dependent magnet flux linkage are included in the controller structure formulation. The authors achieved loss

minimization through appropriate command of the d and q axis machine voltages by closed-loop controllers using a VSI. Therefore, fast speed control is achieved with maximum efficiency with improved torque capability. However, q-axis current, torque and power loss suffers from high ripple. Also authors did not provide any experimental results to verify their simulation results. Vaez-Zadeh, et. al. [71] proposed an efficiency optimization control method for high performance IPMSM drives with online estimation of motor parameters. The control method is based on [70] which sets forth the speed control of the motor drives and simultaneously ensures the minimization of the motor losses. The controllable electrical loss can be minimized by an optimal control of the armature current vector. The model based efficiency optimization control methods are fast and does not produce any torque ripple. However, they are not robust against machine parameter variations. Therefore, the authors developed an observer to estimate stator resistance, iron loss resistance and PM flux linkage to make the system robust. However, authors didn't provide any real-time results to verify the motor parameters and efficiency. Uddin and Abera [72] proposed a model based efficiency optimization algorithm for speed control of IPMSM. The developed efficiency optimization control algorithm determines the optimal d-axis current of the drive for a given speed and torque command to minimize the losses of the IPMSM in a closed loop vector control environment. Uddin and Rebeiro [73] proposed an online loss minimization algorithm (LMA) for a fuzzy-logic-controller based IPMSM drive to yield high efficiency and high dynamic performance over a wide range of speed. The authors developed loss-minimization algorithm based on motor model. The d-axis current is controlled optimally according to the operating speed and load conditions in order to achieve high efficiency. They incorporated LMA with the fuzzy-logic-controller so that the motor can operate over wide speed range while maintaining high efficiency. However, the LMA is still dependent on motor parameters, which were fixed values.

Lim and Nam [74] developed a simplified loss model without sacrificing the leakage inductance. In the simplified model, the loss was represented as a resistance connected to a dependent voltage source. According to the simulation and experimental results, the loss calculation based on this simplified model was closer to that of the full model. Garcia et. al. [75] derived a loss model consisting of resistors reflecting iron loss, rotor and stator copper losses as a function of stator current components in d-q frame. The IM equivalent circuit was simplified by deleting leakage inductance in the induction motor equivalent circuit. Based on this mode, they developed a closed-form equation for the optimum flux level in the field-oriented control. This algorithm allows the electromagnetic losses of IM drive to be decreased while keeping a good dynamic response. The efficiency sensitivity to parameter variation was also studied. Uddin and Nam [76] developed a nonlinear and model-based online loss minimization control of an IM drive. The authors encountered a technical difficulty in deriving the LMC for the full loss model and the online parameter adaptation. Therefore, they presented a new strategy for inverter-fed IM drive for both high efficiency and high dynamic performance. A new LMC incorporated the effect of the leakage inductance and an adaptive-backstepping-based nonlinear controller was designed and combined with each other. Also, the authors estimated load torque and rotor resistance to eliminate uncertainties and to achieve robustness of the system. However, the inductance parameters were considered constant in the LMC.

# 1.7 Thesis Objectives

As mentioned above, IPMSM possesses many appealing characteristics such as high torque to inertia ratio, power to weight ratio, low noise operation and high efficiency. However, due to

the nonlinear nature of IPMSM both the magnitude and the angles of the current vectors need to be controlled. For this reason, the traditional scalar control is not suitable for HPD applications of IPMSM. Thus, the vector control scheme is used in the proposed LMC algorithm for speed control of IPMSM drive to achieve both high efficiency and high dynamic performance.

The first objective is to develop a LMC for IPMSM, which determines an optimum d-axis current to minimize the losses.

Scalar control and conventional fixed gain PI control are not suitable for HPD applications because of the nonlinear nature of the motor. In literature search section several works have been discussed on adaptive control for the IPMSM such as MRAC, SMC etc. However, the absence of proper estimation of the parameters reduces the performance of these controllers. Therefore, the objectives of this thesis is to develop a robust nonlinear controllers for speed control of an IPMSM drive. Then the LMC will be combined with the proposed nonlinear controller. One of the proposed method is based on adaptive backstepping based nonlinear controller (ABNC). The motor parameters such as load torque and friction coefficient are estimated online in order to make the system robust against disturbances and uncertainties. Finally, as an intelligent controller an NFC will be developed for IPMSM as a speed controller. The NFC will also be combined with the LMC to achieve both high performance and high efficiency.

The last objective of this thesis is the simulation and real-time implementation of closed loop vector control of the proposed IPMSM drive system incorporating the control algorithm developed earlier. The simulation is performed using Matlab/Simulink [77]. The real-time implementation is carried out using a DSP board, DS1104 for an available laboratory 5 hp motor [78]. The dynamic performance of the proposed LMC and speed controllers are examined through different operating conditions such as sudden command speed change, load disturbances, etc. A

performance comparison of the NFC and LMA based controller with ABNC and LMA based controller is also provided.

## 1.8 Thesis Organization

The organization of the remaining chapters of this thesis is as follows. Chapter 2 explains Park's transformation and the derivation of the mathematical model of the IPMSM without motor losses. Here it is shown that the vector control technique greatly simplifies the control of the motor. Chapter 3 explains losses which are involved in IPMSM drive and reviews the different methods of loss minimization with the focus being on the control technique based method. The mathematical model for the proposed LMA is also derived based on the motor model from Chapter 2 incorporating motor losses. Chapter 4 shows the control design procedure using adaptive backstepping technique for speed control and parameter adaptation in detail. In the development of the controller, LMC is incorporated. Chapter 4 also shows the detailed simulation results of the complete drive system. In Chapter 5, a new adaptive NFC is developed in which the membership functions and consequent parameters are tuned online. Then the performance of the controller is investigated extensively in simulation. Chapter 6 describes the real-time implementation of the complete 5hp IPMSM drive system in laboratory using dSPACE DS1104 DSP board. The detailed experimental results of the NFC based online loss minimization are shown in this Chapter. The detailed real-time implementation procedures for both hardware and software are also discussed. Finally, Chapter 7 presents summary/conclusions of this work and suggestions for future work. After that all relevant references and appendices are listed.

# Chapter 2

# Mathematical Model of IPMSM

This Chapter explains the concept of the vector control of IPMSM and the necessary coordinate transformations to apply it to an IPMSM drive. The mathematical model of IPMSM is also derived in the d-q rotating reference frame using the coordinate transformations.

## 2.1 Mathematical Modeling of IPMSM

If $\Psi$ is the constant flux linkage provided by the PMs, then the flux linkages in the three phase stator winding due to PM of the rotor can be given as [11]:

$$\begin{bmatrix} \Psi_{am} \\ \Psi_{bm} \\ \Psi_{cm} \end{bmatrix} = \Psi \begin{bmatrix} \sin\theta_r \\ \sin\left(\theta_r - \frac{2\pi}{3}\right) \\ \sin\left(\theta_r + \frac{2\pi}{3}\right) \end{bmatrix} \tag{2.1}$$

where, $\Psi_{am}$, $\Psi_{bm}$ and $\Psi_{cm}$ are the three phase stator flux linkages in the three phase stator winding due to PM of the rotor and $\theta_r$ is the rotor position. The total air gap flux linkage of the three phases are the summation of the flux linkage for the corresponding phase current, the mutual flux linkage

due to currents in the other phases and the flux linkages in the three phase stator winding due to PM of the rotor. The three phase air gap flux linkage equations are given in matrix form as:

$$\begin{bmatrix} \Psi_a \\ \Psi_b \\ \Psi_c \end{bmatrix} = \begin{bmatrix} L_{aa} & M_{ab} & M_{ac} \\ M_{ba} & L_{bb} & M_{bc} \\ M_{ca} & M_{cb} & L_{cc} \end{bmatrix} \begin{bmatrix} i_a \\ i_b \\ i_c \end{bmatrix} + \Psi \begin{bmatrix} \sin\theta_r \\ \sin\left(\theta_r - \frac{2\pi}{3}\right) \\ \sin\left(\theta_r + \frac{2\pi}{3}\right) \end{bmatrix} \tag{2.2}$$

where, $\Psi_a$, $\Psi_b$ and $\Psi_c$ are the air gap flux linkage for the phase a, b, c, respectively; $L_{aa}$, $L_{bb}$, $L_{cc}$ are the self-inductances and $M_{ab}$, $M_{ac}$, $M_{ba}$, $M_{bc}$, $M_{ca}$ and $M_{cb}$ are the mutual inductances, respectively. The mutual inductances are symmetrical. $M_{ab} = M_{ba}$, $M_{bc} = M_{cb}$, and $M_{ca} = M_{ac}$.

The phase voltage is the voltage drop in each phase plus the voltage drop due to the rate of change of flux linkages. Now, the voltage equations of the three phases of the IPMSM can be defined as:

$$v_a = r_a i_a + \frac{d\Psi_a}{dt} \tag{2.3}$$

$$v_b = r_b i_b + \frac{d\Psi_b}{dt} \tag{2.4}$$

$$v_c = r_c i_c + \frac{d\Psi_c}{dt} \tag{2.5}$$

where, $v_a$, $v_b$, $v_c$ are the three phase voltages, $i_a$, $i_b$, $i_c$ are the three phase currents and $r_a$, $r_b$, $r_c$ are the three phase stator resistances. Eqn. (2.5) can be written in matrix form as:

$$\begin{bmatrix} v_a \\ v_b \\ v_c \end{bmatrix} = \begin{bmatrix} r_a & 0 & 0 \\ 0 & r_b & 0 \\ 0 & 0 & r_c \end{bmatrix} \begin{bmatrix} i_a \\ i_b \\ i_c \end{bmatrix} + \frac{d}{dt} \begin{bmatrix} \Psi_a \\ \Psi_b \\ \Psi_c \end{bmatrix} \tag{2.6}$$

$v_a$, $v_b$ and $v_c$ depends on the flux linkage components which are functions of rotor position $\theta_r$ and hence functions of rotor speed $\omega_r$. Therefore, the coefficients of the voltage equations are time varying except when the motor is motionless. In order to keep away from the difficulty of

calculations, all the equations have to be changed to the synchronously rotating rotor reference frame where the machine equations are no longer dependent on the rotor position. These transformations can be achieved in two steps using Park's transformation equations [6]. In the first step, $v_a$, $v_b$ and $v_c$ will be transformed from the three phase stationary a-b-c frame into two phase stationary d-q frame and in the second step, from the stationary d-q frame to the synchronously rotating $d^r$-$q^r$ frame. The transformed phase variables in the stationary d-q-0 axis can be written in matrix form as:

$$\begin{bmatrix} x_a \\ x_b \\ x_c \end{bmatrix} = \begin{bmatrix} \cos\theta_r & \sin\theta_r & 1 \\ \cos\left(\theta_r - \frac{2\pi}{3}\right) & \sin\left(\theta_r - \frac{2\pi}{3}\right) & 1 \\ \cos\left(\theta_r + \frac{2\pi}{3}\right) & \sin\left(\theta_r + \frac{2\pi}{3}\right) & 1 \end{bmatrix} \begin{bmatrix} x_q \\ x_d \\ x_0 \end{bmatrix} \tag{2.7}$$

The corresponding inverse relation can be written as:

$$\begin{bmatrix} x_q \\ x_d \\ x_0 \end{bmatrix} = \frac{2}{3} \begin{bmatrix} \cos\theta_r & \cos\left(\theta_r - \frac{2\pi}{3}\right) & \cos\left(\theta_r + \frac{2\pi}{3}\right) \\ \sin\theta_r & \sin\left(\theta_r - \frac{2\pi}{3}\right) & \sin\left(\theta_r + \frac{2\pi}{3}\right) \\ \frac{1}{2} & \frac{1}{2} & \frac{1}{2} \end{bmatrix} \begin{bmatrix} x_a \\ x_b \\ x_c \end{bmatrix} \tag{2.8}$$

where, $x_a$, $x_b$ and $x_c$ are the a, b and c phase quantities, respectively, $x_d$, $x_q$ and $x_0$ are the d-axis, q-axis and zero sequence components, respectively. The matrix element x may represent either voltage or current.

The rotor location or rotor position angle $\theta_r$ is defined as:

$$\theta_r = \int_0^t \omega_r(\tau)\, d\tau + \theta_r(0) \tag{2.9}$$

For balanced three phase, zero sequence component ($x_0$) does not exist, and it is convenient to set initial rotor position $\theta_r(0) = 0$ so that the q-axis coincides with a-phase. Under these conditions Eqns. (2.7) and (2.8) can be written, respectively, as:

$$\begin{bmatrix} x_a \\ x_b \\ x_c \end{bmatrix} = \begin{bmatrix} 1 & 0 \\ -\frac{1}{2} & -\frac{\sqrt{3}}{2} \\ -\frac{1}{2} & \frac{\sqrt{3}}{2} \end{bmatrix} \begin{bmatrix} x_q \\ x_d \end{bmatrix} \tag{2.10}$$

and

$$\begin{bmatrix} x_q \\ x_d \end{bmatrix} = \begin{bmatrix} \frac{2}{3} & -\frac{1}{3} & -\frac{1}{3} \\ 0 & -\frac{1}{\sqrt{3}} & \frac{1}{\sqrt{3}} \end{bmatrix} \begin{bmatrix} x_a \\ x_b \\ x_c \end{bmatrix} \tag{2.11}$$

The relative position of the stationary d-q frame and the synchronously rotating $d^r$-$q^r$ frame is shown in Fig. 2.1. With the help of Fig. 2.1 the stationary d-q frame can be converted to the synchronously rotating $d^r$-$q^r$ frame as:

$$\begin{bmatrix} x_q^r \\ x_d^r \end{bmatrix} = \begin{bmatrix} \cos\theta_r & -\sin\theta_r \\ \sin\theta_r & \cos\theta_r \end{bmatrix} \begin{bmatrix} x_q \\ x_d \end{bmatrix} \tag{2.12}$$

The inverse relation can be written as:

$$\begin{bmatrix} x_q \\ x_d \end{bmatrix} = \begin{bmatrix} \cos\theta_r & \sin\theta_r \\ -\sin\theta_r & \cos\theta_r \end{bmatrix} \begin{bmatrix} x_q^r \\ x_d^r \end{bmatrix} \tag{2.13}$$

In order to derive the $d^r$-$q^r$ axis model of IPMSM drive, the following four assumptions are made:

a) The eddy current and hysteresis losses are negligible.

b) The induced emf is sinusoidal.

c) The saturation is neglected.

d) The stator resistance of the three phases are balanced.

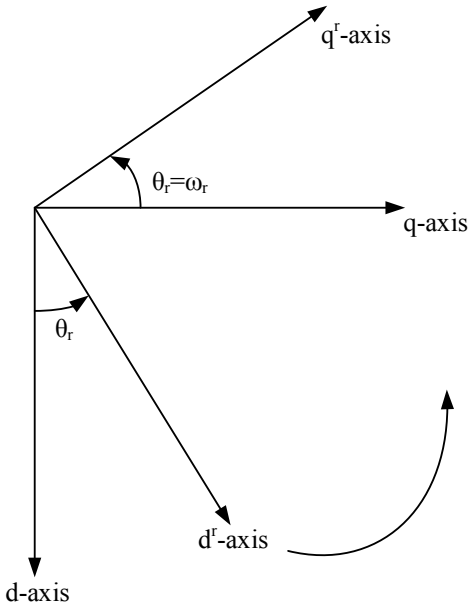


Fig. 2.1: Relative position of stationary d-q axis to the synchronously rotating dr-qr axis.

With the above assumptions and using Eqns. (2.6), (2.7) and (2.13), the $d^r$-$q^r$ axis model of IPMSM can be derived as follows:

$$v_q^r = Ri_q^r + \frac{d\Psi_q^r}{dt} + \omega_s \Psi_d^r \tag{2.14}$$

$$v_d^r = Ri_d^r + \frac{d\Psi_d^r}{dt} - \omega_s \Psi_q^r \tag{2.15}$$

where, $v_d^r$ and $v_q^r$ are d and q axis voltages and $i_d^r$ and $i_q^r$ are d and q axis currents, $\Psi_d^r$ and $\Psi_q^r$ are d and q axis flux linkages, R is the stator resistance per phase and $\omega_s$ is the stator frequency.

$\Psi_q^r$ and $\Psi_d^r$ can be written as:

$$\Psi_q^r = L_q i_q^r \tag{2.16}$$

$$\Psi_d^r = L_d i_d^r + \Psi \tag{2.17}$$

where,

$$L_q = L_l + L_{mq} \tag{2.18}$$

$$L_d = L_l + L_{md} \tag{2.19}$$

$L_d$ and $L_q$ are d and q axis inductances, $L_{md}$ and $L_{mq}$ are d and q axis magnetizing inductances and $L_l$ is the leakage inductance per phase. The stator frequency, $\omega_s$ is related to the rotor frequency $\omega_r$ as:

$$\omega_s = P\omega_r \tag{2.20}$$

where, P is the number of pole-pairs in motor.

Using Eqns. (2.14)-(2.20), the mathematical motor model is given as:

$$v_q^r = Ri_q^r + L_q \frac{di_q^r}{dt} + P\omega_r L_d i_d^r + P\omega_r \Psi \tag{2.21}$$

$$v_d^r = Ri_d^r + L_d \frac{di_d^r}{dt} - P\omega_r L_q i_q^r \tag{2.22}$$

According to Eqns. (2.21) and (2.22) the motor can be represented by the equivalent circuit diagrams shown in Fig. 2.2. The PM flux is represented as a constant current source $I_M$, since a constant field current in a wire wound synchronous machine will supply a constant flux. The total average energy entering the sources which is also the developed power per phase is given by:

$$P_{phase} = \frac{1}{2}\left(-P\omega_r L_q i_q^r i_d^r + P\omega_r L_d i_d^r i_q^r + P\omega_r \Psi i_q^r\right) \tag{2.23}$$

The total power developed by the machine is:

$$P_{mech} = \frac{3P\omega_r}{2}\left\{\Psi i_q^r + \left(L_d - L_q\right) i_q^r i_d^r\right\} \tag{2.24}$$

Now the developed electromagnetic torque is given by:

$$T_e = \frac{P_{mech}}{\omega_r} = \frac{3P}{2}\left\{\Psi i_q^r + \left(L_d - L_q\right) i_q^r i_d^r\right\} \tag{2.25}$$

The magnetic and reluctance torques are given in (2.26) and (2.27), respectively as:

$$T_{mag} = \frac{3P}{2}\Psi i_q^r \tag{2.26}$$

$$T_{rel} = \frac{3P}{2}\left(L_d - L_q\right) i_q^r i_d^r \tag{2.27}$$

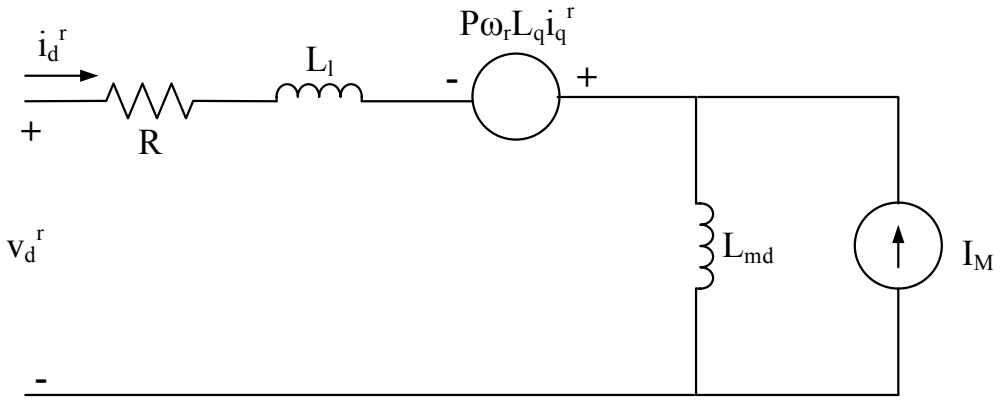


(a) d-axis equivalent circuit

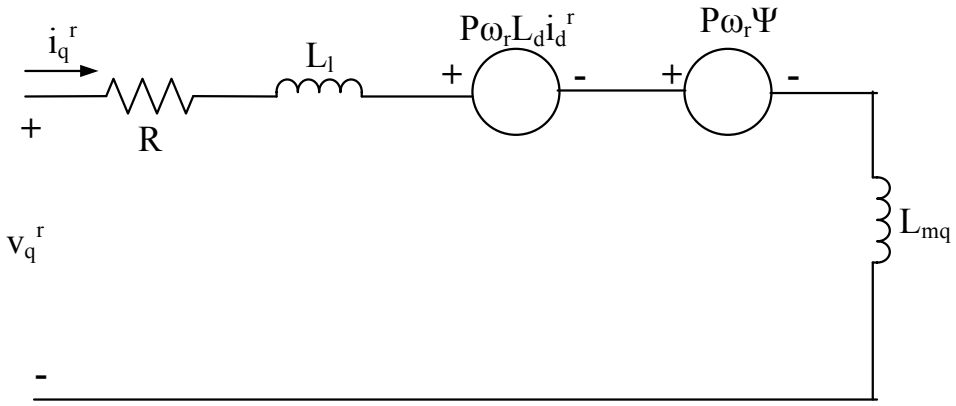


(b) q-axis equivalent circuit

Fig. 2.2: Equivalent circuits model of the IPMSM: (a) d-axis, (b) q-axis.

Finally, the motor dynamics can be represented by the following equation:

$$T_e = T_L + B_m \omega_r + J\frac{d\omega_r}{dt} \tag{2.28}$$

where, $T_L$ is the load torque in Nm, $B_m$ is the friction damping coefficient in Nm/rad/sec and J is the rotor and load inertia constant in kg-$m^2$.

# 2.2 Vector Control Scheme for IPMSM Drive

As mentioned before the objective of vector control is to eliminate the coupling between the direct (d) and quadrature (q) axis currents. By doing so both the phase angle and the magnitude of the current can be controlled. It is also an effective technique for control of ac motors in HPD. The IPMSM can be vector controlled when the machine equations are transformed from the a-b-c frame to the synchronous rotating $d^r$-$q^r$ frame where sinusoidal voltage become constant like a dc voltage. In the case of dc motor control, the developed torque $T_e$ is:

$$T_e = KI_a I_f \tag{2.29}$$

Where, $I_a$ is the armature current, $I_f$ is the field current and K is a constant. Both $I_a$ and $I_f$ are orthogonal and decoupled vectors. So the control task becomes much easier for the separately excited dc motor. In the case of PM motor, the first term of torque Eqn. (2.25) represents the magnet torque produced by the PM flux Ψ and q-axis current and the second term represents the reluctance torque produced by the interaction of q and d axis inductances and the d-q axis currents. The complexity of control of the IPMSM drive arises due to the nonlinear nature of the torque in Eqn. (2.25). In order to operate the motor in a vector control scheme avoiding the complexity, most of the researchers consider the command d-axis current, $i_d^r = 0$. Thus, the torque equation becomes linear and control task becomes easier.

$$T_e = \frac{3P}{2}\Psi i_q^r = K_t i_q^r \tag{2.30}$$

Using phasor notation and taking the $d^r$ axis as the reference phasor, the steady state phase voltage $V_a$ can be derived from Eqns. (2.21) and (2.22) as [11]:

$$V_a = v_d^r + jv_q^r$$

$$V_a = RI_a - \omega_s L_q i_q^r + j\omega_s L_d i_d^r + j\omega_s \Psi \tag{2.31}$$

where, the phase current is:

$$I_a = i_d^r + ji_q^r \tag{2.32}$$

In the case of the IPM motor, the $d^r$-axis current is negative and it demagnetizes the main flux provide by the PMs. Thus, in order to take only the absolute value of $i_d^r$ we can rewrite the Eqn. (2.29) as:

$$V_a = RI_a - \omega_s L_q i_q^r - j\omega_s L_d i_d^r + j\omega_s \Psi \tag{2.33}$$

Based on Eqn. (2.31) the basic vector diagram of IPMSM is shown in Fig. 2.3(a). It is shown in Fig. 2.3(a) that the stator current can be controlled by controlling the $d^r$-$q^r$ axis current components. When $i_d^r = 0$ then all the flux linkages are oriented in the $d^r$-axis as shown in Fig. 2.3(b). The torque then is a function of only the $q^r$-axis current component; hence the torque can be controlled by controlling $i_q^r$. Constant torque can be achieved by ensuring that $i_q^r$ is kept constant. If the flux control is needed then $i_d$ can be calculated as a function of $i_q$ and speed based on some algorithms such as MTPA or FW [11, 42, 46, 81, 82].

# 2.3 Concluding Remarks

The detail mathematical model has been derived in this Chapter. The vector control technique for IPMSM has also been introduced in this chapter. In the next chapter LMA is developed to achieve high efficiency of the IPMSM drive.

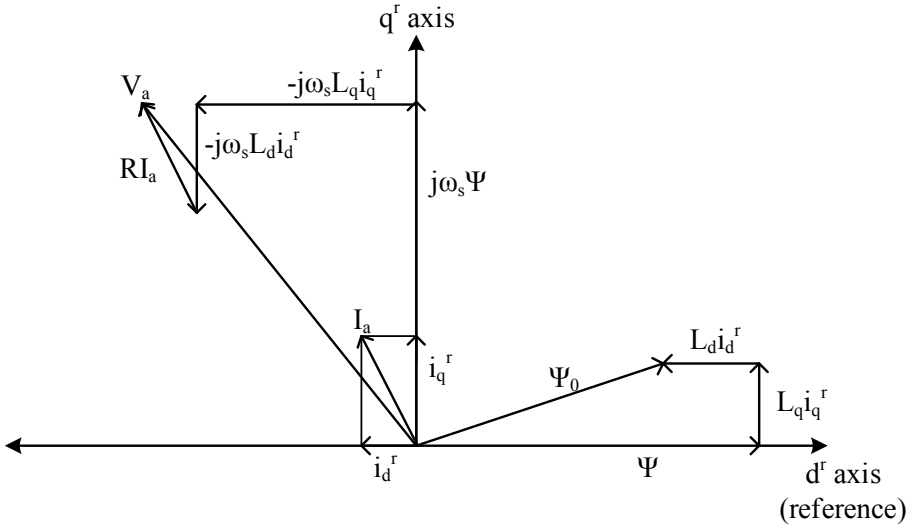


(a) General vector diagram

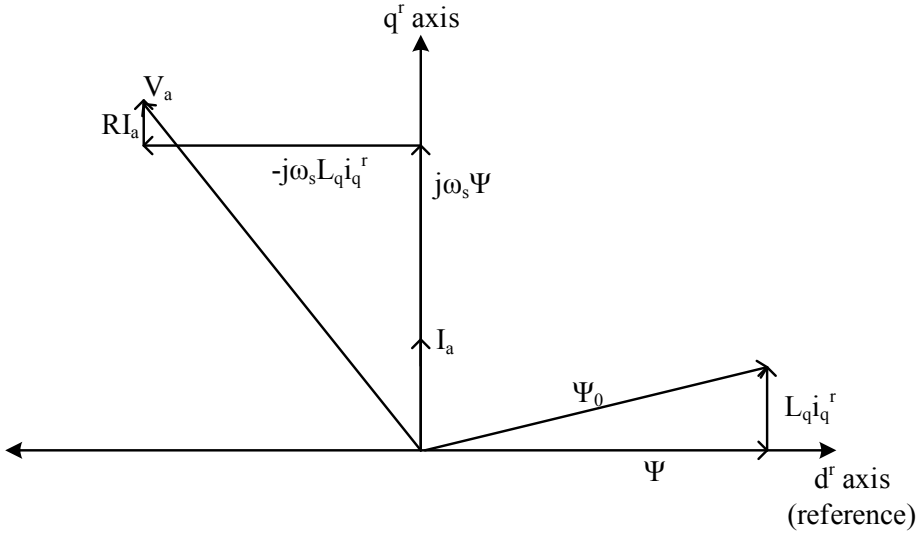


(b) Modified with $i_d=0$

Fig. 2.3: Vector diagrams of the IPMSM: (a) general vector diagram, (b) modified with id=0 diagram.

# Chapter 3

# Loss Minimization Control of IPMSM Drives

This chapter reviews the different methods of loss reduction with the focus on the control technique based method. A new loss minimization algorithm for an adjustable speed/torque IPMSM drive is also derived and presented.

## 3.1 Types of Loss Minimization Algorithms

As mentioned in the literature review, there are two major loss minimization control techniques for IPMSM drives such as (a) Search-based Controller (SC) and (b) Loss Model-based Controller (LMC).

The basic SC approach to optimum efficiency control is to measure the input power to the drive and use a search algorithm to adjust a control variable until it detects a minimum value in the input power while keeping the output power of the motor constant. During the optimization period speed is kept constant and load torque is assumed to be constant as shown in Fig. 3.1. If power measurement is done at the input of the rectifier, converter losses are taken into account in search of minimum input power. However, a voltage sensor and a current sensor are required. In

order to reduce the cost of measurement, the DC-link power can be measured. In this case, only one extra current sensor is required while the inverter loss is considered. The most cost effective and easiest way is to minimize the stator current which does not require extra measuring devices. Because SC offers optimum efficiency based on the exact measurement of power input, it does not depend on the machine parameters. However, the disadvantages in the application of this technique are: (a) torque ripple appears each time the flux is stepped down to reach the optimal operation point. (b) when the optimal operating point is found, electromagnetic torque reserve is so low that motor is very sensitive to load perturbations, and (c) convergence of the magnetizing current toward the optimum value is very slow and wouldn't reach its optimal value but oscillates around it in small steps. [63-67].

The LMC technique employs a loss model of the motor and regulates the controlled quantities such as voltages/currents to minimize the estimated loss. The loss minimization algorithm (LMA) is developed based on motor model and operating conditions. The d-axis armature current is utilized to minimize the losses of the IPMSM in a closed loop vector control. LMC is fast and does not produce any torque ripple. However, the accuracy depends on the correct modeling of the motor drive and the losses, and its performance deteriorates when the parameter changes. The advantages and disadvantages of SC and LMC are summarized in Table 3.1.

Table 3.1: Comparison of loss minimization control strategies.

| | Advantages | Disadvantages |
|---|---|---|
| SC | • No loss model necessary.<br>• No dependency on the parameters.<br>• Include the inverter losses (in some cases). | • Slow Convergence.<br>• Torque pulsations.<br>• Extra sensors for power measurements. |
| LMC | • Fast response.<br>• No torque pulsations.<br>• Simple to implement | • Requires the knowledge of motor and loss model.<br>• Dependency on the parameter. |

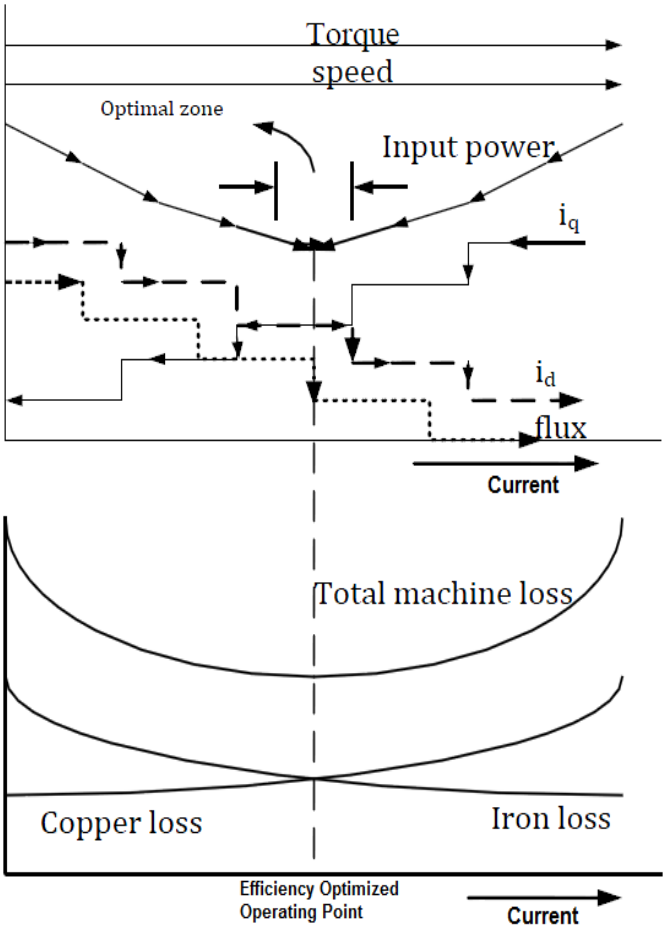


Fig. 3.1: Principle of efficiency optimization control with d-axis current decrement in SC technique.

# 3.2 IPMSM Model Including Motor Losses

A widely used model of a IPMSM drive including copper and iron losses in synchronously rotating $d^r - q^r$ frame is presented in Fig. 3.2 [71].

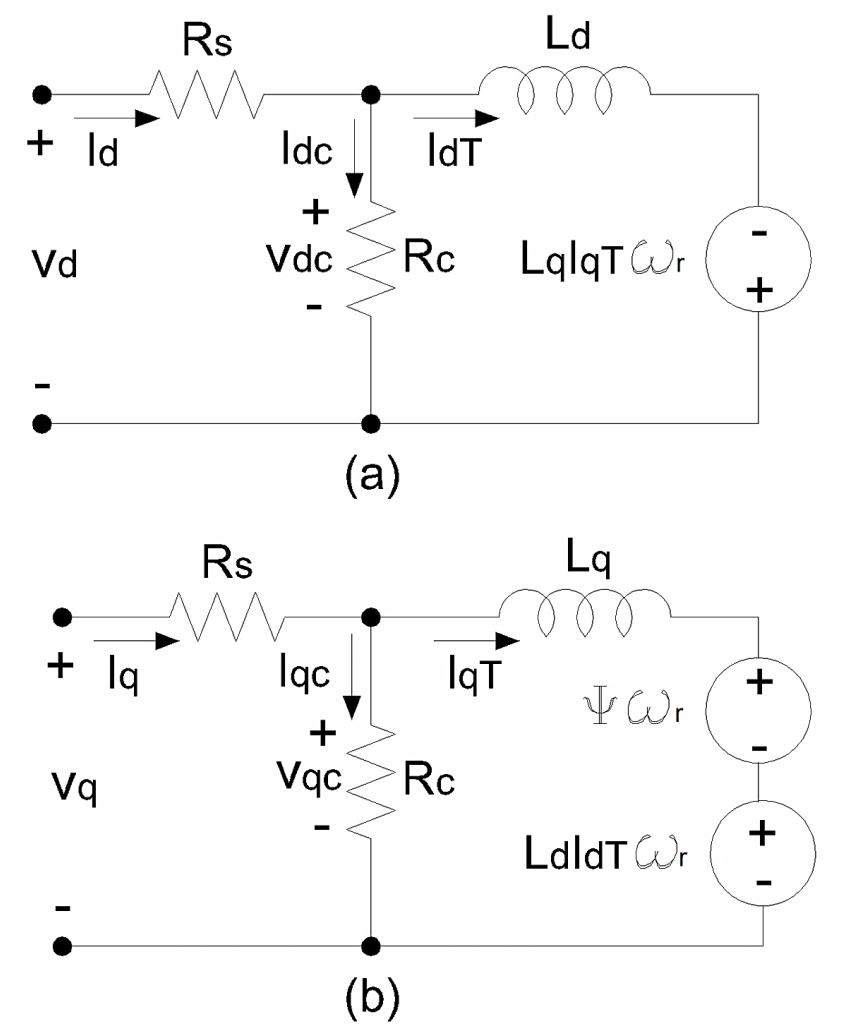


Fig. 3.2: Equivalent circuits for IPMSM including motor losses: (a) d-axis, (b) q-axis.

Fig. 3.2 shows the d-q axis equivalent circuits of IPMSM including the effect of the iron losses. $R_s$ represent the armature copper loss resistance. The iron loss consists of hysteresis loss and eddy current loss, but here they are added into a single quantity and the iron loss is represented by the

iron loss resistance $R_c$ inserted in parallel with the inductances. Thus, the d-q axis armature currents ($I_d$ and $I_q$) are divided into d-axis and q-axis iron loss currents ($I_{dc}$, $I_{qc}$) and d-axis demagnetizing and q-axis torque generating operating point currents ($I_{dT}$, $I_{qT}$). The harmonics in the back electromotive force (EMF) also generate the iron loss. The iron loss due to the harmonics, however, is not controllable by the current vector control, therefore the effects of the harmonics is not considered in this thesis [68]. $V_d$ and $V_q$ are d-axis and q-axis armature voltages. $L_d$ and $L_q$ are d-axis and q-axis inductances, respectively. Whereas $\Psi$ is magnet flux linkage.

From Fig. 3.2, the voltage equations of the IPMSM are expressed as:

$$V_d = R_s I_d + V_{dc} \tag{3.1}$$

$$V_q = R_s I_q + V_{qc} \tag{3.2}$$

$$V_{dc} = L_d \frac{dI_{dT}}{dt} - L_q I_{qT} \omega_r = I_{dc} R_c \tag{3.3}$$

$$V_{qc} = L_q \frac{dI_{qT}}{dt} + \Psi \omega_r + L_d I_{dT} \omega_r = I_{qc} R_c \tag{3.4}$$

where,

$$I_{dc} = I_d - I_{dT}$$

$$I_{dc} = \frac{V_d - R_s I_d}{R_c} = \frac{L_d \frac{dI_{dT}}{dt} - L_q I_{qT} \omega_r}{R_c} \tag{3.5}$$

$$I_{qc} = I_q - I_{qT}$$

$$I_{qc} = \frac{V_q - R_s I_q}{R_c} = \frac{L_q \frac{dI_{qT}}{dt} + \Psi \omega_r + L_d I_{dT} \omega_r}{R_c} \tag{3.6}$$

Expressing the voltage equations in terms of the $I_{dT}$ and $I_{qT}$ currents, hence substituting Eqns. (3.3)-(3.6) in Eqns. (3.1) and (3.2), respectively gives:

$$V_d = R_s I_{dT} + \left(1 + \frac{R_s}{R_c}\right)\left[L_d \frac{dI_{dT}}{dt} - \omega_r L_q I_{qT}\right] \tag{3.7}$$

$$V_q = R_s I_{qT} + \left(1 + \frac{R_s}{R_c}\right)\left[L_q \frac{dI_{qT}}{dt} + \omega_r \left(L_d I_{dT} + \Psi\right)\right] \tag{3.8}$$

By choosing d-q axis currents as the state variable, the IPMSM model given by Eqns. (3.7) and (3.8) can be written in the following explicit form:

$$\frac{dI_{dT}}{dt} = \frac{R_c}{L_d\left(R_s + R_c\right)}\left[V_d - R_s I_{dT}\right] + \frac{L_q}{L_d}\omega_r I_{qT} \tag{3.9}$$

$$\frac{dI_{qT}}{dt} = \frac{R_c}{L_q\left(R_s + R_c\right)}\left[V_q - R_s I_{qT}\right] - \frac{\omega_r}{L_q}\left(L_d I_{dT} + \Psi\right) \tag{3.10}$$

From the equivalent circuits shown in Fig. 3.2, the electromagnetic torque $T_e$ is proportional to the vector product of flux linkages and currents and can be obtained as (3.11), where P denotes the number of poles. Since $R_c$ supplies an additional current path to each axis equivalent circuits, the torque depends not on measured armature currents, $I_d$ and $I_q$, but on the $I_{dT}$ and $I_{qT}$ currents. Therefore, the armature currents can no longer directly govern the torque; hence, the electromagnetic torque equation is given by:

$$T_e = \frac{3P}{2}\left[\Psi I_{qT} + \left(L_d - L_q\right) I_{dT} I_{qT}\right] \tag{3.11}$$

# 3.3 Steady State Conditions

The development of voltage equations that express the transient behaviour of the IPMSM including the motor losses is the first object presented in this thesis. In order to understand the nature of the equivalent circuit parameters and to get parameter approximations in the transient condition, voltage equations in the steady state are developed. In steady state condition, voltages across the d-q axis inductances are zero. Therefore, the steady-state equations are:

$$V_d = R_s I_{dT} - \left(1 + \frac{R_s}{R_c}\right) \omega_r L_q I_{qT} \tag{3.12}$$

$$V_q = R_s I_{qT} + \left(1 + \frac{R_s}{R_c}\right) \left(\mathrm{L_d} I_{dT} + \Psi\right) \omega_r \tag{3.13}$$

Similarly, the d-q axis components of the iron loss current can be expressed in steady state as:

$$I_{dc} = \frac{V_d - R_s I_d}{R_c} = -\frac{L_q I_{qT} \omega_r}{R_c} \tag{3.14}$$

$$I_{qc} = \frac{V_q - R_s I_q}{R_c} = \frac{\Psi \omega_r + L_d I_{dT} \omega_r}{R_c} \tag{3.15}$$

# 3.4 Electrical Power Losses of the IPMSM

Based on the Eqns. (3.14), (3.15) and Fig. 3.2 the copper losses $P_{Cu}$ and iron losses $P_{Fe}$ of the IPMSM can be expressed as:

$$P_{Cu} = \frac{3}{2} R_s \left(I_d^2 + I_q^2\right) \tag{3.16}$$

$$P_{Fe} = \frac{3}{2} R_c \left(I_{dc}^2 + I_{qc}^2\right) \tag{3.17}$$

$$I_d = I_{dc} + I_{dT} \tag{3.18}$$

$$I_q = I_{qc} + I_{qT} \tag{3.19}$$

Substituting Eqns. (3.14) and (3.15) into (3.18) and (3.19), respectively. The copper losses $P_{Cu}$ can be written as:

$$P_{Cu} = \frac{3}{2} R_s \left( \left( I_{dT} - \frac{\omega_r L_q I_{qT}}{R_c} \right)^2 + \left( I_{qT} + \frac{\omega_r \left( \Psi + L_d I_{dT} \right)}{R_c} \right)^2 \right) \tag{3.20}$$

Substituting Eqns. (3.14) and (3.15) into (3.17), the iron losses $P_{Fe}$ can be written as:

$$P_{Fe} = \frac{3}{2} \left( \frac{\omega_r^2 L_q^2 I_{qT}^2}{R_c} + \frac{\omega_r^2 \left( \Psi + L_d I_{dT} \right)^2}{R_c} \right) \tag{3.21}$$

The mechanical loss $P_M$ can be written as:

$$P_M = T_{mec} \omega_r \tag{3.22}$$

where, $T_{mec}$ is the friction torque of the motor and $\omega_r$ is the speed of the motor.

The $P_{Cu}$ and $P_{Fe}$ are the two controllable losses in IPMSM [68]. Iron loss is the combined effect of eddy current and hysteresis losses. Eddy current losses are caused by the flow of induced currents inside the stator core and hysteresis losses are caused by the continuous variation of flux linkages and frequency of the flux variation in the core. The $P_M$ is speed dependent, therefore it is not controllable by LMC. The output power $P_{out}$, the total electrical power loss $P_L$ and the efficiency of the IPMSM, $\eta$ are expressed as:

$$P_{out} = T_e \omega_r \tag{3.23}$$

$$P_L = P_{Cu} + P_{Fe} + P_M$$

$$P_L = \frac{3}{2} \left[ R_s \left\{ \left( I_{dT} - \frac{\omega_r L_q I_{qT}}{R_c} \right)^2 + \left( I_{qT} + \frac{\omega_r \left( \Psi + L_d I_{dT} \right)}{R_c} \right)^2 \right\} + \frac{\omega_r^2 L_q^2 I_{qT}^2}{R_c} + \frac{\omega_r^2 \left( \Psi + L_d I_{dT} \right)^2}{R_c} \right] \tag{3.24}$$

$$\eta = \frac{P_{out}}{P_{out} + P_L} \times 100\% \tag{3.25}$$

Eqn. (3.24) can be simplified as:

$$\begin{aligned} P_L = {} & \frac{3}{2} R_s \left( I_{dT}^2 + I_{qT}^2 \right) + 3 \frac{(R_s + R_c)}{R_c^2} L_d \Psi \omega_r^2 I_{dT} + \frac{3}{2} \frac{\omega_r^2}{R_c^2} \left( R_s + R_c \right) \left[ \Psi^2 + \left( L_d^2 I_{dT}^2 + L_q^2 I_{qT}^2 \right) \right] \\ & + 3 \frac{R_s}{R_c} \left( \Psi + \left( L_d - L_q \right) I_{dT} \right) \omega_r I_{qT} \end{aligned} \tag{3.26}$$

In a conventional machine, operation under rated conditions is found to be highly efficient. This results from a favourable balance between copper and iron losses. However, there are many applications which require adjustable torque and speed different than the rated one. A torque or speed far from the rated operating point causes a significant drop in the efficiency of IPMSM drive. This is due to imbalance between iron and copper losses. Copper and iron losses are the most fundamental and dominant losses in IPMSM [68]. Because of this, in LMC the value of $R_c$ is calculated at the rated torque and rated speed. First the iron loss $P_{Fe}$ is calculated by subtracting $P_M$ and $P_{Cu}$ given by Eqn. (3.22) and Eqn. (3.20), respectively from total power loss $P_L$. The $R_c$ now can be calculated from $P_{Fe}$ based on Eqn. (3.21). However, $R_c$ can change depending on the operating condition, it is assumed to be constant in this thesis. The complete parameters of the IPMSM which is under consideration for loss minimization in this thesis are given in Appendix A. As Eqn. (3.23) depicted efficiency can be improved by minimizing $P_L$ which is given in Eqn. (3.26) where the mechanical loss $P_M$ is not controllable, but the electrical losses $P_{Cu}$ and $P_{Fe}$ are controllable by means of vector control. The electrical losses are controlled by means of vector control.

# 3.5 Proposed Loss Minimization Algorithm

The minimization of IPMSM power losses is regarded as one of the control objectives under the constraint of control torque production. In Fig. 3.3, the constant torque curve can be drawn as a hyperbola on the $I_{dT}$ and $I_{qT}$ plane using Eqn. (3.11). On the same plane, at a constant speed, a curve representing constant power losses takes the form of an ellipse of which the major axis is inclined by δ is given by Eqn. (3.26). As speed increases, the eccentricity of this ellipse and δ increases. Under the constraint of constant torque production, if an operating point is set at point "a" in Fig. 3.3, the curve A is supposed to be a power loss curve producing $P_{LA}$. If an operating point is set at "b", the curve B is a power loss curve, and it produces power losses $P_{LB}$. Based on Lagrange's Theorem, it can be easily found that power losses are minimum when the torque curve and power loss curve are tangent at a point. This is achieved if and only if their gradient vectors are parallel. This means that $\nabla T_e(I_{dT}, I_{qT})$ must be a scalar multiple of $\nabla P_L(I_{dT}, I_{qT})$ at the point of tangency [82].

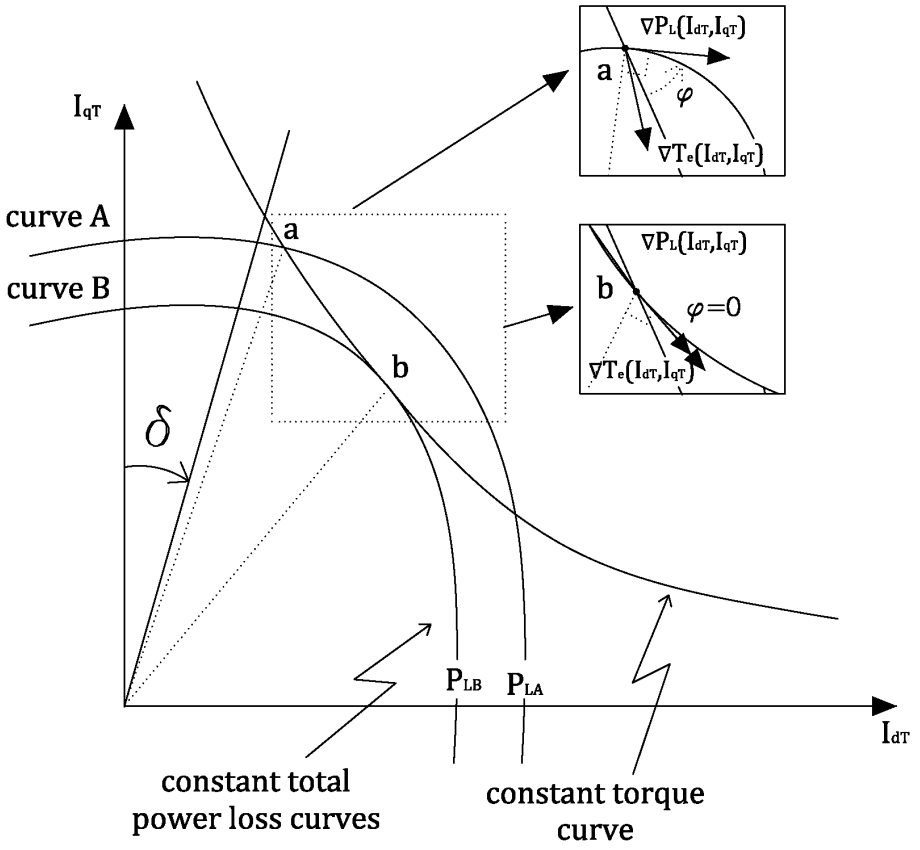


Fig. 3.3: Constant torque curve and power loss curve on $I_{dT}$ - $I_{qT}$ plane.

In order to minimize total electrical losses (copper and iron losses) for any given constant torque (i.e, $T_e = T_L$), the Γ is chosen as output variable which is magnitude of the cross product of $\nabla T_e(I_{dT}, I_{qT})$ and $\nabla P_L(I_{dT}, I_{qT})$.

$$\Gamma = \begin{bmatrix} \frac{\partial P_L}{\partial I_{qT}} & \frac{\partial P_L}{\partial I_{dT}} \\ \frac{\partial T_e}{\partial I_{qT}} & \frac{\partial T_e}{\partial I_{dT}} \end{bmatrix} \tag{3.27}$$

Thus, the output for the proposed LMA is Γ. As per Fig. 3.3 the minimum loss condition is achieved if |Γ| = 0, where, |Γ| is determinant of Eqn. (3.27).

$$\gamma = \det(\Gamma) = \frac{\partial P_L}{\partial I_{qT}} \frac{\partial T_e}{\partial I_{dT}} - \frac{\partial P_L}{\partial I_{dT}} \frac{\partial T_e}{\partial I_{qT}} = 0 \tag{3.28}$$

The objective of the nonlinear controller is to force the output γ to zero, so that the reached operating point corresponds to a minimum value of $P_L$ along a constant torque trajectory.

Differentiating Eqn. (3.26) with respect to $I_{qT}$ gives:

$$\frac{\partial P_L}{\partial I_{qT}} = 3R_s I_{qT} + 3\frac{\omega_r^2}{R_c^2}\left(R_s + R_c\right)L_q^2 I_{qT} + 3\frac{R_s}{R_c}\left(\Psi + \left(L_d - L_q\right)I_{dT}\right)\omega_r \tag{3.29}$$

Differentiating Eqn. (3.26) with respect to $I_{dT}$ gives:

$$\frac{\partial P_L}{\partial I_{dT}} = 3R_s I_{dT} + 3\frac{(R_s + R_c)}{R_c^2} L_d \Psi \omega_r^2 + 3\frac{\omega_r^2}{R_c^2}\left(R_s + R_c\right)L_d^2 I_{dT} + 3\frac{R_s}{R_c}\left(L_d - L_q\right)\omega_r I_{qT} \tag{3.30}$$

Differentiating Eqn. (3.11) with respect to $I_{qT}$ gives:

$$\frac{\partial T_e}{\partial I_{qT}} = \frac{3P}{2}\left[\Psi + \left(L_d - L_q\right)I_{dT}\right] \tag{3.31}$$

Differentiating Eqn. (3.11) with respect to $I_{dT}$ gives:

$$\frac{\partial T_e}{\partial I_{dT}} = \frac{3P}{2}\left(L_d - L_q\right)I_{qT} \tag{3.32}$$

Substituting Eqns. (3.29)-(3.31) in Eqn. (3.28) gives:

$$\begin{aligned}\gamma = {} & \frac{3P}{2}\left(L_d - L_q\right)I_{qT}\left[3R_s I_{qT} + 3\frac{\omega_r^2}{R_c^2}\left(R_s + R_c\right)L_q^2 I_{qT} + 3\frac{R_s}{R_c}\left(\Psi + \left(L_d - L_q\right)I_{dT}\right)\omega_r\right] \\ & - \frac{3P}{2}\left(\Psi + \left(L_d - L_q\right)I_{dT}\right)\left[3R_s I_{dT} + 3\frac{(R_s + R_c)}{R_c^2} L_d \Psi \omega_r^2 + 3\frac{\omega_r^2}{R_c^2}\left(R_s + R_c\right)L_d^2 I_{dT}\right. \\ & \left. + 3\frac{R_s}{R_c}\left(L_d - L_q\right)\omega_r I_{qT}\right]\end{aligned} \tag{3.33}$$

The optimal operating point d-axis current which provides the minimum electrical loss can be found by equating (3.33) to zero in order to achieve optimal $I_{dT}^*$.

$$0 = I_{dT}^2\left\{\frac{9P}{2}\left(Ld-Lq\right)\left[R_s+\frac{\omega_r^2}{R_c^2}\left(R_s+R_c\right)L_q^2\right]\right\}+I_{dT}\left\{\frac{9P}{2}\Psi\left[R_s+\frac{\omega_r^2}{R_c^2}\left(R_s+R_c\right)L_d\left[2L_d-L_q\right]\right]\right\}$$
$$-\left[\frac{9P}{2}\left(L_d-L_q\right)I_{qT}^2\left[R_s+\frac{\omega_r^2}{R_c^2}\left(R_s+R_c\right)L_q^2\right]-\frac{9P}{2}\frac{\omega_r^2}{R_c^2}\left(R_s+R_c\right)L_d\Psi^2\right] \quad (3.34)$$

For given torque ($T_e$) and speed ($\omega_r$) the optimal d-axis current $I_{dT}$ is derived from (3.34) as shown below:

$$I_{dT}^* = \frac{-b\pm\sqrt{b^2-4ac}}{2a} \quad (3.35)$$

where, a, b and c are given as:

$$a = \frac{9P}{2}\left(Ld-Lq\right)\left[R_s+\frac{\omega_r^2}{R_c^2}\left(R_s+R_c\right)L_q^2\right]$$

$$b = \frac{9P}{2}\Psi\left[R_s+\frac{\omega_r^2}{R_c^2}\left(R_s+R_c\right)L_d\left[2L_d-L_q\right]\right]$$

$$c = -\left[\frac{9P}{2}\left(L_d-L_q\right)I_{qT}^2\left[R_s+\frac{\omega_r^2}{R_c^2}\left(R_s+R_c\right)L_q^2\right]-\frac{9P}{2}\frac{\omega_r^2}{R_c^2}\left(R_s+R_c\right)L_d\Psi^2\right] \quad (3.36)$$

Eqn. (3.35) have two solutions. The solution with negative sign gave positive and very high value of $I_{dT}^*$ and the solution with positive sign gave negative and small value of $I_{dT}^*$. The control objective was met with the second solution of the $I_{dT}^*$. Thus, the optimal d-axis current from Eqns. (3.35) and (3.36) is obtained as:

$$I_{dT}^* = \frac{-\frac{9P}{2}\Psi\left[R_s+\frac{\omega_r^2}{R_c^2}\left(R_s+R_c\right)L_d\left[2L_d-L_q\right]\right]+\sqrt{\left(\frac{9P}{2}\Psi\left[R_s+\frac{\omega_r^2}{R_c^2}\left(R_s+R_c\right)L_d\left[2L_d-L_q\right]\right]\right)^2-}}{2\left(\frac{9P}{2}\left(Ld-Lq\right)\left[R_s+\frac{\omega_r^2}{R_c^2}\left(R_s+R_c\right)L_q^2\right]\right)} \quad (3.37)$$

$$\frac{4\left(\frac{9P}{2}\left(Ld-Lq\right)\left[R_s+\frac{\omega_r^2}{R_c^2}\left(R_s+R_c\right)L_q^2\right]\right)\left(\left[-\frac{9P}{2}\left(L_d-L_q\right)I_{qT}^2\left[R_s+\frac{\omega_r^2}{R_c^2}\left(R_s+R_c\right)L_q^2\right]+\frac{9P}{2}\frac{\omega_r^2}{R_c^2}\left(R_s+R_c\right)L_d\Psi^2\right]\right)}{2\left(\frac{9P}{2}\left(Ld-Lq\right)\left[R_s+\frac{\omega_r^2}{R_c^2}\left(R_s+R_c\right)L_q^2\right]\right)}$$

Eqn. (3.37) is used to control the flux to achieve minimum loss condition of the motor.

# Chapter 4

# Nonlinear Controller Design for IPMSM Drive

In this Chapter, a nonlinear controller for IPMSM is developed based on adaptive backstepping technique. In order to achieve high performance operation from the IPMSM drive, the vector control technique is utilized for the proposed drive. The basic principle of the adaptive backstepping technique is explained here. Step-by-step design procedures to derive control and parameter update laws for IPMSM drive are presented in detail. Stability analysis for the proposed controller is also provided.

## 4.1 Adaptive Backstepping Technique

The conventional gain PI and PID controllers are sensitive to plant parameter variations, load variation and other disturbances. For the purpose of obtaining high dynamic performance, several non-linear controllers have been developed for IPMSM [31-43]. Recently, feedback linearization control (FBLC) has been applied to IPMSM with an aim to design the nonlinear controller by changing the original dynamics into linear one, which has limitations in terms of incorporating all system nonlinearities [70, 71, 82]. Thus, the performance of the system utilizing

FBLC for reported works were not at an optimum level. Therefore, it is necessary to develop an adaptive controller which incorporates system nonlinearities particularly, mechanical parameters, sometimes which are not possible to measure at all. These parameters may also vary with different operation conditions especially with mechanical load variation.

Adaptive Backstepping is a systematic and recursive design methodology for nonlinear feedback control which makes use of the Lyapunov stability theory [79]. The key idea of adaptive backstepping is to systematically decompose a complex nonlinear control problem into simpler and smaller ones and to select recursively appropriate functions of state variables as so-called "virtual-control". Each backstepping stage results in a new virtual-control to deal with a decomposed subsystem problem and this virtual-control becomes a reference to the next design step for another subsystem. At the final stage, true control input for the original control objectives can be formed by summing up the Lyapunov functions associated with each individual design stage. While feedback linearization methods require precise models and often cancel some useful nonlinearity, the adaptive backstepping design offers a choice of design tools for accommodation of uncertainties and nonlinearities and can avoid wasteful cancellations. Another important feature of the backstepping design method is that it can be easily combined with adaptive control techniques. Parameter update laws can be obtained simultaneously with design steps of control laws. Hence, no extra effort to build other means for parameter adaptation is needed and the compensation of the parameter uncertainties in the system is quite straightforward. To guarantee the robustness, mechanical parameters are estimated online based on adaptive backstepping technique [37, 80, 81]. Therefore, the proposed adaptive backstepping-based nonlinear controller (ABNC) is capable of conserving the system robustness and stability against mechanical parameter variations and external load torque disturbances. Among the IPMSM parameters, the load torque

is unknown in most applications and has a great influence in servo performance. Therefore, in this thesis we design an adaptive backstepping controller with parameter uncertainties of the load torque and friction coefficient.

## 4.2 Proposed LMA Based Nonlinear Controller Design

The fundamental of backstepping controller is the identification of a virtual control variable and forcing it to become a stabilizing function. Thus, it generates a corresponding error variable which can be stabilized by proper input selection via Lyapunov's stability theory [79]. In order to derive the adaptive control algorithms the mathematical model of IPMSM as derived in Chapters 2 and 3 are considered.

$$\frac{dI_{dT}}{dt} = \frac{R_c}{L_d\left(R_s + R_c\right)}\left[V_d - R_s I_{dT}\right] + \frac{L_q}{L_d}\omega_r I_{qT} \tag{4.1}$$

$$\frac{dI_{qT}}{dt} = \frac{R_c}{L_q\left(R_s + R_c\right)}\left[V_q - R_s I_{qT}\right] - \frac{\omega_r}{L_q}\left(L_d I_{dT} + \Psi\right) \tag{4.2}$$

$$T_e = \frac{3P}{2}\left[\Psi I_{qT} + \left(L_d - L_q\right) I_{qT} I_{dT}\right] \tag{4.3}$$

$$T_e = T_L + B_m\omega_r + J\frac{d\omega_r}{dt} \tag{4.4}$$

In order to achieve high dynamic performance from an IPMSM, the vector control technique is utilized for the proposed ABNC of IPMSM drive. Command d-axis and q-axis input voltages are developed in the proposed controller to guarantee high speed tracking performance of the IPMSM. The first step for the purpose of speed tracking is to select the input variable with

proper value in order to ensure the convergence of the motor speed to the command/reference speed. The speed error is defined as:

$$e = \omega_r^* - \omega_r \tag{4.5}$$

Then from (4.3) – (4.5) speed error dynamic is given by:

$$\dot{e} = -\dot{\omega}_r = \frac{1}{J}\left[ B_m\omega_r + T_L - \frac{3P}{2}\left(\Psi I_{qT} + \left(L_d - L_q\right) I_{dT} I_{qT}\right)\right] \tag{4.6}$$

The Lyapunov function is given by:

$$V = \frac{1}{2}e^2 \tag{4.7}$$

The stabilizing function is determined by differentiating the Lyapunov function (4.7) to get:

$$\dot{V} = e\dot{e}$$

$$= \frac{e}{J}\left[ B_m\omega_r + T_L - \frac{3P}{2}\left(\Psi I_{qT} + \left(L_d - L_q\right) I_{dT} I_{qT}\right)\right] \tag{4.8}$$

In order to stabilize the motor speed the d-q axis currents are identified as virtual control variables. From Eqn. (4.8) we choose the following stabilizing functions:

$$I_{qT}^* = \frac{2}{3P\Psi}\left[B_m\omega_r + T_L + k_1 Je\right] \tag{4.9}$$

$$I_{dT}^* = 0 \tag{4.10}$$

where, $k_1$ is a constant gain, $I_{qT}^*$ and $I_{dT}^*$ are the command currents. Substituting Eqns. (4.9) and (4.10) back into Eqn. (4.8) the Lyapunov function becomes:

$$\dot{V} = -k_1 e^2 \tag{4.11}$$

If $k_1 > 0$ then the function is negative semi-definite which ensures asymptotic stability.

If the γ and q-axis current are identified as the virtual control variables the corresponding error functions are defined as:

$$e_\gamma = \gamma^* - \gamma \tag{4.12}$$

$$e_q = I_{qT}^* - I_{qT} \tag{4.13}$$

Like the speed error, these error functions must also be reduced to zero. The error dynamics given with $\dot{\gamma}^* = 0$ are:

$$\dot{e}_\gamma = -\dot{\gamma} \tag{4.14}$$

$$\dot{e}_q = \dot{I}_{qT}^* - \dot{I}_{qT} \tag{4.15}$$

The parameters that must be estimated in this work are the load torque ($T_L$) and friction coefficient ($B_m$). Since the value of load torque is unknown and the motor parameters are varying with different operation condition, these values should be estimated adaptively. The corresponding error variables are given by:

$$\tilde{T}_L = \hat{T}_L - T_L \tag{4.16}$$

$$\tilde{B}_m = \hat{B}_m - B_m \tag{4.17}$$

The q-axis command current Eqn. (4.9) must be modified to incorporate the estimated load torque and estimated friction coefficient as:

$$I_{qT}^* = \frac{2}{3P\Psi}\left[\hat{B}_m\omega_r + \hat{T}_L + k_1 Je\right] \tag{4.18}$$

where, $\hat{T}_L$ and $\hat{B}_m$ are the estimated values of load torque and friction coefficient, respectively. The speed error dynamic from Eqns. (4.6), (4.13) and (4.18) can be rewritten as:

$$\dot{e} = \frac{1}{J}\left[B_m\omega_r + T_L - \frac{3P\Psi}{2}\left(\frac{2}{3P\Psi}\left[\hat{B}_m\omega_r + \hat{T}_L + k_1 Je\right] - e_q\right) - \frac{3P}{2}\left(L_d - L_q\right)I_{dT}I_{qT}\right]$$

$$= \frac{1}{J}\left[-\tilde{B}_m\omega_r - \tilde{T}_L - k_1 Je + \frac{3P}{2}\Psi e_q - \frac{3P}{2}\left(L_d - L_q\right)I_{dT}I_{qT}\right] \tag{4.19}$$

The time derivative of Eqn. (3.32) is given by:

$$\dot{\gamma} = 9P\left(L_d - L_q\right)R_s I_{qT}\frac{dI_{qT}}{dt} + 9P\frac{\left(R_s + R_c\right)}{R_c^2}\left(L_d - L_q\right)L_q^2\omega_r I_{qT}^2\frac{d\omega_r}{dt} + 9P\frac{\left(R_s + R_c\right)}{R_c^2}\left(L_d - L_q\right)L_q^2\omega_r^2 I_{qT}\frac{dI_{qT}}{dt}$$
$$-\frac{9P}{2}R_s\Psi\frac{dI_{dT}}{dt} - 9P\frac{\left(R_s + R_c\right)}{R_c^2}L_d\omega_r\Psi^2\frac{d\omega_r}{dt} - 9P\frac{\left(R_s + R_c\right)}{R_c^2}L_d^2\Psi\omega_r I_{dT}\frac{d\omega_r}{dt} - \frac{9P}{2}\frac{\left(R_s + R_c\right)}{R_c^2}L_d^2\Psi\omega_r^2\frac{dI_{dT}}{dt}$$
$$-9P\left(L_d - L_q\right)R_s I_{dT}\frac{dI_{dT}}{dt} - 9P\frac{\left(R_s + R_c\right)}{R_c^2}\left(L_d - L_q\right)L_d\Psi\omega_r I_{dT}\frac{d\omega_r}{dt} - \frac{9P}{2}\frac{\left(R_s + R_c\right)}{R_c^2}\left(L_d - L_q\right)L_d\Psi\omega_r^2\frac{dI_{dT}}{dt}$$
$$-9P\frac{\left(R_s + R_c\right)}{R_c^2}\left(L_d - L_q\right)L_d^2\omega_r I_{dT}^2\frac{d\omega_r}{dt} - 9P\frac{\left(R_s + R_c\right)}{R_c^2}\left(L_d - L_q\right)L_d^2\omega_r^2 I_{dT}\frac{dI_{dT}}{dt}$$

$$= \left[9P\frac{\left(R_s + R_c\right)}{R_c^2}\left(L_d - L_q\right)L_q^2\omega_r I_{qT}^2 - 9P\frac{\left(R_s + R_c\right)}{R_c^2}L_d\omega_r\Psi^2 - 9P\frac{\left(R_s + R_c\right)}{R_c^2}L_d^2\Psi\omega_r I_{dT}\right.$$
$$\left. -9P\frac{\left(R_s + R_c\right)}{R_c^2}\left(L_d - L_q\right)L_d\Psi\omega_r I_{dT} - 9P\frac{\left(R_s + R_c\right)}{R_c^2}\left(L_d - L_q\right)L_d^2\omega_r I_{dT}^2\right]\frac{d\omega_r}{dt}$$
$$+\left[9P\left(L_d - L_q\right)R_s I_{qT} + 9P\frac{\left(R_s + R_c\right)}{R_c^2}\left(L_d - L_q\right)L_q^2\omega_r^2 I_{qT}\right]\frac{dI_{qT}}{dt} - \left[\frac{9P}{2}R_s\Psi\right.$$
$$+\frac{9P}{2}\frac{\left(R_s + R_c\right)}{R_c^2}L_d^2\Psi\omega_r^2 + 9P\left(L_d - L_q\right)R_s I_{dT} + \frac{9P}{2}\frac{\left(R_s + R_c\right)}{R_c^2}\left(L_d - L_q\right)L_d\Psi\omega_r^2$$
$$\left. +9P\frac{\left(R_s + R_c\right)}{R_c^2}\left(L_d - L_q\right)L_d^2\omega_r^2 I_{dT}\right]\frac{dI_{dT}}{dt}$$

$$= 9P\frac{\left(R_s + R_c\right)}{R_c^2}\left(L_d - L_q\right)\omega_r\left(L_q^2 I_{qT}^2 - \frac{L_d}{\left(L_d - L_q\right)}\Psi^2 - \frac{L_d^2}{\left(L_d - L_q\right)}\Psi I_{dT} - L_d\Psi I_{dT} - L_d^2 I_{dT}^2\right)$$
$$\left[\frac{1}{J}\left(T_e - T_L - B_m\omega_r\right)\right] + 9P\left(L_d - L_q\right)\frac{R_c}{L_q\left(R_s + R_c\right)}I_{qT}\left[R_s + \frac{\left(R_s + R_c\right)}{R_c^2}L_q^2\omega_r^2\right]$$
$$\left(V_q - R_s I_{qT} - \frac{\left(R_s + R_c\right)}{R_c}L_d\omega_r I_{dT} - \frac{\left(R_s + R_c\right)}{R_c}\Psi\omega_r\right) - \frac{9P}{2}\frac{R_c}{L_d\left(R_s + R_c\right)}$$
$$\left(R_s\Psi + \frac{\left(R_s + R_c\right)}{R_c^2}L_d^2\Psi\omega_r^2 + 2\left(L_d - L_q\right)R_s I_{dT} + \frac{\left(R_s + R_c\right)}{R_c^2}\left(L_d - L_q\right)L_d\Psi\omega_r^2\right.$$
$$\left. +2\frac{\left(R_s + R_c\right)}{R_c^2}\left(L_d - L_q\right)L_d^2\omega_r^2 I_{dT}\right)\left[V_d - R_s I_{dT} + \frac{\left(R_s + R_c\right)}{R_c}L_q\omega_r I_{qT}\right]$$

$$
\begin{aligned}
&= \frac{9P}{J}\frac{\left(R_s+R_c\right)}{R_c^2}\left(L_d-L_q\right)\omega_r\left[L_q^2I_{qT}^2-L_dI_{dT}\left(\Psi+L_dI_{dT}\right)-\frac{L_d\Psi\left(\Psi+L_dI_{dT}\right)}{\left(L_d-L_q\right)}\right]\left(T_e-T_L-B_m\omega_r\right)\\
&+\frac{9P\left(L_d-L_q\right)I_{qT}}{L_q\left(R_s+R_c\right)R_c}\left[R_sR_c^2+\left(R_s+R_c\right)L_q^2\omega_r^2\right]\left[V_q-R_sI_{qT}-\frac{\left(R_s+R_c\right)}{R_c}L_d\omega_rI_{dT}-\frac{\left(R_s+R_c\right)}{R_c}\Psi\omega_r\right]\\
&-\frac{9P}{2L_d\left(R_s+R_c\right)R_c}\left[R_sR_c^2\left(\Psi+2\left(L_d-L_q\right)I_{dT}\right)+\left(R_s+R_c\right)L_d^2\Psi\omega_r^2\right.\\
&\left.+\left(R_s+R_c\right)\left(L_d-L_q\right)L_d\omega_r^2\left(\Psi+2L_dI_{dT}\right)\right]\left[V_d-R_sI_{dT}+\frac{\left(R_s+R_c\right)}{R_c}L_q\omega_rI_{qT}\right]
\end{aligned}
\tag{4.20}
$$

For stabilizing γ and q-axis current vectors, the Eqns. (4.14) and (4.15) can be defined as:

Substituting Eqn. (4.20) into γ error dynamic Eqn. (4.14) is defined as:

$$\dot{e}_\gamma = 0-\dot{\gamma}$$

$$
\begin{aligned}
&= -\frac{9P}{J}\frac{\left(R_s+R_c\right)}{R_c^2}\left(L_d-L_q\right)\omega_r\left[L_q^2I_{qT}^2-L_dI_{dT}\left(\Psi+L_dI_{dT}\right)-\frac{L_d\Psi\left(\Psi+L_dI_{dT}\right)}{\left(L_d-L_q\right)}\right]\left(T_e-T_L-B_m\omega_r\right)\\
&-\frac{9P\left(L_d-L_q\right)I_{qT}}{L_q\left(R_s+R_c\right)R_c}\left[R_sR_c^2+\left(R_s+R_c\right)L_q^2\omega_r^2\right]\left[V_q-R_sI_{qT}-\frac{\left(R_s+R_c\right)}{R_c}L_d\omega_rI_{dT}-\frac{\left(R_s+R_c\right)}{R_c}\Psi\omega_r\right]\\
&+\frac{9P}{2L_d\left(R_s+R_c\right)R_c}\left[R_sR_c^2\left(\Psi+2\left(L_d-L_q\right)I_{dT}\right)+\left(R_s+R_c\right)L_d^2\Psi\omega_r^2\right.\\
&\left.+\left(R_s+R_c\right)\left(L_d-L_q\right)L_d\omega_r^2\left(\Psi+2L_dI_{dT}\right)\right]\left[V_d-R_sI_{dT}+\frac{\left(R_s+R_c\right)}{R_c}L_q\omega_rI_{qT}\right]
\end{aligned}
\tag{4.21}
$$

Substituting Eqns. (4.2) and (4.18) into the q-axis current error dynamic Eqn. (4.15) gives:

$$\dot{e}_q = \frac{2}{3P\Psi}\left[\hat{B}_m\frac{d\omega_r}{dt}+0+k_1J\frac{de}{dt}\right]-\frac{dI_{qT}}{dt}$$

$$= \frac{2}{3P\Psi}\left[\hat{B}_m\frac{d\omega_r}{dt}-k_1J\frac{d\omega_r}{dt}\right]-\frac{dI_{qT}}{dt}$$

$$= \frac{2}{3P\Psi}\left(\hat{B}_m-k_1J\right)\frac{d\omega_r}{dt}-\frac{dI_{qT}}{dt}$$

$$= \frac{2\left(\hat{B}_m - k_1 J\right)}{3P\Psi J}\left[T_e - T_L - B_m\omega_r\right] - \frac{R_c}{L_q\left(R_s + R_c\right)}\left[V_q - R_s I_{qT} - \frac{\left(R_s + R_c\right)}{R_c} L_d \omega_r I_{dT} - \frac{\left(R_s + R_c\right)}{R_c}\Psi\omega_r\right] \tag{4.22}$$

As the mechanical parameters of the system change at different operating conditions, those should be determined adaptively. Based on the error dynamics, new Lyapunov function including the γ and q-axis current error variables and estimation error variables is presented for reduction of estimated errors to zero.

$$V_1 = \frac{1}{2}\left(e^2 + e_\gamma^2 + e_q^2 + \frac{1}{\phi_1}\tilde{T}_L^{\,2} + \frac{1}{\phi_2}\tilde{B}_m^{\,2}\right) \tag{4.23}$$

where, $\varphi_1, \varphi_2$ are constant adaptive gains. By differentiating the new Lyapunov function and using the value of error dynamics one can achieve:

$$\dot{V}_1 = e\dot{e} + e_\gamma\dot{e}_\gamma + e_q\dot{e}_q + \frac{1}{\phi_1}\tilde{T}_L\dot{\tilde{T}}_L + \frac{1}{\phi_2}\tilde{B}_m\dot{\tilde{B}}_m$$

$$\begin{aligned}
&= \frac{e}{J}\left[-\tilde{B}_m\omega_r - \tilde{T}_L - k_1 Je + \frac{3P}{2}\Psi e_q - \frac{3P}{2}\left(L_d - L_q\right) I_{dT} I_{qT}\right] \\
&+ e_\gamma\left\{-\frac{9P}{J}\frac{\left(R_s + R_c\right)}{R_c^2}\left(L_d - L_q\right)\omega_r\left[L_q^2 I_{qT}^2 - L_d I_{dT}\left(\Psi + L_d I_{dT}\right) - \frac{L_d\Psi\left(\Psi + L_d I_{dT}\right)}{\left(L_d - L_q\right)}\right]\right. \\
&\left(T_e - T_L - B_m\omega_r\right) + \frac{9P}{2L_d\left(R_s + R_c\right)R_c}\left[R_s R_c^2\left(\Psi + 2\left(L_d - L_q\right) I_{dT}\right) + \left(R_s + R_c\right) L_d^2\Psi\omega_r^2\right. \\
&\left.\left.+ \left(R_s + R_c\right)\left(L_d - L_q\right) L_d\omega_r^2\left(\Psi + 2L_d I_{dT}\right)\right]\left(V_d - R_s I_{dT} + \frac{\left(R_s + R_c\right)}{R_c} L_q\omega_r I_{qT}\right)\right\} \\
&+ e_q\left\{\frac{2\left(\hat{B}_m - k_1 J\right)}{3P\Psi J}\left[T_e - T_L - B_m\omega_r\right] - \left[\frac{R_c^2 e_q + 9Pe_\Gamma\left(L_d - L_q\right) I_{qT}\left[R_s R_c^2 + \left(R_s + R_c\right) L_q^2\omega_r^2\right]}{L_q\left(R_s + R_c\right) R_c e_q}\right]\right. \\
&\left.\left(V_q - R_s I_{qT} - \frac{\left(R_s + R_c\right)}{R_c} L_d\omega_r I_{dT} - \frac{\left(R_s + R_c\right)}{R_c}\Psi\omega_r\right)\right\} + \frac{1}{\phi_1}\tilde{T}_L\dot{\tilde{T}}_L + \frac{1}{\phi_2}\tilde{B}_m\dot{\tilde{B}}_m
\end{aligned} \tag{4.24}$$

The control input $V_d$ and $V_q$ voltages are derived to make Eqn. (4.24) negative semi-definite to guarantee global stability [42, 43].

$$V_d = \frac{2L_d\left(R_s+R_c\right)R_c}{9P\left[R_sR_c^2\left(\Psi+2\left(L_d-L_q\right)I_{dT}\right)+\left(R_s+R_c\right)L_d^2\Psi\omega_r^2+\left(R_s+R_c\right)\left(L_d-L_q\right)L_d\omega_r^2\left(\Psi+2L_dI_{dT}\right)\right]}$$
$$\left(\frac{9P}{J}\frac{\left(R_s+R_c\right)}{R_c^2}\left(L_d-L_q\right)\omega_r\left[L_q^2I_{qT}^2-L_dI_{dT}\left(\Psi+L_dI_{dT}\right)-\frac{L_d\Psi\left(\Psi+\mathrm{L_d}I_{dT}\right)}{\left(L_d-L_q\right)}\right]\left(T_e-\hat{T}_L-\hat{B}_m\omega_r\right)\right. \quad (4.25)$$
$$\left.-k_2e_\gamma\right)+R_sI_{dT}-\frac{\left(R_s+R_c\right)}{R_c}L_q\omega_rI_{qT}$$

$$V_q = \frac{L_q\left(R_s+R_c\right)R_ce_q}{R_c^2e_q+9Pe_\gamma\left(L_d-L_q\right)I_{qT}\left[R_sR_c^2+\left(R_s+R_c\right)L_q^2\omega_r^2\right]}\left[\frac{2\left(\hat{B}_m-k_1J\right)}{3P\Psi J}\left(T_e-\hat{T}_L-\hat{B}_m\omega_r\right)+\frac{3P}{2J}\Psi e\right.$$
$$\left.-\frac{3P}{2Je_q}\left(L_d-L_q\right)I_{qT}I_{dT}e+k_3e_q\right]+R_sI_{qT}+\frac{\left(R_s+R_c\right)}{R_c}L_d\omega_rI_{dT}+\frac{\left(R_s+R_c\right)}{R_c}\Psi\omega_r \quad (4.26)$$

where, $k_1$, $k_2$ and $k_3$ are the closed loop feedback gains.

# 4.3 Development of Parameter Adaptation

Now substituting Eqns. (4.25) and (4.26) into (4.24) with further simplification, the Lyapunov function becomes:

$$\dot{V}_1 = \frac{e}{J}\left[-\tilde{B}_m\omega_r-\tilde{T}_L-k_1Je\right]+e_\Gamma\left\{-\frac{9P}{J}\frac{\left(R_s+R_c\right)}{R_c^2}\left(L_d-L_q\right)\omega_r\left[L_q^2I_{qT}^2-L_dI_{dT}\left(\Psi+L_dI_{dT}\right)\right.\right.$$
$$\left.-\frac{L_d\Psi\left(\Psi+L_dI_{dT}\right)}{\left(L_d-L_q\right)}\right]\left(T_e-T_L-B_m\omega_r\right)+\left[-k_2e_\gamma+\frac{9P}{J}\frac{\left(R_s+R_c\right)}{R_c^2}\left(L_d-L_q\right)\omega_r\left[L_q^2I_{qT}^2\right.\right.$$
$$\left.\left.-L_dI_{dT}\left(\Psi+L_dI_{dT}\right)-\frac{L_d\Psi\left(\Psi+L_dI_{dT}\right)}{\left(L_d-L_q\right)}\right]\left(T_e-\hat{T}_L-\hat{B}_m\omega_r\right)\right]\right\}+e_q\left\{\frac{2\left(\hat{B}_m-k_1J\right)}{3P\Psi J}\left(T_e-T_L-B_m\omega_r\right)\right. \quad (4.27)$$
$$\left.-\left[k_3e_q+\frac{2\left(\hat{B}_m-k_1J\right)}{3P\Psi J}\left(T_e-\hat{T}_L-\hat{B}_m\omega_r\right)\right]\right\}+\frac{1}{\phi_1}\tilde{T}_L\dot{\tilde{T}}_L+\frac{1}{\phi_2}\tilde{B}_m\dot{\tilde{B}}_m$$

Eqn. (4.27) can be simplified in the following form:

$$\dot{V}_1 = -k_1 e^2 - k_2 e_\gamma^2 - k_3 e_q^2 + \tilde{T}_L \left( -\frac{e}{J} + \frac{2\left(\hat{B}_m - k_1 J\right) e_q}{3P\Psi J} - \frac{9P}{J}\frac{\left(R_s + R_c\right)}{R_c^2}\left(L_d - L_q\right) e_\gamma \omega_r \left[ L_q^2 I_{qT}^2 \right.\right.$$
$$\left.\left. - L_d I_{dT}\left(\Psi + L_d I_{dT}\right) - \frac{L_d \Psi\left(\Psi + L_d I_{dT}\right)}{\left(L_d - L_q\right)} \right] + \frac{1}{\phi_1}\dot{\tilde{T}}_L \right) + \tilde{B}_m \left( -\frac{e}{J}\omega_r + \frac{2\left(\hat{B}_m - k_1 J\right) e_q}{3P\Psi J}\omega_r \right. \quad (4.28)$$
$$\left. - \frac{9P}{J}\frac{\left(R_s + R_c\right)}{R_c^2}\left(L_d - L_q\right) e_\gamma \omega_r^2 \left[ L_q^2 I_{qT}^2 - L_d I_{dT}\left(\Psi + L_d I_{dT}\right) - \frac{L_d \Psi\left(\Psi + L_d I_{dT}\right)}{\left(L_d - L_q\right)} \right] + \frac{1}{\phi_2}\dot{\tilde{B}}_m \right)$$

Where, $\varphi_1$ and $\varphi_2$ are adaptive gains. The parameter adaptation for the estimated adaptive values can be derived as:

$$\dot{\tilde{T}}_L = -\phi_1 \left( -\frac{e}{J} + \frac{2\left(\hat{B}_m - k_1 J\right) e_q}{3P\Psi J} - \frac{9P}{J}\frac{\left(R_s + R_c\right)}{R_c^2}\left(L_d - L_q\right) e_\gamma \omega_r \left[ L_q^2 I_{qT}^2 - L_d I_{dT}\left(\Psi + L_d I_{dT}\right) \right.\right.$$
$$\left.\left. - \frac{L_d \Psi\left(\Psi + L_d I_{dT}\right)}{\left(L_d - L_q\right)} \right] \right) \quad (4.29)$$

$$\dot{\tilde{B}}_m = -\phi_2 \omega_r \left( -\frac{e}{J} + \frac{2\left(\hat{B}_m - k_1 J\right) e_q}{3P\Psi J} - \frac{9P}{J}\frac{\left(R_s + R_c\right)}{R_c^2}\left(L_d - L_q\right) e_\gamma \omega_r \left[ L_q^2 I_{qT}^2 - L_d I_{dT}\left(\Psi + L_d I_{dT}\right) \right.\right.$$
$$\left.\left. - \frac{L_d \Psi\left(\Psi + L_d I_{dT}\right)}{\left(L_d - L_q\right)} \right] \right) \quad (4.30)$$

As we can see from Eqns. (4.29) and (4.30) the right hand side of the parameter adaptation laws also contain the updated parameter. For the first sample, the nominal value of the parameter is used in the right hand side and then updated parameter is used from the next sample.

The following expression of Eqn. (4.28) is obtained as:

$$\dot{V}_1 = -k_1 e^2 - k_2 e_\gamma^2 - k_3 e_q^2 \quad (4.31)$$

If $k_1$, $k_2$, $k_3 > 0$ the Eqn. (4.31) becomes negative semi-definite which guarantees asymptotic stability of the complete system.

# 4.4 Simulation Results of the Proposed Loss Minimization based ABNC for IPMSM

The dynamics of the IPMSM drive is complex because of its nonlinear nature and also the discrete time nature of the inverter and motor system. After developing the control strategy of the complete drive system and to verify the effectiveness of the proposed controller, digital simulations are performed to predict the behaviour of the system before it is implemented in real-time. The simulation of the proposed IPMSM drive controller has been study using MATLAB/Simulink software as per Fig. 4.1 [77]. The gains used in the simulation model of ABNC drive system are $k_1$=2500, $k_2$=8000, $k_3$=15000. The extensive simulation results are presented after an explanation about the complete drive system with particular attention to the three-phase inverter and its operation by PWM control scheme.

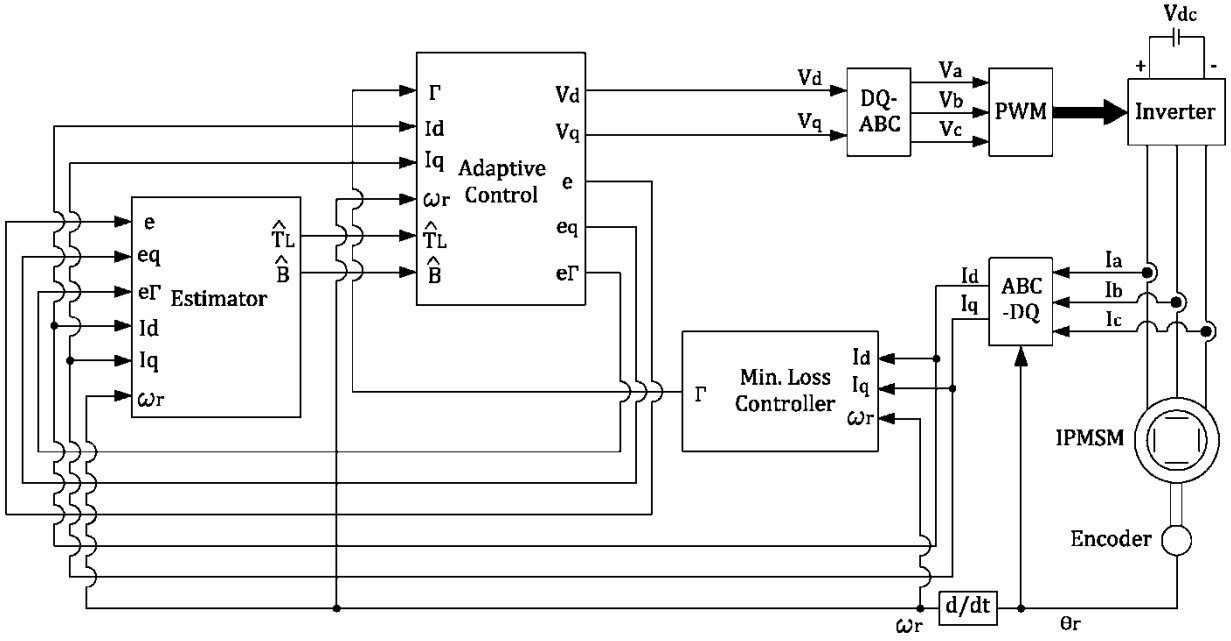


Fig. 4.1: Block diagram of the proposed loss minimization based ABNC for IPMSM drive.

The proposed loss minimization based ABNC scheme of the IPMSM drive is shown in Fig. 4.1. The equivalent Simulink schematic diagram is shown in Fig. 4.2. The motor parameters used for this simulation are given in Appendix A. The details of each subsystem are shown in Appendix B. The Eqns. (4.1)–(4.4) for IPMSM are used for motor model in Simulink. The command q-axis current generated using Eqn. (4.18). Adaptive controller is simulated in the controller block using control law Eqns. (4.25)-(4.26) to give the command d- and q-axis voltages. The command d-q axis voltages are applied to the inverse Clark and Park transformations (*dq/abc*) to get the command *abc* coordinate values. These command voltages are compared with high frequency carrier signals to generate pulse width modulation (PWM) signals for inverter switches. The inverter runs the motor. The estimator block estimates the mechanical motor parameters using the update laws (4.29)-(4.30). The details about the operation of the three-phase inverter and PWM techniques are explained in the following sub-sections.

### 4.4.1 Three-Phase Inverter

3-phase inverters are widely used for ac motor drives and general-purpose ac supplies. The inverter converts DC power to AC power as well as offers an easy way to regulate both the frequency and magnitude of the voltage and current applied to a motor [3]. As shown in Fig. 4.3, the inverter consists of three half-bridge units, each made up of two transistor switches and two anti-parallel freewheeling diodes. The motor terminals (*a*, *b* and *c*) are connected to the mid-point of each inverter leg. The motor phase windings are Y-connected, ‘n’ is the neutral point which is not grounded and ‘g’ is the inverter ground. The inverter leg voltages (with respect to ground ‘g’) are denoted by $V_{ag}$, $V_{bg}$ and $V_{cg}$ and the motor phase voltages (with respect to neutral ‘n’) are

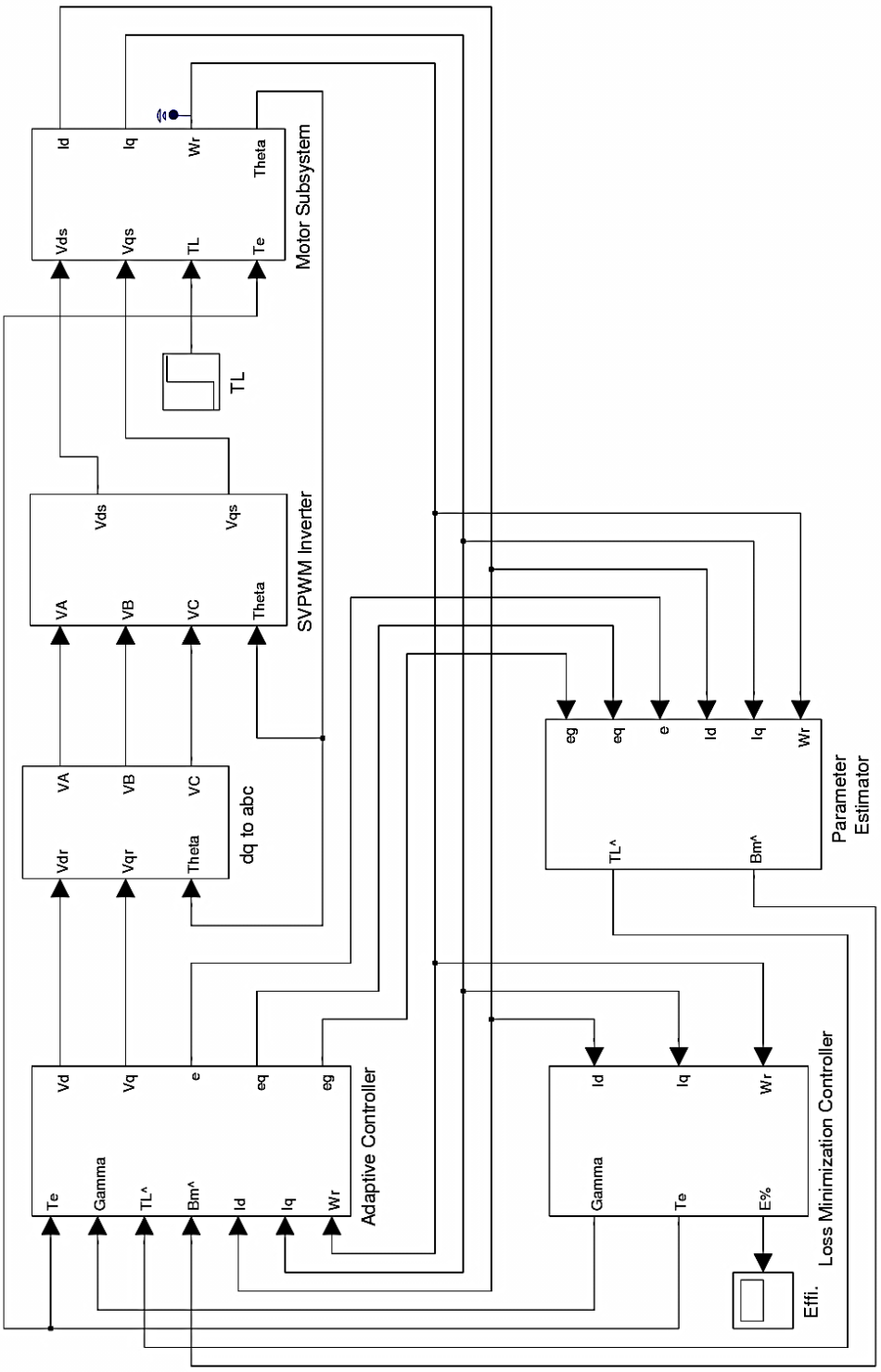


Fig. 4.2: Simulink schematic of the complete loss minimization based ABNC for IPMSM drive.

denoted by $V_{an}$, $V_{bn}$, and $V_{cn}$. By using Kirchhoff's voltage law to the inverter motor circuit $V_{an}$, $V_{bn}$, and $V_{cn}$ can be easily derived as:

$$\begin{bmatrix} V_{an} \\ V_{bn} \\ V_{cn} \end{bmatrix} = \begin{bmatrix} \frac{2}{3} & -\frac{1}{3} & -\frac{1}{3} \\ -\frac{1}{3} & \frac{2}{3} & -\frac{1}{3} \\ -\frac{1}{3} & -\frac{1}{3} & \frac{2}{3} \end{bmatrix} \begin{bmatrix} V_{ag} \\ V_{bg} \\ V_{cg} \end{bmatrix} \tag{4.32}$$

Eqn. (4.32) implies that it is possible to express the motor phase voltages $V_{abcn}$ from the inverter leg voltage $V_{abcg}$. The basic operation of the 3-phase inverter can be explained by considering the single inverter leg. For example, if switch SW1 is logic '1' or 'on' and switch is logic '0' or 'off' would establish $V_{dc}$ across terminals 'a' and 'g', therefore $V_{ag} = V_{dc}$. On the other hand, if switch SW1 is logic '0' and switch SW4 is logic '1' would apply zero voltage across 'a' and 'g', therefore $V_{ag} = 0$. Setting both SW1 and SW4 to logic '1' would short the voltage bus to ground, thus a dead time must be included in switching logic intentionally delaying the all off-on transitions of the transistor switches.

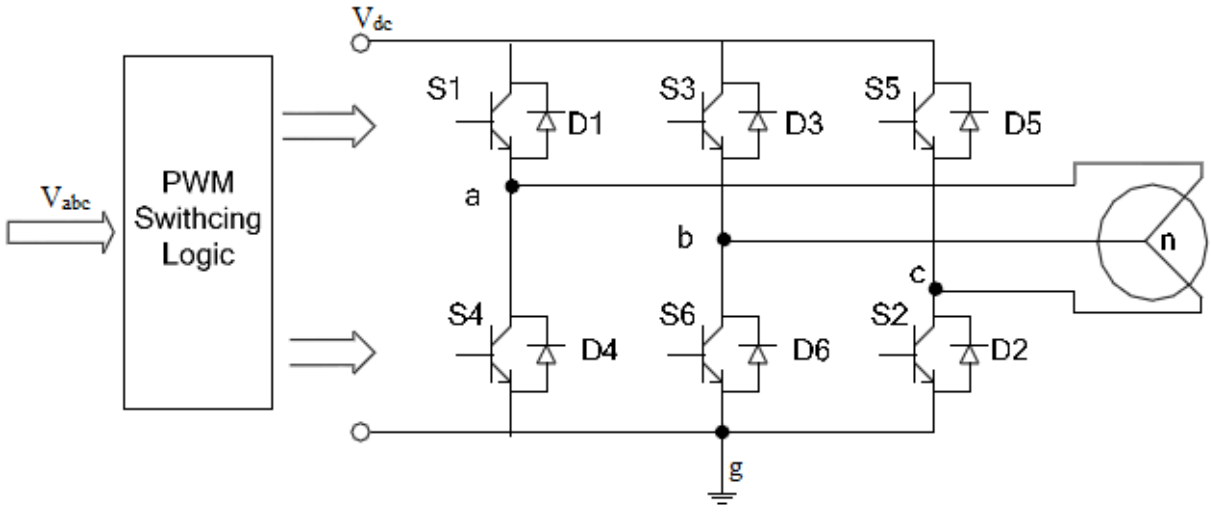


Fig. 4.3: Three-phase inverter feeding a Y-connected IPMSM.

Table 4.1: Inverter states and corresponding invert leg voltages and motor phase voltages.

| Phase state 'abc' | $V_{ag}$ | $V_{bg}$ | $V_{cg}$ | $V_{an}$ | $V_{bn}$ | $V_{cn}$ |
|---|---|---|---|---|---|---|
| 000 | 0 | 0 | 0 | 0 | 0 | 0 |
| 001 | 0 | 0 | $V_{dc}$ | $-1/3V_{dc}$ | $-1/3V_{dc}$ | $2/3V_{dc}$ |
| 010 | 0 | $V_{dc}$ | 0 | $-1/3V_{dc}$ | $2/3V_{dc}$ | $-1/3V_{dc}$ |
| 011 | 0 | $V_{dc}$ | $V_{dc}$ | $-2/3V_{dc}$ | $1/3V_{dc}$ | $1/3V_{dc}$ |
| 100 | $V_{dc}$ | 0 | 0 | $2/3V_{dc}$ | $-1/3V_{dc}$ | $-1/3V_{dc}$ |
| 101 | $V_{dc}$ | 0 | $V_{dc}$ | $1/3V_{dc}$ | $-2/3V_{dc}$ | $1/3V_{dc}$ |
| 110 | $V_{dc}$ | $V_{dc}$ | 0 | $1/3V_{dc}$ | $1/3V_{dc}$ | $-2/3V_{dc}$ |
| 111 | $V_{dc}$ | $V_{dc}$ | $V_{dc}$ | 0 | 0 | 0 |

During the dead time, both SW1 and SW4 are simultaneously logic '0' and the direction of current $i_a$ will determine the actual voltage. If $i_a < 0$, then $V_{ag} = V_{dc}$ and diode D1 will conduct. If $i_a > 0$, then $V_{ag} = 0$ and diode D4 will conduct. Since the on-and-off states of the power switches in one inverter leg are always opposite without considering the dead time, each inverter leg can be in either of two states. Therefore, the 3-phase inverter as a whole can be in any of possible eight states. Table 4.1 summarizes these eight inverter states and corresponding invert leg voltages and motor phase voltage using the relations in Eqn. (4.32).

## 4.4.2 Pulse Width Modulation (PWM)

There are many possible PWM techniques proposed. The classifications of PWM techniques can be given as follows [3]:

- Sinusoidal PWM (SPWM)

- Selected harmonic elimination PWM
- Minimum ripple current PWM
- Space vector modulation PWM (SVM)
- Random PWM
- Hysteresis band current control PWM
- Sinusoidal PWM with instantaneous current control
- Delta modulation
- Sigma-delta modulation

Often, PWM techniques are classified on the basis of voltage or current control, feed-forward or feedback methods, carrier- or non-carrier-based control, etc. The well-known PWM techniques are sinusoidal PWM, hysteresis PWM, and SVM. The PWM strategies considered in this thesis are sinusoidal PWM and hysteresis PWM.

The sinusoidal PWM technique is very popular for industrial converters. Fig. 4.4 explains the general principle of SPWM, where common triangle carrier wave of fixed amplitude and frequency is compared with the 3-phase reference voltages of variable amplitude and frequency from the controller and the points of intersection determine the switching points of power devices [3]. In the entire control system, the inverter reference signals are initially issued in the *dq* coordinates from the controller and then transformed into the *abc* coordinates. Each comparator output forms the switching-state of the corresponding inverter leg. The switching logic of the corresponding inverter leg are given as follows:

If $V_{a,ref} > V_{triangle}$, SW1 = 1 (on) and SW4 = 0 (off), State 1 for phase a

If $V_{a,ref} < V_{triangle}$, SW1 = 0 and SW4 = 1, State 0 for phase a

If $V_{b,ref} > V_{triangle}$, SW3 = 1 and SW6 = 0, State 1 for phase b

If $V_{b,ref} < V_{triangle}$, SW3 = 0 and SW6 = 1, State 0 for phase b

If $V_{c,ref} > V_{triangle}$, SW5 = 1 and SW2 = 0, State 1 for phase c

If $V_{c,ref} < V_{triangle}$, SW5 = 0 and SW6 = 1, State 0 for phase c

The sinusoidal reference voltage establishes the desired fundamental frequency of the inverter output, while the triangular carrier wave establishes the switching frequency of the inverter.

Hysteresis PWM is basically an instantaneous feedback current control method of PWM. It is very simple to implement and taking care directly for the current control. In hysteresis PWM, the switch logic is realized by three hysteresis controllers, one for each phase. Each controller determines the switching state of one inverter leg in such a way that the corresponding actual current is maintained within a hysteresis band $\Delta i$ of reference current. To increase a phase current,

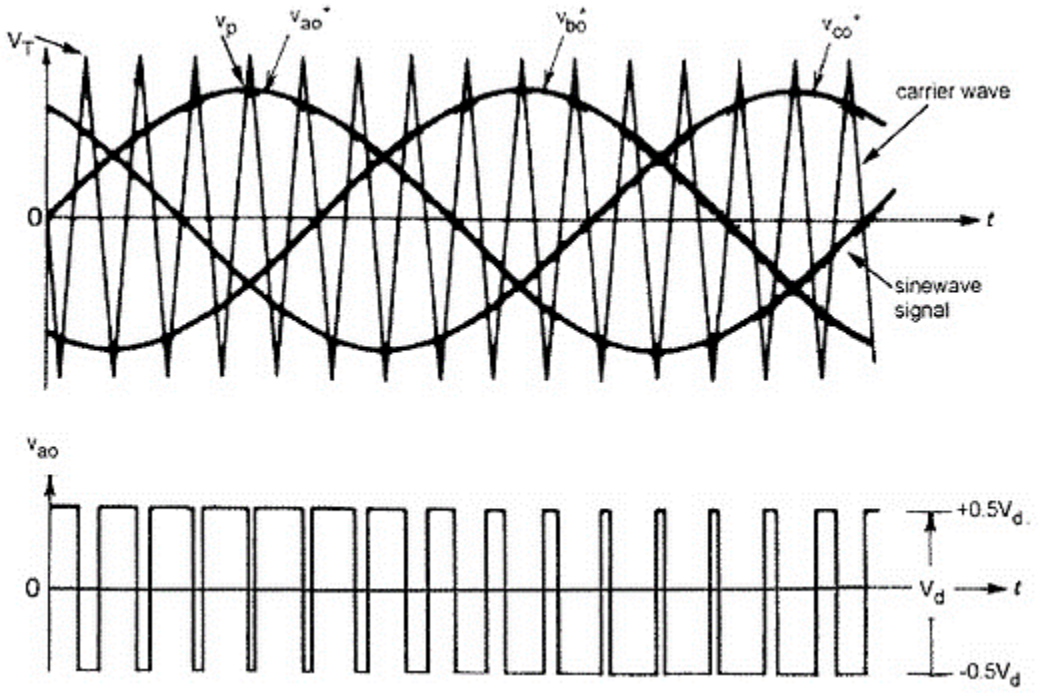


Fig. 4.4: Principle of sinusoidal PWM for three-phase bridge inverter.

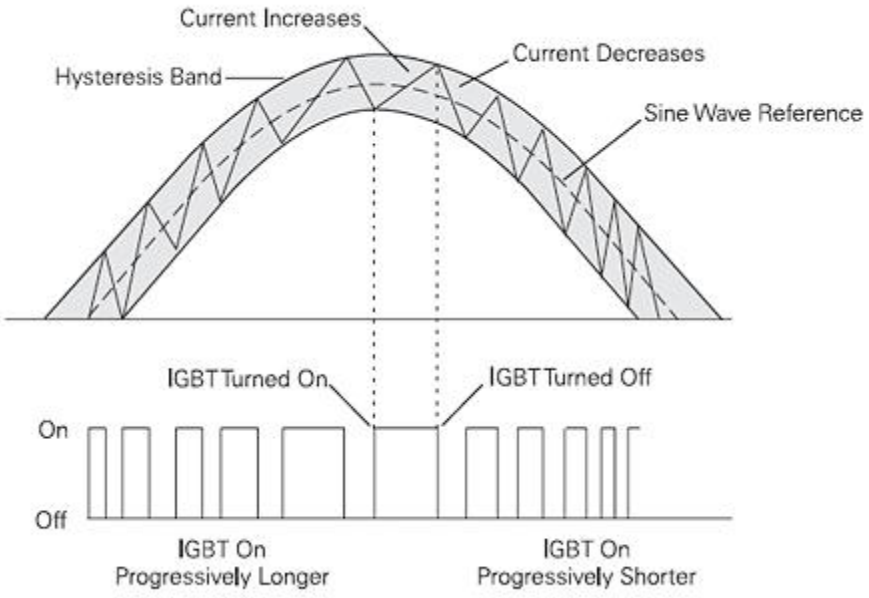


Fig. 4.5: Principle of hysteresis-band current control PWM.

the corresponding inverter leg voltage is equal to the $V_{dc}$ until the upper band-range is reached. Then, the negative $V_{dc}$ is applied until the phase current drops to the lower limit of a hysteresis. Due to the elimination of an additional current controller, the motor parameter dependence is very low. However, PWM frequency is not fixed and switching frequency increase at lower modulation. Fig. 4.5 explains the operation principle of hysteresis PWM for a half-bridge inverter. In simulation the sinusoidal PWM and hysteresis PWM are used for ABNC and PI control, respectively.

### 4.4.3 Design of PI Controller for Comparison

In order to prove the superiority of the proposed ABNC and NFC, a simple PI controller is designed for speed control. The input to the PI controller is the speed error and the output is the torque component current $i_q^*$. The speed controller can be described as:

$$i_q^* = K_P \Delta\omega_r + K_I \int \Delta\omega_r \, dt$$

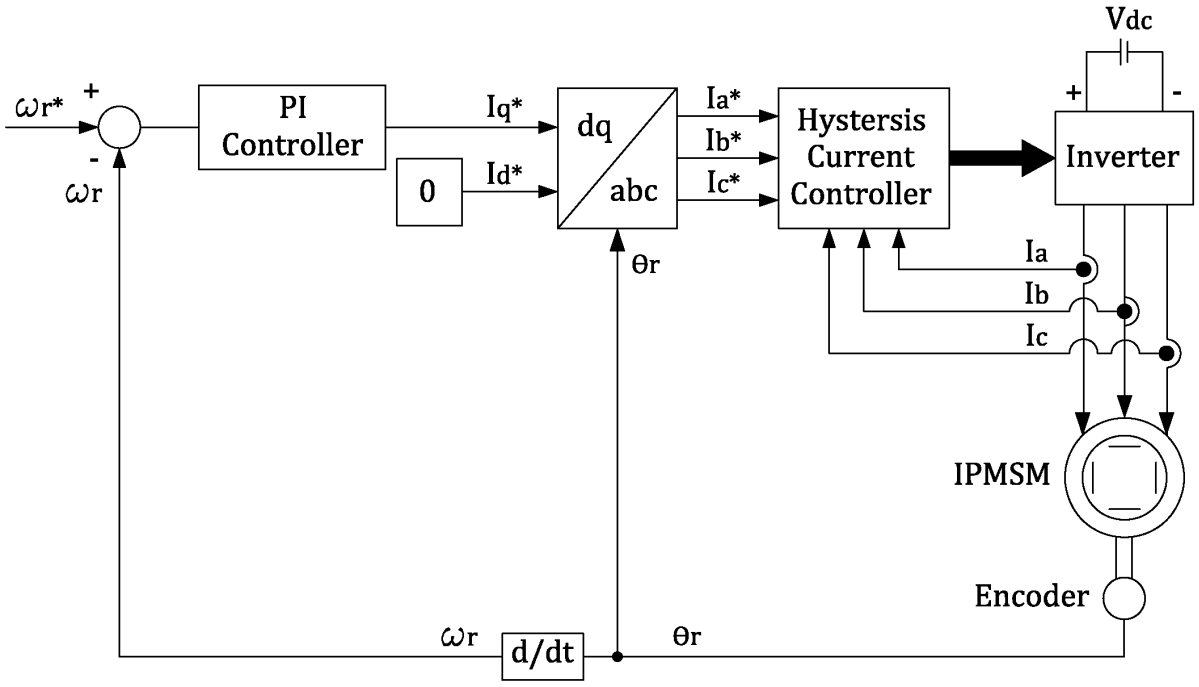


Fig. 4.6: Block diagram of the simple PI controller based IPMSM drive for speed control.

where, $\Delta\omega_r$ is the speed error between actual and command speeds, $K_P$ is the proportional gain and $K_I$ is the integral gain for the PI type speed controller. At first the PI controller gains are selected as $K_P = 0.7$ and $K_I = 2$ to avoid overshoot but the controller becomes sluggish. In order to get the best performance, the PI control parameters are played around these values by trial and error. The parameters of the PI controller are chosen by trial and error such that it gives the best performance at the steady-state condition with minimum overshoot, minimum settling time and zero steady-state error based on simulation results. The final controller gains are found to be $K_P = 1$ and $K_I = 7$. The command d-axis current is considered as zero. These d- and q-axis command currents are transformed into *abc* coordinates and fed to a hysteresis current controller, which is used to generate the PWM gate signals for the inverter. The block diagram of the IPMSM drive with PI speed controller is shown in Fig. 4.6.

### 4.4.4 Simulation Results and Discussion

The complete closed loop vector control of IPMSM drive incorporating the proposed loss minimization based ABNC has been investigated extensively at different operating conditions. A performance comparison between conventional PI controller and proposed ABNC is also provided to show the superiority of the controllers. The performance of the proposed LMA is also compared with conventional $i_d = 0$ control scheme. First, the high dynamic performance results are shown for PI controller and ABNC, then the loss minimization results are shown for proposed controller with LMA and without LMA at different operating conditions. The sample results are shown below.

Fig. 4.7(a) shows the PI control speed response for the command speed of 183 rad/s at full load (19 Nm) condition. The actual speed converges to the command speed with an overshoot. The starting current is also high as seen from Fig. 4.7(b). The actual motor phase current $i_a$, speed error and three phase currents are shown in Fig. 4.7(c)-(e), respectively. It is found in Fig. 4.8 that the settling time is less and the actual speed converges with the command speed with negligible overshoot and no steady state error for ABNC scheme. The starting current is also less compared with conventional PI controller. The d- and q-axis currents and line current are shown in Fig. 4.8(b) and (c), respectively. Fig. 4.9(a)-(c) show the corresponding tracking errors of q-axis current, gamma function and speed defined in backstepping design which all converge to zero. Thus, it ensures the global stability of the drive system. The estimated load torque, friction constant and developed torque are shown in Fig. 4.10. These estimated values are not exactly following the nominal values. The reason is that the nominal values are measured with lot of assumptions and the purpose of adaptive controller is to adjust the parameter values with online changing conditions. The speed response and corresponding three phase currents, d- and q-axis currents and

speed error of the PI controller at rated speed (183 rad/s) with 50% rated load (9.5 Nm) are shown in Fig. 4.11. It is observed that it has high overshoot of about 3.83% and long settling time (0.6sec) at that condition. The speed response, line current, and d-q axes currents of the proposed ABNC at rated speed (183 rad/s) with 50% rated load (9.5 Nm) are shown in Fig. 4. 12 (a)-(c). The speed of the proposed ABNC drive can follow the command speed with less (1.64%) overshoot. But the settling time is little longer (0.7sec). The corresponding speed error and virtual control variable errors are shown in Fig. 4.13. All the errors converges to zero which indicate that stability of the drive at 50% rated load. Fig. 4.14 (a)-(c) shows the corresponding estimated load torque, friction coefficient and developed torque, respectively.

To test the robustness of the controller, disturbance is applied by change of load which is a very common type of disturbance. The robustness of the proposed controller is tested and compared with PI controller. Fig. 4.15 (a)-(d) shows the speed response, d- and q- axis currents, line current and speed error with step increase of load from 50% load (9.5 Nm) to rated load (19 Nm) at t=1s for PI controller, and proposed ABNC responses are shown in Fig. 4.16. In the case of PI controller, speed response has a high overshoot at start with 50% load and the speed deviation from the command speed is high with change of load. On other side, the proposed ABNC has a fairly low overshoot at start with 50% load as compared to conventional PI controller. But the speed deviation from the command speed is higher with change of load and also the settling time is longer. The d axis and q axis current converge to new value so that the motor actual speed follows the command speed. The line current of the controller is shown in Fig. 4.16(c) and the corresponding d-q axis currents are shown in Fig. 4.16(b). The speed error and virtual control errors are shown in Fig. 4.17. In Fig. 4.18(a)-(c), estimated load torque, friction constant and developed torque are shown. The developed torque converges to load torque with change of load

and all error variables converge to zero. The estimated load torque tries to follow the actual load torque.

For high performance drive application it is essential to follow the command speed when sudden change of command speed is needed without any overshoot, and zero steady-state error. The responses of the PI controller and ABNC for a change of command speed from 150 rad/s to 183 rad/s at t=1s at 50% rated load (9.5 Nm) are shown in Figs. 4.19 and 4.20, respectively. Fig. 4.19 shows that actual speed follows the command speed with 3% overshoot and settling time of 0.6 sec. which is not good for high performance system. Fig. 4.19(b)-(d) shows the corresponding d-q axis currents, phase currents and speed error. Fig. 4.20(a) shows the speed response which follows the command speed with 0.67% overshoot and settling time of approximately 0.4 sec. Fig. 4.20(b) and (c) shows the d-q axis currents and line ('a' phase) current, respectively. The virtual control errors and speed error are shown in Fig. 4.21. The estimated load torque, friction constant and developed torque are shown in Fig. 4.22. Thus, it is found that the proposed ABNC based drive has better performance than PI controller in the case of changing reference speed.

The performance of the proposed LMA along with ABNC is examined. Fig. 4.23 shows the responses of the efficiency and power loss with and without LMA. The simulation started with load torque of 19 Nm and the command speed of 183 rad/s. When the loss minimization is on, LMA calculates the optimum d-axis current level online based on the speed and motor parameters. It is observer that the LMA can improve the efficiency by almost 3% as compared to without any LMA. Next, the efficiency of the motor is observed in Fig. 4.24 with and without LMA at 50% load (9.5 Nm) and rated speed (183 rad/s). In Fig. 4.25 the efficiency is observed at full load (19 Nm) and command change in speed from 150 rad/s to 183 rad/s condition.

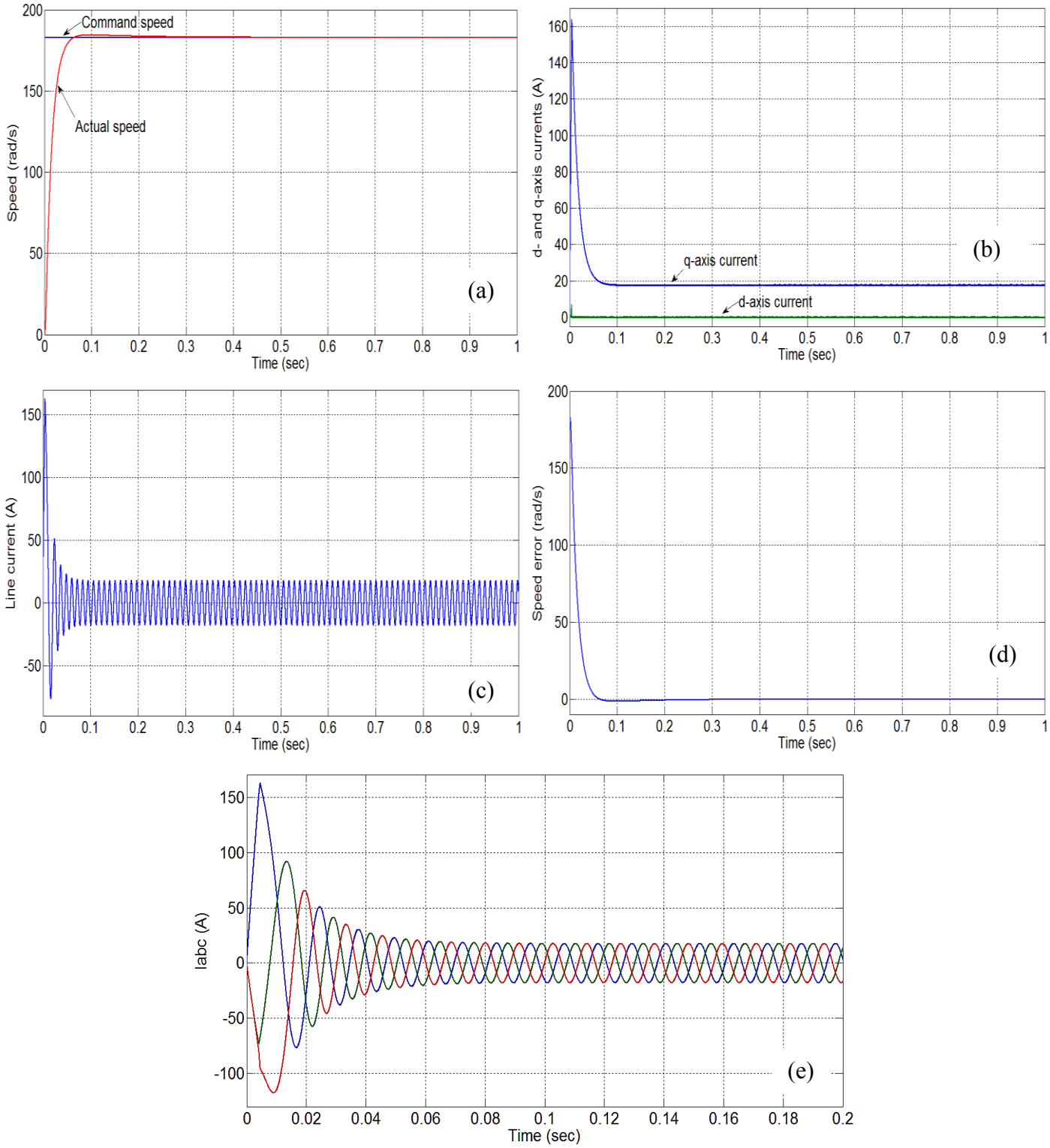


Fig. 4.7: Simulated response of PI controller based IPMSM drive at full load (19 Nm) and rated speed (183 rad/s); (a) speed, (b) d- and q-axis currents, (c) line current, (d) speed error, and (e) a, b and c phase currents.

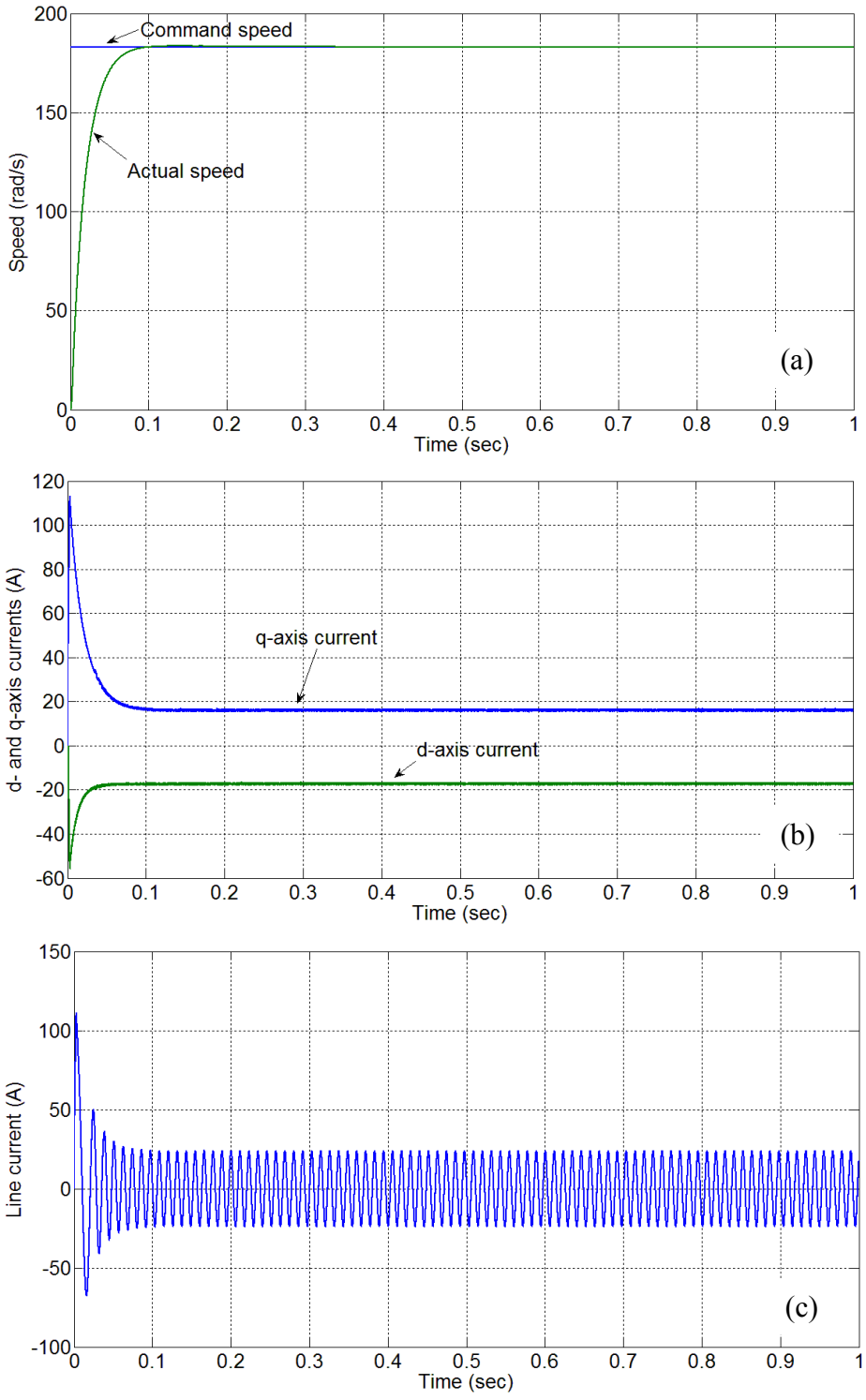


Fig. 4.8: Simulated response of the proposed ABNC based IPMSM drive at full load (19 Nm) and rated speed (183 rad/s); (a) speed, (b) d- and q-axis currents, and (c) line current.

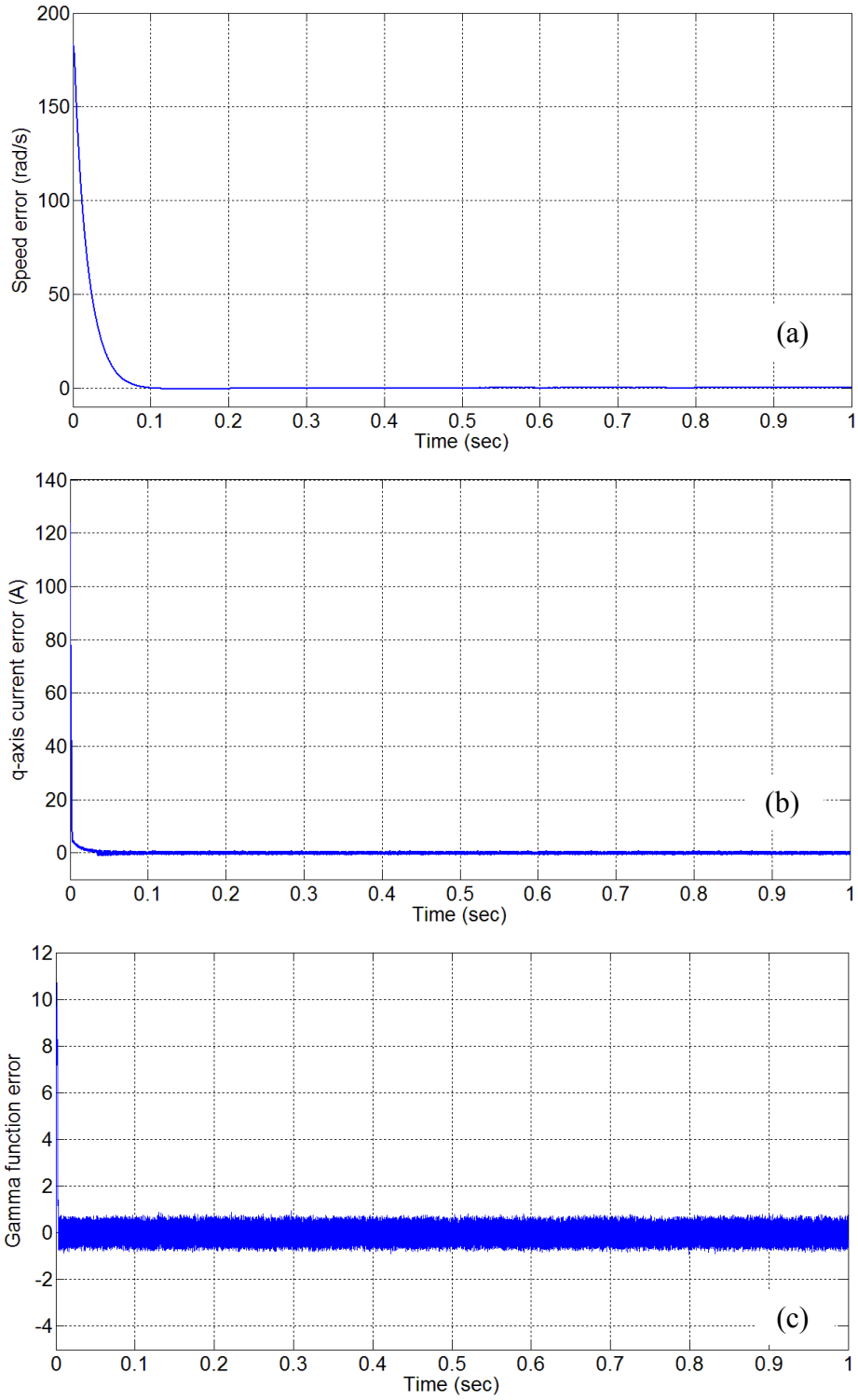


Fig. 4.9: Simulated response of the proposed ABNC based IPMSM drive at full load (19 Nm) and rated speed (183 rad/s); (a) speed error, (b) q-axis current error, $e_q$, and (c) gamma function error, $e_\gamma$.

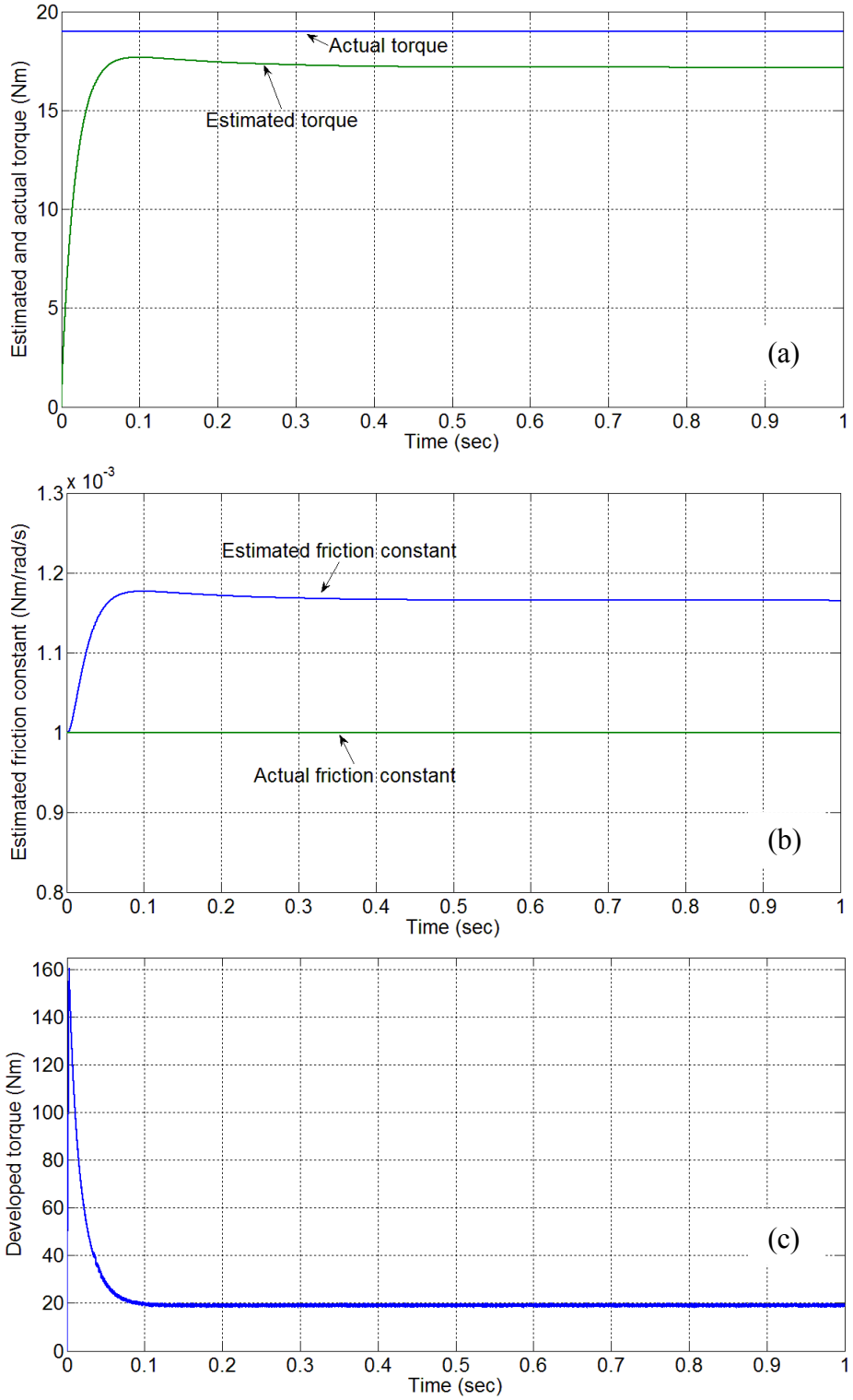


Fig. 4.10: Simulated response of proposed ABNC based IPMSM drive at full load (19 Nm) and rated speed (183 rad/s); (a) estimated load torque, (b) estimated friction constant, and (c) developed torque.

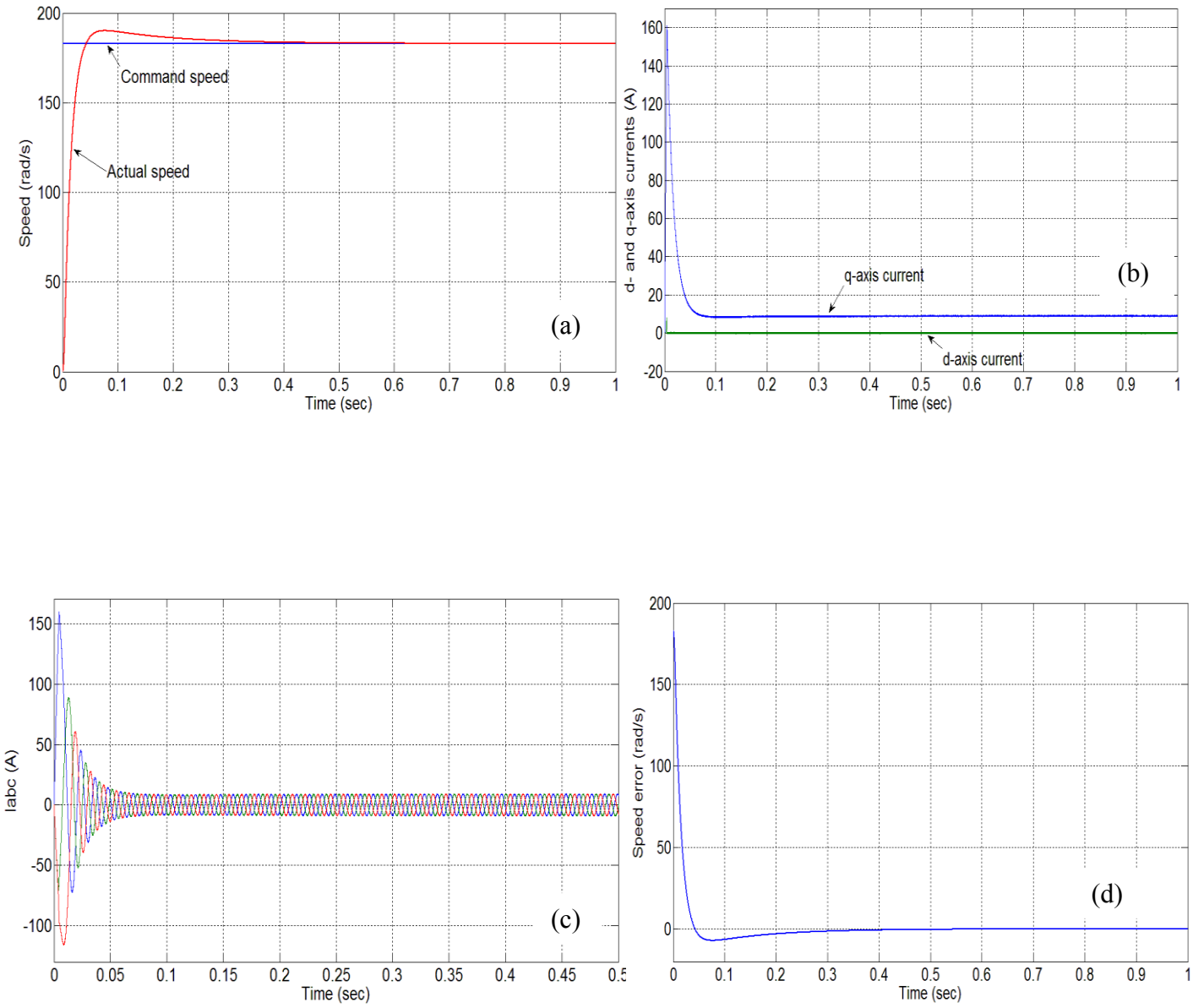


Fig. 4.11: Simulated response of the PI based IPMSM drive at 50% load (9.5 Nm) and rated speed (183 rad/s); (a) speed, (b) d- and q-axis currents, (c) three phase currents, and (d) speed error.

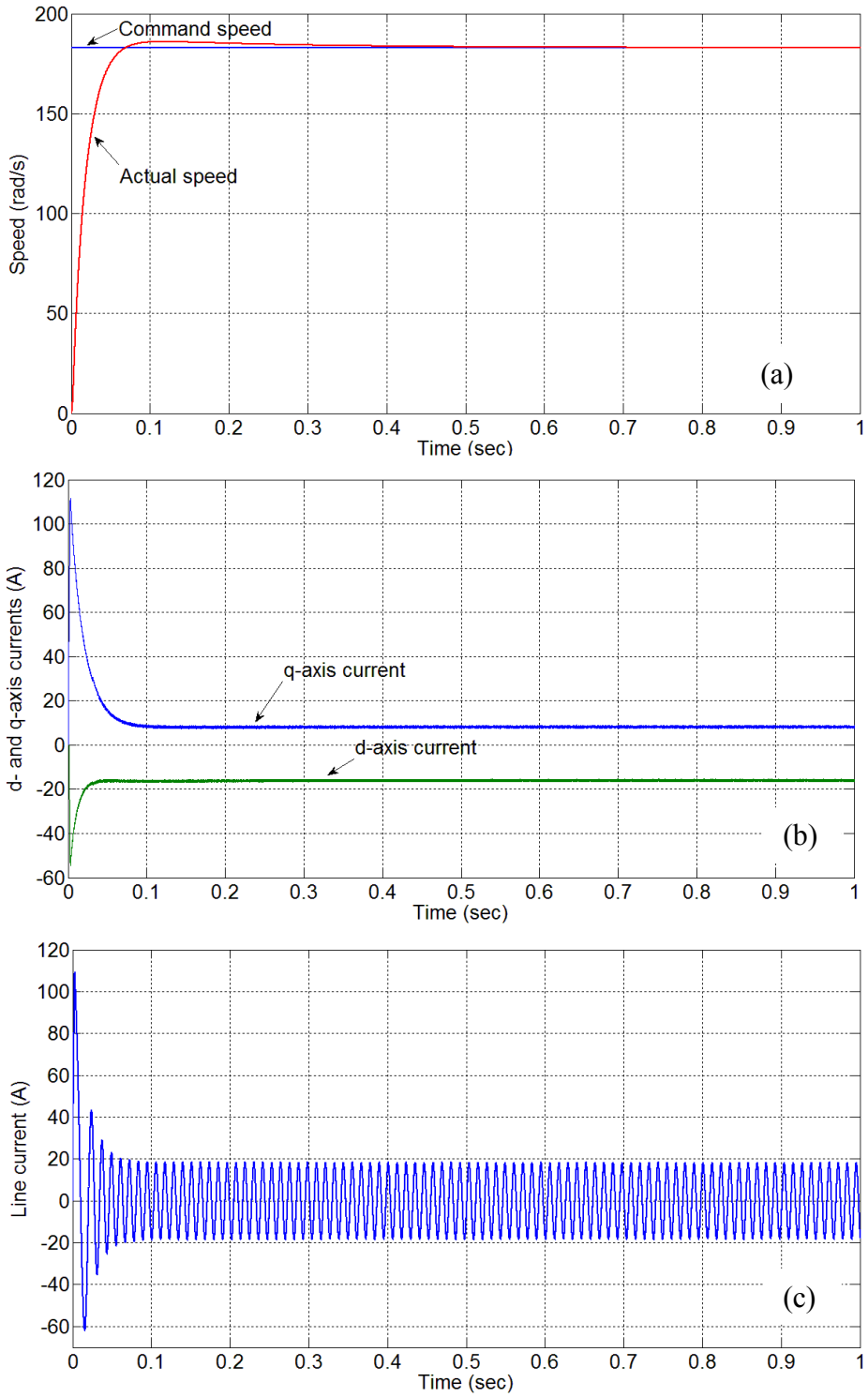


Fig. 4.12: Simulated response of the proposed ABNC based IPMSM drive at 50% load (9.5 Nm) and rated speed (183 rad/s); (a) speed, (b) d- and q-axis currents, and (c) line current.

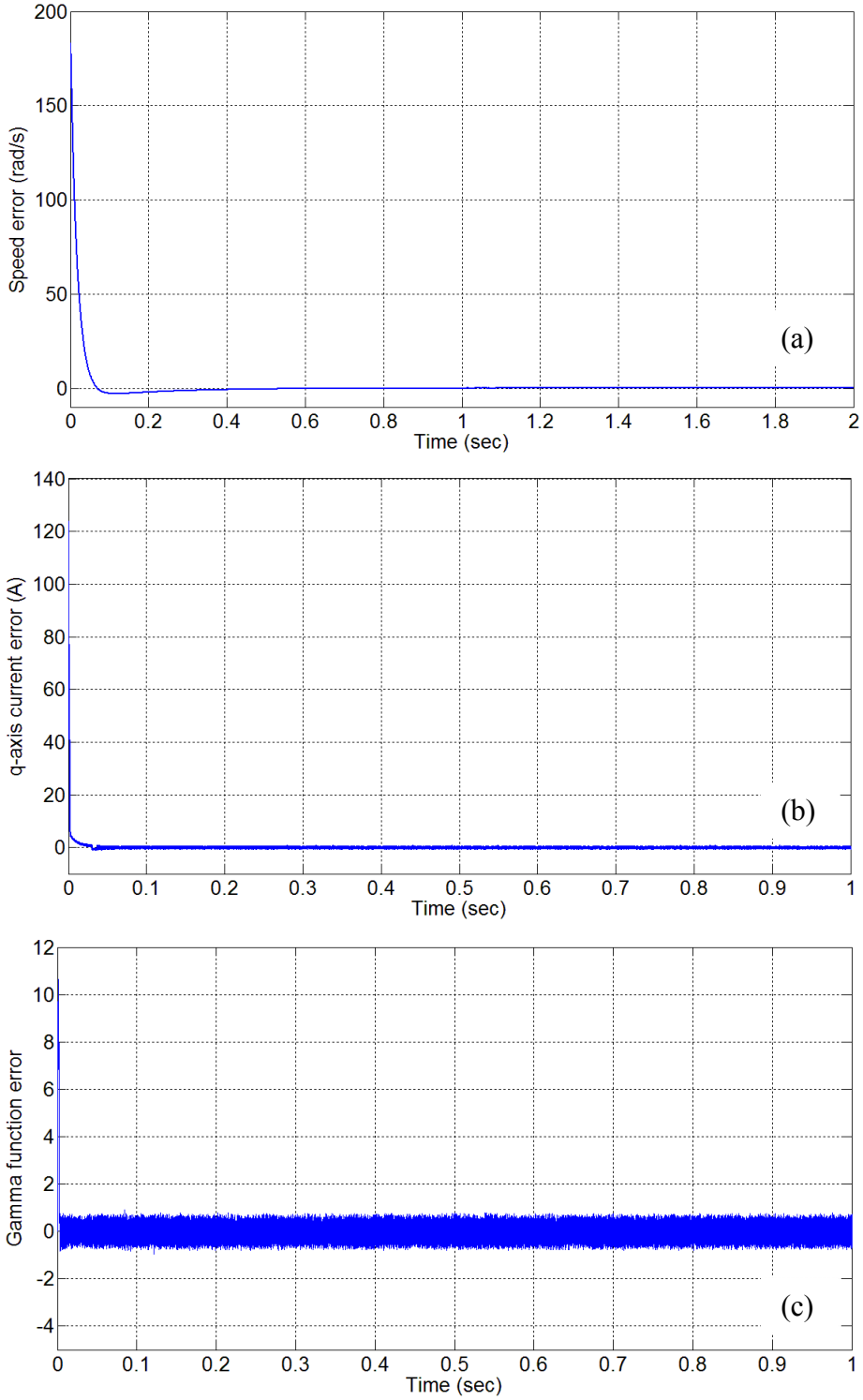


Fig. 4.13: Simulated response of the proposed ABNC based IPMSM drive at 50% load (9.5 Nm) and rated speed (183 rad/s); (a) speed error, (b) q-axis current error, $e_q$, and (c) gamma function tracking error, $e_\gamma$.

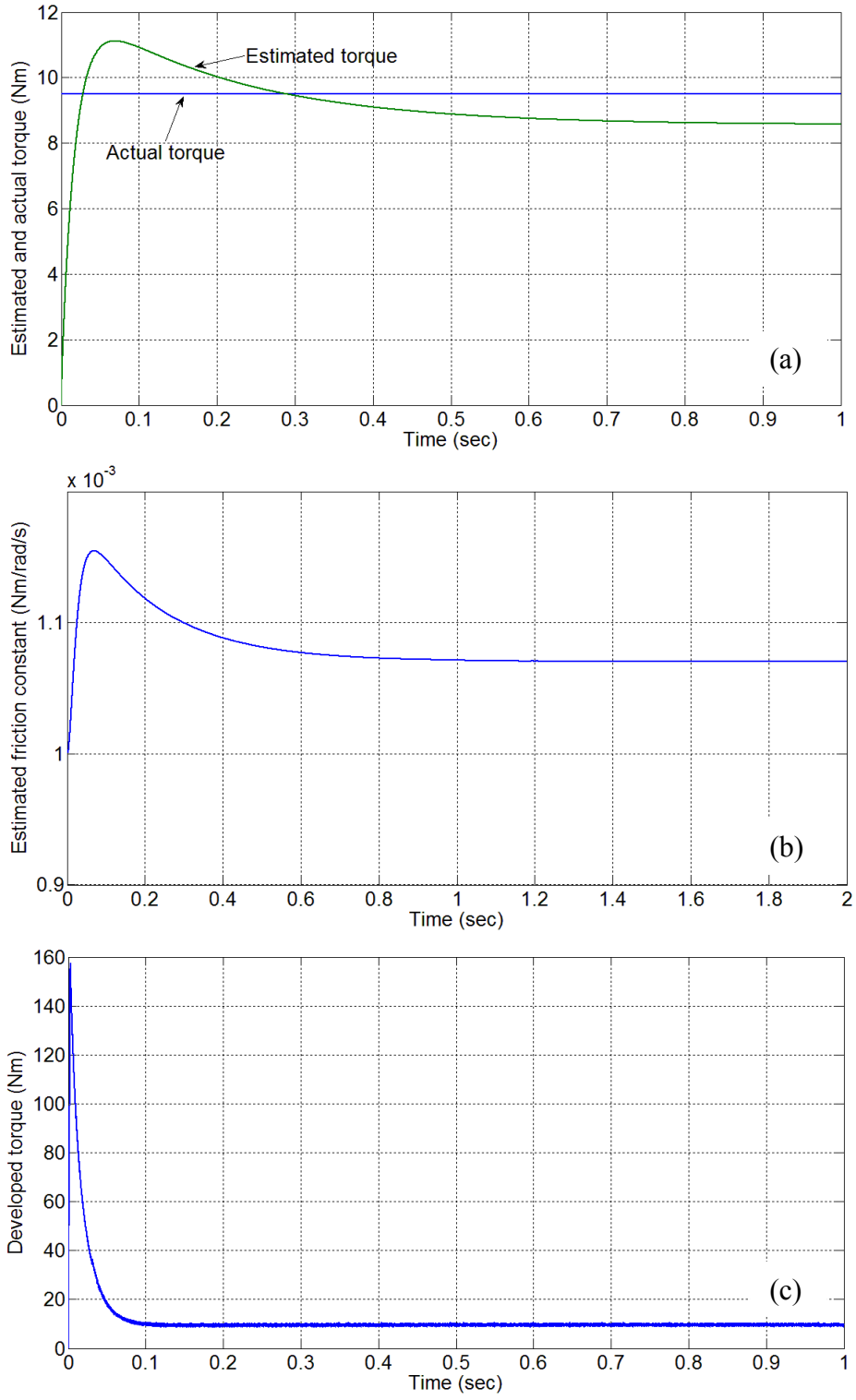


Fig. 4.14: Simulated response of the proposed ABNC based IPMSM drive at 50% load (9.5 Nm) and rated speed (183 rad/s); (a) estimated load torque, (b) estimated friction constant, and (c) developed torque.

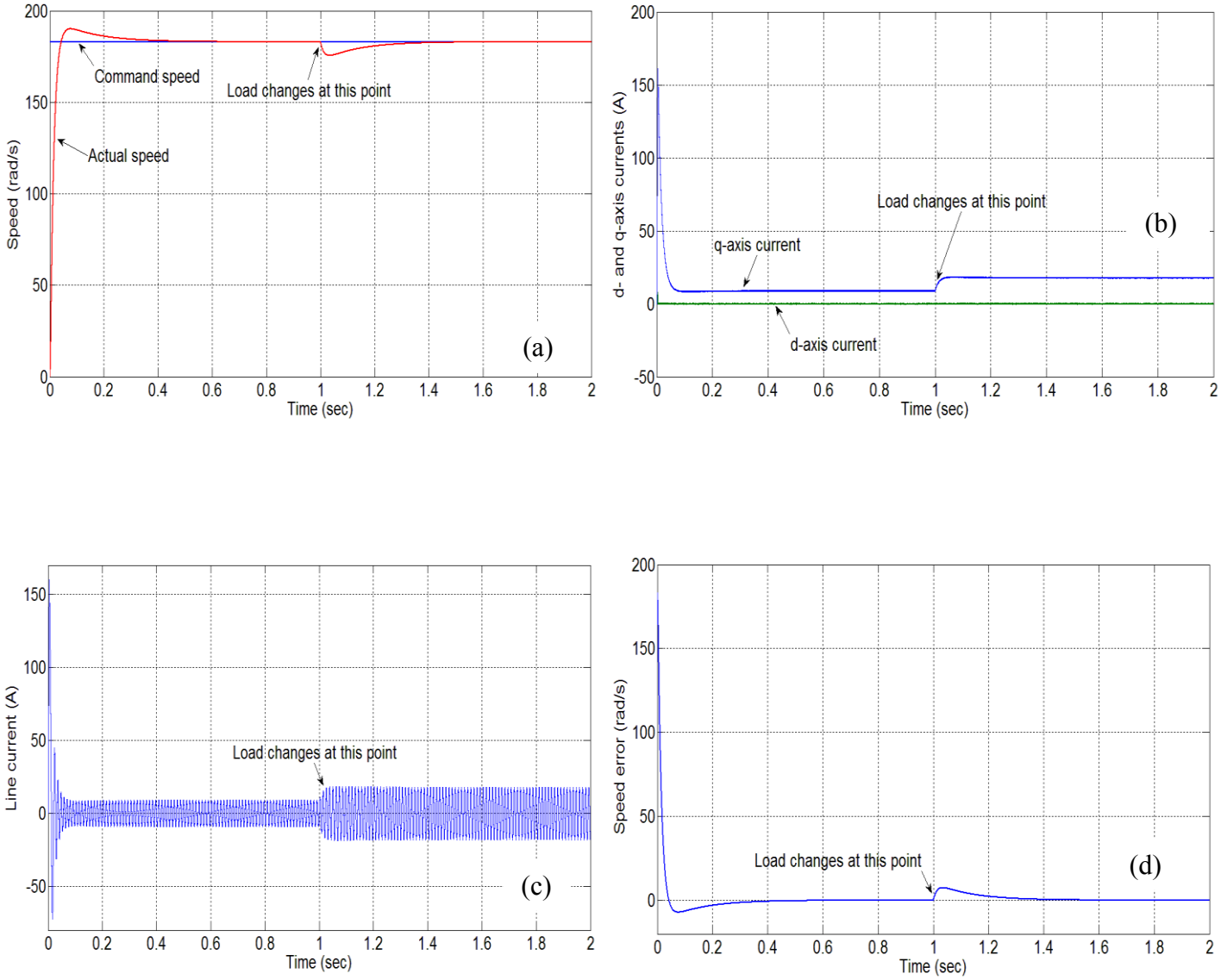


Fig. 4.15: Simulated response of PI controller based IPMSM drive for a step increase of load from 9.5 Nm to 19 Nm and rated speed (183 rad/s); (a) speed, (b) d- and q-axis currents, (c) line current, and (d) speed error.

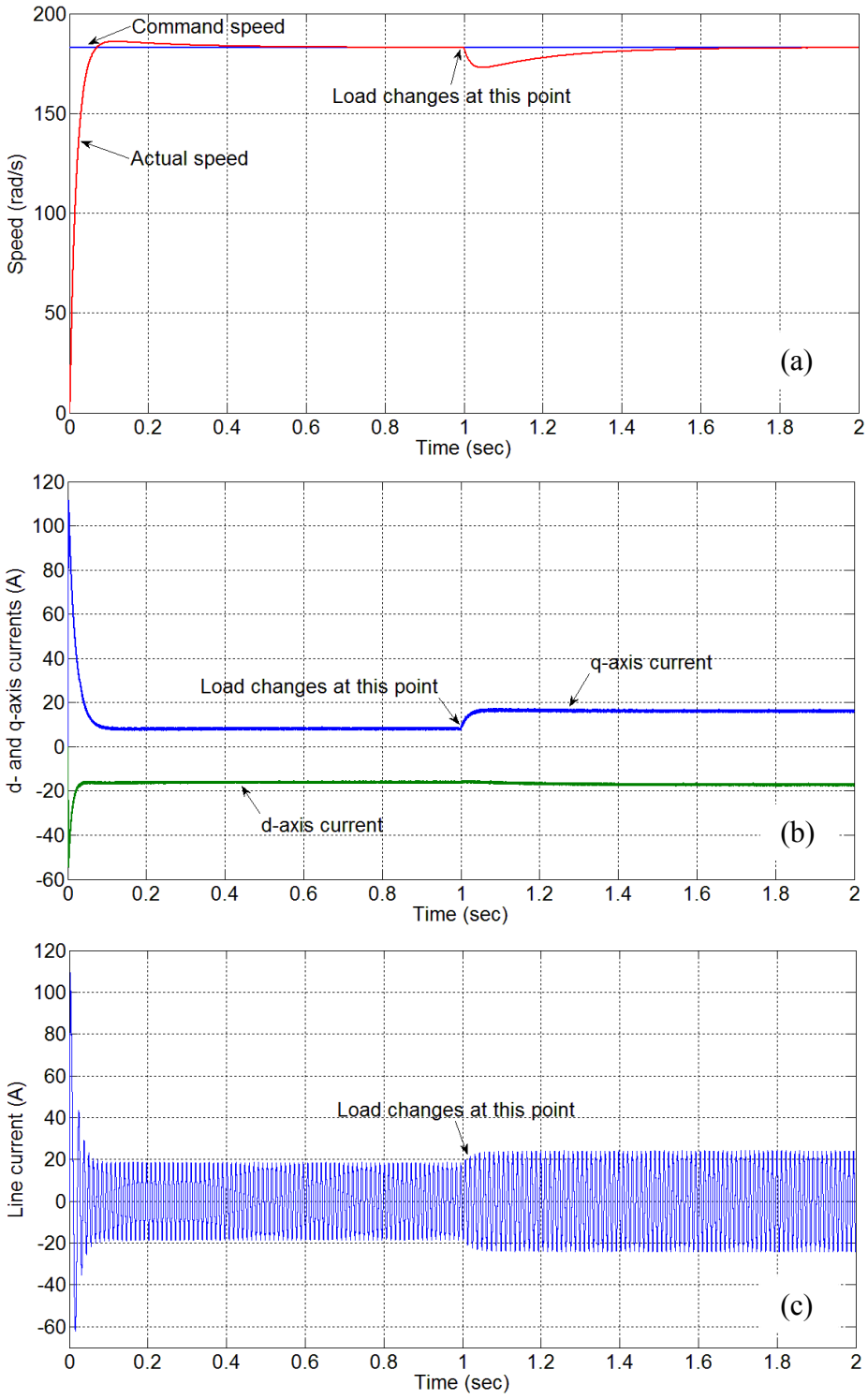


Fig. 4.16: Simulated response of the proposed ABNC based IPMSM drive for a step increase of load from 9.5 Nm to 19 Nm and rated speed (183 rad/s); (a) speed, (b) d- and q-axis currents, and (c) line current

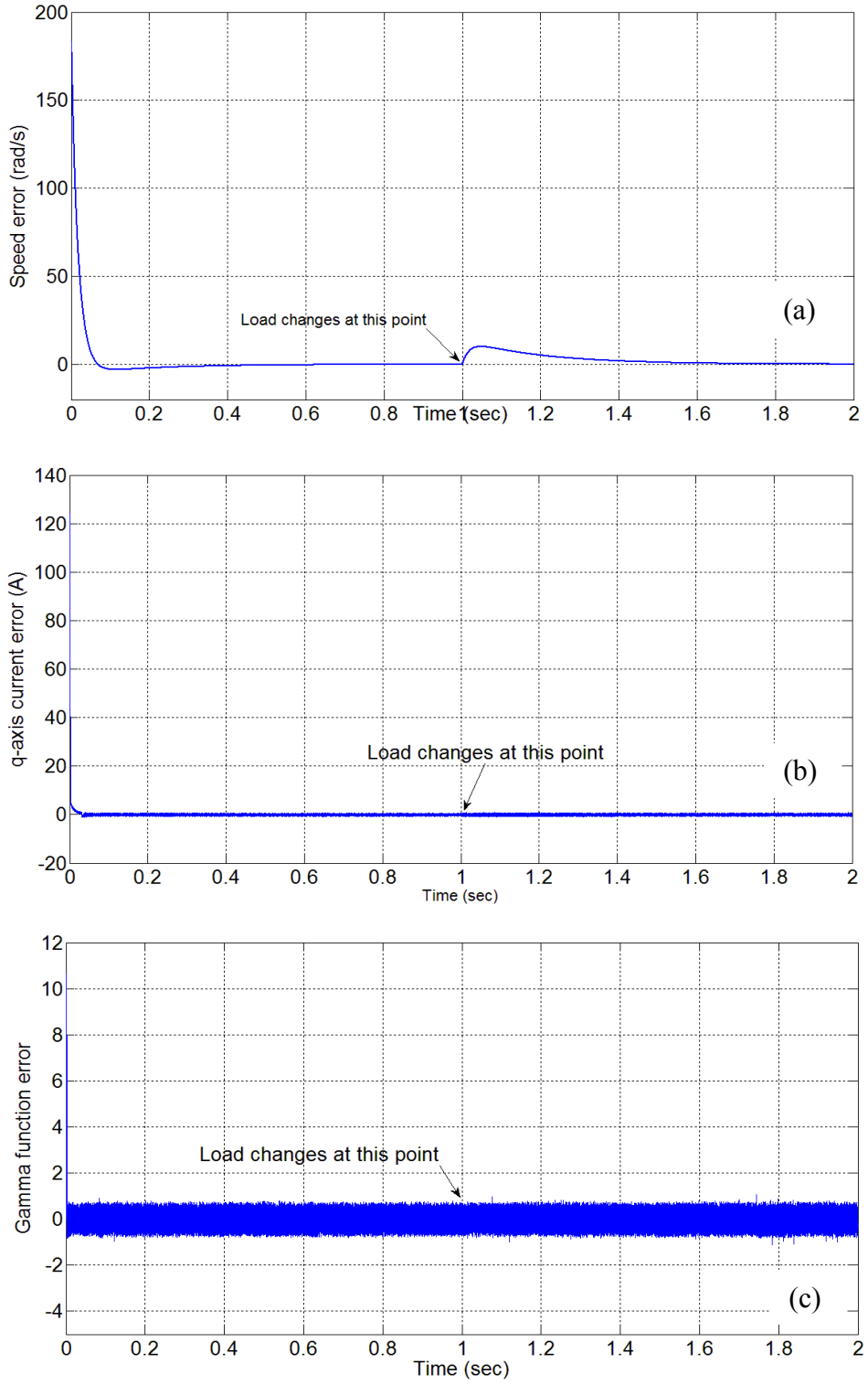


Fig. 4.17: Simulated response of the proposed ABNC based IPMSM drive for a step increase of load from 9.5 Nm to 19 Nm and rated speed (183 rad/s); (a) speed error, (b) q-axis current error, $e_q$, and (c) gamma function tracking error, $e_\gamma$.

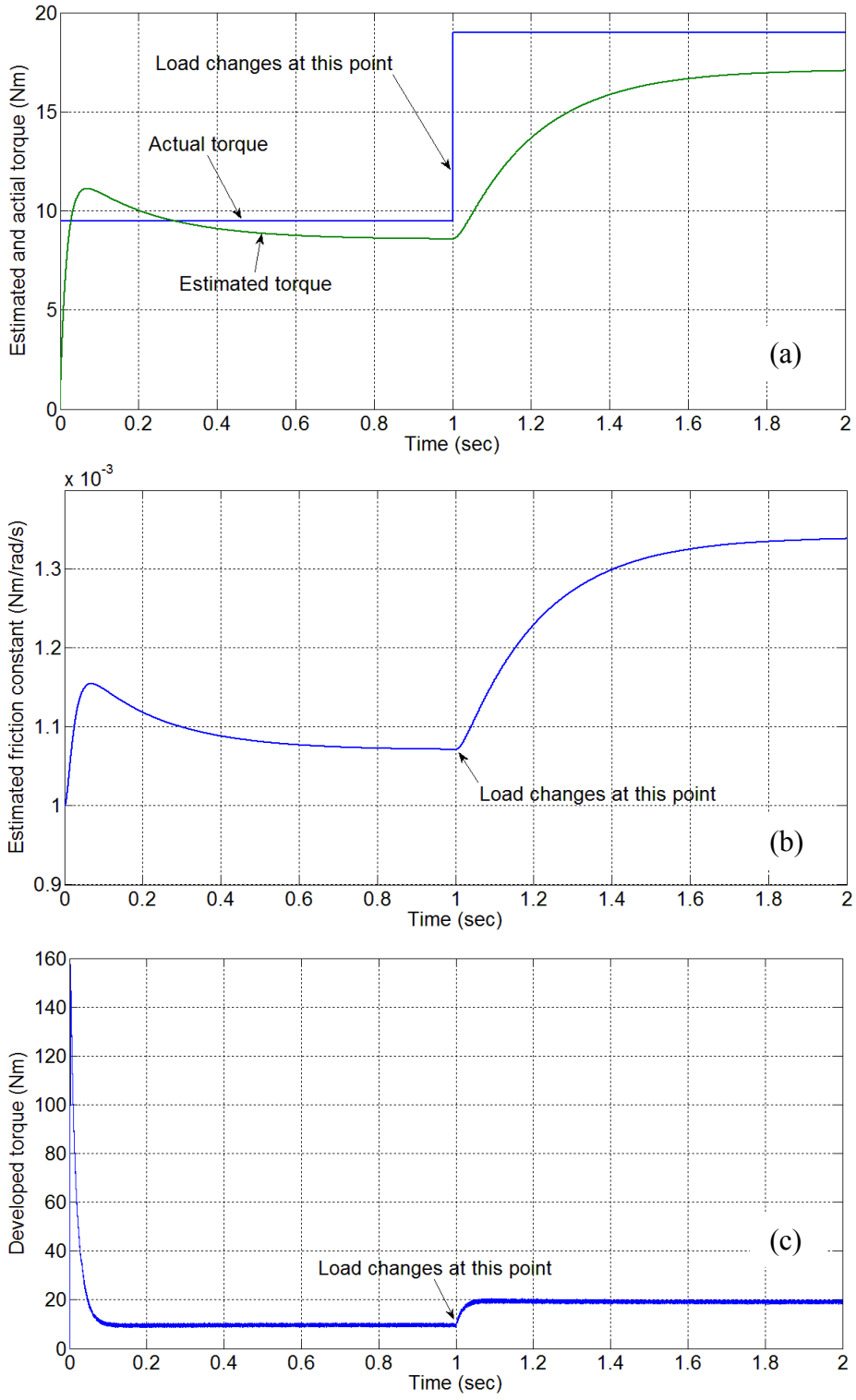


Fig. 4.18: Simulated response of the proposed ABNC based IPMSM drive for a step increase of load from 9.5 Nm to 19 Nm and rated speed (183 rad/s); (a) estimated load torque, (b) estimated friction constant, and (c) developed torque.

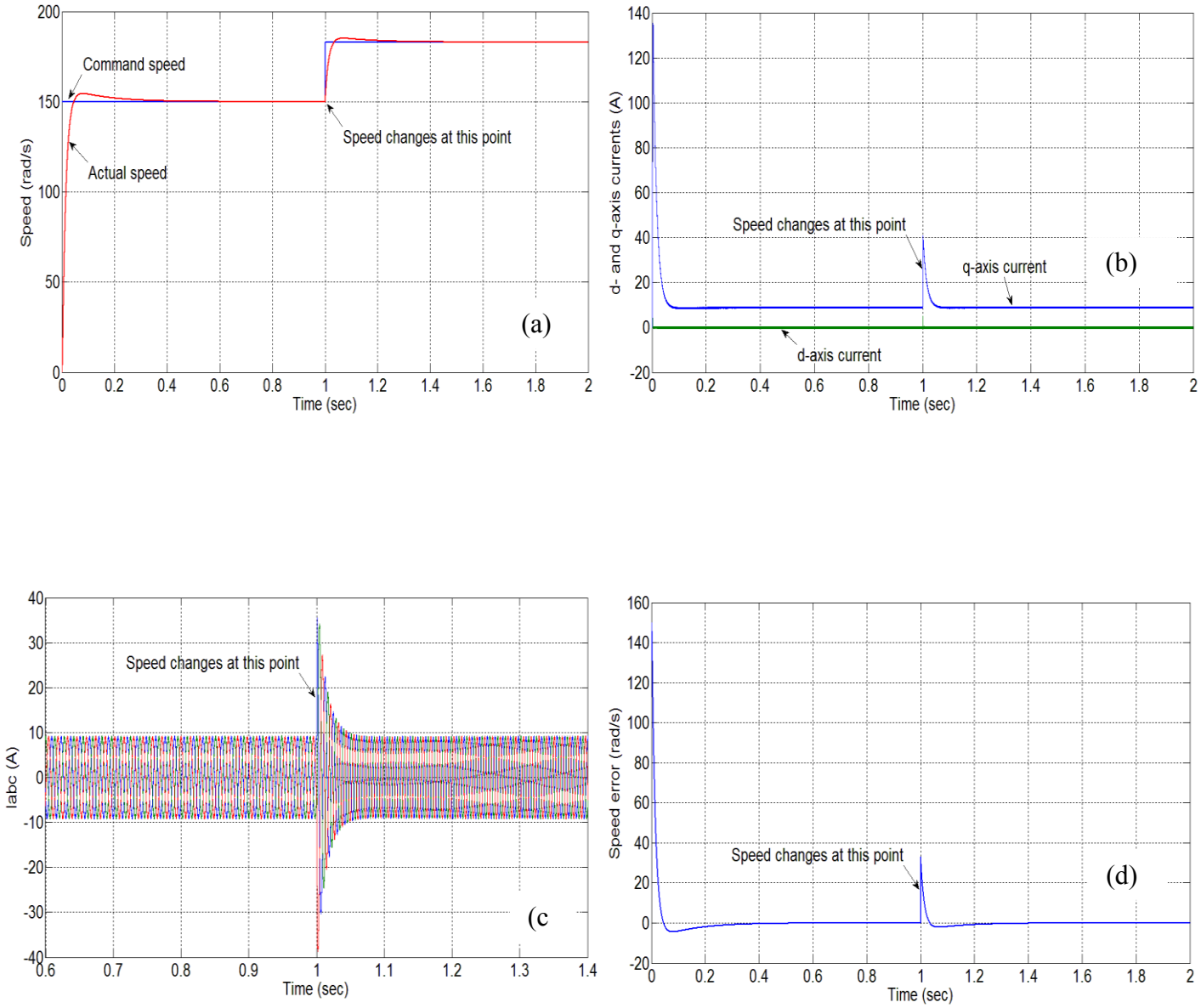


Fig. 4.19: Simulated response of PI controller based IPMSM drive for a step increase of speed command from 150 rad/s to 183 rad/s at 50% load (9.5 Nm); (a) speed, (b) d- and q-axis currents, (c) actual a, b and c phase currents, and (d) speed error.

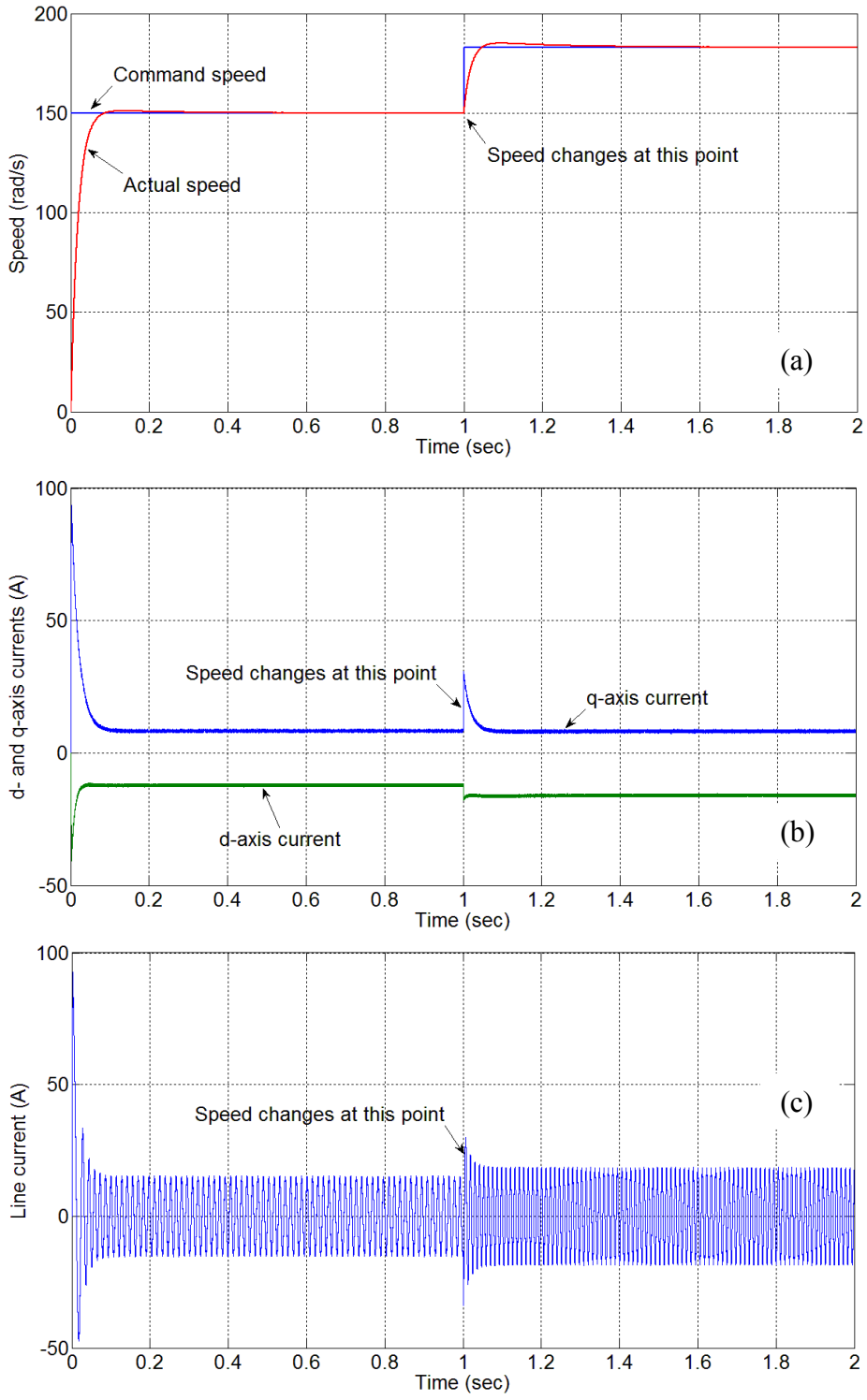


Fig. 4.20: Simulated response of the proposed ABNC based IPMSM drive for a step increase of speed command from 150 rad/s to 183 rad/s at 50% load (9.5 Nm); (a) speed, (b) d- and q-axis currents, and (c) line current.

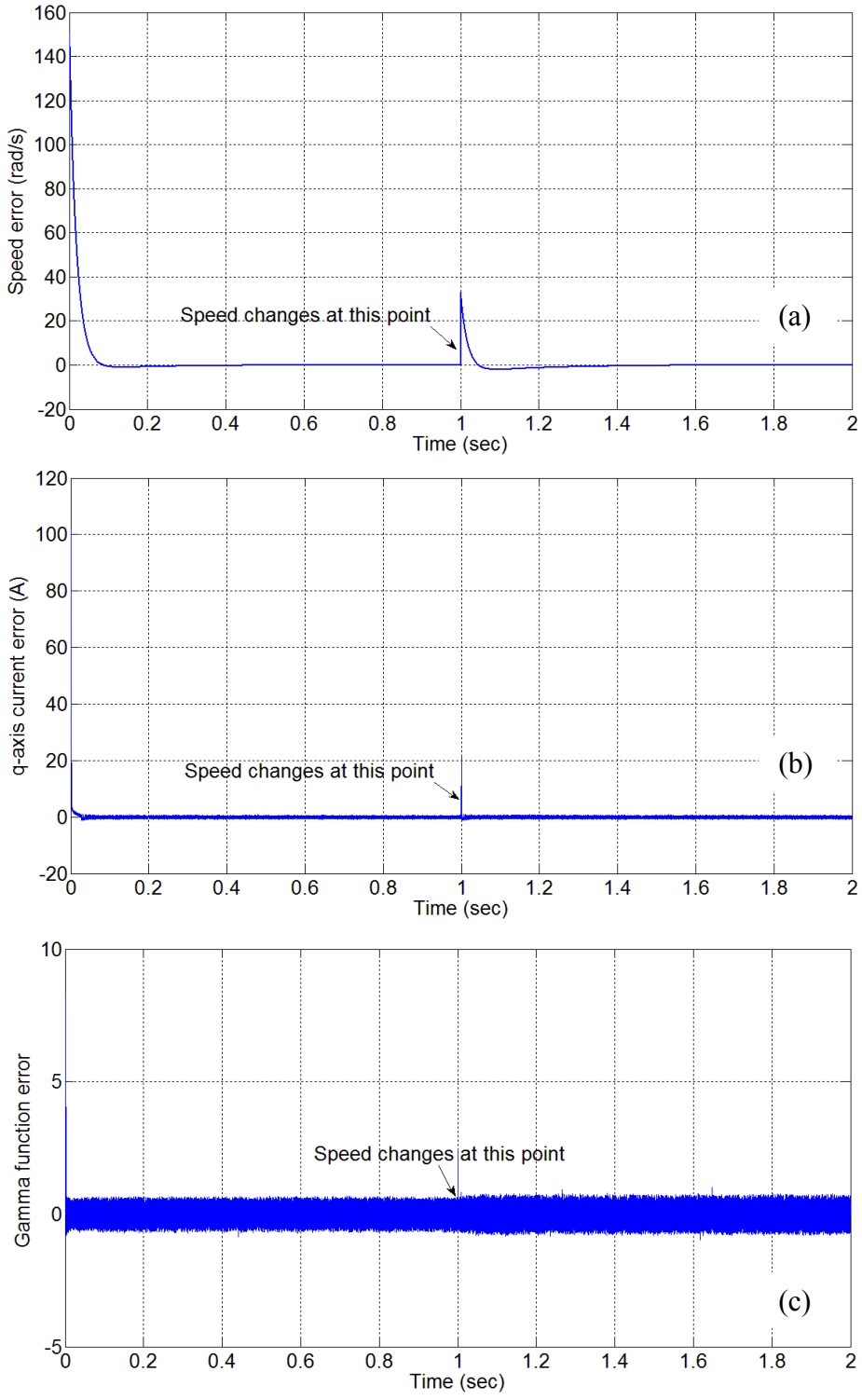


Fig. 4.21: Simulated response of the proposed ABNC based IPMSM drive for a step increase of speed command from 150 rad/s to 183 rad/s at 50% load (9.5 Nm); (a) speed error, (b) q-axis current error, $e_q$, and (c) gamma function tracking error, $e_\gamma$.

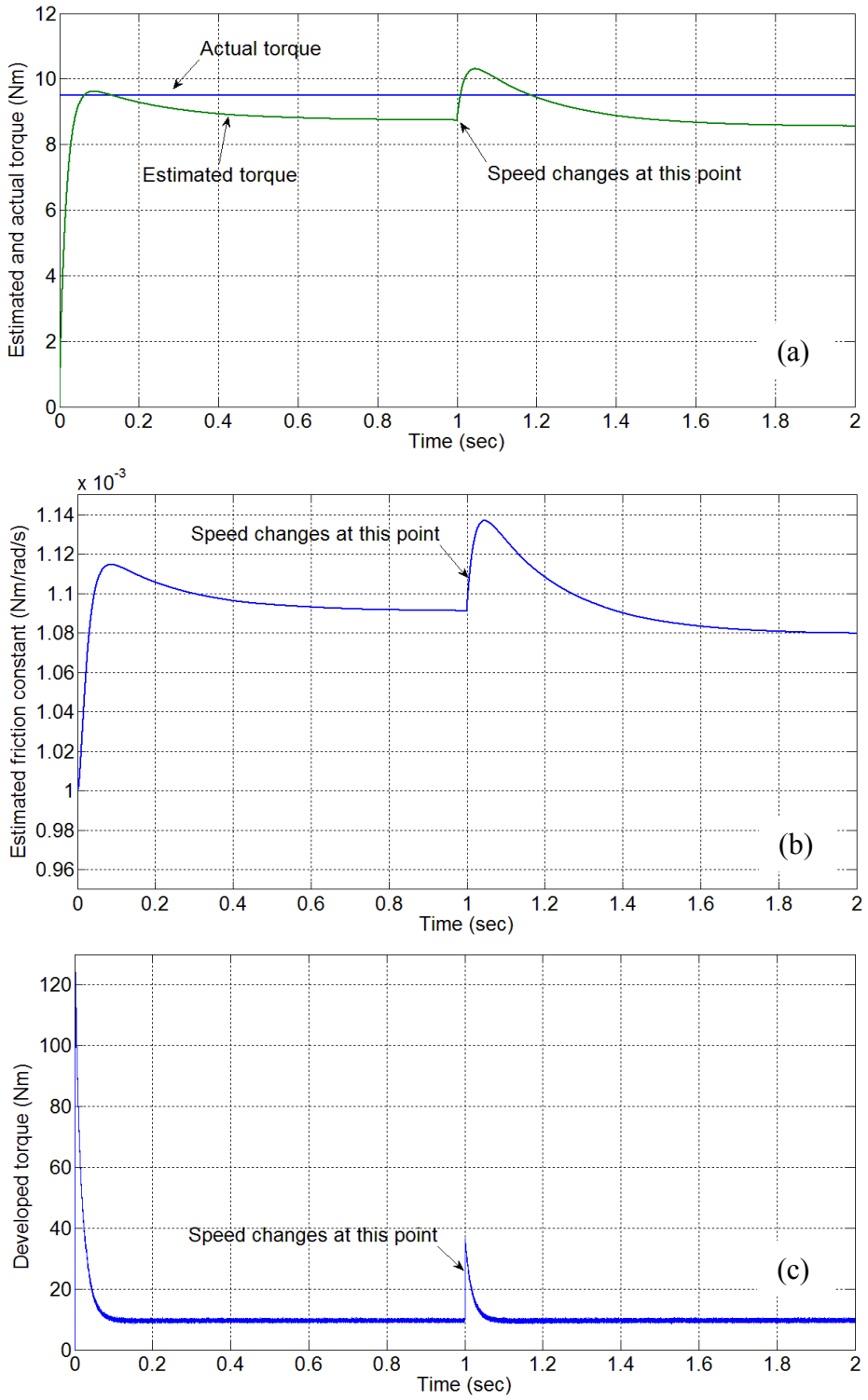


Fig. 4.22: Simulated response of the proposed ABNC based IPMSM drive for a step increase of speed command from 150 rad/s to 183 rad/s at 50% load (9.5 Nm); (a) estimated load torque, (b) estimated friction constant, and (c) developed torque.

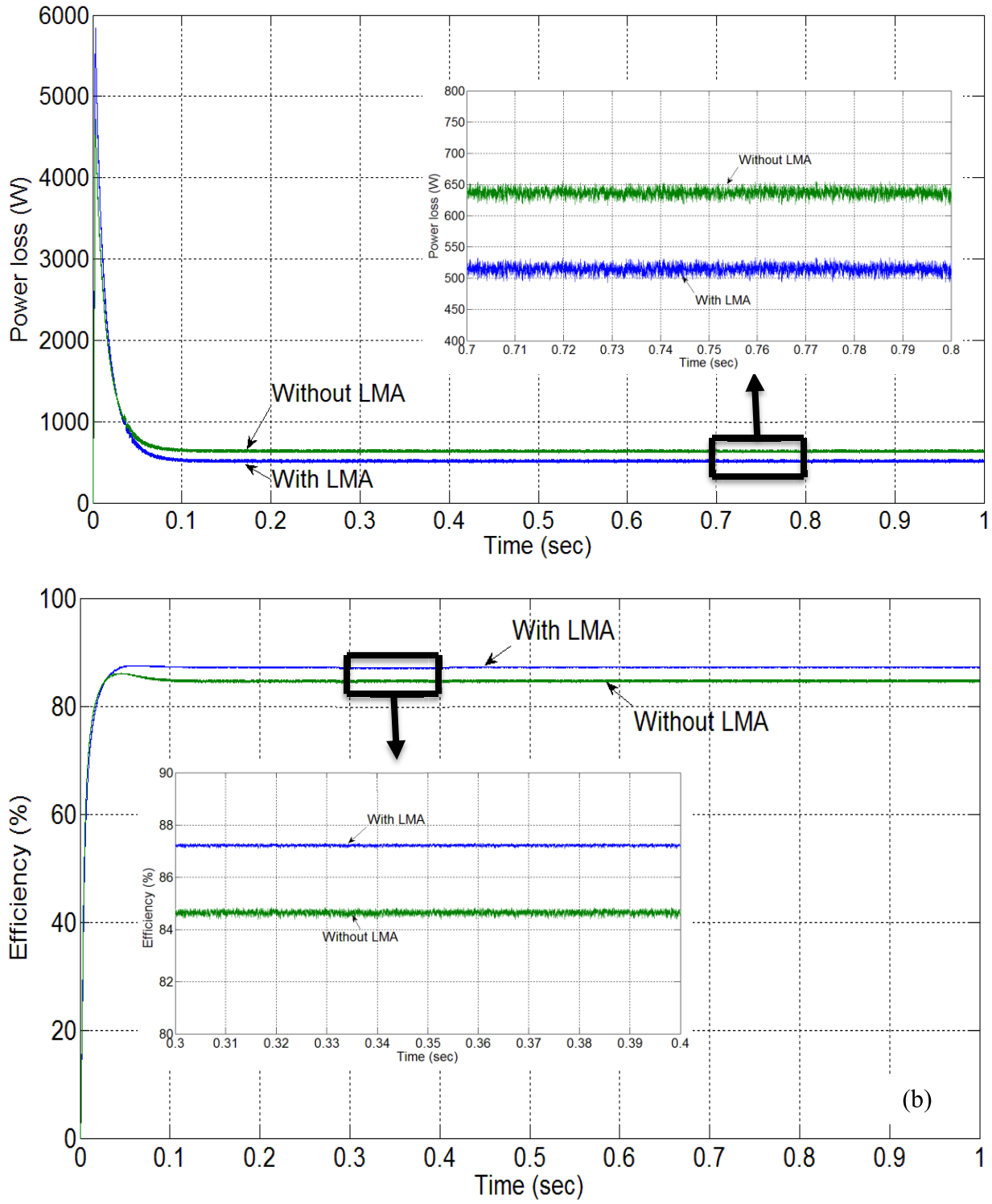


Fig. 4.23: Simulated response of the proposed LMA based ABNC for IPMSM drive for rated speed (183 rad/s) and rated load (19 Nm); (a) power loss with and without LMA, and (b) efficiency with and without LMA.

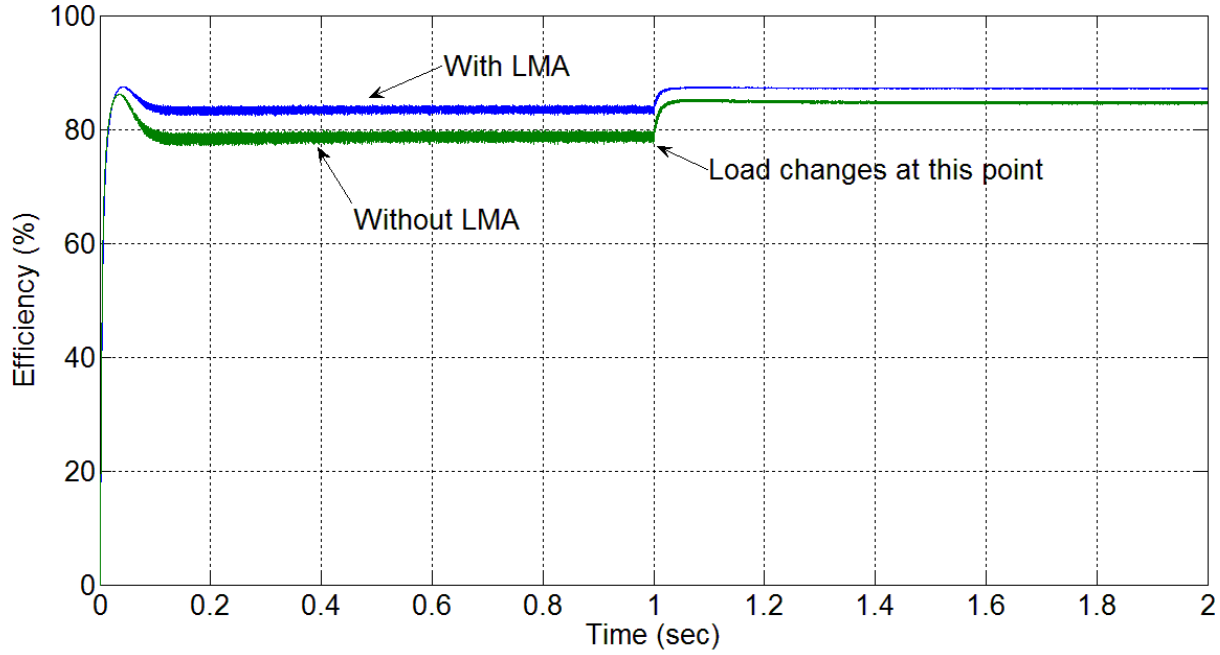


Fig. 4.24: Simulated response of the propose LMA based ABNC for IPMSM drive for a step increase of load from 9.5 Nm to 19 Nm and rated speed (183 rad/s).

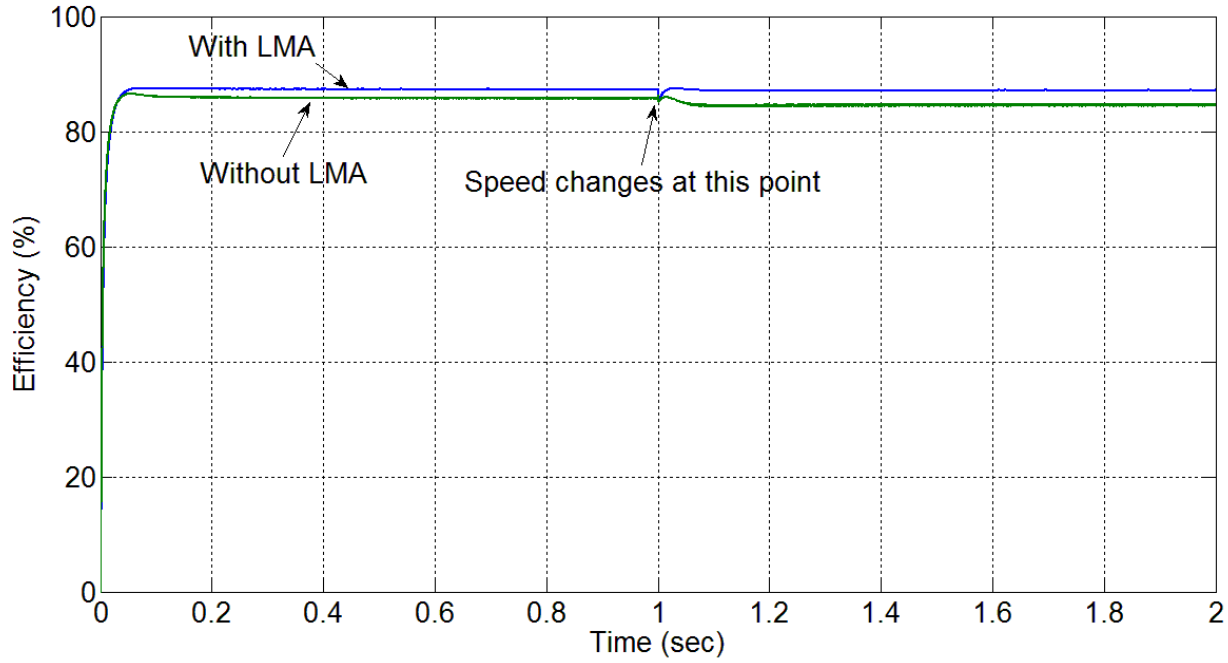


Fig. 4.25: Simulated response of the proposed LMA based ABNC for IPMSM drive for a step increase of speed command from 150 rad/s to 183 rad/s at rated load (19 Nm).

Fig. 4.26 shows the simulation results to test the effectiveness of parameter adaptation. The motor is started with wrong parameter value of $T_L$ = 1 Nm to the controller at a command speed of 183 rad/s while the true value is $T_L$ = 5 Nm. At t=0.3 sec, parameter adaptation is activated, and t=2 sec, a step load of 19 Nm is applied suddenly. Fig. 4.26(a) shows the successful parameter adaptation result. Fig. 4.26(b) shows the speed response. There was a steady-state error in speed due to the wrong parameter before the parameter adaptation is activated as shown in Fig. 4.26(b). However, once parameter adaptation is initiated at t=0.3sec, this steady-state error becomes zero. At t=1 sec, speed increase is observed due to sudden load increase, but speed is recovered to its reference value in a short time due to the effectiveness of the adaptation laws.

# 4.5 Concluding Remarks

A loss minimization based adaptive backstepping-based nonlinear controller for an IPMSM drive has been developed. The control laws were derived based on the motor model incorporating various system uncertainties. This proposed scheme successfully estimate the parameter values at different operating conditions. Global stability of the developed nonlinear controller has been verified analytically using Lyapunov's stability theory. The performance of the proposed control technique has been tested in simulation at different operating conditions. The performance of the proposed ABNC was found to be superior when compared with conventional PI controller at different operating conditions. However, ABNC depends on the exact mathematical model of the system and suffers from high computational burden, which may cause problem while implementing it in real-time. Therefore, an NFC based online loss minimization of an IPMSM drive is proposed.

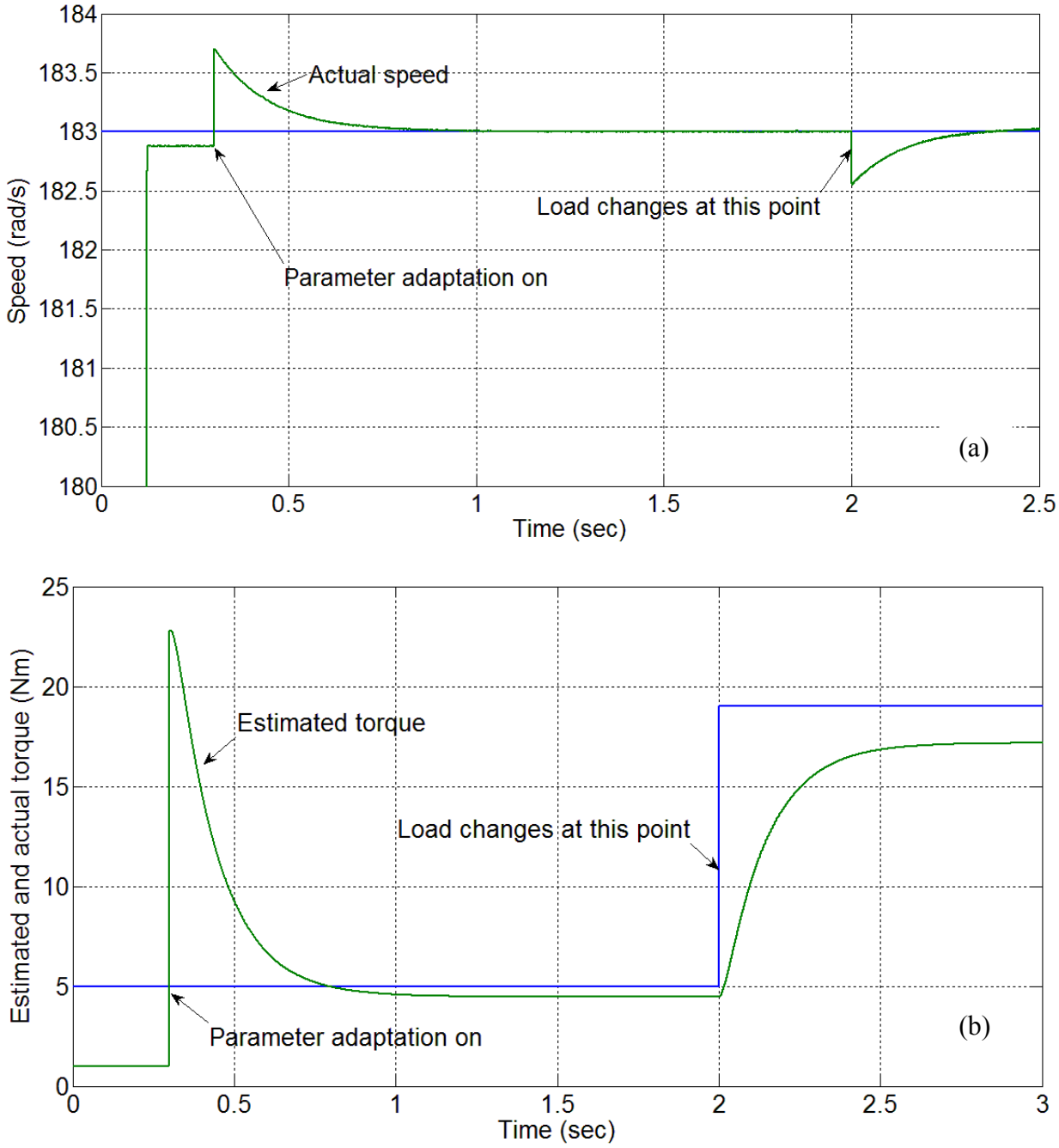


Fig. 4.26: Simulated response of the proposed ABNC based IPMSM drive at rated speed (183 rad/s) with step change in load from 5 Nm to 19 Nm at t=2sec; (a) speed, and (b) estimated load torque.

# Chapter 5

# Performance of Neuro-Fuzzy and Loss Minimization Based IPMSM Drive

In this chapter, a simple online adaptive network-based fuzzy inference system (ANFIS) is used for speed control of IPMSM drive [59]. Some of the advantages of ANFIS are very fast convergence due to hybrid learning and the ability to construct reasonably good input membership functions. The most appealing feature of ANFIS based neuro-fuzzy controller (NFC) is that it provides more choices over membership functions. An online self-tuning algorithm is also used to adjust the precondition and consequent parameters of the ANFIS. Moreover, the model-based LMA developed in Chapter 3 is incorporated with the NFC to achieve both high efficiency and high dynamic performance.

## 5.1 Design of Proposed NFC

As mentioned earlier in Chapter 1, the designs of intelligent controllers do not need exact mathematical model of the system. Simplicity and less intensive mathematical design requirements are the main features of intelligent controller, which are suitable to deal with nonlinearities and uncertainties of electric motors [83]. Therefore, the intelligent controllers demand particular

attention for high performance nonlinear IPMSM drive systems. However, the fuzzy logic controller (FLC) and artificial neural network (ANN) have disadvantages such as, a simple FLC has a narrow speed operation and needs much more manual adjusting by trial and error if high performance is required [83-89]. On the other, it is extremely hard to create a series of training data for ANN that can handle all the operating modes [83-89]. In order to achieve the advantages of both FLC and ANN and not the disadvantages, researchers developed neuro-fuzzy controller (NFC) for motor drive applications. In [55], a conventional NFC is applied to tune the PI controller parameters for IPMSM drive. Moreover, in those works the centers and weights of the NFC were tuned offline. In most of NFC, large number of membership functions and rules are used for designing the controller, these cause high computational burden for the conventional NFC, which is the major limitation for practical industrial applications. Therefore, an ANFIS is designed in such a way that the computational burden remains at the low level.

The Takagi-Sugino-Kang (TSK) fuzzy inference system and the corresponding ANFIS based general NFC architecture are shown in Figs. 5.1 and 5.2, respectively. The proposed NFC incorporates a six-layer ANN structure. In six layer ANN structure the first layer represents for inputs, the second layer represents for fuzzification, the third represent for fuzzy rules, the forth represents firing strength, the fifth represents consequent value and the sixth layer represents output. The TSK fuzzy rule-based control systems were enunciated in defuzzification process. As it is more accurate than the Mamdani method [83]. Moreover, in addition, if they are based on local semantic, the rules have more freedom to improve their performance at the expense of a loss of interpretability which is very useful when the main objective is the accuracy. It requires less computation than Mamdani method as it utilizes a linear defuzzification. The details of each layers are given in the next section.

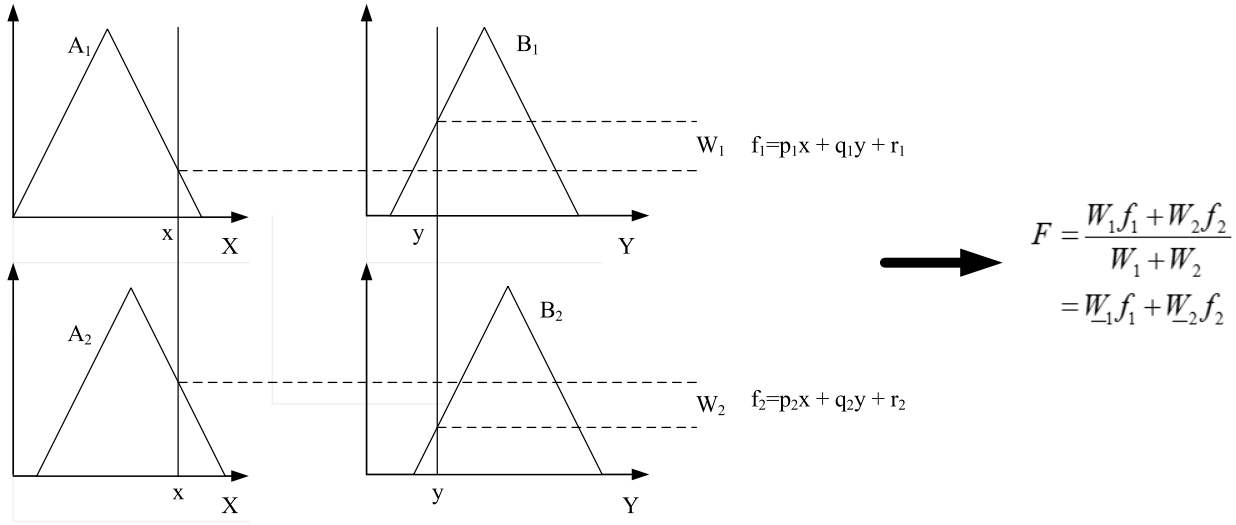


Fig. 5.1: TSK based fuzzy inference system.

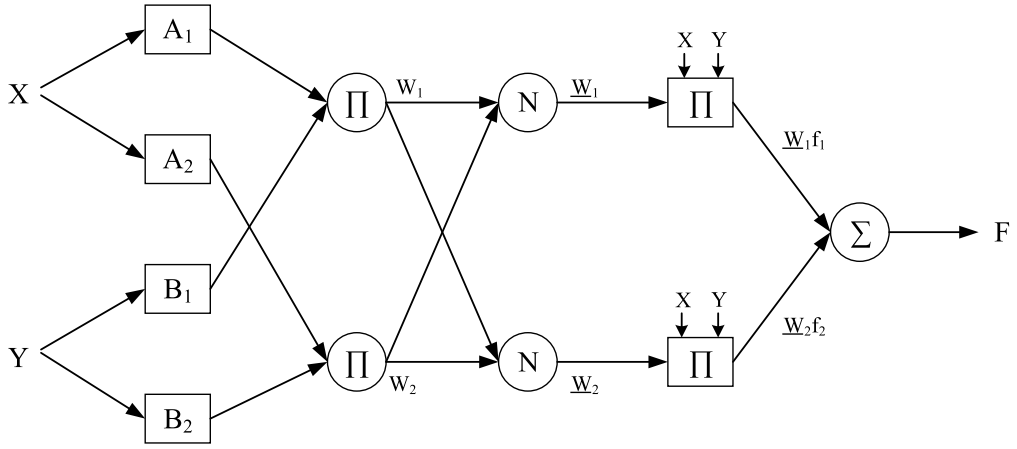


Layer 1 Layer 2 Layer 3 Layer 4 Layer 5 Layer 6

Fig. 5.2: General structure of an ANFIS.

# 5.2 Detailed Structure of NFC

The specific structure of the proposed ANFIS based NFC is shown in Fig. 5.3 [59]. For the proposed NFC only one input (speed error, e) is used to keep the computation burden low. However, an online tuning method is used to adjust input and output variables with drive uncertainties. The function of each layer of the ANFIS is briefly described as follows:

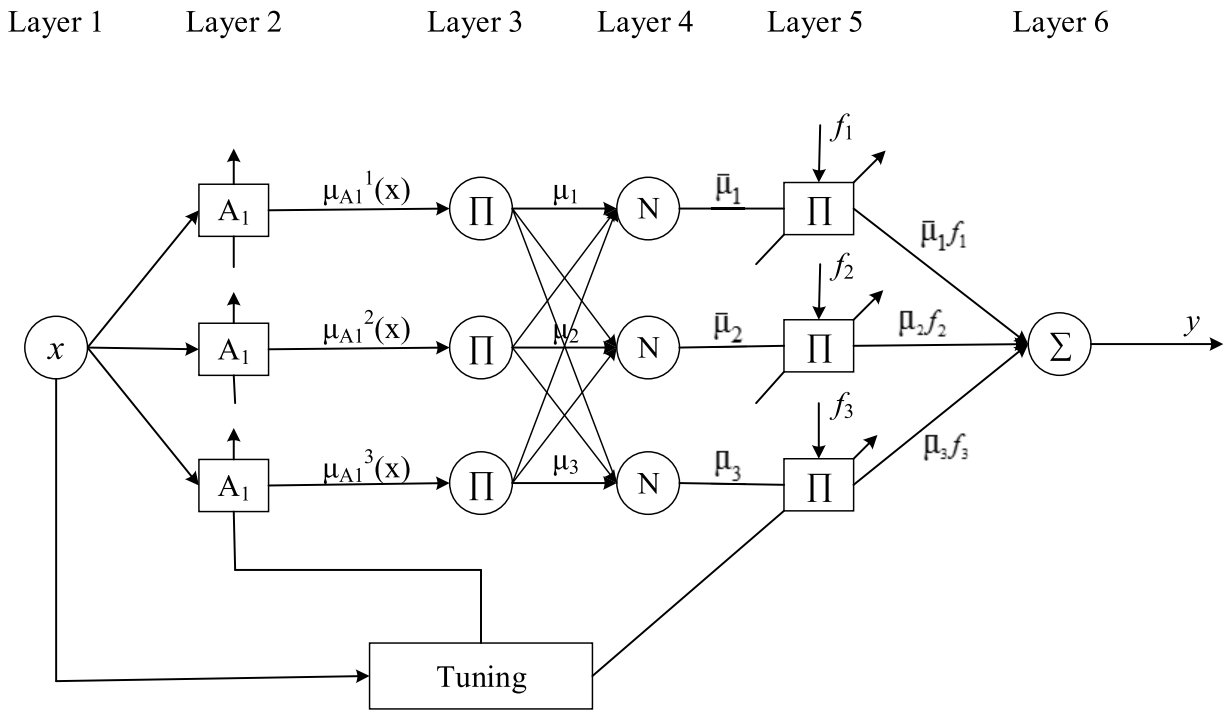


Fig. 5.3: Proposed structure of ANFIS based NFC.

*Layer 1:*

This layer is called input layer. Every node in this layer just passes external signal to the next layer. For simplicity only normalized speed error is considered, which is given by:

$$x = O^I = \frac{\omega_r^* - \omega_r}{\omega_r^*} \times 100\% \tag{5.1}$$

where, $\omega_r$ is the measure speed, $\omega_r^*$ is the reference speed, I denotes the 1st layer.

*Layer 2:*

This layer is called fuzzification layer, where the crisp value of each input is transformed to the fuzzy number through the membership functions. In the fuzzification process three membership functions are chosen. For less computational burden, triangular and trapezoidal functions are chosen as the membership functions for an ANFIS, as shown in Fig. 5.4.

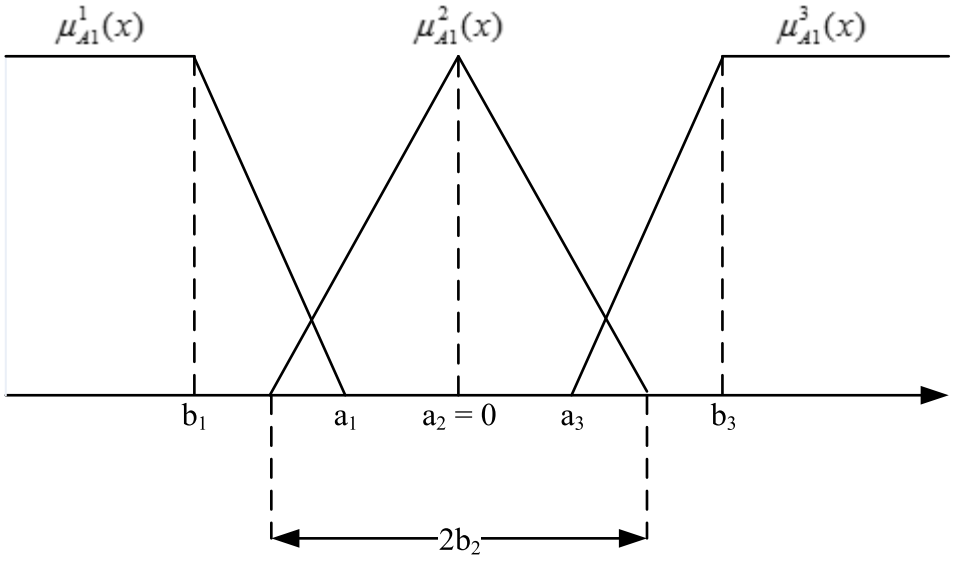


Fig. 5.4: Membership functions for input.

The corresponding node equations for three membership functions are given by:

$$\mu_{A1}^1(x) = \begin{cases} 1 & x \le b_1 \\ \dfrac{x - a_1}{b_1 - a_1} & b_1 < x < a_1 \\ 0 & x \ge a_1 \end{cases} \tag{5.2}$$

$$\mu_{A1}^2(x) = \begin{cases} 0 & |x| \ge b_2 \\ 1 - \dfrac{x - a_2}{b_2} & |x| < b_2 \end{cases} \tag{5.3}$$

$$\mu_{A1}^{3}(x)=\begin{cases}0 & x \le a_3 \\ \dfrac{x-a_3}{b_3-a_3} & a_3 < x < b_3 \\ 1 & x \ge b_3\end{cases} \tag{5.4}$$

where, x is the input of the 2nd layer which is the same as the output of 1st layer, superscript indicate the membership function and subscript indicate input. For example, $\mu_{A1}^{1}(x)$ is the first membership function of input 1. It is considered that $a_2 = 0$ in order for further reduction of computational burden. Parameters in this layer are referred to as precondition parameters, which need to be tuned online based on operating conditions of the motor.

*Layer 3:*

This layer is called rule layer. Every node in this layer multiplies incoming signals and sends the product. The node equations in rule layer are specified as:

$$\mu_j = \mu_{A1}^{j}(x_1), \mu_{A2}^{j}(x_2), \ldots, \mu_{Aj}^{j}(x_i), \ldots, \mu_{An}^{i}(x_n) \tag{5.5}$$

However, for the proposed controller, this layer can be ignored, since the number of input is one. Therefore, the output of the second layer is directly passed to the fourth layer.

So, $$\mu_1 = \mu_{A1}^{1}(x),\ \mu_2 = \mu_{A1}^{2}(x),\ \mu_3 = \mu_{A1}^{3}(x) \tag{5.6}$$

*Layer 4:*

Every node in this layer calculates the normalized firing strength of a rule in the proposed NFC.

$$\bar{\mu}_1 = \frac{\mu_1}{\mu_1 + \mu_2 + \mu_3} \tag{5.7a}$$

$$\bar{\mu}_2 = \frac{\mu_2}{\mu_1 + \mu_2 + \mu_3} \tag{5.7b}$$

$$\bar{\mu}_3 = \frac{\mu_3}{\mu_1 + \mu_2 + \mu_3} \tag{5.7c}$$

*Layer 5:*

Every node in this layer calculates weighted consequent values $\bar{\mu}_1 f_1$, $\bar{\mu}_2 f_2$, and $\bar{\mu}_3 f_3$, where $f_1, f_2$, and $f_3$ are considered as linear consequent functions as:

$$f_1 = a_0^1 + a_1^1 x \tag{5.8a}$$

$$f_2 = a_0^2 + a_1^2 x \tag{5.8b}$$

$$f_3 = a_0^3 + a_1^3 x \tag{5.8c}$$

Where, $x$ is normalized speed error.

In order to make the activation function nonlinear with time, parameters $\{a_0^1, a_1^1, a_0^2, a_1^2, a_0^3, a_1^3\}$ need to be tuned based on operating conditions of the motor. Parameters in this layer are referred to as consequent parameters.

*Layer 6:*

This layer is called the output layer. This layer sums all the incoming inputs.

$$y = \bar{\mu}_1 f_1 + \bar{\mu}_2 f_2 + \bar{\mu}_3 f_3 \tag{5.9}$$

For the proposed NFC based IPMSM drive this control output (y) represents the q-axis command current of the stator $(i_q^*)$. This current is responsible to force the motor to follow the reference speed trajectory. The proposed NFC acts as a speed controller. Now, the LMA developed in Chapter 3 is integrated with the NFC so that high dynamic performance of IPMSM can be achieved while maintaining high efficiency. The block diagram of the proposed ANFIS and LMC based IPMSM drive is shown in Fig. 5.5.

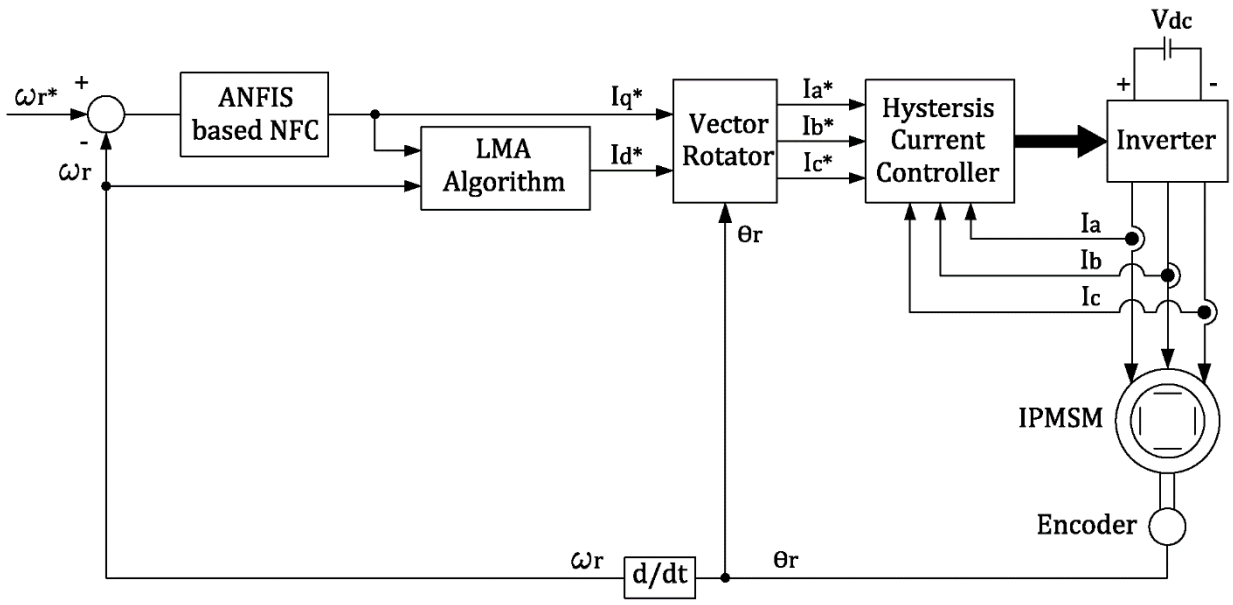


Fig. 5.5: Block diagram of the proposed NFC and LMC based IPMSM drive.

# 5.3 On-line Tuning Method

Since it is almost impossible to determine or calculate desired ANFIS controller output, $i_q^*$ and find training data off-line covering all operating conditions, an unsupervised on-line self-tuning method is used in this thesis. Instead of using desired controller's output $i_q^*$ as target, reinforcement signal, r, which is equal to the normalized speed error of the IPMSM and is the same as $x$ variable input to the controller is utilized to generate control action to produce the desired speed response. The corresponding equation is given as:

$$E = \frac{1}{2} r^2 = \frac{1}{2}\left(\omega_r^* - \omega_r\right)^2 \tag{5.10}$$

The back propagation algorithm is used to tune the input membership functions and the coefficients of linear activation functions at the output.

### 5.3.1 Tuning of Precondition Parameters

The learning rules can be derived as follows:

$$a_i(n+1) = a_i(n) - \eta_{a_i} \frac{\partial E}{\partial a_i} \tag{5.11a}$$

$$b_i(n+1) = b_i(n) - \eta_{b_i} \frac{\partial E}{\partial b_i} \tag{5.11b}$$

where, $\eta_{a_i}$, $\eta_{b_i}$ are the learning rate of the corresponding parameters. The derivatives can be found by chain rule as:

$$\frac{\partial E}{\partial a_i} = \frac{\partial E}{\partial r}\frac{\partial r}{\partial \omega_r}\frac{\partial \omega_r}{\partial i_q^*}\frac{\partial i_q^*}{\partial \mu_{A1}^i}\frac{\partial \mu_{A1}^i}{\partial a_i} \tag{5.12a}$$

$$\frac{\partial E}{\partial b_i} = \frac{\partial E}{\partial r}\frac{\partial r}{\partial \omega_r}\frac{\partial \omega_r}{\partial i_q^*}\frac{\partial i_q^*}{\partial \mu_{A1}^i}\frac{\partial \mu_{A1}^i}{\partial b_i} \tag{5.12b}$$

The common parts of Eqn. (5.12) are:

$$\frac{\partial E}{\partial r} = r = \omega_r^* - \omega_r \tag{5.13}$$

$$\frac{\partial r}{\partial \omega_r} = -1 \tag{5.14}$$

$$\frac{\partial \omega_r}{\partial i_q^*} = J \tag{5.15}$$

where, J is the Jacobian matrix of the system [52]. System Jacobian matrix cannot be found easily. For field oriented control, the PMSM system can be viewed as a single input single output system and then the Jacobian matrix can be estimated as a constant positive value. Considering that the effect of J is included in tuning rate parameter, the update rules can be determined from Eqns. (5.10)-(5.15), as follows:

$$a_1(n+1) = a_1(n) - \eta_{a_1} r(n) \frac{f_1(n)}{\sum \mu_{A1}^i(n)} \frac{1-\mu_{A1}^1(n)}{b_1(n)-a_1(n)} \tag{5.16a}$$

$$a_3(n+1) = a_3(n) - \eta_{a_3} r(n) \frac{f_3(n)}{\sum \mu_{A1}^i(n)} \frac{1-\mu_{A1}^3(n)}{b_3(n)-a_3(n)} \tag{5.16b}$$

$$b_1(n+1) = b_1(n) - \eta_{b_1} r(n) \frac{f_1(n)}{\sum \mu_{A1}^i(n)} \frac{\mu_{A1}^1(n)}{b_1(n)-a_1(n)} \tag{5.16c}$$

$$b_2(n+1) = b_2(n) + \eta_{b_2} r(n) \frac{f_2(n)}{\sum \mu_{A1}^i(n)} \frac{1-\mu_{A1}^2(n)}{b_2(n)} \tag{5.16d}$$

$$b_3(n+1) = b_3(n) - \eta_{b_3} r(n) \frac{f_3(n)}{\sum \mu_{A1}^i(n)} \frac{\mu_{A1}^3(n)}{b_3(n)-a_3(n)} \tag{5.16e}$$

Based on these update rules, the parameters of $a_1$, $a_3$, $b_1$, $b_2$, and $b_3$ can be tuned.

## 5.3.2 Tuning of Consequent Parameters

To tune the consequent parameters, the following update laws are developed:

$$a_0^i(n+1) = a_0^i(n) - \eta_{a_0^i} \frac{\partial E}{\partial a_0^i} \tag{5.17a}$$

$$a_1^i(n+1) = a_1^i(n) - \eta_{a_1^i} \frac{\partial E}{\partial a_1^i} \tag{5.17b}$$

where, $\eta_{a_0^i}$ and $\eta_{a_1^i}$ are the learning rate of the corresponding parameters. As with the precondition parameters adjustment discussed earlier, the derivatives can be found by chain rule as:

$$\frac{\partial E}{\partial a_0^i} = \frac{\partial E}{\partial r} \frac{\partial r}{\partial \omega_r} \frac{\partial \omega_r}{\partial i_q^*} \frac{\partial i_q^*}{\partial a_0^i} \tag{5.18a}$$

$$\frac{\partial E}{\partial a_1^i} = \frac{\partial E}{\partial r} \frac{\partial r}{\partial \omega_r} \frac{\partial \omega_r}{\partial i_q^*} \frac{\partial i_q^*}{\partial a_1^i} \tag{5.18b}$$

Using Eqns. (5.8) and (5.9):

$$\frac{\partial i_q^*}{\partial a_0^1} = \frac{\mu_1}{\mu_1 + \mu_2 + \mu_3}$$
$$\frac{\partial i_q^*}{\partial a_0^2} = \frac{\mu_2}{\mu_1 + \mu_2 + \mu_3} \tag{5.19a}$$
$$\frac{\partial i_q^*}{\partial a_0^3} = \frac{\mu_3}{\mu_1 + \mu_2 + \mu_3}$$

$$\frac{\partial i_q^*}{\partial a_1^1} = \frac{\mu_1 x}{\mu_1 + \mu_2 + \mu_3}$$
$$\frac{\partial i_q^*}{\partial a_1^2} = \frac{\mu_2 x}{\mu_1 + \mu_2 + \mu_3} \tag{5.19b}$$
$$\frac{\partial i_q^*}{\partial a_1^3} = \frac{\mu_3 x}{\mu_1 + \mu_2 + \mu_3}$$

The update laws for tuning consequent parameters can be obtained from Eqns. (5.10), (5.13)-(5.15), and (5.17)-(5.19) as:

$$a_0^i(n+1) = a_0^i(n) + \eta_{a_0^i} r(n) \frac{\mu_i}{\mu_1 + \mu_2 + \mu_3} \tag{5.20a}$$

$$a_1^i(n+1) = a_1^i(n) + \eta_{a_1^i} r(n) \frac{\mu_i x}{\mu_1 + \mu_2 + \mu_3} \tag{5.20b}$$

Therefore, the overall tuning method can be summarized as:

*Step 1:* An initial setting of fuzzy logic rules and initial values of $a_1$, $a_3$, $b_1$, $b_2$, $b_3$ and $\{a_0^1,\ a_1^1,\ a_0^2,\ a_1^2,\ a_0^3,\ a_1^3\}$ are selected.

*Step 2:* The normalized speed error is calculated, which is input to the controller.

*Step 3:* Fuzzy reasoning is performed for the normalized speed error data input using Eqns. (5.1)-(5.10). The membership values are calculated for the input speed error by using Eqns. (5.2)-(5.4), and output fuzzy reasoning $i_q^*$ is calculated.

*Step 4:* The tuning of the $a_1,\ a_3,\ b_1,\ b_2$ and $b_3$ is done by substituting the measured reinforcement signal, *r*, the membership value $\mu_{A1}^{i}$, and consequent value $f_1$ into Eqn. (5.16).

*Step 5:* Fuzzy reasoning is repeated as in step 3.

*Step 6:* Tune the consequent parameters $\{a_0^1,\ a_1^1,\ a_0^2,\ a_1^2,\ a_0^3,\ a_1^3\}$ using Eqn. (5.20) by substituting the input normalized speed error data (*x*), measured reinforcement signal, *r*, and calculated firing strength of rules from membership functions.

*Step 7:* Repeat from step 3.

# 5.4 Simulation Results and Discussion

In order to demonstrate the performance of the ANFIS along with loss minimization capability of loss model-based controller (LMC), numerous extensive simulations were performed. A simulation model for the proposed ANFIS and LMA based closed loop vector control of IPMSM drive is developed using MATLAB/Simulink as per Fig. 5.6. The initial values of precondition and consequent parameters used in the simulation model are $a_1 = 0,\ a_3 = 0,\ b_1 = -0.5,\ b_2 = 0.001,\ b_3 = 0.5$ and $a_0^1 = 0,\ a_1^1 = 3,\ a_0^2 = 0,\ a_1^2 = 3,\ a_0^3 = 0,\ a_1^3 = 3$. The values of tuning rate of precondition and consequent parameters are 1e-6 and 0.05, respectively. These values were obtained by trial and error in simulation under rated conditions. The learning rate were chosen small values so that the transition from one state to another becomes smooth. The details of the Simulink model are shown in Appendix B.

First, the dynamic performance of the proposed drive is tested. Fig. 5.7(a) shows the starting speed response of the proposed NFC and LMC based IPMSM drive at full load (19 Nm)

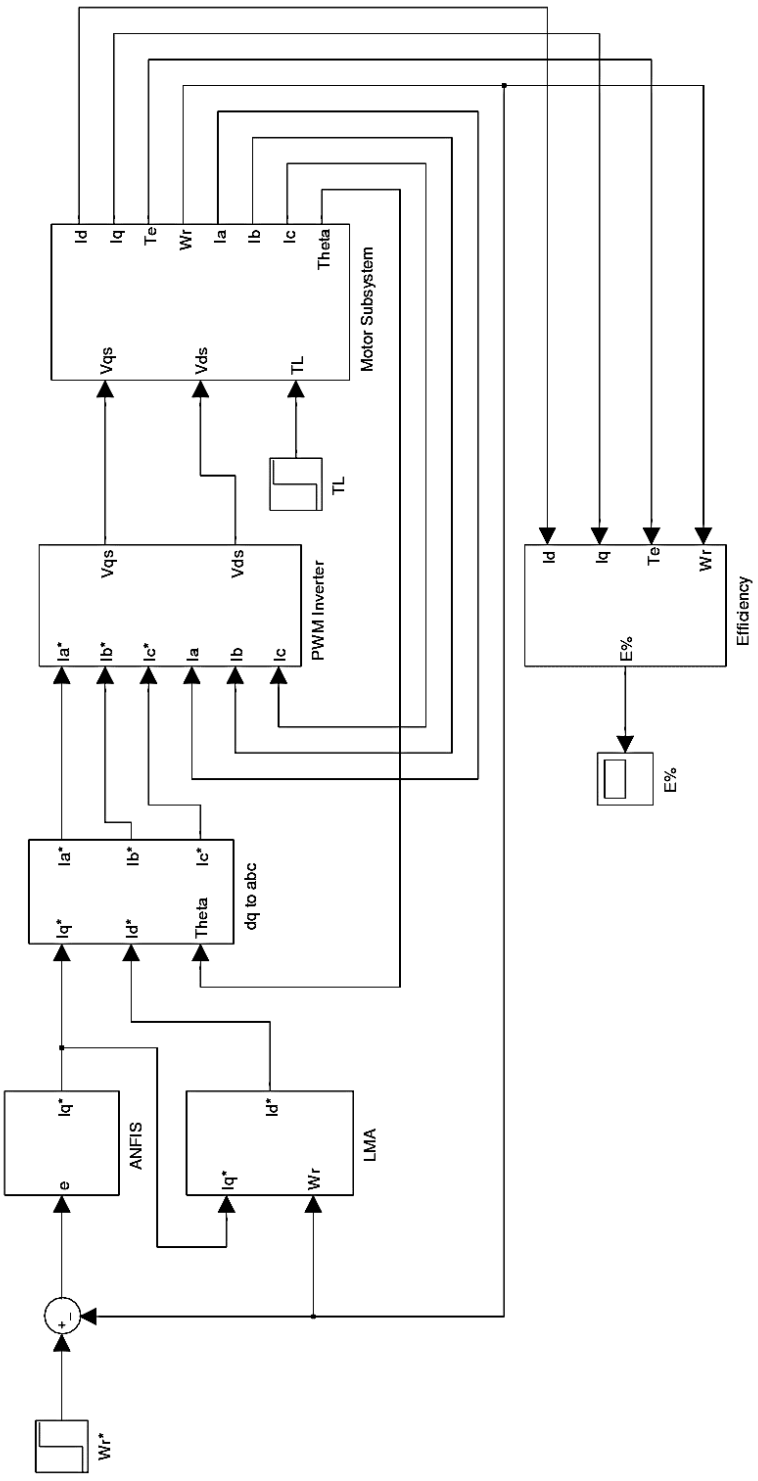


Fig. 5.6: Simulink schematic of the complete proposed NFC and LMC based IPMSM drive.

condition. It is shown from this Figure that the performance of the proposed controller is fast and smooth. It is also seen that the actual speed follows the reference speed without any overshoot or undershoot and with zero steady-state error. The corresponding d-q axis currents, line current are shown in Fig. 5.7(b) and (c), respectively. Fig. 5.8(a) shows the corresponding steady-state actual three phase currents. This verifies the balanced operation of the motor. The developed torque, magnetic torque and the reluctance torque are shown in Fig. 5.8(b) and (c), respectively. It shows that the reluctance torque due to nonzero d- axis current contribute a part to the total developed torque by the drive. Traditionally, $i_d$ is set to zero and hence the reluctance torque becomes zero. Therefore, the LMA is contributing to produce some reluctance torque. Fig. 5.9(a) shows the starting speed response of the proposed controller at no load. The actual speed converges with the reference speed within very short period of time with minimum overshoot and no steady-state error. The corresponding d-q axis currents, magnetic torque, reluctance torque and line current are shown in Fig. 5.9(b)-(d), respectively. The effectiveness of the proposed controller is also tested for a step increase in load from no load to full load (19 Nm) at rated reference speed (183 rad/s), which are shown in Figs. 5.10 and 5.11. The corresponding motor developed torque, magnetic torque, and reluctance torque are given in Fig. 5.10(b) and (c), respectively. With the increase of load q-axis current increases and d-axis current decreases as shown in Fig. 5.11(a). The effect in line current and three phase currents are shown in Fig. 5.11(b) and (c), respectively. Fig. 5.12 shows the response of the proposed controller for IPMSM drive for step change in reference speed from 150 rad/s to 183 rad/s at no load condition. From Fig. 5.12(a), it is observed that the motor can follow the reference speed with very small overshoot (0.16%). The simulated d-q axis current vector trajectories for step increase in reference speed are shown in Fig. 5.12(b). Line current and the developed torque of the motor are shown in Fig. 5.12(c) and (d), respectively. Fig. 5.13(a) and

(b) show the speed response of the proposed controller of IPMSM drive under rated speed (183 rad/s) and load (19 Nm) condition with doubled inertia (J → 2J) and doubled friction constant ($B_m$ → $2B_m$), respectively. It is evident from Figs. 5.13(a) and (b) that the proposed ANFIS and LMA controller for IPMSM drive can follow the reference speed with increased inertia and friction constant smoothly without overshoot/undershoot and steady-state error.

Next the loss minimization capability of the proposed ANFIS and LMC based IPMSM drive is tested at different operating conditions. Fig. 5.14 shows the efficiency and power loss of the drive for rated speed and load condition. From the Fig. 5.14(a), it is seen that the efficiency of the drive is approximately 87.5 % at rated conditions, it is same as in Fig. 4.24(b). In Fig. 5.15, the simulation started with the rated speed (183 rad/s) and rated torque (19 Nm) with the LMC. The loss minimization control technique is activated at t=0.5s. When the LMC is activated, it adjusts the optimum d-axis current level online based on the speed and motor parameters. This also leads to the rearrangement of $i_q$ in order to maintain the same torque. As a result of this arrangements, the efficiency is increased and the total loss is significantly reduced as shown in Fig. 5.15(a) and (b), respectively. The change in three phase current and d-q axis currents are shown in Fig. 5.15(c) and (d), respectively. Fig. 5.16 shows the efficiency and torque responses with and without LMA for change in load (9.5 Nm to 19 Nm) at t=0.5s and rated speed. It is seen from Fig. 16(a) that the proposed LMC can maintain higher efficiency at different load conditions as compared to without any LMA. Fig. 5.17 shows the efficiency response for IPMSM drive with and without LMA for change in speed (150 rad/s to 183 rad/s) at t=0.5s and rated load. From Fig. 5.17, one can see that when LMA is incorporated in proposed ANFIS based NFC the efficiency had almost no effect when there was speed change. However, without LMA the efficiency decreases when the speed is increased.

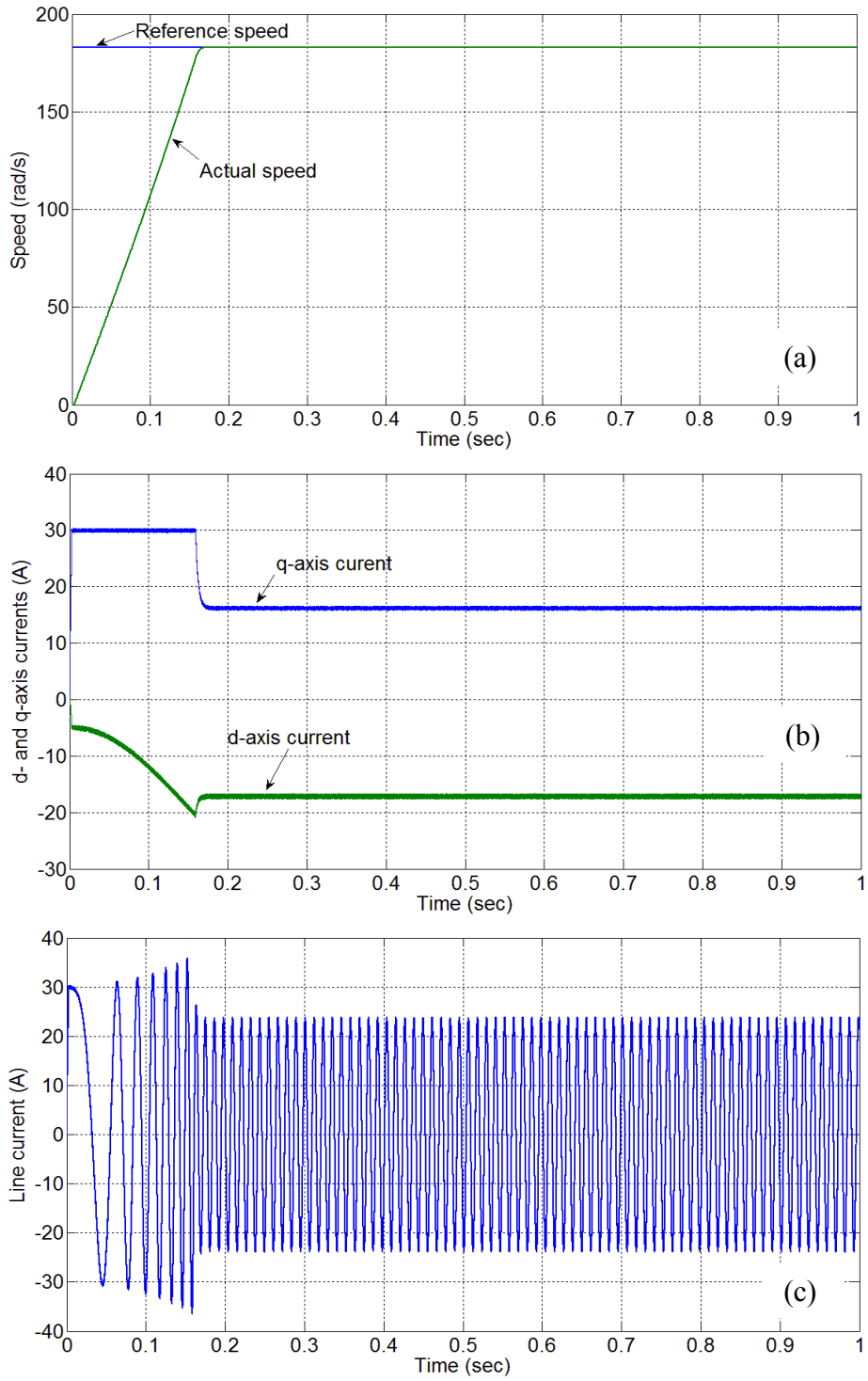


Fig. 5.7: Simulated response of the proposed ANFIS and LMC based IPMSM drive at rated speed (183 rad/s) and rated load (19 Nm); (a) speed, (b) d-q axis currents, (c) line current.

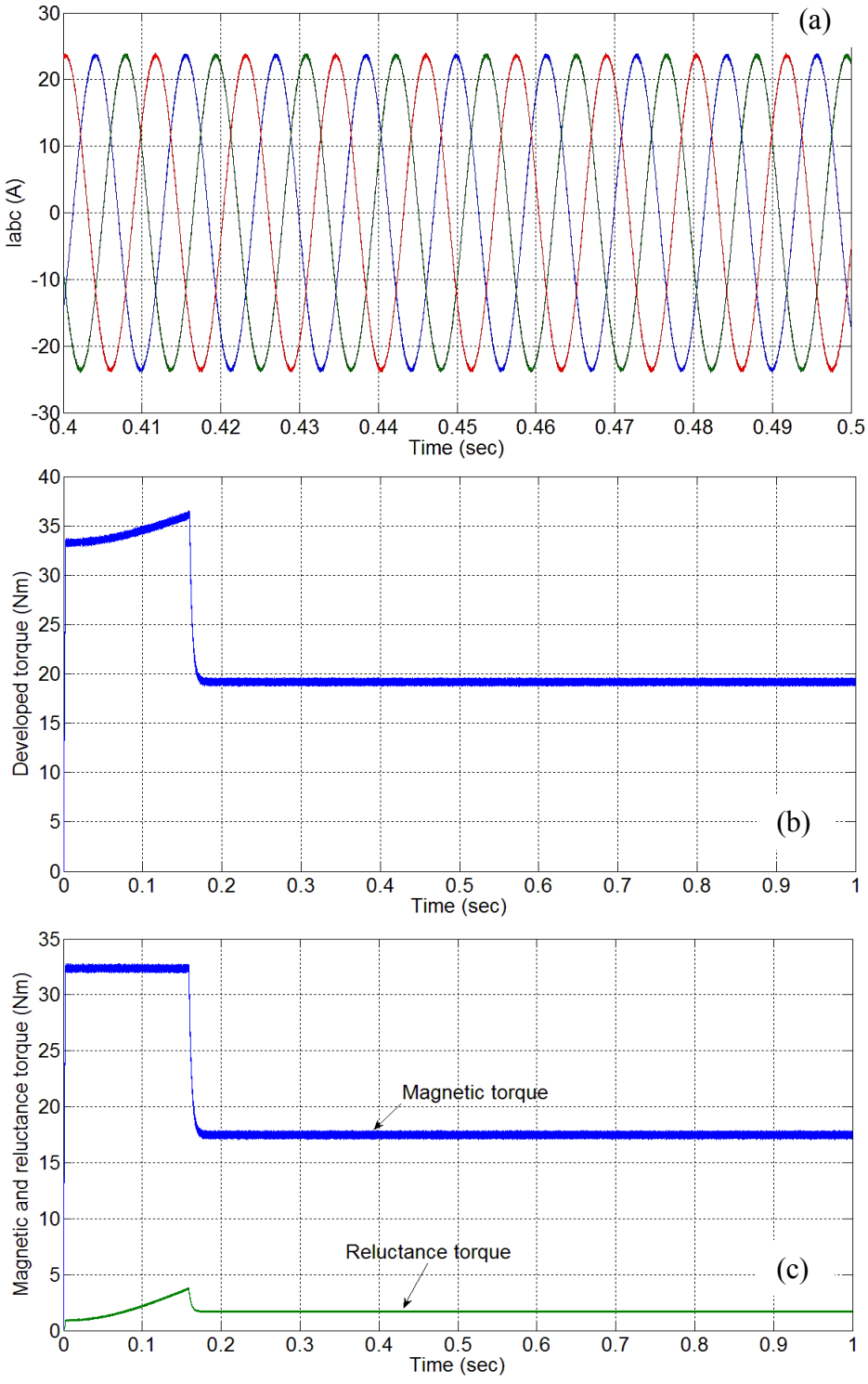


Fig. 5.8: Simulated response of the proposed ANFIS and LMC based IPMSM drive at rated speed (183 rad/s) and rated load (19 Nm); (a) steady-state three phase currents, (b) developed torque, and (c) steady-state magnetic and reluctance torque.

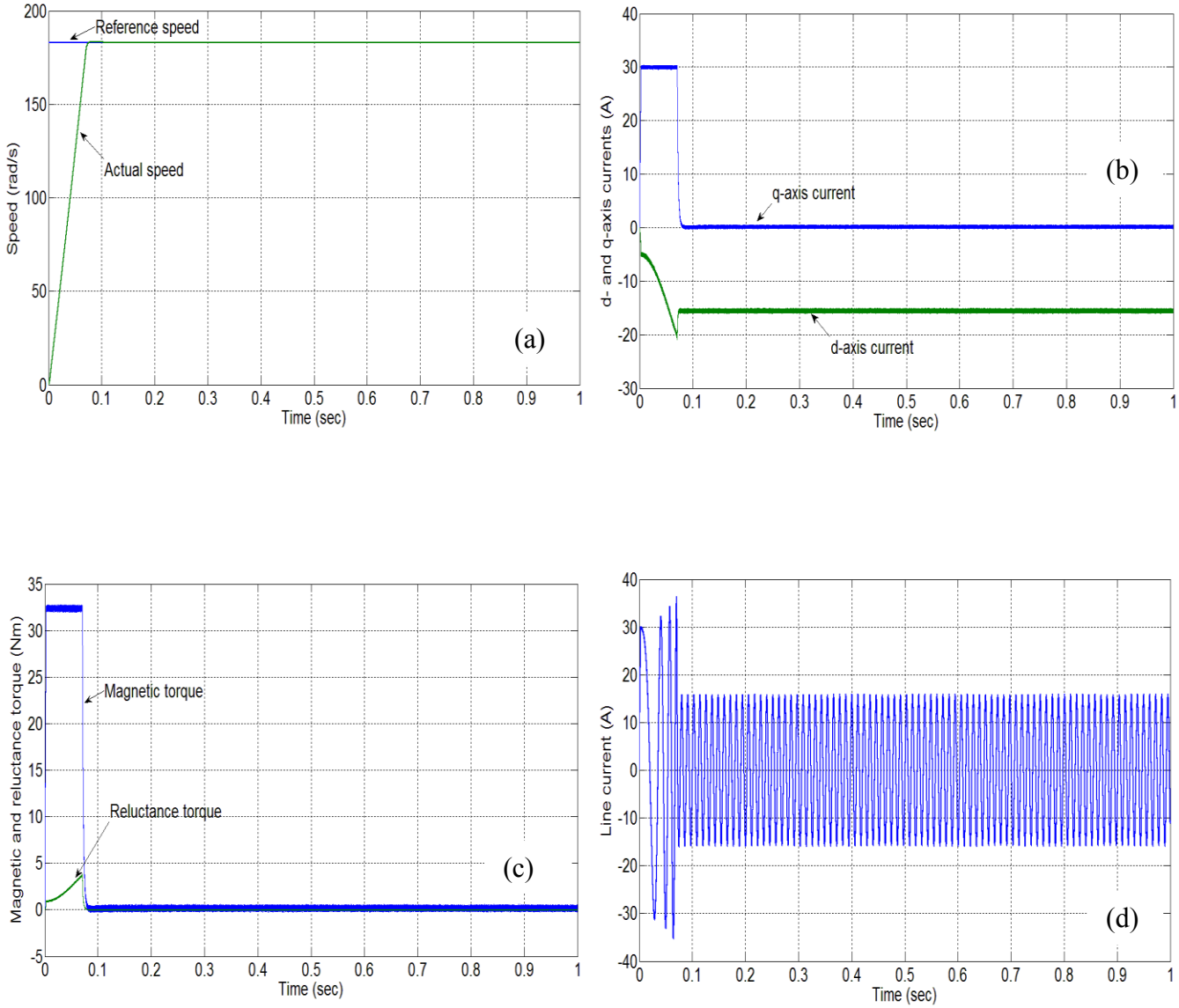


Fig. 5.9: Simulated response of the proposed ANFIS and LMC based IPMSM drive with no load and rated speed (183 rad/s); (a) speed, (b) d-q axis currents, (c) magnetic and reluctance torque, and (d) line current.

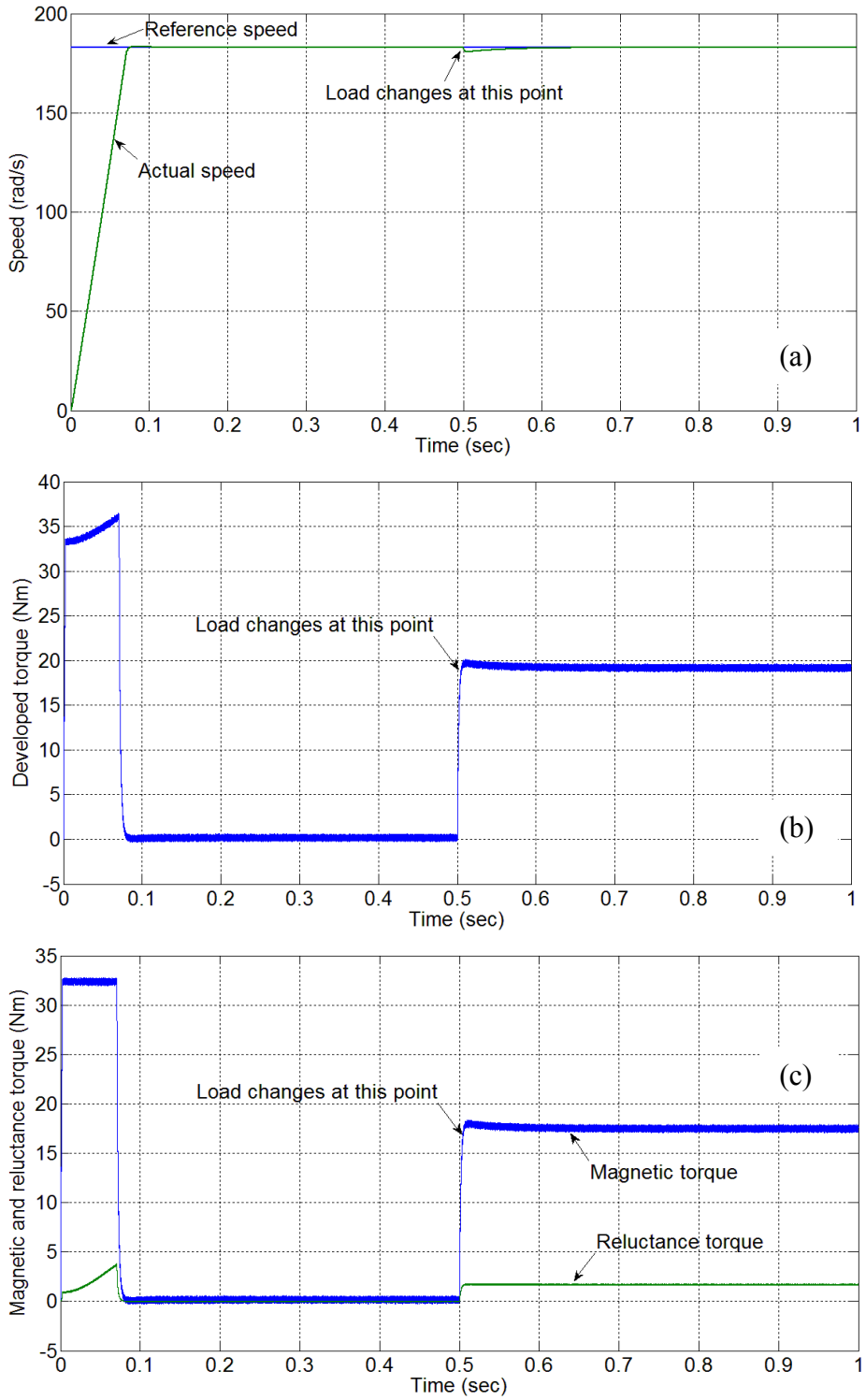


Fig. 5.10: Simulated response of the proposed ANFIS and LMC based IPMSM drive for step change in load from no load to full load (19 Nm) at rated speed (183 rad/s); (a) speed, (b) developed torque, and (c) magnetic and reluctance torque.

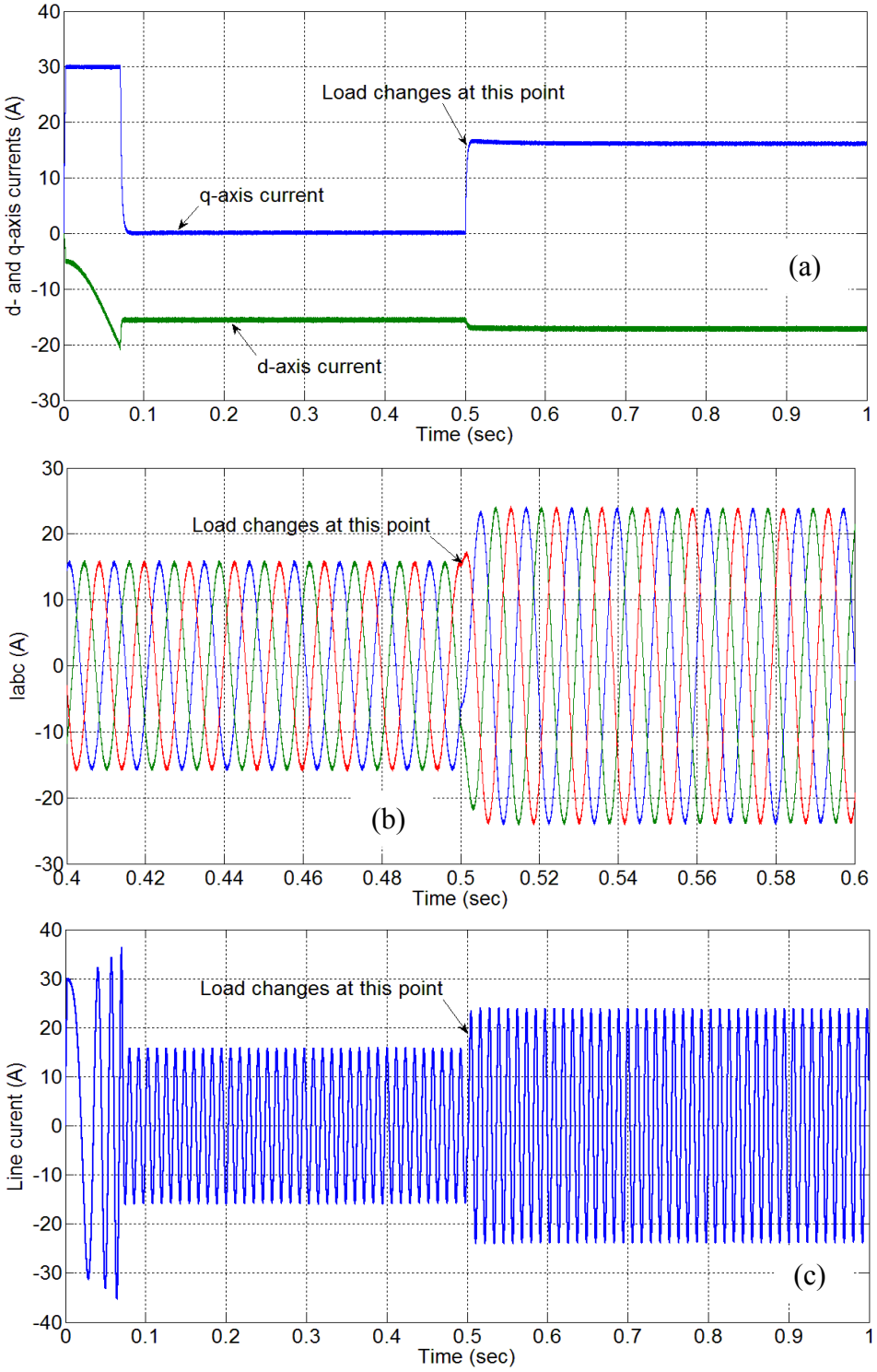


Fig. 5.11: Simulated response of the proposed ANFIS and LMC based IPMSM drive for step change in load from no load to full load (19 Nm) at rated speed (183 rad/s); (a) d-q axis currents, (b) steady-state three phase currents, and (c) line current.

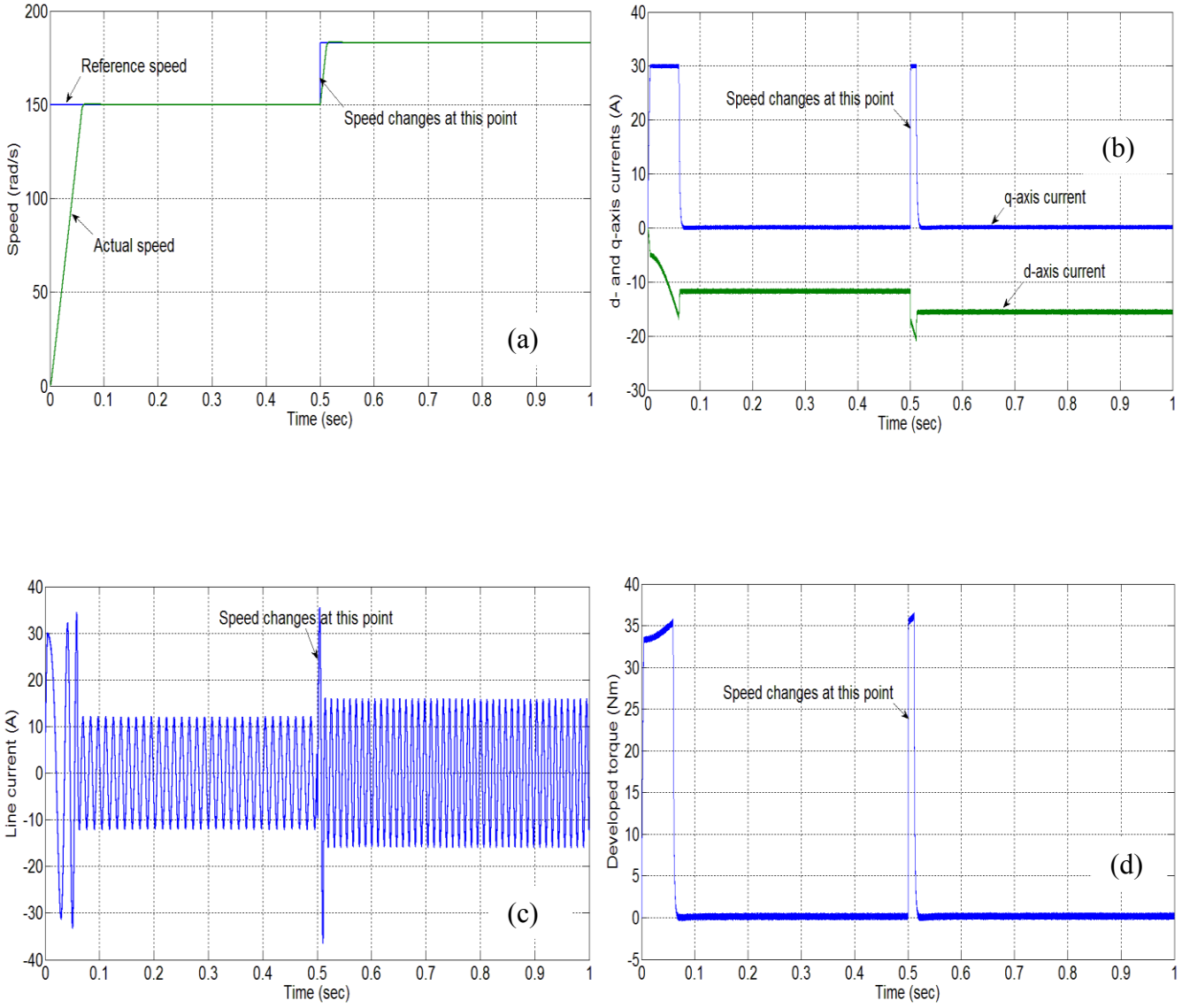


Fig. 5.12: Simulated response of the proposed ANFIS and LMC based IPMSM drive for step change in reference speed from 150 rad/s to 183 rad/s at no load; (a) speed, (b) d-q axis currents, (c) line current, and (d) developed torque.

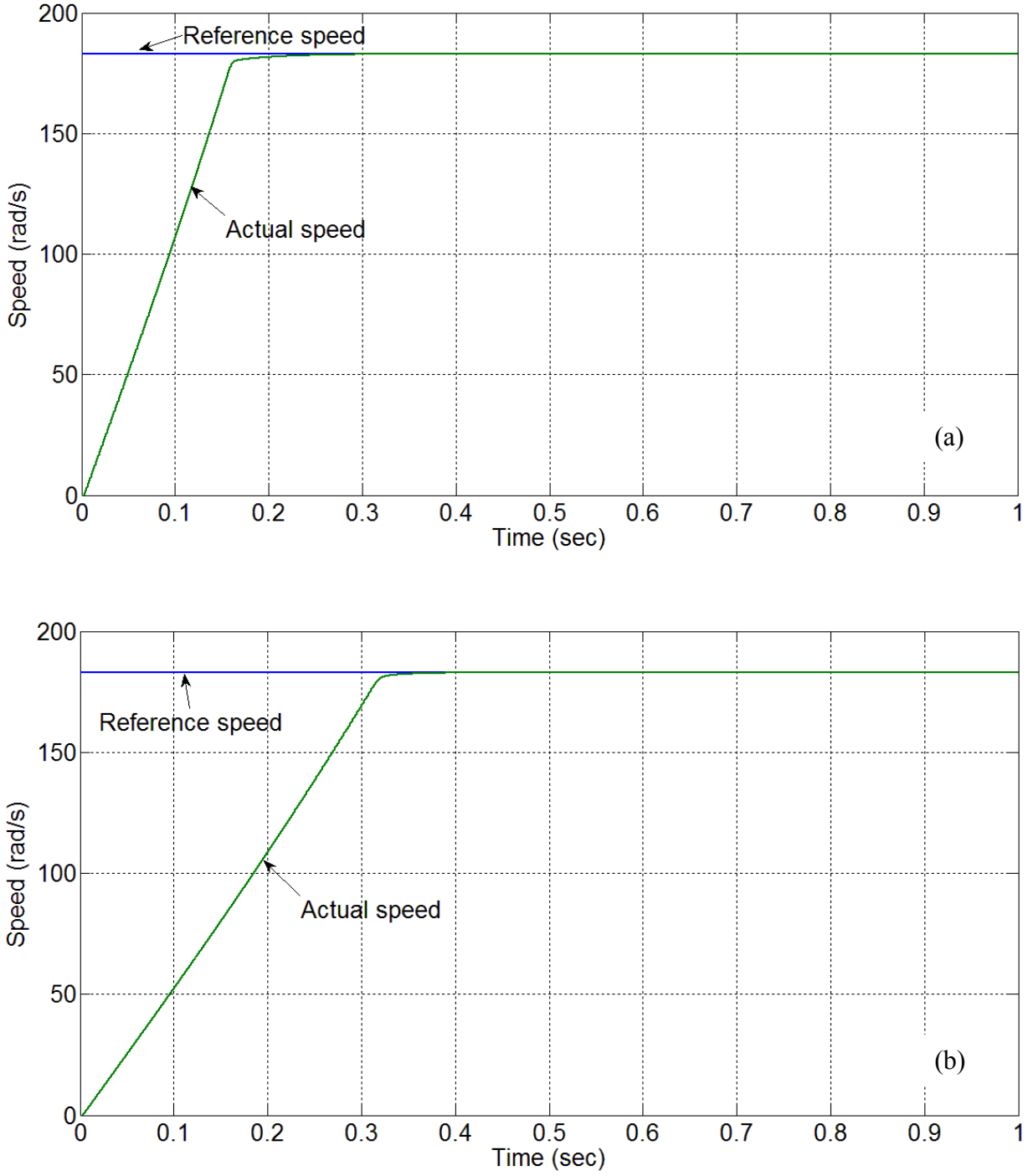


Fig. 5.13: Simulated speed response of the proposed ANFIS and LMC based IPMSM drive under rated speed (183 rad/s) and load (19 Nm); (a) doubled inertia (J → 2J) at start, and (b) doubled friction constant ($B_m \rightarrow 2B_m$) at start.

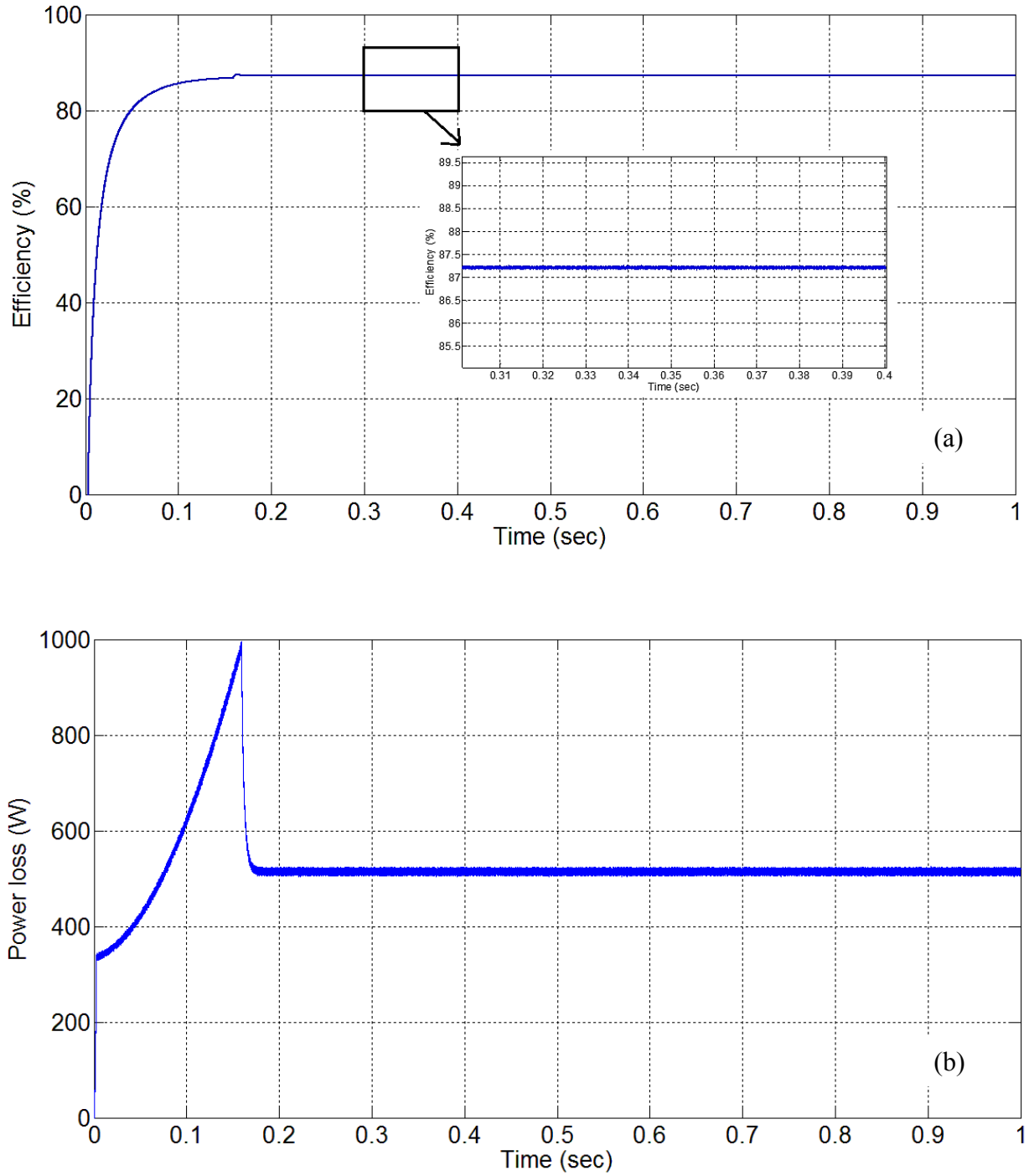


Fig. 5.14: Simulated response of the proposed LMC for IPMSM drive at rated speed (183 rad/s) and load (19 Nm); (a) efficiency with LMA, and (b) power loss with LMA.

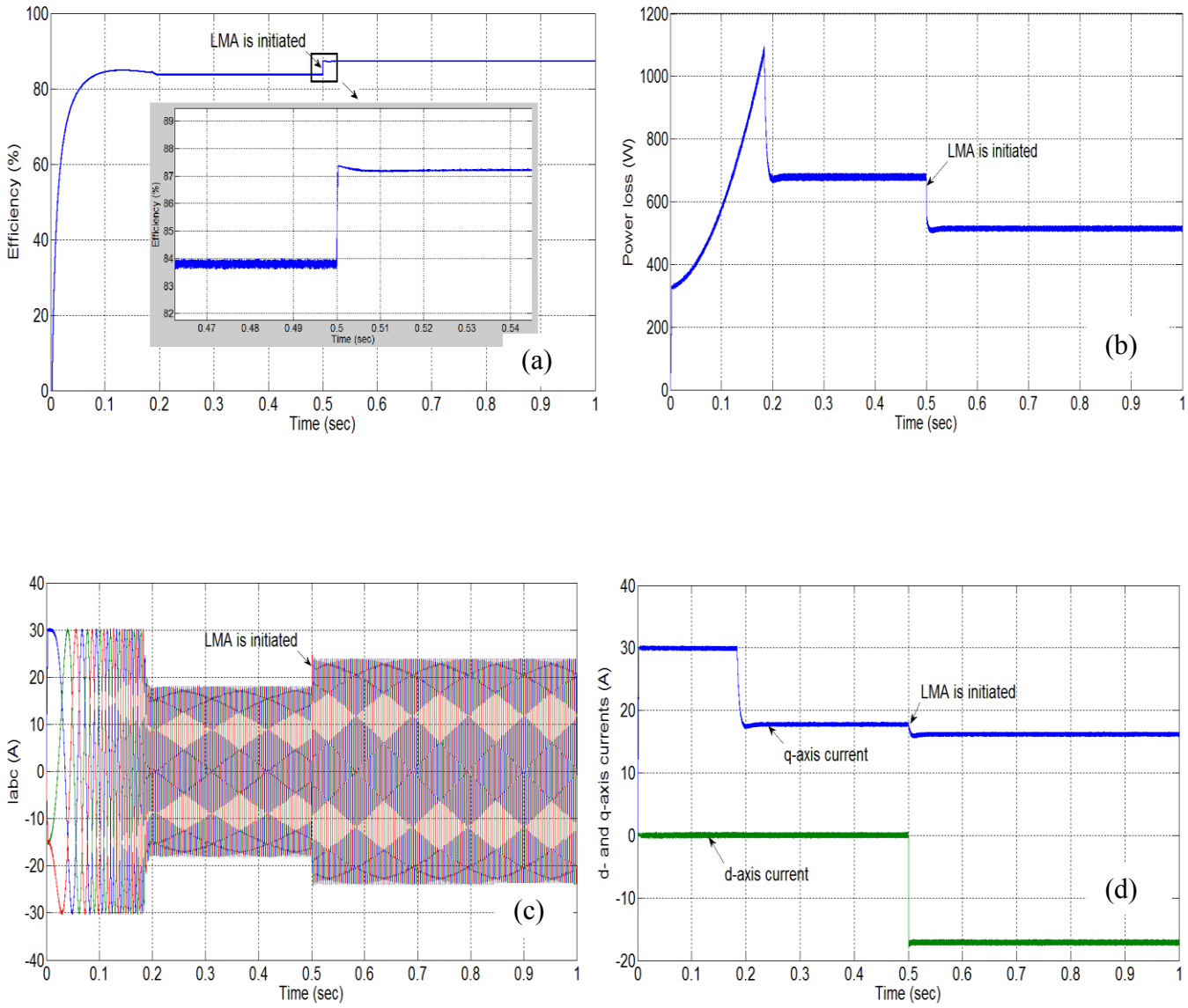


Fig. 5.15: Simulated response of the proposed LMC for IPMSM drive at rated speed and load condition; (a) efficiency, (b) power loss, (c) three phase current, and (d) d- and q-axis currents.

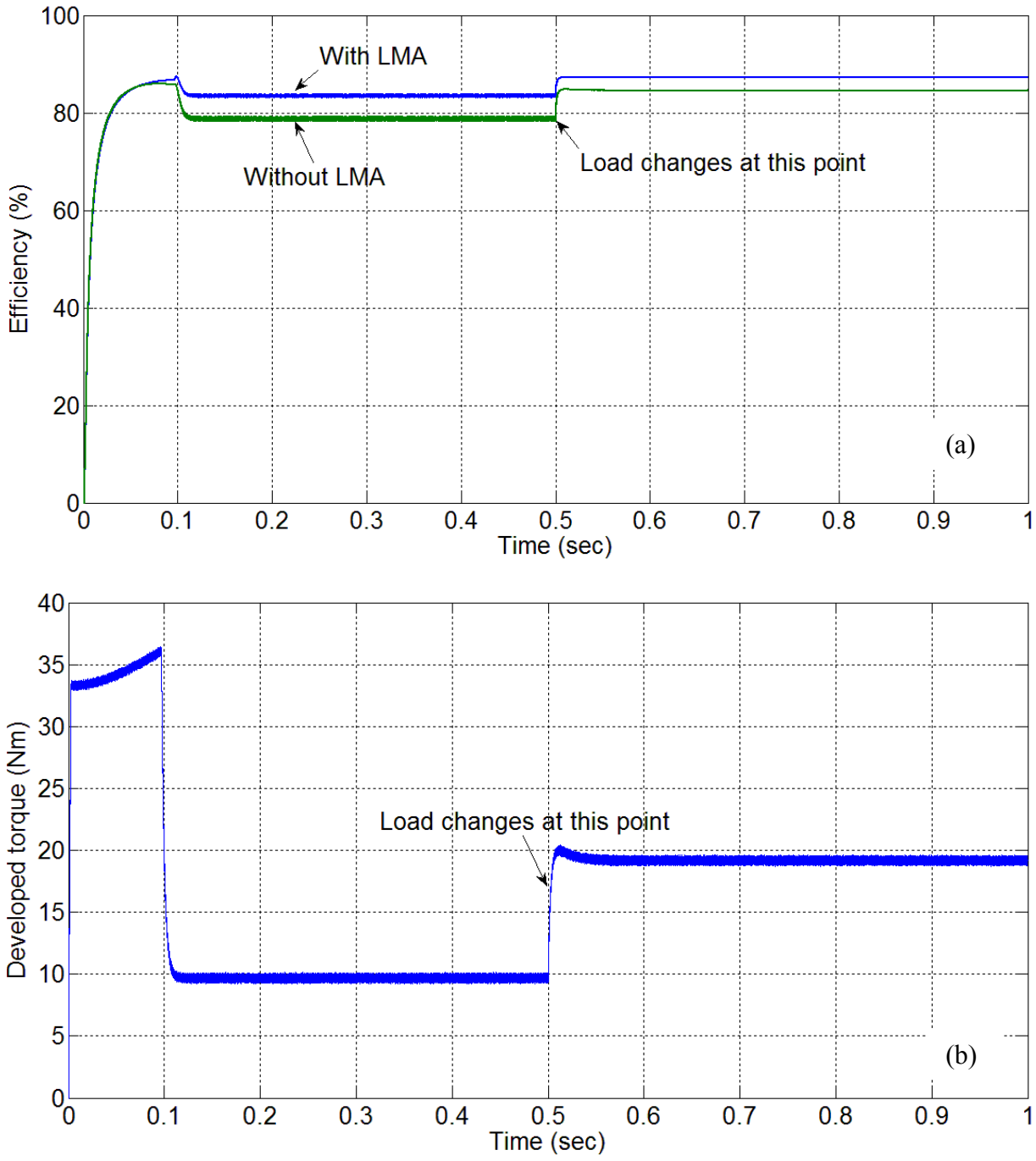


Fig. 5.16: Simulated responses of the proposed IPMSM drive with and without LMA at rated speed (183 rad/s) and step change in load 9.5 Nm to 19 Nm at t=0.5s; (a) efficiency, and (b) developed torque.

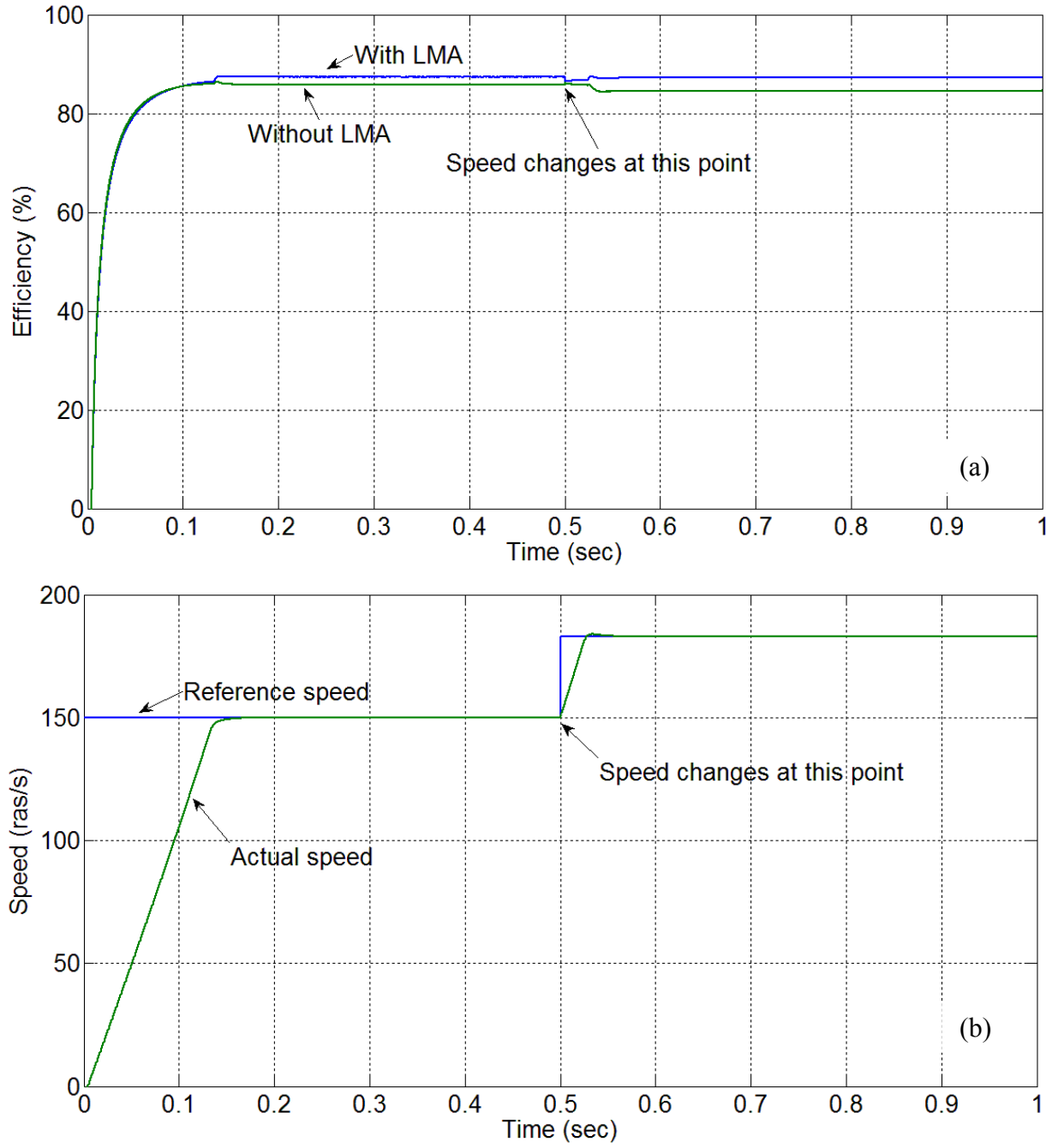


Fig. 5.17: Simulated responses of the proposed IPMSM drive with and without LMA for rated load (19 Nm) and step change in command speed 150 rad/s to 183 rad/s at t=0.5s; (a) efficiency, and (b) speed.

## 5.5 Concluding Remarks

An ANFIS based NFC has been proposed in this thesis. The NFC has been utilized to achieve both the good features of FLC and ANN controller. The proposed NFC is simple and therefore has low computational burden. Therefore, the proposed ANFIS based NFC is developed in real-time. The LMC technique developed in Chapter 3 has also been incorporated to achieve high efficiency while maintaining high dynamic performance. The simulation results verify the feasibility of the proposed drive. The performance of the proposed NFC and LMC based IPMSM drive has been found superior to the nonlinear and PI controller presented in Chapter 4. Therefore, the proposed ANFIS and LMC based drive is developed in real-time which is presented in next chapter. The proposed ANFIS and LMC based provide an efficient and robust IPMSM drive. The weights and membership functions are updated online based on back propagation technique which provide a unique feature of the adaptive controller.

# Chapter 6

# Experimental Implementation

This chapter presents the experimental implementation of the proposed IPMSM drive system in real-time using DSP controller board DS 1104 on an available laboratory 5hp IPMSM. The detail hardware and software implementation are described below. Experimental results and discussion are also presented in order to verify the effectiveness of the proposed controllers in real-time.

## 6.1 DSP-Based Hardware Implementation of IPMSM Drive

The DSP controller board DS 1104 is used for the real-time implementation of the proposed IPMSM drive system. The board is installed in an Intel PC with uninterrupted communication through dual port memory. The block diagram of the DSP board is shown in Fig. 6.2.The DS1104 board is mainly based on a Texas Instrument MPC8240 64-bit floating point digital signal processor. The DS1104 board uses a PowerPC type PPC603e processor which operates at the clock of 250 MHz with 32 KB cache. This board has a 32 MB of SDRAM global memory and 8 MB of flash memory. The DSP is supplemented by a set of on-board peripherals used in digital control

systems including analog to digital (A/D), digital to analog (D/A) converters and digital incremental encoder interfaces. This board is also equipped with a TI TMS320F240 16-bit micro controller DSP that acts as a slave processor and provides the necessary digital I/O ports configuration and powerful timer functions such as input capture, output capture and PWM generation. In this work, the slave processor is used for only digital I/O subsystem configuration. Rotor position is sensed by an optical incremental encoder mounted at the rotor shaft and is fed back to the DSP board through the encoder interface. The encoder used in this work generates 1024 pulses per revolution. A 24-bit position counter is used to count the encoder pulses and is

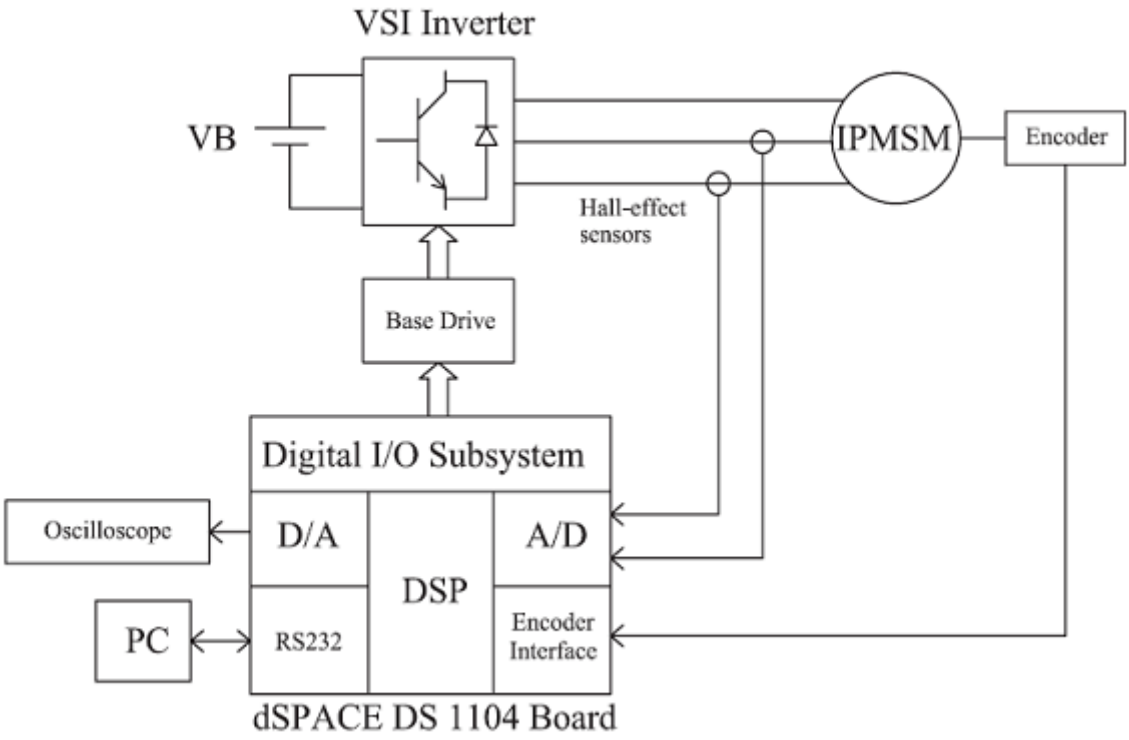


Fig. 6.1: Hardware schematic for experimental implementation of VSI fed IPMSM drive.

read by a calling function in the software. The counter is reset in each revolution by the index pulse generated from the encoder. The motor speed is computed from the measured rotor position angles using discrete difference equation. The actual motor currents are measured by the Half-effect

sensors, which have current range of 0 ~ ±200A and a frequency range of 0 ~ 250 kHz. The current signals are fed back to DSP board through A/D channels. The output current signal of these sensors is converted to a voltage across the resistor connected between the output terminal of the sensor and ground. One can scale the output voltage by selecting the value of the resistors. These resistors can be within the range 0~100Ω. As the output voltages due to these current sensors are low, interface circuit is used to amplify the output of the sensor. The interface circuit consists of non-inverting amplifier with operational amplifier LM741CN as shown in Appendix C. As the motor neutral is not grounded, only two phases current are measured and third phase current is calculated using Kirchoff's Current Law in software.

The hysteresis-band current control PWM is used to generate the logic signals which act as firing pulses for the inverter switches. Thus, these six logic signals are the output of the DSP Board and fed to the base drive circuit of the IGBT inverter power module. The outputs of the digital I/O subsystem of the DS 1104 are six pulses with a magnitude of 5 V. This voltage level is not sufficient for the gate drive of IGBTs. Therefore, the voltage level is shifted from +5 V to +15V through the base drive circuit with the chip SN7407N as shown in Appendix C. At the same time it also provides isolation between low power and high power circuits.

# 6.2 Software Development of IPMSM Drive

The dSPACE DS1104 board is a self-contained system, not an embedded system. This means that board installed in the lab computer through a PCI slot is its own entity and none of the processing for a system implemented on the board is done by the host PC. As a result, the board requires that software be created and downloaded to the board for the system to function.

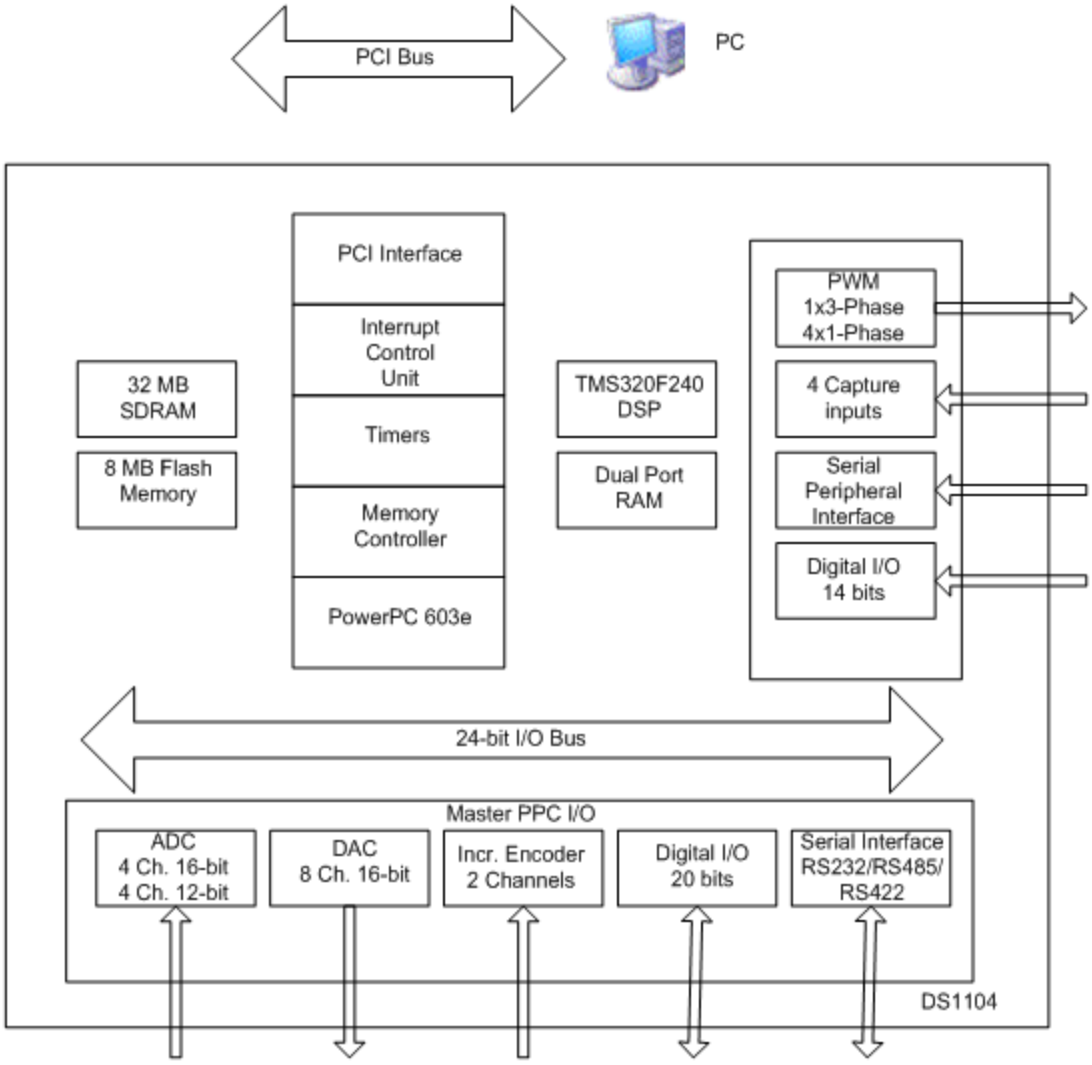


Fig. 6.2: Block diagram of the DS1104 board.

As a first step for the implementation of the proposed control algorithm, a real-time Simulink model for the complete drive system is developed and the dSPACE program code in ANSI ‘C’ is generated from it by the real-time workshop (RTW). The real-time Simulink model for the proposed control scheme is shown in detail in Appendix D. Then, ControlDesk software is used to download software to the DSP board, start and stop function of the DS1104 as well as create a layout for interfacing with global variables in dSPACE programs. The sampling frequency used

in this work is found to be 10 kHz. If the sampling frequency that is higher than 10 kHz is chosen, the 'overrun error' occurs, which indicates too much computational burden for the processor. The flow chart of the software is shown in Fig. 6.3. After initializing all the required variables, the timer interrupt routine is set up to read the values of the currents and rotor position every 100 μs. The motor currents obtained through analog to digital converter (ADC) channels 1 and 2 are multiplied by the gain 18.814 and 16.667, respectively in order to obtain the actual current values in software. These constants depend on the Hall-effect sensors specifications and the resistors used at the output node of these sensors and the resistors used in the interface circuit. After these digitalized currents in *abc* coordinates are converted into rotating reference frame of *d-q* axes coordinates.

The rotor position is measured by encoder and can be calculated in radian by the equation of $2\pi/1024$ x P, where P is the number of pulses counted in the counter. Once the rotor position angle is calculated, the rotor speed is computed from the measured rotor position angles using numerical backward differentiation. The speed error between actual and command is the input to the NFC which gives q-axis current, $i_q$ as output. Based on the proposed LMC and optimum $i_d$ is calculated form $i_q$ and actual motor speed. to achieve high efficiency.

# 6.3 Experimental Results and Discussion

Experimental tests are performed to verify the effectiveness of the proposed NFC and LMC based IPMSM drive at different operating conditions. Experimental tests are also carried out for conventional PI controller in order to prove the superiority of the ANFIS to the PI controller. The

gains of the PI controller are chosen as $K_P$=0.01 and $K_I$=0.4 by trial and error method in order to get minimum overshoot and settling time at rated conditions.

First the dynamic speed performance of the proposed ANFIS based LMC is tested. The starting responses of the IPMSM drive with PI and proposed ANFIS controller are shown in Fig. 6.4. It is seen from Fig. 6.4(a) that with PI controller the motor can follow the command speed but it has high overshoot and higher settling time than the proposed ANFIS based NFC controller. It is seen from Fig. 6.4(b) that the proposed NFC can follow command speed with almost no steady-state error and without overshoot/undershoot. The corresponding d-q axis currents, a-b phase currents and b-c phase currents for the proposed ANFIS controller are shown in Fig. 6.4(c)-(e), respectively. As the d-axis current is nonzero, it contributes to utilize the reluctance torque of the motor. The a-b and b-c phase currents indicate the balanced operation of the motor in real-time. Due to the limitation of the oscilloscope which have only 2 channels, the three phase currents could not be obtained, simultaneously. The performance for a step change in reference speed from 120 rad/s to 150 rad/s is also investigated for both PI and proposed ANFIS controller at no load. The step change of command speed is applied using real-time Simulink step block and a timer. It is seen from Fig. 6.5(a) and (b) that the proposed ANFIS based IPMSM drive can follow the command speed faster and smoothly as compared to the PI controller. Even the PI controller exhibits small steady-state error.

The robustness of the proposed ANFIS based NFC with sudden load variation is also tested in real-time. Fig. 6.6(a) and (b) show the experimental speed responses of the PI and proposed ANFIS controller for step decrease in load, respectively. It is clearly seen from these figures that the ANFIS based IPMSM drive can follow the command speed very quickly as compared to the conventional PI controller. Initially the motor was started with half load and then suddenly the

load was released. The resistance load was hooked up to a DC machine side of IPMSM and by turning the switches "on" and "off" the load was changed. Again, the proposed ANFIS based IPMSM drive is tested with step increase in load, the results are shown in Fig. 6.7. It is seen that the motor converges to its reference speed very quickly with a small dip in speed. The corresponding adjustments in q-axis current, line current and speed error are shown in Fig. 6.7(b)-(d), respectively. With the increase of load the q-axis current increases to supply more torque.

Fig. 6.8 shows another response of reference speed change from 130 rad/s to 170 rad/s for the proposed ANFIS controller. Fig. 6.8(a) shows the speed response, it is observed the actual speed follows the command speed quickly almost without any steady-state error. Fig. 6.8(b) and (c) shows the corresponding d-q axis currents and speed error, respectively.

Now, the effectiveness of the LMC is tested in real-time. Fig. 6.9 shows the efficiency of approximately 84% when no LMA is used with ANFIS based IPMSM drive while the motor is running at rated speed with 30% rated load condition. Fig. 6.10 show the real-time experimental response of IPMSM drive with proposed LMA at rated speed and 30% rated load. The motor is tested at light load condition as the efficiency drops at light load. From Fig. 6.10, it clearly seen that the efficiency of the motor is approximately 87%. Which is almost 3% higher than without any LMA. Thus, it verifies the simulation results. Fig. 6.11 shows the power loss before and after LMA is initiated. As expected the significant power loss reduction is achieved by the proposed LMA. Therefore, the performance of the proposed ANFIS and LMC based IPMSM drive has been found to be robust and stable while maintaining high efficiency in real-time for different operating conditions. However, there is some ripple in speed, which needs to be minimized. The total power loss $P_L$ and output power $P_{out}$ is calculated using the Eqns. (3.26) and (3.23), respectively. From the $P_L$ and $P_{out}$ the efficiency is calculated using Eqn. (3.25) and measured in real-time.

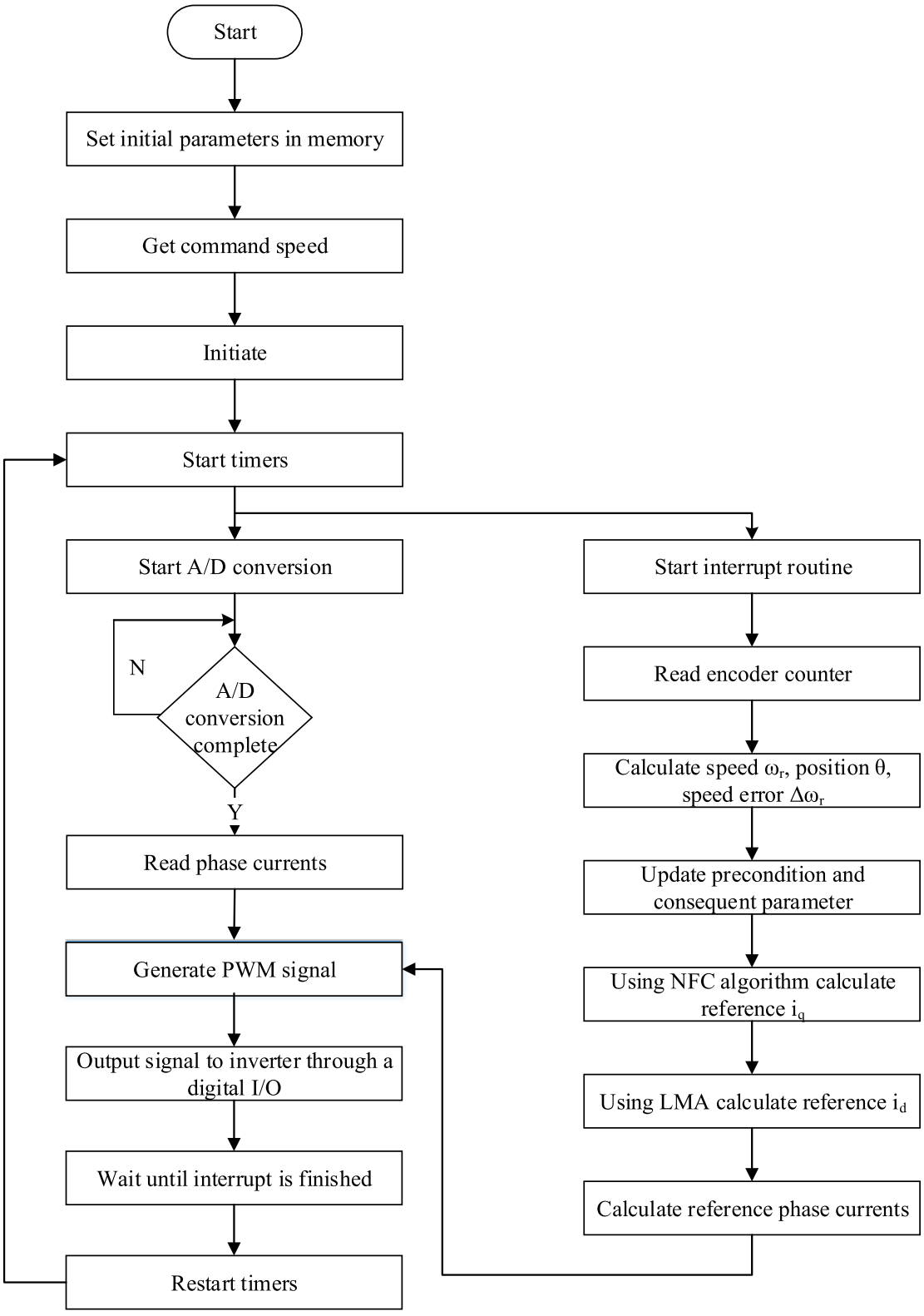


Fig. 6.3: Flow chart for the Real-time implementation of the proposed ANFIS and LMC based IPMSM.

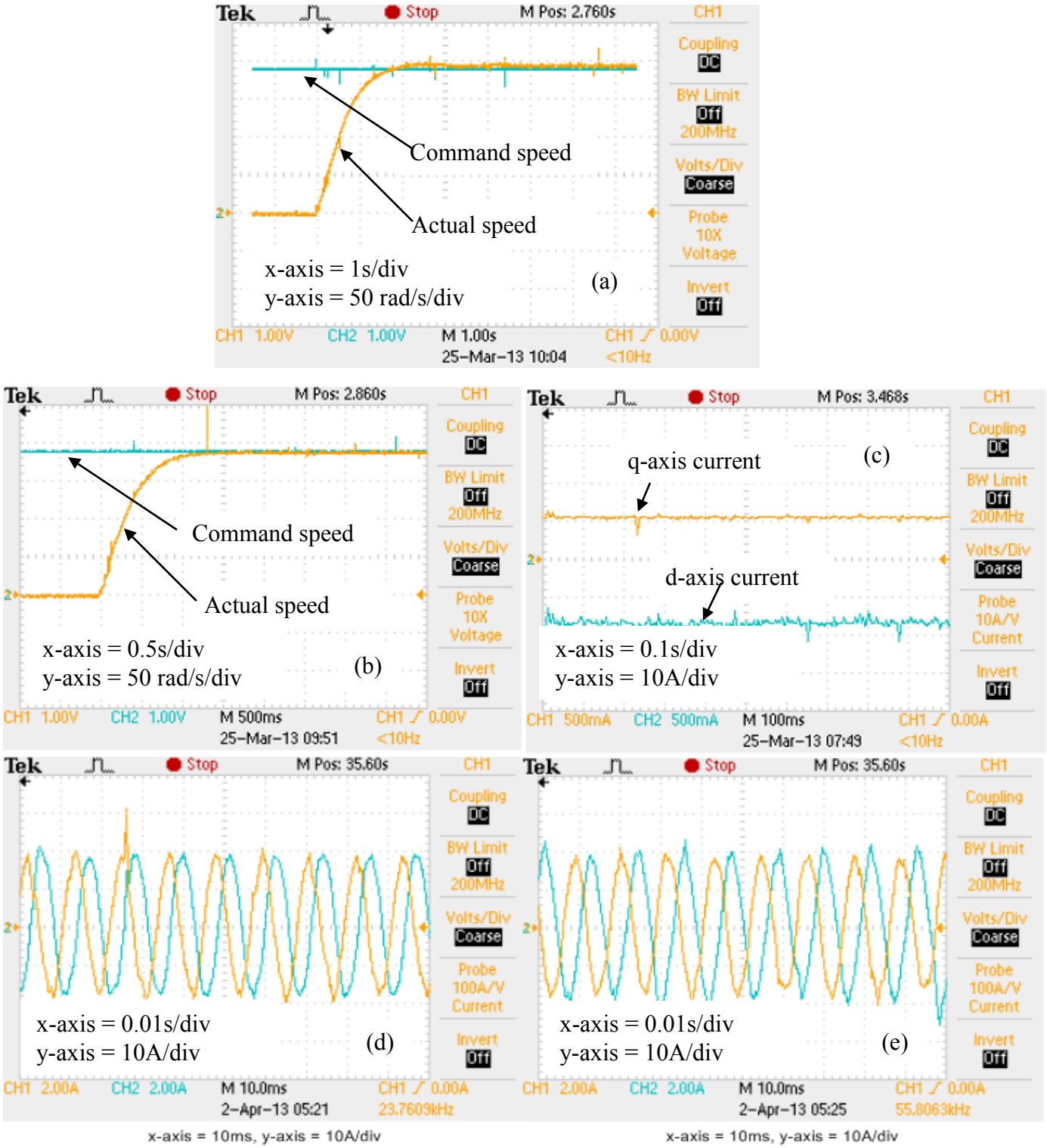


Fig. 6.4: Experimental starting responses at rated speed (183 rad/s) at 30% load; (a) PI based speed, (b) ANFIS based speed, (c) ANFIS based $i_d$ and $i_q$, (d) ANFIS based $i_a$ and $i_b$, and (e) ANFIS based $i_b$ and $i_c$.

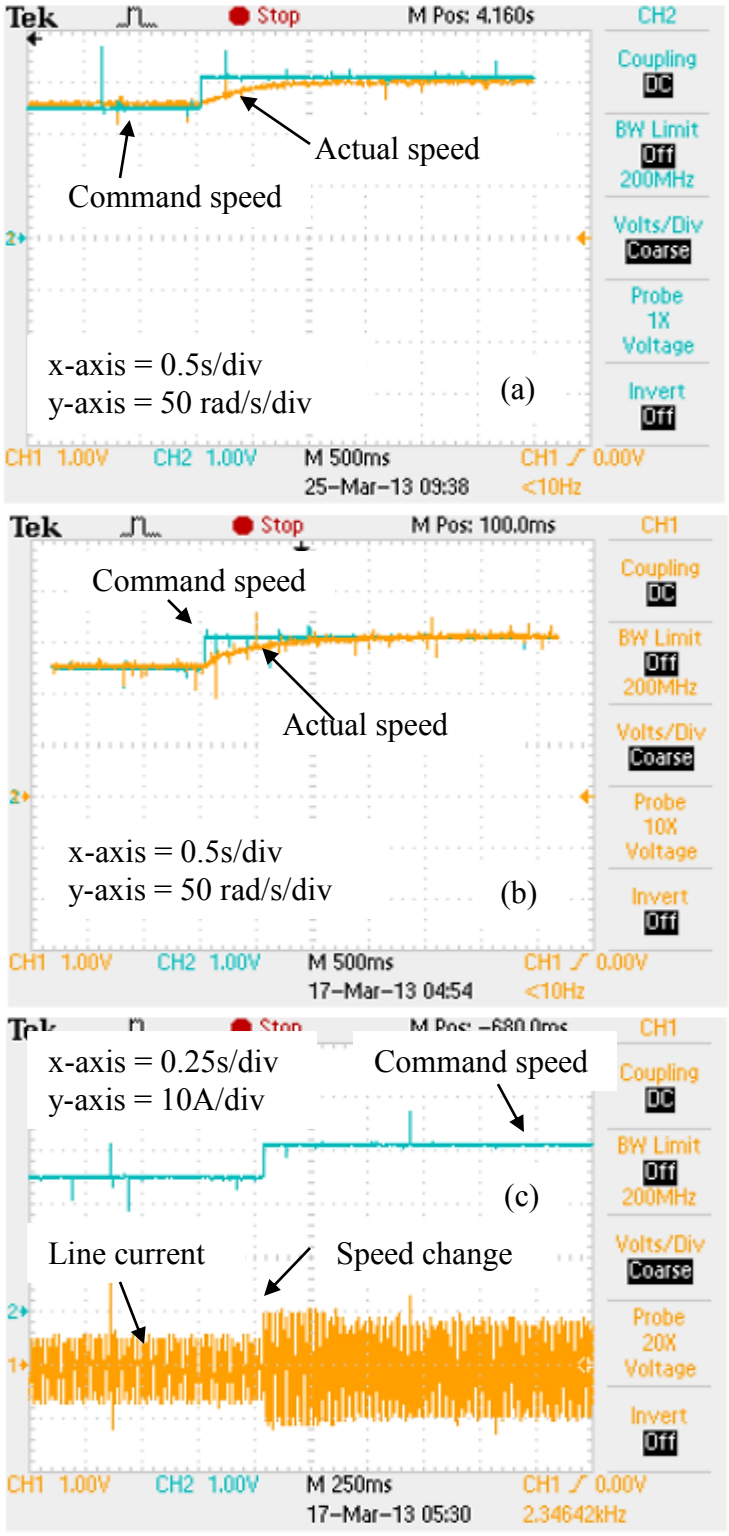


Fig. 6.5: Experimental responses for a step increase in speed reference from 120 rad/s to 150 rad/s; (a) PI based speed, (b) ANFIS based speed, and (c) ANFIS based line current.

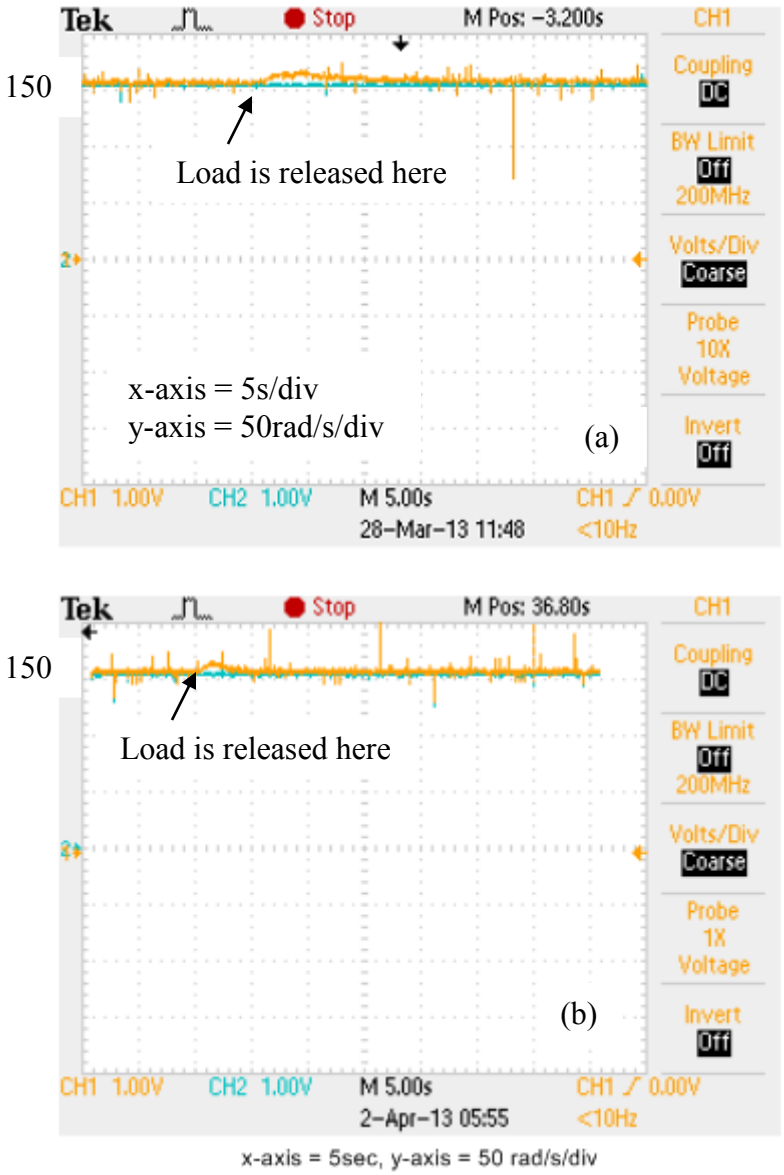


Fig. 6.6: Experimental speed responses for step decrease in load at 150 rad/s; (a) PI, and (b) ANFIS.

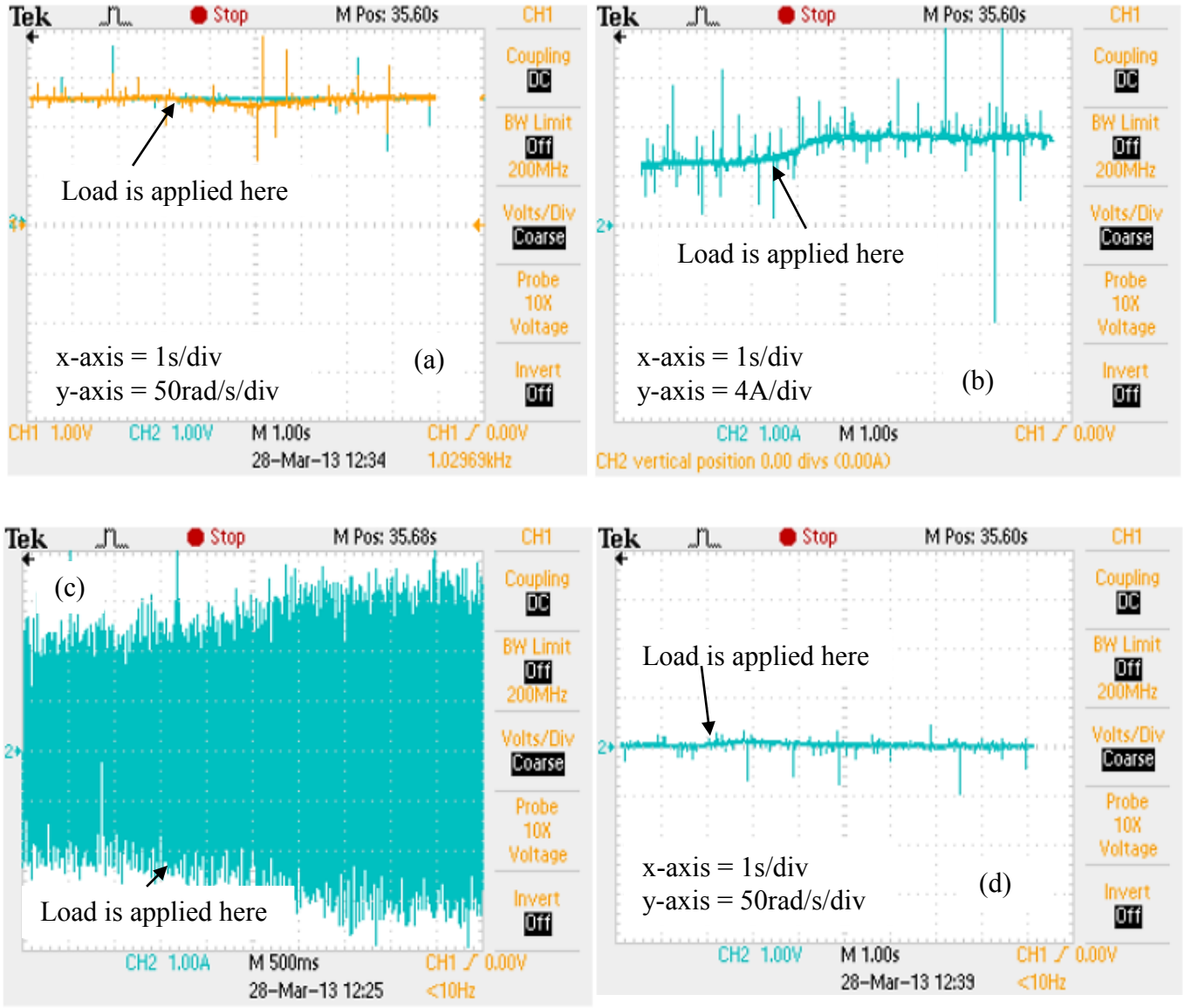


Fig. 6.7: Experimental responses of the proposed ANFIS and LMC based drive for a step increase in load at 120 rad/s speed; (a) speed, (b), q-axis current, (c) line current, and (d) speed error.

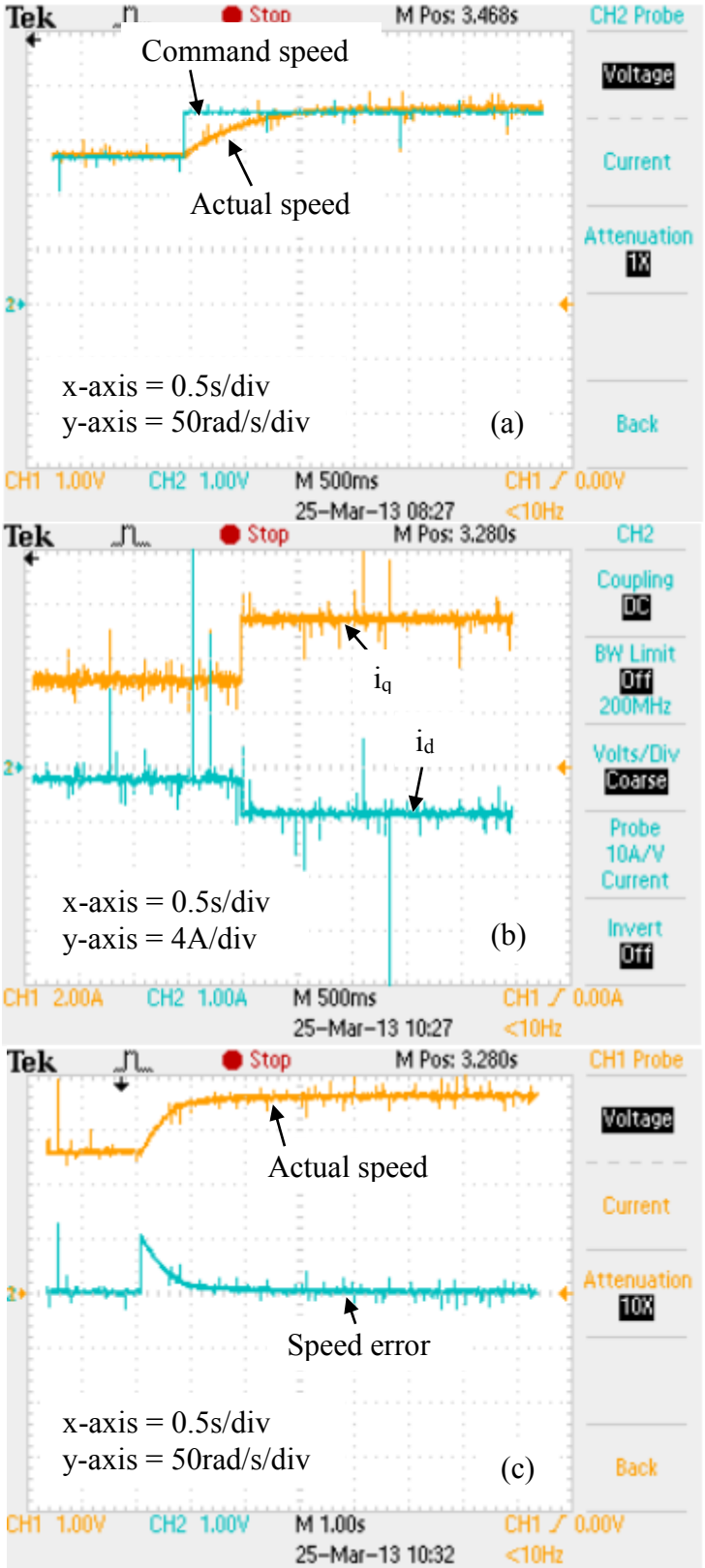


Fig. 6.8: Experimental responses of the proposed ANFIS and LMC based drive for a step increase in speed reference from 130 rad/s to 170 rad/s; (a) speed, (b) $i_d$ and $i_q$ currents, and (c) speed error.

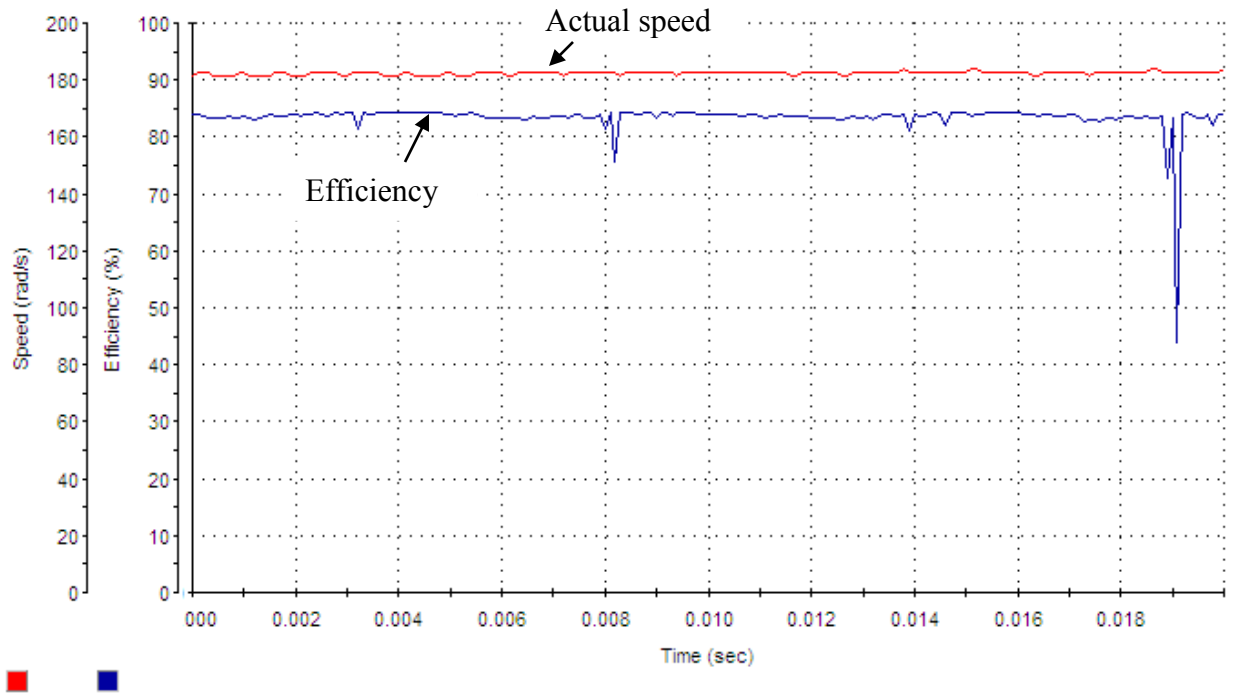


Fig. 6.9: Experimental efficiency response of the proposed ANFIS without any LMA at rated speed (183 rad/s) and 30% rated load.

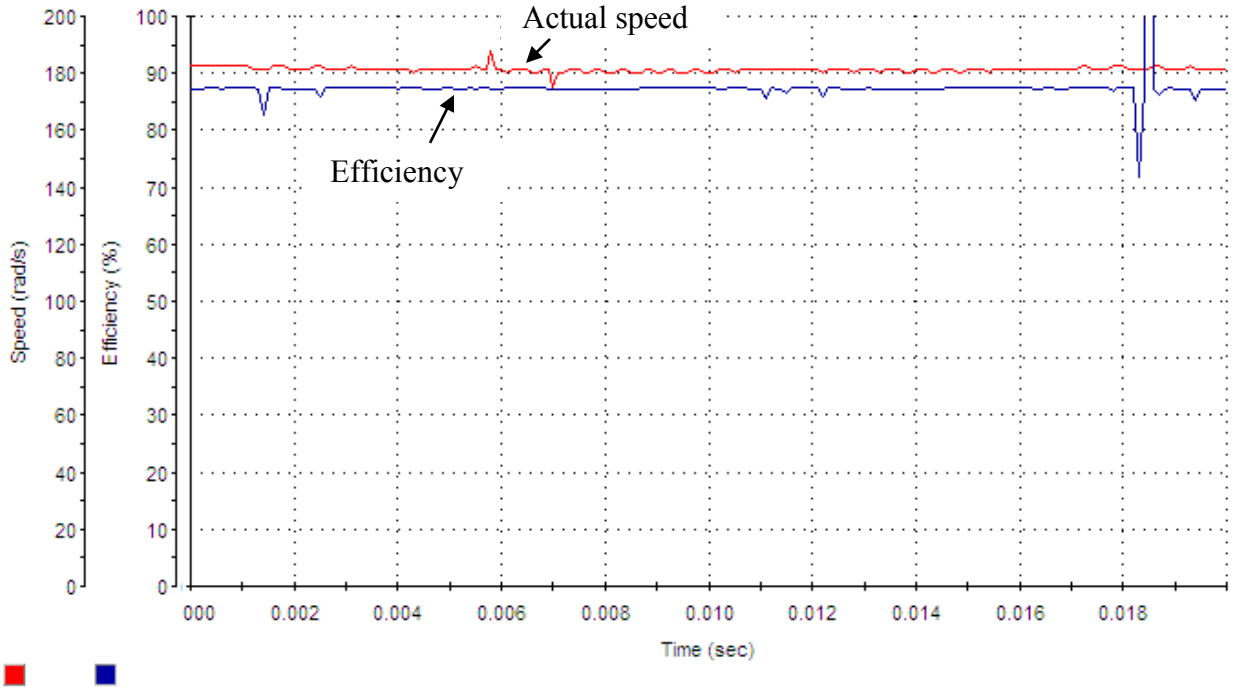


Fig. 6.10: Experimental efficiency response for the proposed ANFIS with LMC at rated speed (183 rad/s) and 30% rate load.

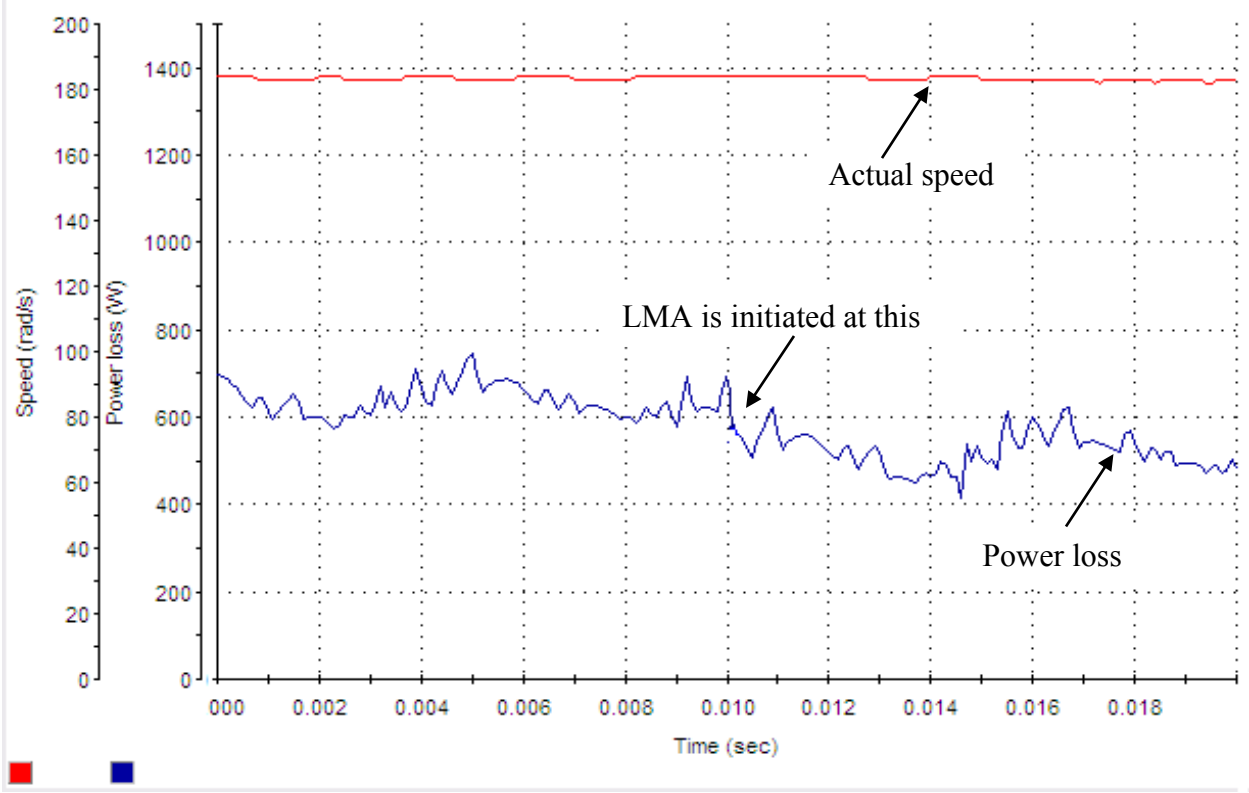


Fig. 6.11: Experimental power loss response for the proposed ANFIS with and without LMA at rated speed 183 rad/s and 30% rated load.

# 6.4 Concluding Remarks

The detailed experimental implementation of the proposed NFC and LMC based IPMSM drive using dSPACE DSP board DS1104 has been presented in this Chapter. The performance of the proposed drive has been tested in real-time at different operating conditions such as sudden change in reference speed and load. In order to prove the superiority, the performance of the proposed NFC based drive has been compared with a conventional PI controller based drive. Due to incorporation of LMA, efficiency is improved as compared to without any LMA scheme. The performance of the proposed ANFIS and LMC drive has been found robust while maintaining high efficiency.

# Chapter 7

# Conclusions

As mentioned in Chapter 1 of this thesis, the loss minimization of IPMSMs can significantly contribute to overall energy saving considering the fact, that the ac motors consume more than half of the electric energy generated in the world. At the same time, the excellent dynamic performance of a controller has to be achieved in order to be used in high performance applications. In agreement with these requirements, in this thesis a loss model-based efficiency algorithm for vector controlled IPMSM drive has been developed. In order to achieve high dynamic performance (HPD), an adaptive backstepping-based nonlinear controller (ABNC) has been proposed. However, ABNC depends on the motor parameters and it requires lot of computation. To overcome these disadvantages, a new intelligent control has been proposed based on neuro-fuzzy controller (NFC). In recent years intelligent controllers such as FLC, ANN and NFC become popular for control of electric motors due to their inherent properties of generalization, parameter insensitivity, parallel processing and nonlinear mapping between input and output. The problem of controlling the electric motors in HPD is uncertainty of the motor model parameters. The intelligent controller adjusts the control output with different dynamic conditions with its inherent adaptive nature. Therefore, an ANFIS based NFC is developed with tuning the membership function. The design, analysis, simulation, real-time implementation and extensive experimental test results have been presented in this thesis.

In Chapter 1, the basic background of ac and dc motors have been presented. The literature review of conventional PI controller, adaptive controller, intelligent controller and various loss minimization algorithms (LMA) has been discussed in this thesis. In the literature review of LMA, few of the drawbacks were identified i.e. a long search time, torque pulsations, demand for the precise knowledge of a loss model and parameter dependency. A new loss model-based controller (LMC) combined with ABNC and NFC has been proposed in order to overcome the limitations and drawbacks of the existing loss minimization controllers.

In Chapter 2, the mathematical model of IPMSM has been derived for vector control scheme.

In Chapter 3, losses that are involved in IPMSM drives were classified and possible methods of loss reduction were explained. A mathematical model of IPMSM incorporating copper and iron losses has been developed. A new LMA has been developed based on the steady state motor model.

In Chapter 4, an ABNC has been developed for IPMSM drive incorporating LMA. Step-by-step procedures for the control and parameter adaptation design have been proved. Stability analysis has also been presented. The simulation model for the proposed ABNC based LMA has been developed. The extensive simulation results at different operating conditions were shown. For the comparison purpose a conventional PI controller have also been developed. From the simulation results, the ABNC have been found to follow the reference speed smoothly and quickly maintaining the global stability.

In Chapter 5, an ANFIS based NFC has been developed with tuning the membership function online. The tuning of the membership functions of the NFC is discussed in this chapter. The NFC is designed in such a way that the computational burdens remain low which is suitable

for real-time implementation. For the proposed NFC, the LMA has also been incorporated to achieve high efficiency while maintaining high performance. The extensive simulation results at different operating conditions were also shown. The performance of the proposed ANFIS based NFC has been found as superior to other controllers presented in this thesis as the membership functions as well as weights were tuned online for NFC. Therefore, only ANFIS real-time results have been presented.

In Chapter 6 detailed implementation technique and experimental result of the proposed ANFIS and LMC based IPMSM drive have been presented. It has been found that the experimental results verify the simulation results shown in chapter 5.

# 7.1 Achievements of the Thesis

Achievements of the thesis can be summarized as follows:

- Mathematical model of an IPMSM incorporating copper and iron losses has been derived. In these equations, no extra state variables are added while the losses are incorporated into the equations. Hence, this set of equation can be used to develop controllers that take copper and iron losses into account without adding too much complexity to the design.
- A new loss model-based controller (LMC), which operates an IPMSM at the minimum loss point has been developed based on the steady-state motor model described in chapter 3.
- An adaptive backstepping-based nonlinear control technique incorporating LMA has been developed for IPMSM. Stability of the ABNC based IPMSM drive has been proved by Lyapunov's stability theory. Besides control laws, mechanical parameter estimation update laws have also been developed.

- An ANFIS and LMC based IPMSM has been developed. The performance of the controller has been investigated both in simulation and experiment at different operating conditions. The performance of the proposed ANFIS has been found as superior to other controllers presented in this thesis.
- In development of an ANFIS based NFC, a back propagation algorithm for tuning of the membership functions and weights have been developed. Tuning of weights were performed indirectly by tuning precondition and consequent parameters.

# 7.2 Future Work

This thesis develops an LMA and different types of speed controller to achieve both high efficiency and high performance of IPMSM. Although simulation and experimental results show efficiency improvement and robustness of the controller but there are some possible improvement margins for the system which are as follows:

- More research studies are being reported using the speed sensorless approach. Implementing speed sensorless will eliminate the need for an encoder as well as any difficulties associated with it.
- In the development of the adaptive controller, only the mechanical parameters were estimated, d-q axes inductances are varying with different operating condition. So future work can be done with the estimation of electrical parameters too.
- In future a speed ripple minimization technique need to be design to reduce the speed ripple in real-time.

# References


[1] A. J. Pansini, Basics of Electric Motors, 2 ed., Tulsa, Oklahoma: Pennwell Books, 1996.

[2] P. L. Alger and R. E. Arnold, "The History of Induction Motors in America," *Proceedings of The IEEE,* vol. 64, no. 9, pp. 1380-1393, Sept. 1976.

[3] B. K. Bose, Modern Power Electronics and AC Drives, Upper Saddle River, NJ: Prentice Hall, 2002.

[4] M. A. Rahman and P. Zhou, "Analysis of brushless permanent magnet synchronous motors," *IEEE Trans. on Industrial Electronics,* vol. 43, no. 2, pp. 256-267, April 1996.

[5] R. M. Crowder, Electric Drives and Their Controls, Clarendon Press, 1995.

[6] R. H. Park, "Two-reaction theory of synchronous machines generalized method of analysis-part I," *Trans. of the American Institute of Electrical Engineers,* vol. 48, no. 3, pp. 716-727, July 1929.

[7] F. Blaschke, "The principle of field orientation as applied to the new TRANSVECTOR-closed loop control systems for rotating field machines," *Siemens* Review, vol. 34, pp. 217-220, May 1972.

[8] A. Abbondanti, "Methods of flux control in induction motors driven by variable frequency, variable voltage supplies," in *Conf. Rec. Int. Semiconducotr Power Converter*, 1977.

[9] S. J. Chapman, Electic Machinery Fundamentals, New York, NY: McGraw-Hill, 1999.

[10] E. C. Lister and M. R. Golding, Electric Circuits and Machines, McGraw-Hill Ryerson Limited, 1987.

[11] M. N. Uddin, "Intelligent Control of an Interior Permanent Magnet Synchronous Motor," PhD. Thesis, Memorial University of New Foundland, St. John, 2000.

[12] G. R. Slemon, Electric Machines and Drives, Addison-Wesley Pub, 1992.

[13] K. J. Overshott, "Magnetism: it is permanent," *IEE Proceedings A Science, Measurement & Technology,* vol. 139, no. 1, pp. 22-30, Jan. 1991.

[14] A. Consoli and A. Raciti, "Analysis of permanent magnet synchronous motors," *IEEE Trans. on Industry Applications,* vol. 43, no. 2, pp. 350-354, March/April 1991.

[15] T. A. Lipo, "Comparative analysis of permanent magnet AC machines in variable speed applications," *University of Wisconsin - Madison*, *ECE Dept.*, WEMPEC Research Report No. 82-12, Sept. 1982.

[16] R. S. Colby, "Classification of inverter driven permanent magnet synchronous motors," in *Conference Record of IEEE Industry Applications Society Annual Meeting*, Pittsburgh, 1988.

[17] J. T. Boys and S. J. Walton, "Scalar control: an alternative AC drive philosophy," *IEE Proceedings B Electric Power Applications,* vol. 135, no. 3, pp. 151-158, May 1988.

[18] G. Kohlrusz and D. Fodor, "Comparison of scalar and vector control strategies of induction motors," *Hungarian Journal of Industrial Chemistry,* vol. 39, no. 2, pp. 265-270, 2011.

[19] *Super energy saving variable speed drives manual,* Yaskawa Electric Inc..

[20] W. Shepherd and L. N. Hulley, Power Electronics and Motor Control, Cambridge University Press, 1987.

[21] P. Zhou, M. A. Rahman and M. A. Jabbar, "Field circuit analysis of permanent magnet synchronous motors," *IEEE Trans. on Magnetics,* vol. 30, no. 4, pp. 1350-1359, July 1994.

[22] G. R. Slemon and A. V. Gumaste, "Steady State Analysis of a Permanent Magnet Synchronous Motor Drive With Current Source Inverter," *IEEE Trans. on Industrial Applications,* Vols. IA-19, no. 2, pp. 190-197, March/April 1983.

[23] A. V. Gumaste and G. R. Slemon, "Steady State Analysis of a Permanent Magnet Synchronous Motor Drive With Voltage Source Inverter," *IEEE Trans. on Industrial Applications,* Vols. IA-17, no. 2, pp. 143-151, March/April 1981.

[24] B. K. Bose and P. M. Szczesny, "A microcomputer-based control and simulation of an advanced IPM synchronous machine drive system for electric vehicle propulsion," *IEEE Trans. on Industrial Applications,* vol. 35, no. 4, pp. 547-559, Nov. 1988.

[25] P. Pillay and R. Krishnan, "Control characteristics and speed controller design for a high performance permanent magnet synchronous motor drive," *IEEE Trans. on Power Electronics,* vol. 5, no. 2, pp. 151-159, April 1990.

[26] Y. Kazunori, S. Ogasawara and H. Akagi, "Performance evaluations of a position-sensorless IPM motor drive system based on detection of current switching ripples," in *IEEE 31st Annual Power Electronics Specialists Conference*, Galway, 2000.

[27] S. Ogasawara and H. Akagi, "Implementation and position control performance of a position-sensorless IPM motor drive system based on magnetic saliency," *IEEE Trans. on Industry Applications,* vol. 34, no. 4, pp. 806-812, July-Aug. 1998.

[28] C. Mademlis and V. G. Agelidis, "A high-performance vector controlled interior PM synchronous motor drive with extended speed range capability," in *Annual Conference of IEEE Industrial Electronics Society*, Denver, 2001.

[29] S. Bolognani, L. Tubiana and M. Zigliotto, "EKF-based sensorless IPM synchronous motor drive for flux-weakening applications," *IEEE Trans. on Industry Applications,* vol. 39, no. 3, pp. 768-775, May-June 2003.

[30] S. Morimoto, M. Sanada and Y. Takeda, "Effects and compensation of magnetic saturation in flux-weakening controlled permanent magnet synchronous motor drives," *IEEE Trans. on Industry Applications,* vol. 30, no. 6, pp. 1632-1637, Nov./Dec. 1994.

[31] E. Cerruto, A. Consoli, A. Raciti and A. Testa, "A robust adaptive controller for PM motor drives in robotic applications," *IEEE Trans. on Power Electronics,* vol. 10, no. 1, pp. 62-71, Jan. 1995.

[32] A. Consoli and C. Antonio, "A DSP based Sliding Mode Field Oriented Control of an Interior Permanent Magnet Synchronous Motor Drive," in *Conference Proceedings IPEC*, Tokyo, 1990.

[33] M. Ghribi and H. Le-Huy, "Optimal control and variable structure combination using a permanent-magnet synchronous motor," in *Conference Record of the IEEE Industry Applications Society Annual Meeting*, Denver, 1994.

[34] B. Zhang and Y. Li, "A PMSM sliding mode control system based on model reference adaptive control," in *The Third Int. Power Electronics and Motion Control Conference*, Beijing, 2000.

[35] R. B. Sepe and J. H. Lang, "Real-time adaptive control of the permanent-magnet synchronous motor," *IEEE Trans. on Industry Applications,* vol. 27, no. 4, pp. 706-714, July/Aug, 1991.

[36] J. Zhou, Y. Q. Wang and R. J. Zhou, "Adaptive backstepping control of separately excited DC motor with uncertainties," in *International Conf. on Power System Technology*, Perth, 2000.

[37] M. A. Rahman, M. Vilathgamuwa, K. Tseng and M. N. Uddin, "Non-linear control of interior permanent magnet synchronous motor," *IEEE Trans. on Industry Applications,* vol. 39, no. 2, pp. 408-415, March/April 2003.

[38] H. Tan and J. Chang, "Adaptive backstepping control of induction motor with uncertainties," in *Proceedings of the American Control Conference*, San Diego, 1999.

[39] H. Tan and J. Chang, "Adaptive position control of induction motor systems under mechanical uncertainties," in *Proceedings of the IEEE Int. Conference on Power Electronics and Drive Systems*, 1999.

[40] C. I. Huang and L. C. Fu, "Adaptive backstepping speed/position control with friction compensation for linear induction motor," in *Proceedings of the IEEE Conference on Decision and Control*, 2002.

[41] H. Shieh and K. Shyu, "Nonlinear sliding-mode torque control with adaptive backstepping approach for induction motor drive," *IEEE Trans. on Industrial Electronics,* vol. 46, no. 2, pp. 380-389, April 1999.

[42] M. N. Uddin and M. M. I. Chy, "Online Parameter-Estimation-Based Speed Control of PM AC Motor Drive in Flux-Weakening Region," *IEEE Trans. on Industry Applications,* vol. 44, no. 5, pp. 1486-1494, Sept./Oct. 2008.

[43] M. N. Uddin and J. Lau, "Adaptive-backstepping-based design of a nonlinear position controller for an IPMSM servo drive," *Canadian Journal of Electrical and Computer Engineering,* vol. 32, no. 2, pp. 97-102, June 2007.

[44] Y. Tang and L. Xu, "Fuzzy logic application for intelligent control of a variable speed drive," *IEEE Trans. on Energy Conversion,* vol. 9, no. 4, pp. 679-685, Dec. 1994.

[45] M. N. Uddin and M. A. Rahman, "Fuzzy logic based speed control of an IPM synchronous motor drive," in *IEEE Canadian Conference on Electrical and Computer Engineering*, Edmonton, 1999.

[46] C. B. Butt, M. A. Hoque and M. A. Rahman, "Simplified fuzzy logic based MTPA speed control of IPMSM drive," *IEEE Trans. on Industry Applications,* vol. 40, no. 6, pp. 1529-1535, Nov./Dec. 2004.

[47] M. N. Uddin, M. A. Abido and M. A. Rahman, "Real-time performance evaluation of a genetic algorithm based fuzzy logic controller for IPM motor drives," *IEEE Trans. on Industry Applications,* vol. 41, no. 1, pp. 246-252, Jan./Feb. 2005.

[48] K. Zawirski, "Fuzzy robust speed control for permanent magnet synchronous motor servo drive," in *Preceeding of Int. Power Electronics & Motion Control Coference*, Prague, 1998.

[49] S. Bolognami and M. Zigliono, "Fuzzy logic control of a switched reluctance motor drive," *IEEE Trans. on Industry Applications,* vol. 32, no. 5, pp. 1063-1068, Sept./Oct. 1996.

[50] M. A. Rahman, M. N. Uddin and M. A. Abido, "An artificial neural network for online tuning of genetic algorithm-based PI controller for interior permanent magnet synchronous motor drive," *Canadian Journal of Electrical and Computer Engineering,* vol. 31, no. 3, pp. 159-165, 2006.

[51] M. A. Rahman and M. A. Hoque, "On-line adaptive artificial neural network based vector control of permanent magnet synchronous motors," *IEEE Trans. on Energy Conversion,* vol. 13, no. 4, pp. 311-318, Dec. 1998.

[52] M. E. Elbuluk, L. Long and I. Husain, "Neural-network-based model reference adaptive systems for high-performance motor drives and motion controls," *IEEE Trans. on Industry Applications,* vol. 38, no. 3, pp. 879-886, May/June 2002.

[53] N. Urasaki, T. . Senjyu and K. Uezato, "Neural network based high efficiency drive for interior permanent magnet synchronous motors compensating EMF constant variation," in *Proceedings of the Power Conversion Conference*, Osaka, 2002.

[54] M. A. El-Sharkawi, A. A. El-Samahy and M. L. El-Sayed, "High performance drive of DC brushless motors using neural network," *IEEE Trans. on Energy Conversion,* vol. 9, no. 2, pp. 317-322, June 1994.

[55] M. N. Uddin, M. A. Abido and M. A. Rahman, "Development and implementation of a hybrid intelligent controller for interior permanent magnet synchronous motor drive," *IEEE Trans. on Industry Applications,* vol. 40, no. 1, pp. 68-76, Jan./Feb. 2004.

[56] A. Rubaai, D. Ricketts and M. D. Kankam, "Development and implementaion of an adaptive fuzzy-neural-network controller for brushless drives," *IEEE Trans. on Industry Applications,* vol. 38, no. 2, pp. 441-447, March/April 2002.

[57] C. T. Lin, "A neural fuzzy control system with structure and parameter learning," *Fuzzy Sets and Systems,* vol. 70, no. 2-3, pp. 183-212, March 1995.

[58] F. J. Lin, C. H. Lin and P. H. Shen, "Self-constructing fuzzy neural network speed controller for permanent-magnet synchronous motor drive," *IEEE Trans. on Fuzzy Systems,* vol. 9, no. 5, pp. 751-759, Oct. 2001.

[59] M. M. I. Chy and M. N. Uddin, "Development and Implementation of a New Adaptive Intelligent Speed Controller for IPMSM Drive," *IEEE Trans. on Industry Applications,* vol. 45, no. 3, pp. 1106-1115, May/June 2009.

[60] Z. Ibrahim and E. Levi, "A comparative analysis of fuzzy logic and PI speed control in high performance AC drives using experimental approach," *IEEE Trans. on Industry Applications,* vol. 38, no. 5, pp. 1210-1218, Sept./Oct. 2002.

[61] C. B. Butt and M. A. Rahman, "Limitations of simplified fuzzy logic controller for IPM motor drive," in *Conference Record of IEEE Industry Applications Conference*, 2004.

[62] S. Y. Yi and M. J. Chung, "Robustness of fuzzy logic control for an uncertain dynamic system," *IEEE Trans. on Fuzzy Systems,* vol. 6, no. 2, pp. 216-225, May 1998.

[63] R. S. Colby and D. W. Novotny, "An efficiency-optimizing permanent magnet synchronous motor drive," *IEEE Trans. on Industry Applications,* vol. 24, no. 3, pp. 462-469, May/June 1988.

[64] D. S. Kirschen, D. W. Novotny and W. Suwanwisoot, "On-Line Efficiency Optimization of a Variable Frequency Induction Motor Drive," *IEEE Trans. on Industry Applications,* Vols. IA-21, no. 3, pp. 610-616, May 1985.

[65] S. Vaez, V. John and M. A. Rahman, "An on-line loss minimization controller for interior permanent magnet motor drives," *IEEE Trans. on Energy Conversion,* vol. 14, no. 4, pp. 1435-1440, Dec. 1999.

[66] S. Sul and M. Park, "A novel technique for optimal efficiency control of a current-source inverter-fed induction motor," *IEEE Trans. on Power Electronics,* vol. 3, no. 2, pp. 192-199, April 1988.

[67] G. S. Kim, I. J. Ha and M. S. Ko, "Control of induction motors for both high dynamic performance and high power efficiency," *IEEE Trans. on Industrial Electronics,* vol. 39, no. 4, pp. 323-333, Aug. 1993.

[68] S. Morimoto, Y. Tong, Y. Takeda and T. Hirasa, "Loss minimization control of permanent magnet synchronous motor drives," *IEEE Trans. on Industrial Electronics,* vol. 41, no. 5, pp. 511-517, Oct. 1994.

[69] C. Mademlis, I. Kioskeridis and N. I. Margaris, "Optimal efficiency control strategy for interior permanent-magnet synchronous motor drives," *IEEE Trans. on Energy Conversion,* vol. 19, no. 4, pp. 715-723, Dec. 2004.

[70] O. Ojo, F. Osaloni, Z. Wu and M. O. Omoigui, "A control strategy for optimum efficiency operation of high performance interior permanent magnet motor drives," in *Conference Record of the Industry Applications Conference*, 2003.

[71] S. Vaez-Zadeh, M. Zamanifar and J. Soltani, "Nonlinear Efficiency Optimization Control of IPM Synchronous Motor Drives with Online Parameter Estimation," in *IEEE Power Electronics Specialists Conference*, Jeju, 2006.

[72] M. N. Uddin and F. Abera, "Online loss minimization based vector control of IPMSM drive," in *IEEE International Electric Machines and Drives Conference*, Miami, 2009.

[73] M. N. Uddin and R. S. Rebeiro, "Online Efficiency Optimization of a Fuzzy-Logic-Controller-Based IPMSM Drive," *IEEE Trans. on Industry Applications,* vol. 47, no. 2, pp. 1043-1050, March/April 2011.

[74] S. K. Lim and K. H. Nam, "Loss-minimising control scheme for induction motors," *IEEE Proceedings - Electric Power Applications,* vol. 151, no. 4, pp. 385-397, 7 July 2004.

[75] G. O. Garcia, J. C. Luis, R. M. Stephan and E. H. Watanabe, "An efficient controller for an adjustable speed induction motor drive," *IEEE Trans. on Industrial Electronics,* vol. 41, no. 5, pp. 533-539, Oct. 1994.

[76] M. N. Uddin and S. W. Nam, "Development of a Nonlinear and Model-Based Online Loss Minimization Control of an IM Drive," *IEEE Trans. on Energy Conversion,* vol. 23, no. 4, pp. 1015-1024, Dec. 2008.

[77] Simulink User Guide, The Mathworks Inc., 2004.

[78] dSPACE Implementation Guide, dSPACE, 2008.

[79] M. Krstic, I. Kanellakopoulos and P. V. Kokotovic, Nonlinear and Adaptive Control Design, 1 ed., S. Haykin, Ed., Wiley-Interscience, 1995.

[80] J. Soltani and M. Pahlavaninezhad, "Adaptive backstepping based Controller design for Interior type PMSM using Maximum Torque Per Ampere Strategy," in *International Conf. on Power Electronics and Drives Systems*, Kuala Lumpur, 2005.

[81] M. M. I. Chy, "Development and Implementation of Various Speed Controllers for Wide Speed Range Operation of IPMSM Drive," MSc. Thesis, Lakehead University, Thunder Bay, 2007.

[82] H. D. Lee, S. J. Kang and S. K. Sul, "Efficiency-Optimized Direct Torque Control of Synchronous Reluctance Motor Using Feedback Linearization," *IEEE Trans. on Industrial Electronics,* vol. 46, no. 1, pp. 192-198, Feb. 1999.

[83] C.-T. Lin and C. S. George Lee, Neural Fuzzy Systems: A Neuro-Fuzzy Synergism to Intelligent Systems, NJ: Prentice Hall, 1996.

[84] H. D. Mathur and S. Ghosh, "A comprehensive analysis of intelligent controllers for load frequency control," in *IEEE Power India Conference*, New Delhi, 2006.

[85] D. Driankov, H. Hellendoorn and M. Reinfrank, An Introduction to Fuzzy Control, 2 ed., Berlin: Springer, 1996.

[86] M. N. Uddin and R. S. Rebeiro, "Neuro-fuzzy and fuzzy logic controllers based speed control of IPMSM drive — A torque ripple optimization approach," in *IEEE Industrial Electronics Society*, Glendale, 2010.

[87] Y. Sheng, Y. Shou-Yi and W. Z. Zhou, "Research on efficiency optimization of interior permanent magnet synchronous motor based on intelligent integrated control," in *Chinese Control and Decision Conference*, Xuzhou, 2010.

[88] H. Chaoui, W. Gueaieb and M. E. Yagoub, "Neural network based speed observer for interior permanent magnet synchronous motor drives," in *IEEE Electrical Power & Energy Conference*, Montreal, 2009.

[89] C. Butt and M. A. Rahman, "Untrained artificial neuron based speed control of interior permanent magnet motor drives over full operating speed range," in *IEEE Industry Applications Society Annual Meeting*, Orlando, 2011.

# Appendix – A

# IPMSM Parameters

| | |
|---|---|
| Number of phases | 3 |
| Number of poles (P) | 6 |
| Rated frequency (*f*) | 87.5 Hz |
| Rated power | 5 HP |
| Rated input voltage ($V_a$) | 183 V |
| Rated input current ($I_a$) | 14.2 A |
| Rated torque ($T_L$) | 19 Nm |
| Rated speed ($\omega_r$) | 183 rad/s |
| q-axis inductance ($L_q$) | 5.06 mH |
| d-axis inductance ($L_d$) | 6.42 mH |
| Stator resistance ($R_s$) | 0.242 Ω |
| Iron loss resistance ($R_c$) | 7.5 Ω |
| Inertia constant (J) | 0.0133 kg·m$^2$ |
| Rotor friction constant ($B_m$) | 0.001 Nm/rad/s |
| Permanent magnet flux linkage (Ψ) | 0.24 V/rad/s |

# Appendix – B

# Simulink Model

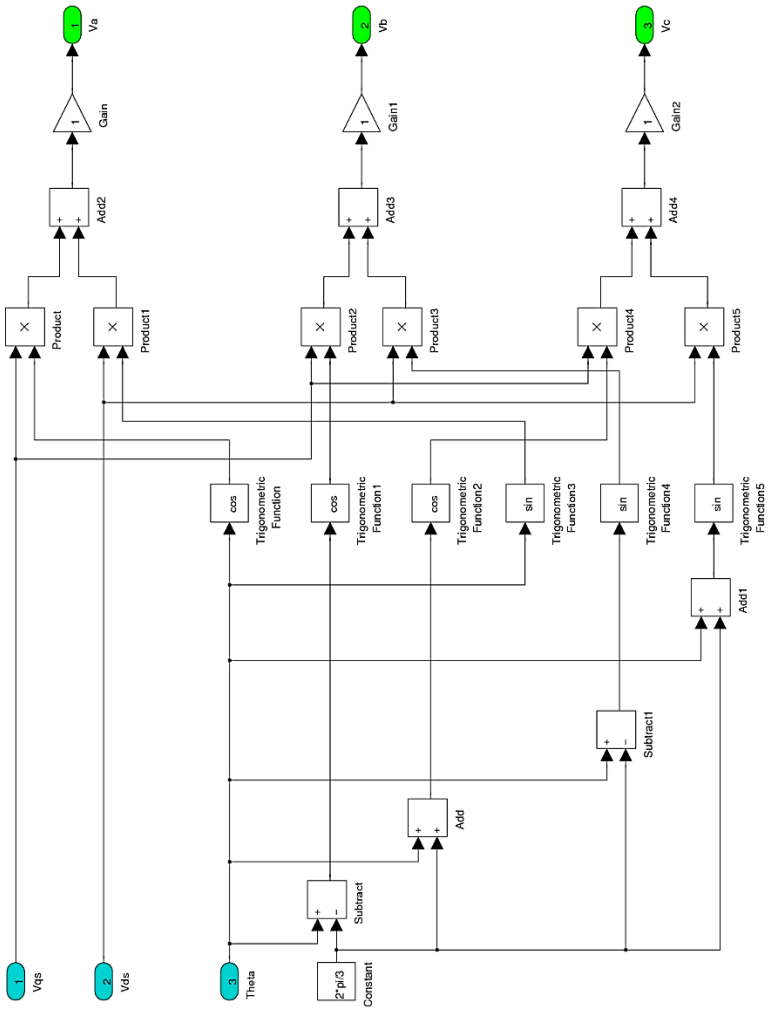


Appendix B.1: DQ/ABC Vector Rotator

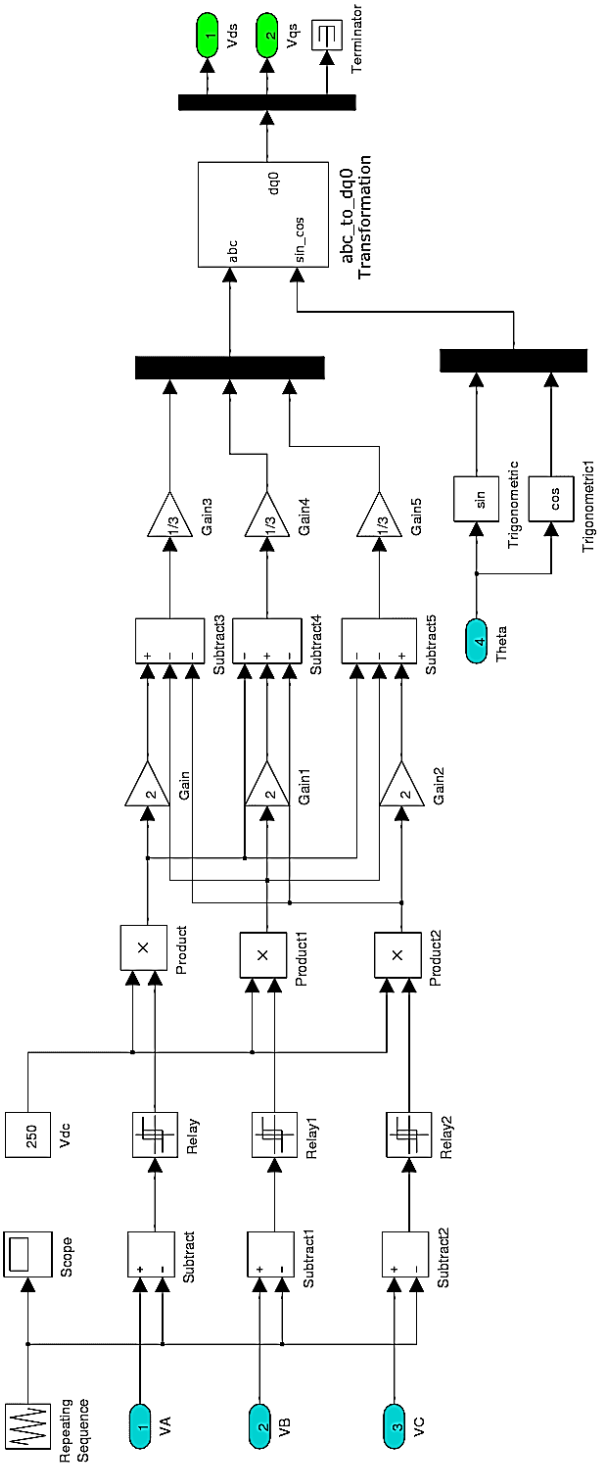


Appendix B.2: PWM Inverter Subsystem

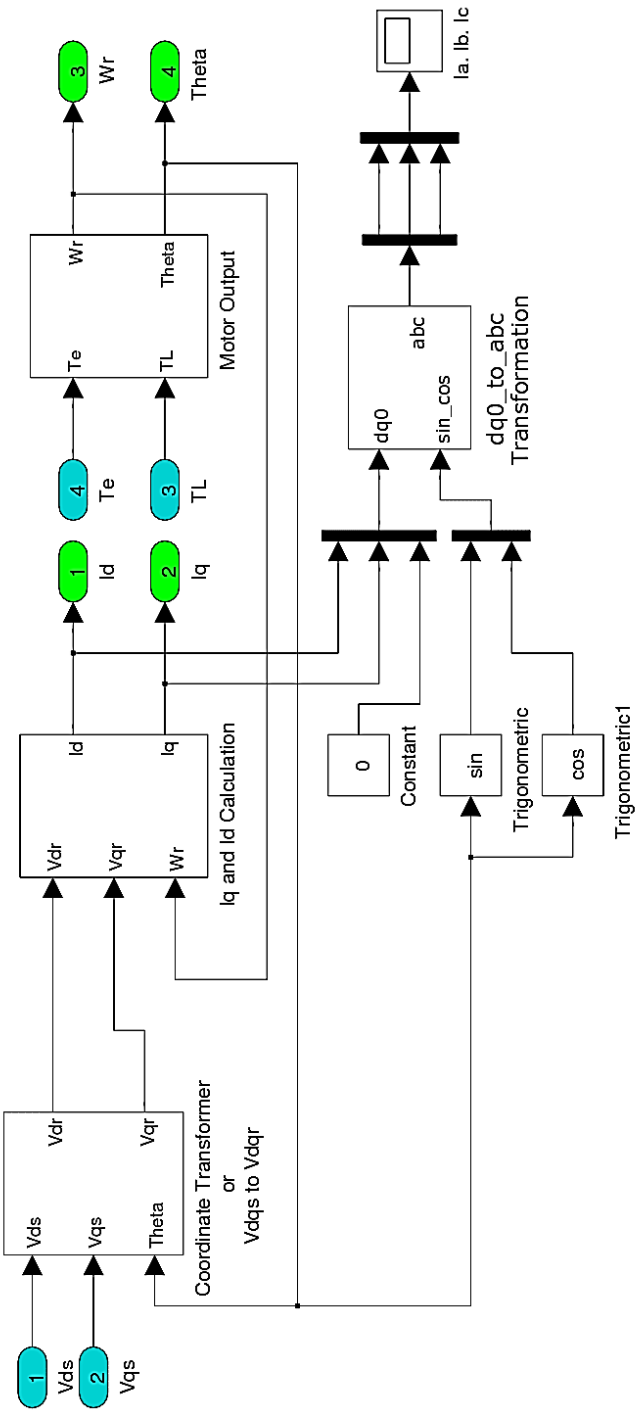


Appendix B.3: Motor Subsystem

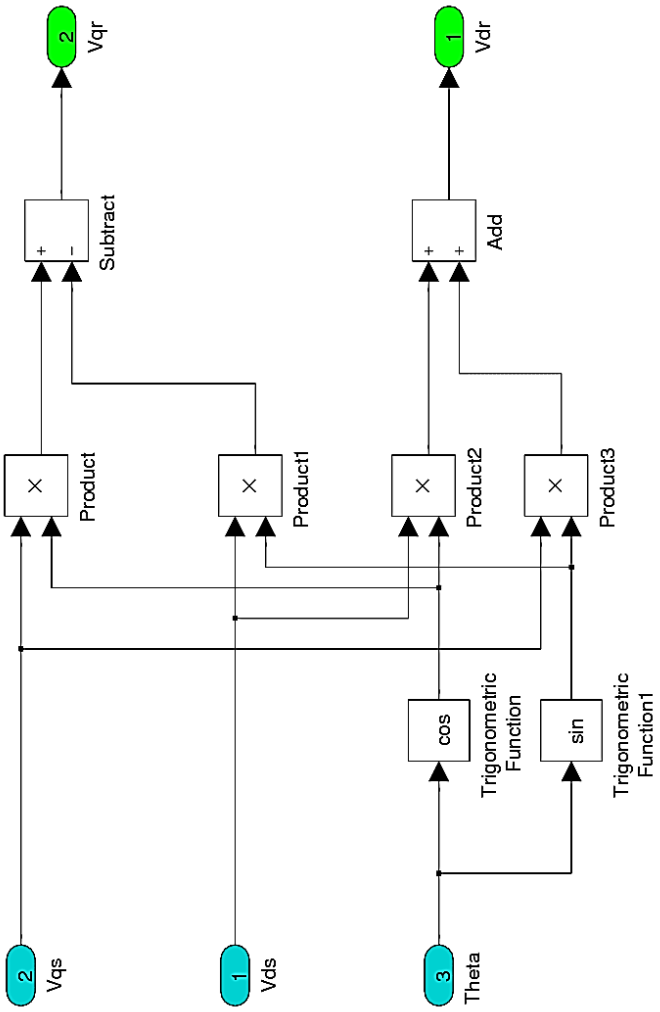


Appendix B.3.1: Co-ordinate Transformer Subsystem

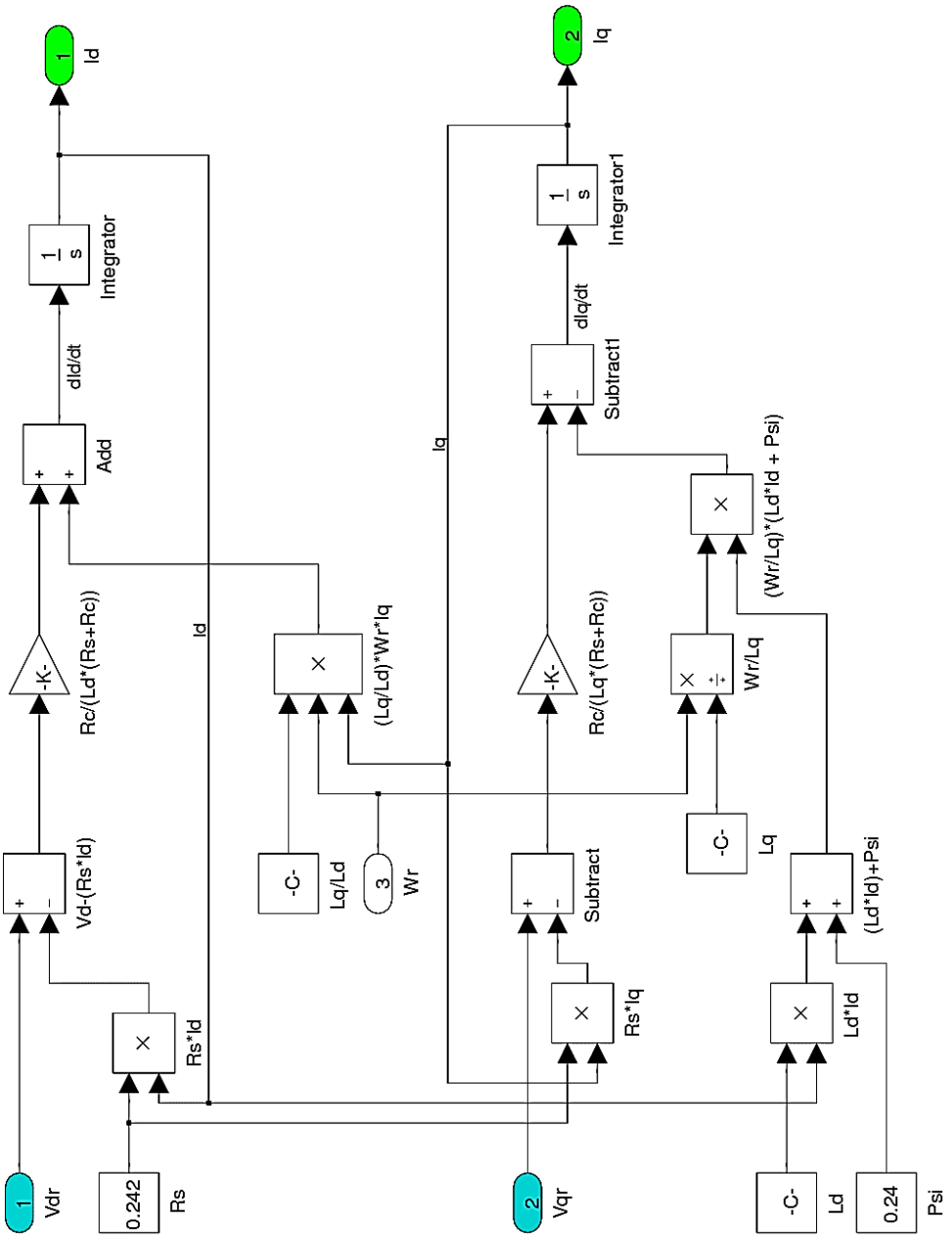


Appendix B.3.2: Current Transformer Subsystem ($I_q$ and $I_d$ Calculation)

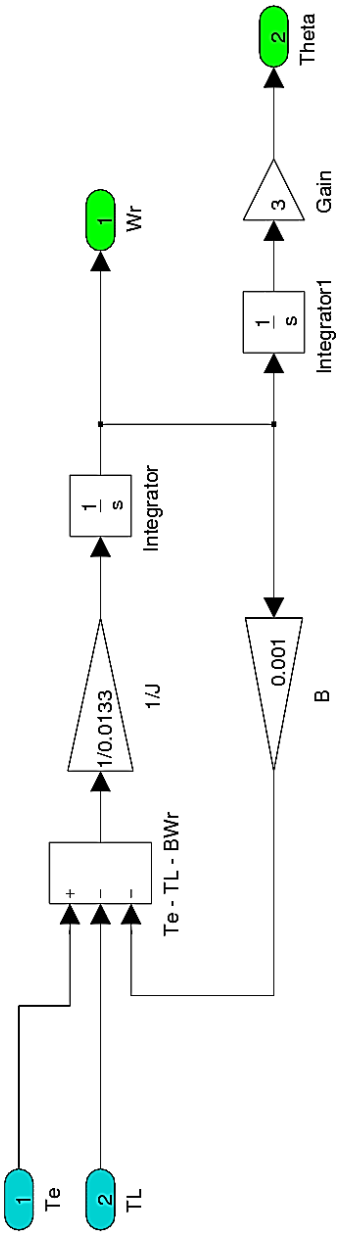


Appendix B.3.3: Motor Output Subsystem

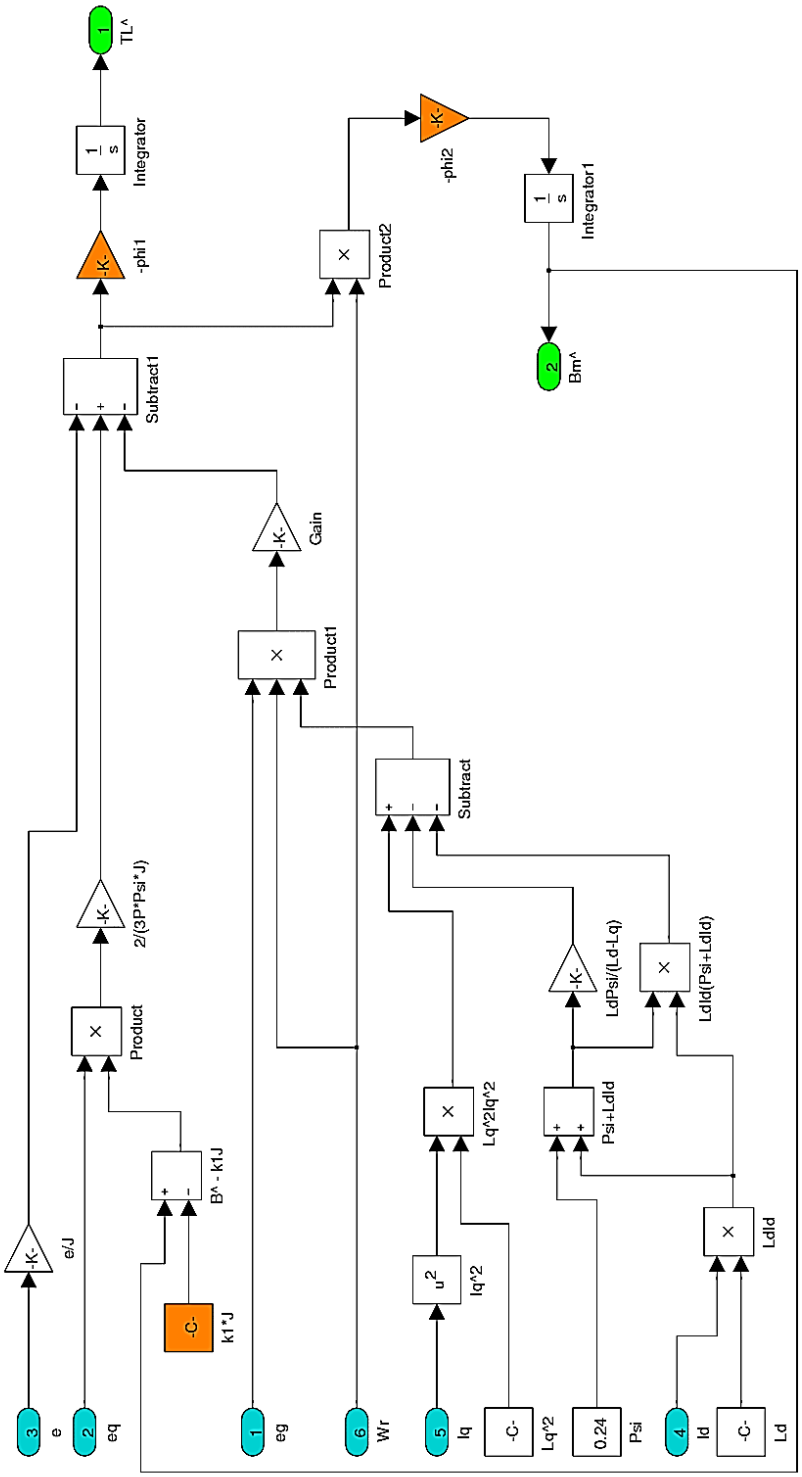


Appendix B.4: Parameter Estimator

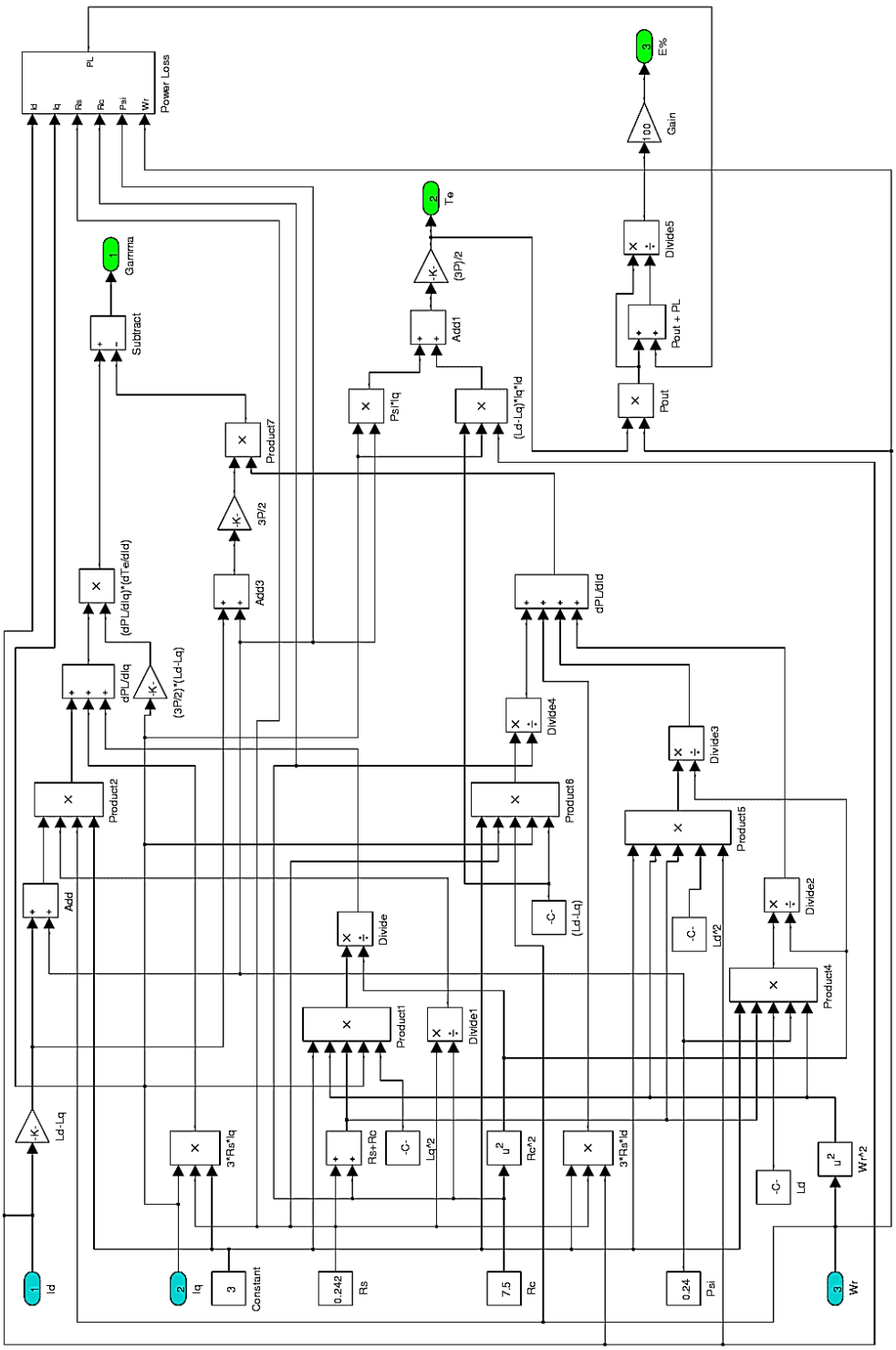


Appendix B.5: Loss Minimization Controller

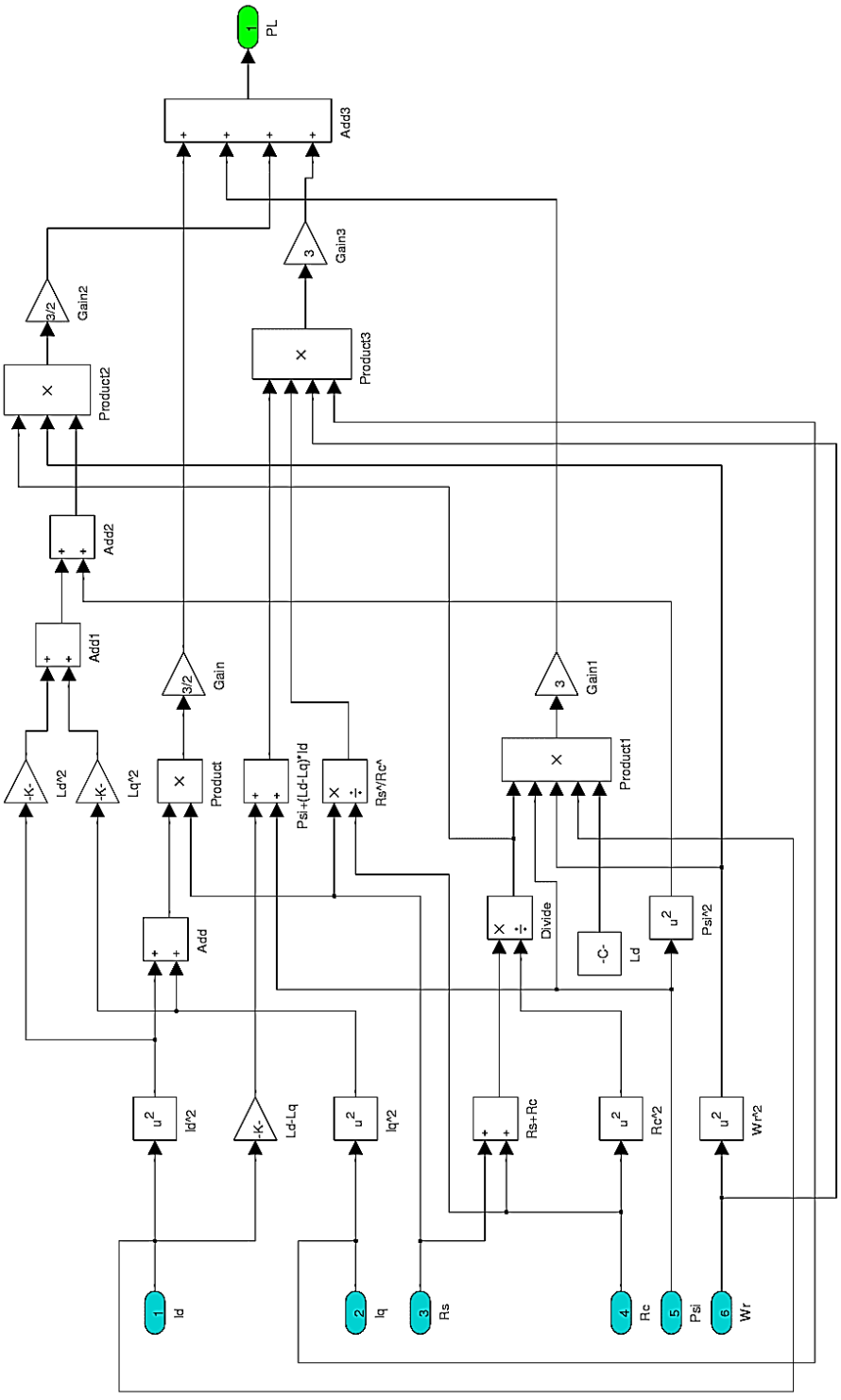


Appendix B.5.1: Power Loss Subsystem

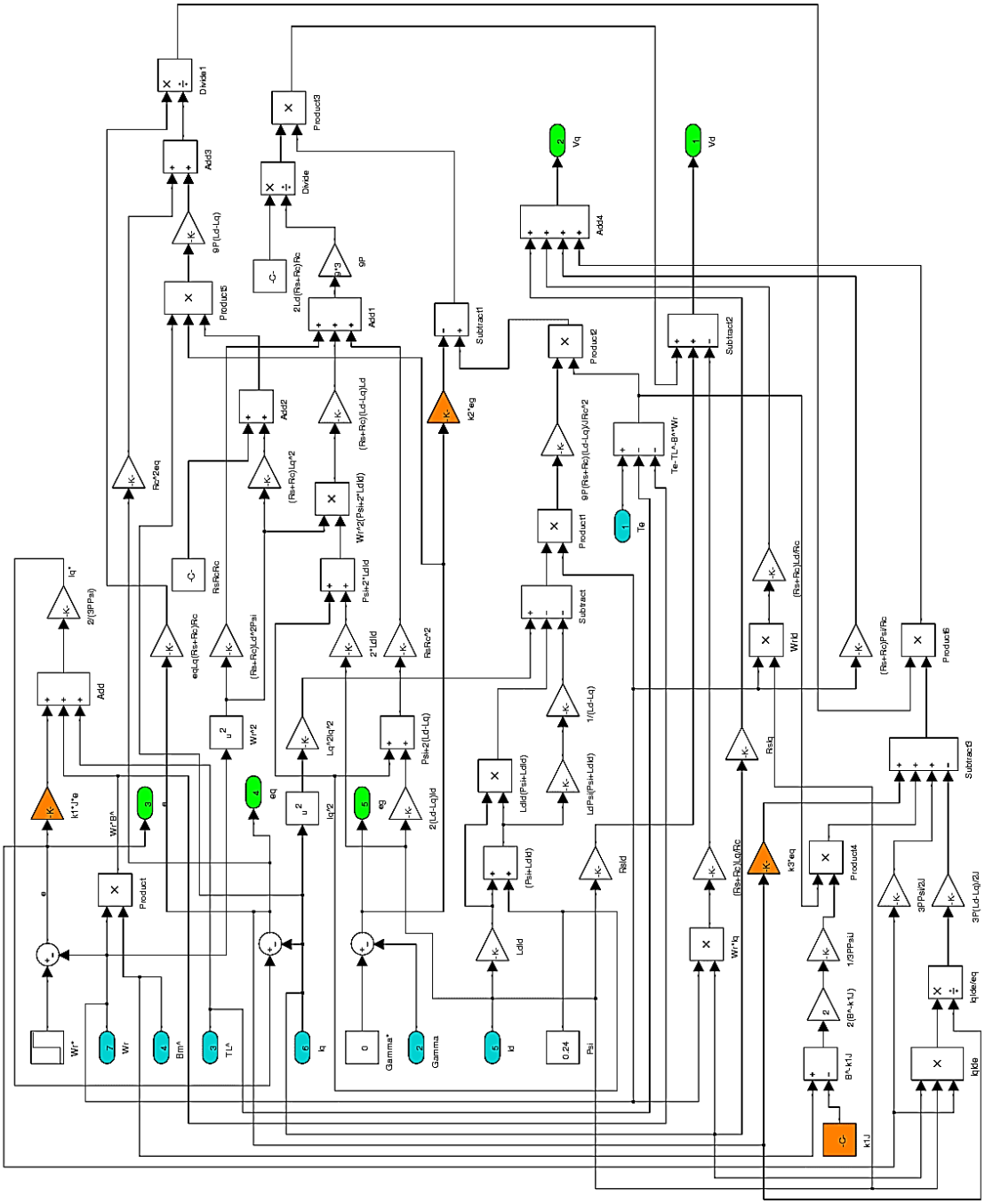


Appendix B.6: Adaptive Controller

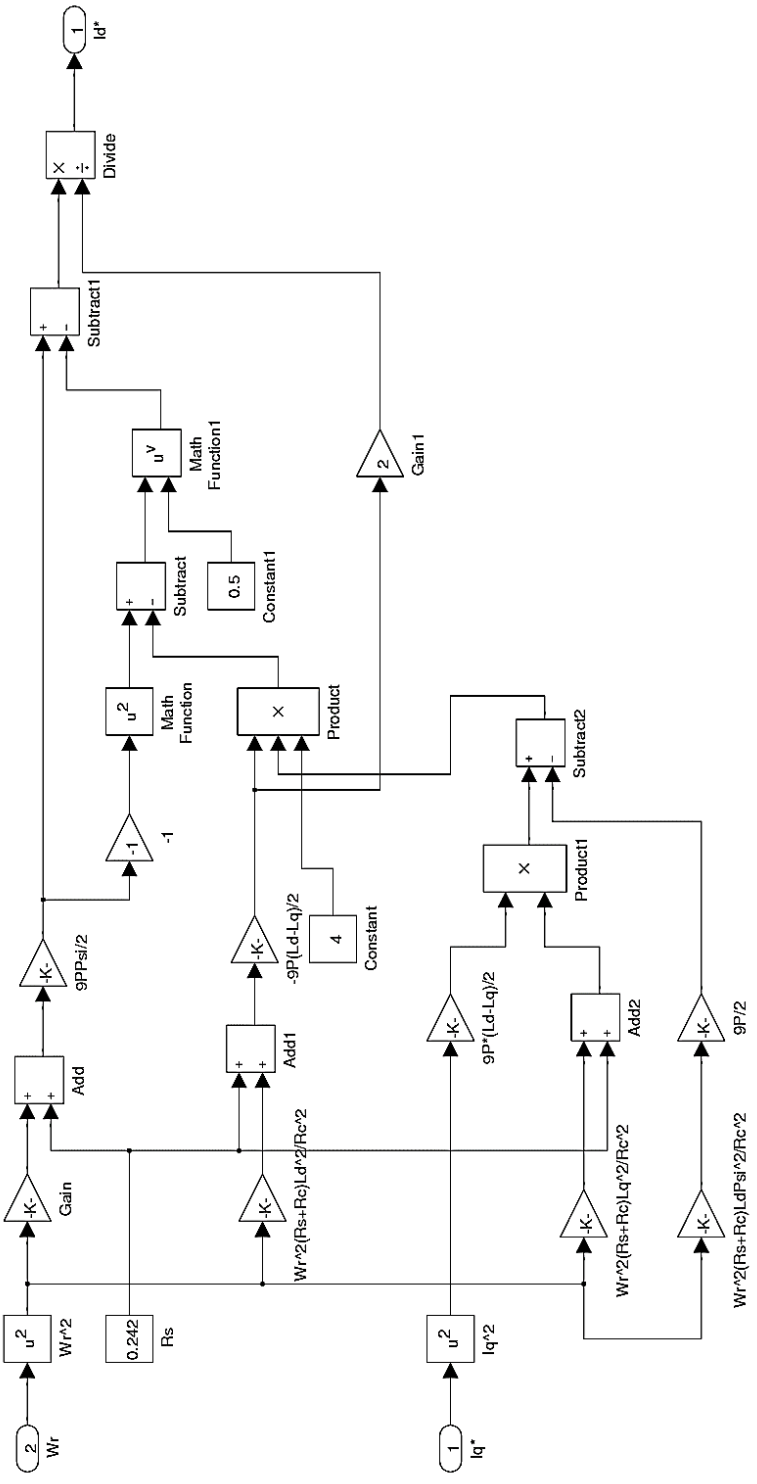


Appendix B.7: Loss Minimization Controller for NFC

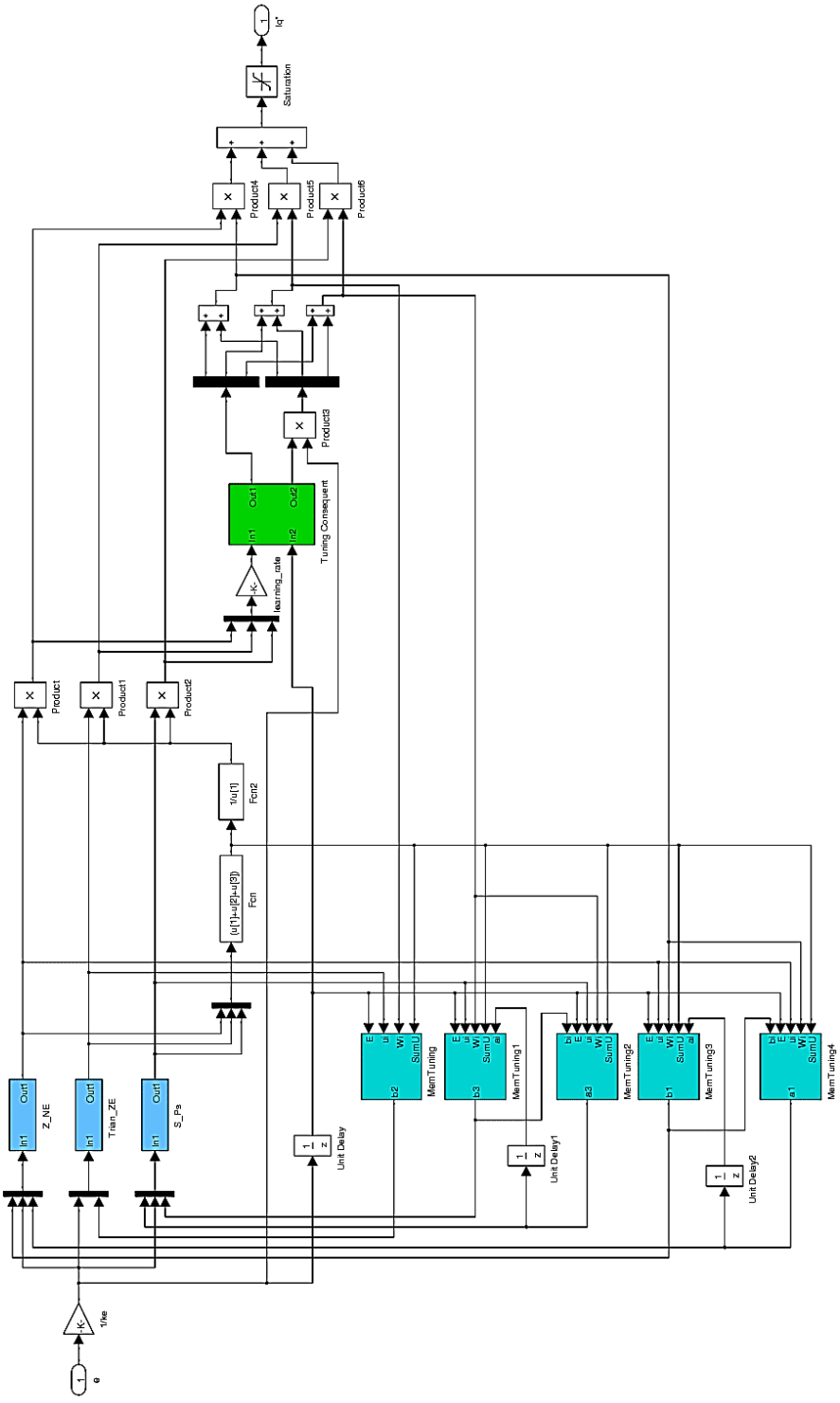


Appendix B.8: Neuro Fuzzy Controller

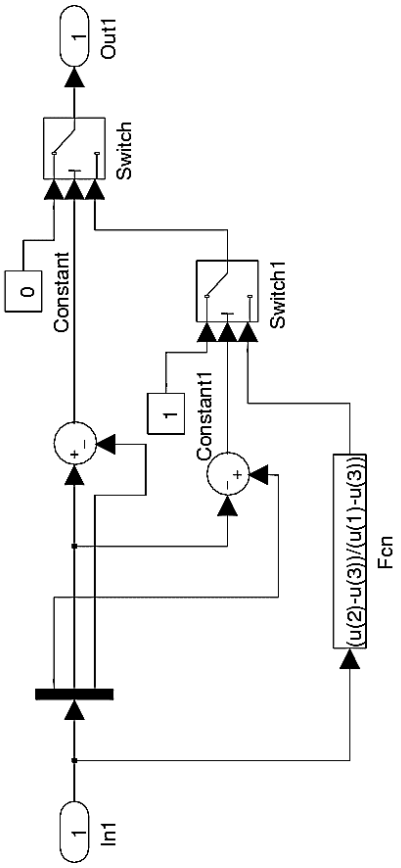


Appendix B.8.1: Fuzzy Value Calculator Subsystem for Z function

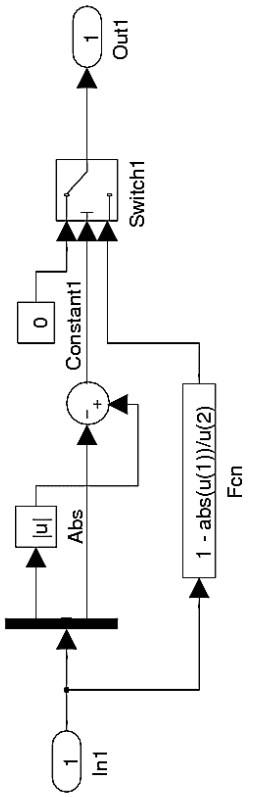


Appendix B.8.2: Fuzzy Value Calculator Subsystem for Triangle function

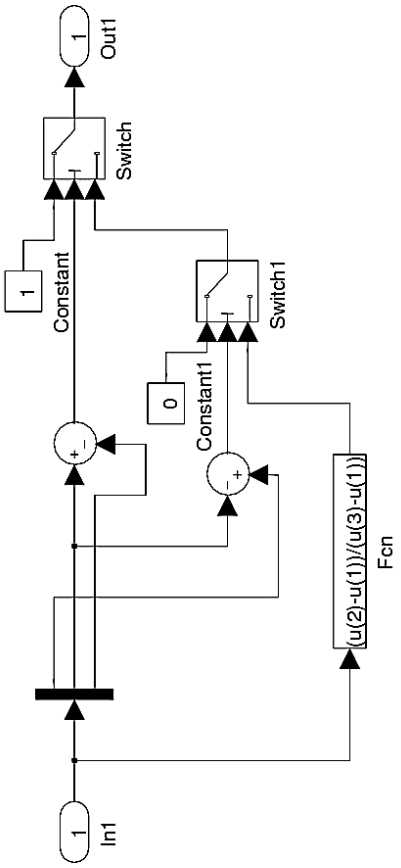


Appendix B.8.3: Fuzzy Value Calculator Subsystem for S function

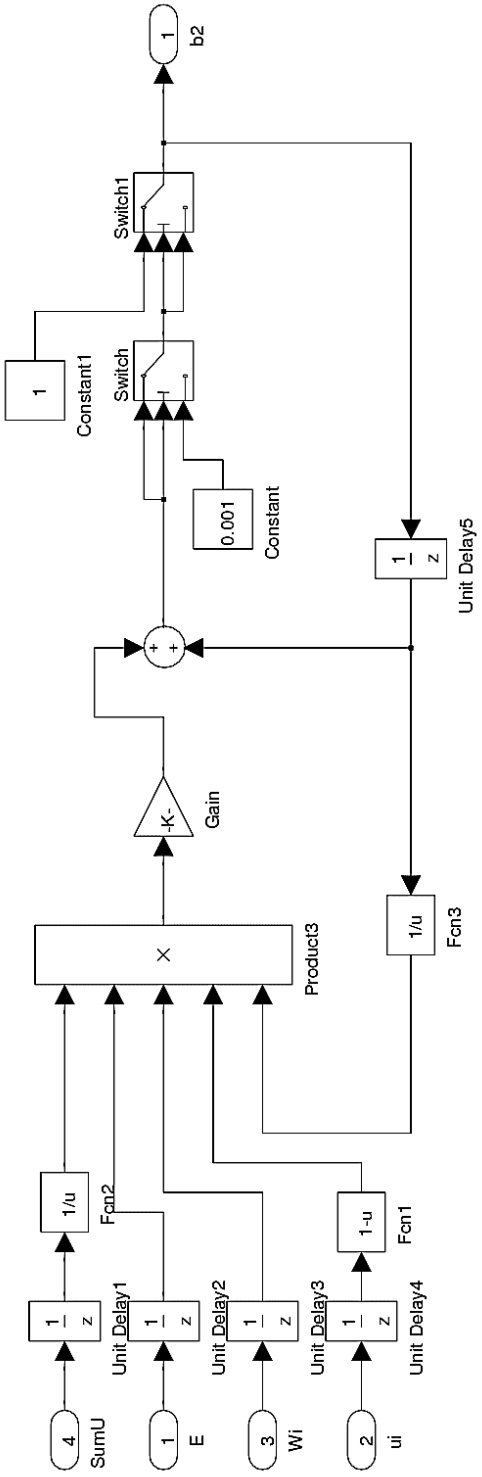


Appendix B.8.4: Membership Tuning Subsystem for $b_2$

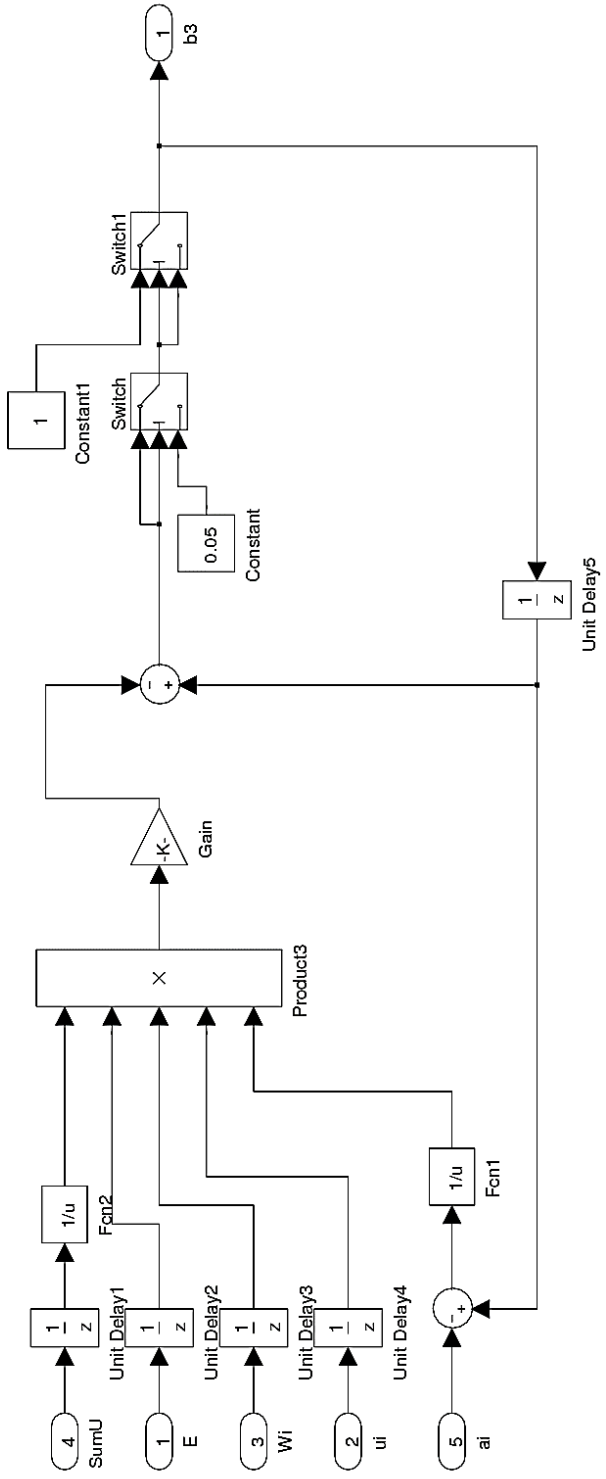


Appendix B.8.5: Membership Tuning Subsystem for $b_3$

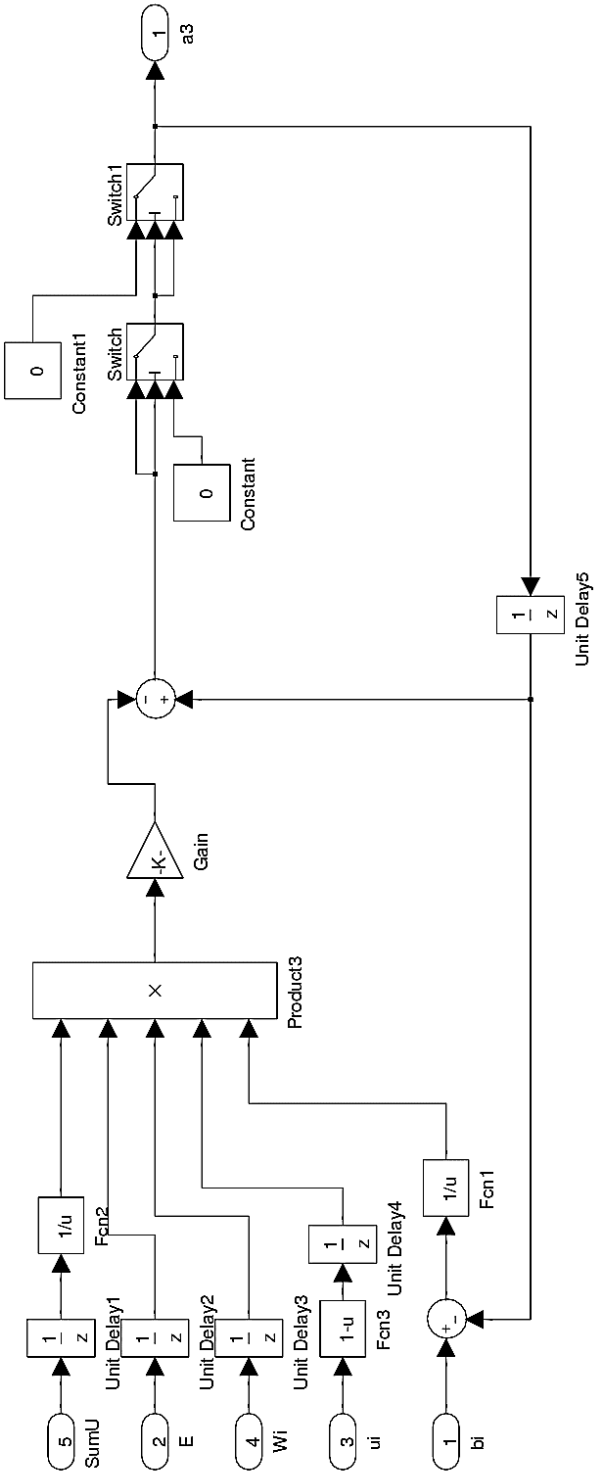


Appendix B.8.6: Membership Tuning Subsystem for $a_3$

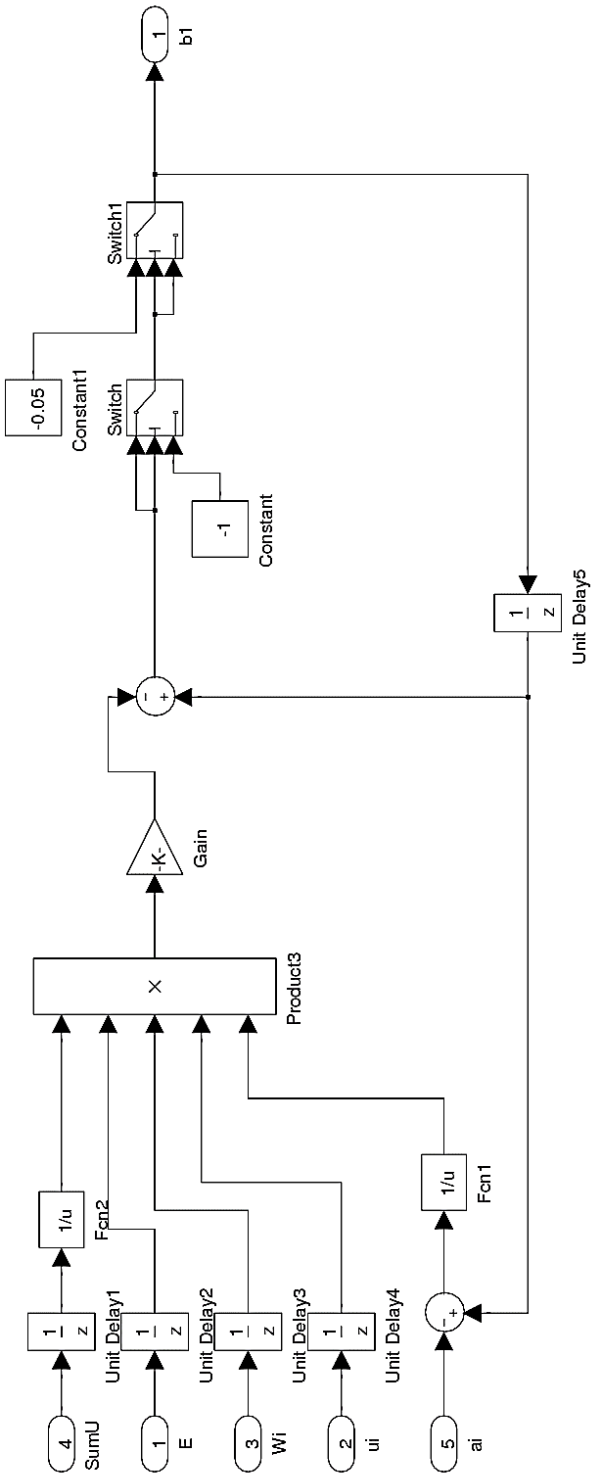


Appendix B.8.7: Membership Tuning Subsystem for $b_1$

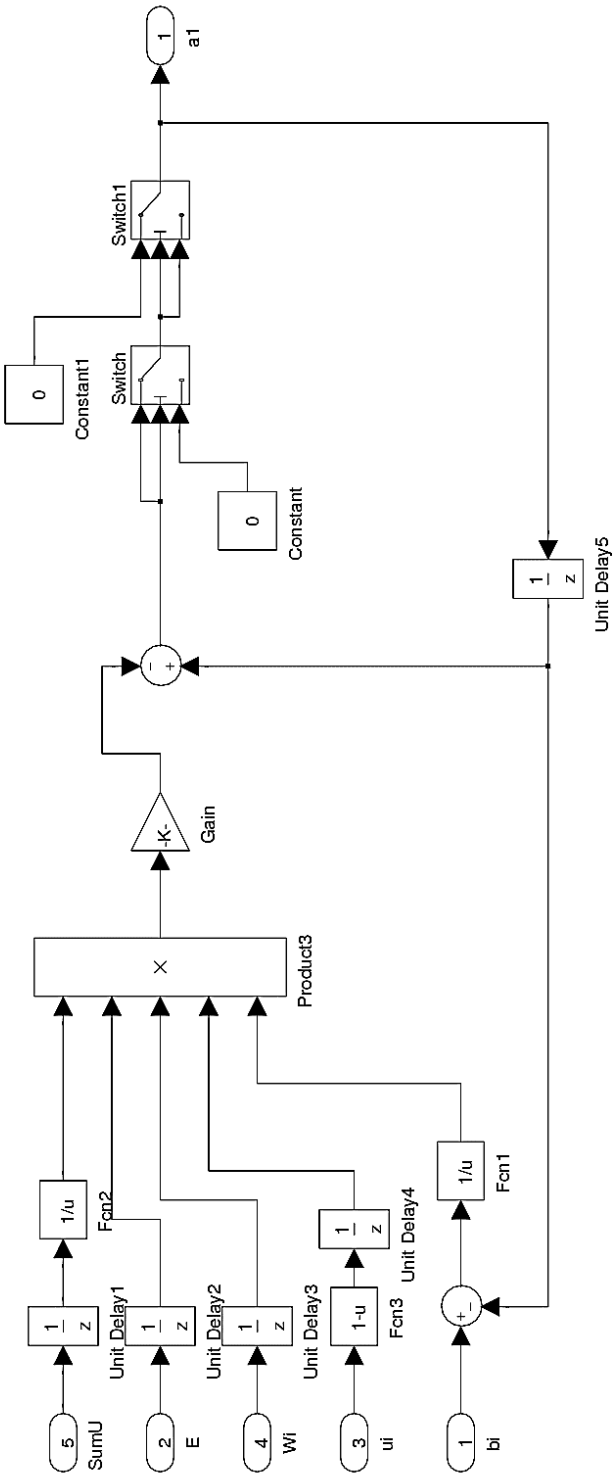


Appendix B.8.8: Membership Tuning Subsystem for $a_1$

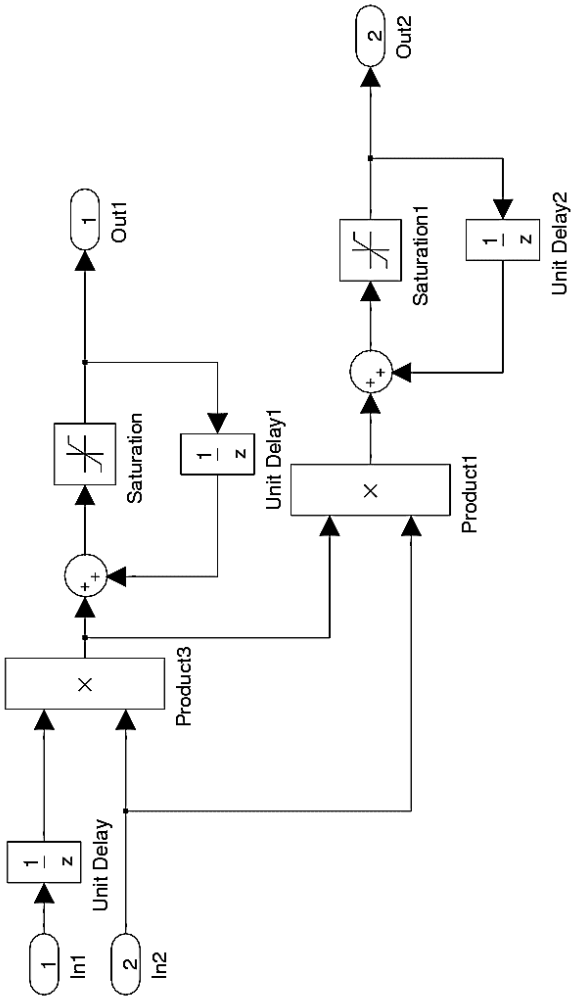


Appendix B.8.9: Tuning Subsystem for Consequent Parameter

# Appendix C

# Drive and Interface Circuit

$R_1=R_2=R_3=R_4=R_5=R_6=1.5k\Omega$

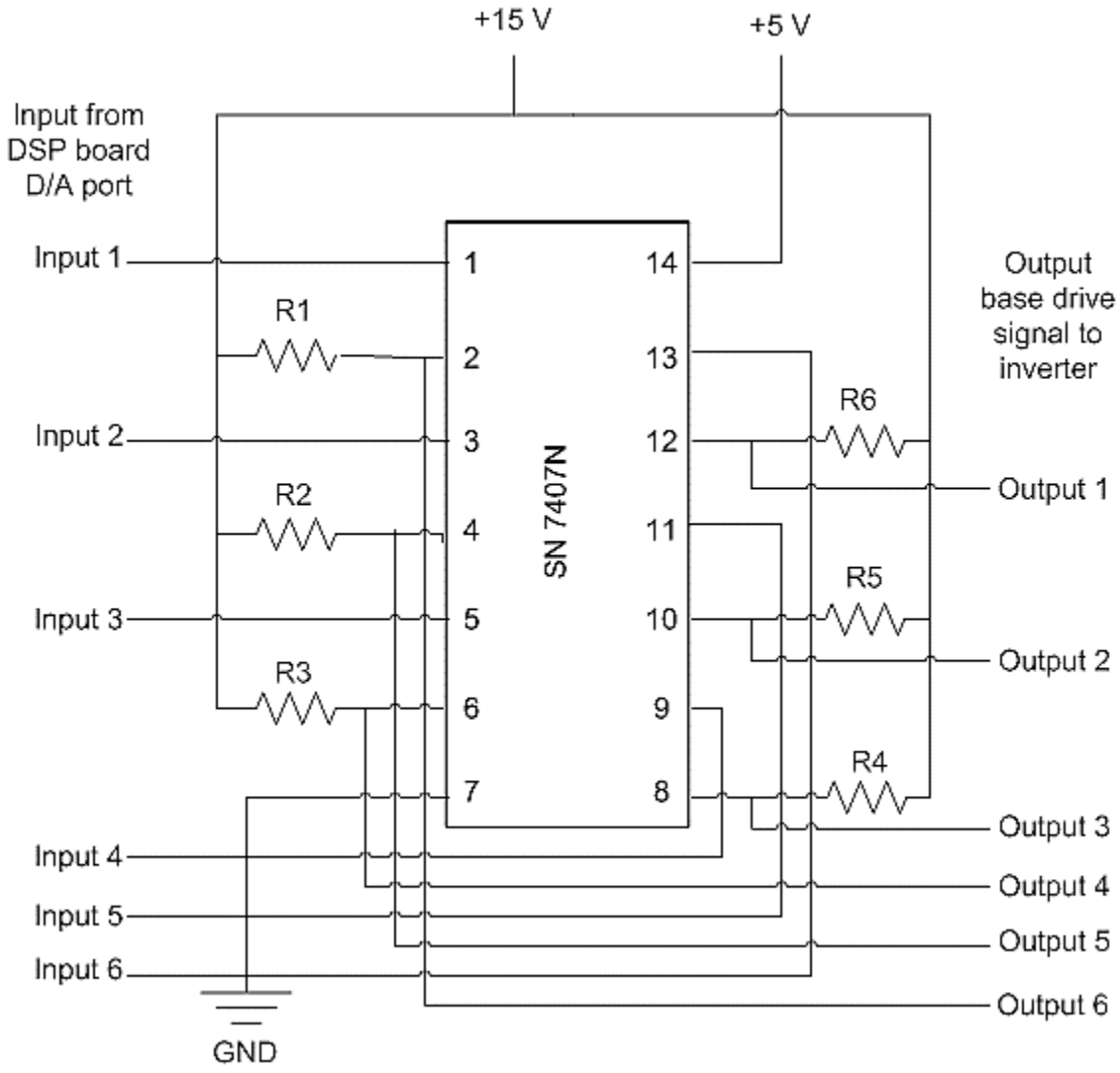


Appendix C.1: Base drive circuit for the inverter

Gain of Op-Amp (741CN) = 1+(R3/R2)

Magnitude of resistors:

| | Current sensor for phase ‘a’ | Current sensor for phase ‘b’ |
|---|---|---|
| $R_1$ | 98.7 Ω | 99 Ω |
| $R_2$ | 1.8 kΩ | 2 kΩ |
| $R_3$ | 5.5 kΩ | 5.1 kΩ |

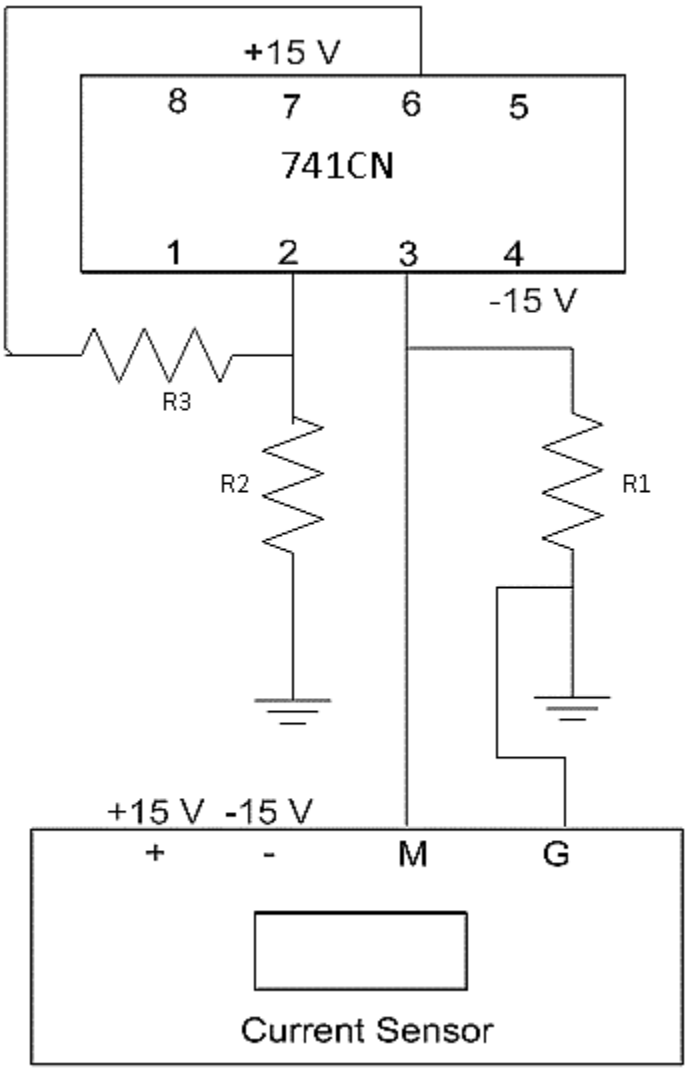


Appendix C.2: Interface circuit for the current sensor

# Appendix D
## Real-Time Simulink Model

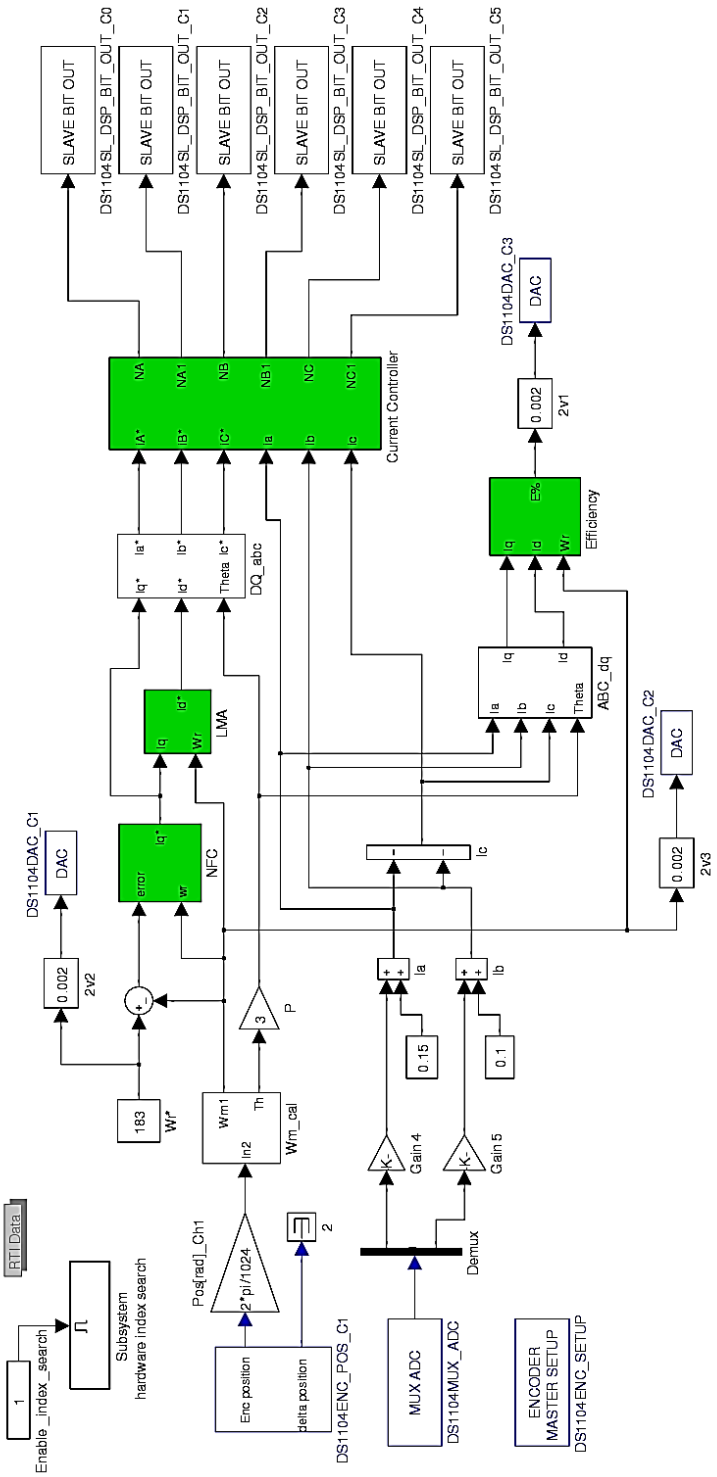


Appendix D.1: Real-time Simulink model for the proposed NFC and LMC based IPMSM drive.